

**Comparative Anatomy of the Mammalian
Bony Cochlea and its Ontogenetic
Development in Humans**

**Thesis submitted in accordance with the requirements of
the University of Liverpool for the degree of Doctor in Philosophy**

by

Thanakul Wannaprasert

October 2013

Dedication

I dedicate this thesis to my beloved father, grandparents and aunt for bringing me up with affections and love.

Acknowledgements

This research project would not have been possible without the support of many people. Foremost, I would like to express my sincere gratitude to my supervisor, Dr. Nathan Jeffery, for the continuous support of my doctoral research, for his patience, enthusiasm, encouragement and immense knowledge. Nathan is always available for giving helpful advice and ideas when they are needed. His guidance helps me in all the time of research and writing of this thesis. I cannot imagine having a better supervisor for my Ph.D. study.

I would like to thank Professor Robin Crompton (co-supervisor) for his support throughout my studies. Also I would like to extend my thanks to the Department of Musculoskeletal Biology for all the facilities and support.

My sincere thanks also go to Dr. Philip Cox for advice on the use of morphometric techniques and computer software, and for micro-CT image files of rodent inner ears. He is a nice friend, knowledgeable about language and helped me to adapt to living abroad when I arrived in Liverpool in 2009.

I would also like to convey thanks to several museums for providing skull specimens and to The University of Manchester for micro-CT imaging.

Furthermore, I thank Kathy Tinoco from Visage Imaging, Inc. for useful suggestions in Amira techniques.

Special thanks to Angela Fonceca for proof-reading of my thesis.

I owe a very important debt to Thai government for their financial support granted throughout the study. They gave me an opportunity to study abroad and to have experience in learning a wide range of life and technical skills.

Many Thai friends in Liverpool and in Thailand help me stay sane through these difficult years. Their support and care help me overcome difficulties and stay focused on my study. I greatly value their friendship and deeply appreciate their belief in me.

Lastly, I would like to most gratefully thank my parents for their endless love, support and encouragement, both academically and personally.

Comparative Anatomy of the Mammalian Bony Cochlea and its Ontogenetic Development in Humans

Abstract

The cochlea is the organ for sound reception. Mammals place varied functional demands on their sense of hearing to meet the requirements of a broad range of ecological niches and diverse behaviours. However, documenting potentially related adaptations of the cochlea to eco-behavioural traits is difficult due to its complex geometry. The present study aims to determine whether the bony cochlea carries eco-behavioural traits that can be used to contextualize our understanding of the fossil record and evolutionary transitions. This study also includes work on ontogenetic changes since these can yield important insights into evolutionary processes resulting in differences of the adult phenotypes.

Advanced techniques in micro-CT imaging, 3D image visualization, geometric morphometrics and statistical methods were used to study morphological variations of the bony cochlea across 45 adult eutherian species. Also, the same set of techniques was used to study 12 human fetal (approximately four to nine months of gestation) cochleae in comparison with five adult cochleae.

Results revealed that there was a considerable range of variation in form of the mammalian bony cochlea. Potential links between the bony cochlear morphology and hearing, ecology and behaviour were found. Dimensions of the bony cochlea may be indicative of the eco-behavioural niche that a mammal occupies; e.g., fewer than two spiral turns is associated with obligate marine species. Rodents also showed remarkable variation in the cochlear morphology, more so than any other group of mammals studied, reflecting their diverse eco-behavioural traits. Results from the human developmental study showed that whilst the general coiled shape was achieved at the midgestational age, there was size related morphological change during the postnatal period. The round window size reached mature state prior to birth, by approximately the second trimester, whereas the oval window continued to change in size after birth. The postnatal enlargement may be determined by functional requirements of air-borne hearing, particularly with respect to frequency range and sensitivity.

Table of contents

Chapter 1 Introduction	1
1.1 Basic anatomy of the mammalian ear	1
1.1.1 The outer (external) ear	1
1.1.2 The middle ear	2
1.1.3 The inner ear	3
1.1.4 Pathway of sound perception	6
1.2 Evolution of vertebrate hearing	8
1.2.1 Fish	12
1.2.2 Tetapods	15
1.2.3 Mammals	16
1.2.3.1 Monotremes	21
1.2.3.2 Therians	22
1.3 Evolution of hearing with reference to example eutherian groups with differing habitats or behaviours	24
1.3.1 Aquatic or semi-aquatic eutherians (Cetacea, Sirenia and Pinnipedia)	25
1.3.1.1 Cetacea	25
1.3.1.2 Sirenia	31
1.3.1.3 Pinnipedia	36
1.3.2 Subterranean and fossorial eutherians (Rodentia and Insectivora)	43
1.4 Summary of functional anatomy of the bony mammalian cochlea and potential correlates	50

1.4.1	The gross dimensions of the bony cochlea	50
1.4.2	Interaural distance	55
1.4.3	Ecology and behavioural influences	59
1.4.4	Hypotheses: the adult interspecific mammalian cochlea	62
1.5	Ontogeny of the cochlea and auditory frequency mapping	64
1.5.1	Ontogenetic changes of the mammalian cochlea	65
1.5.2	Ontogenetic changes in sound frequency analysis	68
1.5.3	Ontogenetic changes of the human bony cochlea	71
1.5.4	Hypotheses regarding development of the bony cochlear morphology in human	75
Chapter 2 Review: capturing the cochlear morphology		77
2.1	Early methods versus computed tomography	77
2.2	Basic principles of X-ray physics in CT	79
2.2.1	Quality and quantity of X-ray beam	79
2.2.2	X-ray interaction with matter	82
2.3	Computed tomography	87
2.3.1	Technical background of CT data processing	88
2.3.2	CT image artifacts	93
2.3.3	Micro-computed tomography (micro-CT)	95
2.3.4	Processing and visualization of images	97
Chapter 3 Review: analyzing the cochlea form		102
3.1	Traditional morphometrics	102
3.2	Geometric morphometrics	103

3.2.1	Procrustes superimposition and morphometric spaces	106
3.2.1.1	Configuration matrix and configuration space	107
3.2.1.2	Pre-shape space	107
3.2.1.3	Shape spaces	109
3.2.1.4	Tangent space	113
3.2.1.5	Reference configuration	115
3.2.2	Analysis of shape differences	117
Chapter 4	Materials and methods	121
4.1	Samples	121
4.1.1	Adult interspecific study	121
4.1.2	Human developmental study	126
4.2	Micro-CT image processing	127
4.3	Standardization and 3D reconstruction	129
4.3.1	Standardization	129
4.3.2	Reconstruction of 3D images of the inner ear	129
4.4	Landmark methods	130
4.5	Measurement protocols of the cochlear variables	133
4.6	Data analyses of the adult interspecific study	139
4.6.1	Repeatability of Measurements	139
4.6.2	Statistical analyses with body mass	140
4.6.3	Quantifying shape with geometric morphometrics and related statistics	140
4.6.4	Test of phylogenetic signal	142
4.7	Data analyses of the human developmental study	146

4.7.1	Comparison between adult and fetal cochleae	146
4.7.2	Comparison between large and small fetal cochleae	147
Chapter 5	Results: adult interspecific study	149
5.1	Descriptive morphology of the inner ear	149
5.1.1	The number of spiral turns	149
5.1.2	The general appearance of the bony cochlea	151
5.1.3	The internal architecture of the bony cochlea	152
5.1.4	Semicircular canals	153
5.1.5	The cochlear fenestrae	154
5.1.6	Variation of the auditory bullae	155
5.2	Repeatability of measurements of the cochlear form analyses	157
5.3	Bivariate analysis—allometry with body mass	160
5.4	Bivariate analysis—pairwise measurement comparisons	164
5.5	General geometric morphometrics	165
5.6	Relationships between the bony cochlear morphology and ecological and hearing influences	172
5.6.1	Habitat selection	172
5.6.2	Activity period	178
5.6.3	Sociality	178
5.6.4	High frequency limit of hearing	179
5.6.5	Low frequency limit of hearing	180
5.6.6	Best frequency of hearing	182
5.6.7	Intermeatal distance	183
5.7	Test of phylogenetic signal	184

Chapter 6 Results: human developmental study	191
6.1 Cochlear development from micro-CT images	192
6.2 Repeatability	195
6.3 Developmental study: fetal cochleae	197
6.3.1 Bivariate analysis—allometry with the length of the petrous bone	197
6.3.2 Differences in the cochlear morphology between large and small fetuses	198
6.3.3 Geometric Morphometrics	200
6.4 Developmental study: adult versus fetal cochleae	207
6.4.1 Differences in the cochlear morphology between adults and fetuses	207
6.4.2 Geometric morphometrics	208
Chapter 7 Discussions and Conclusions	216
7.1 Adult interspecific study	217
7.1.1 General description of the cochlea in relation to hearing abilities	217
7.1.2 Allometric relationship with body mass	220
7.1.3 Relationships between the bony cochlear morphology, ecology and hearing abilities	221
7.1.3.1 The number of cochlear turns	221
7.1.3.2 The height-to-width ratio of the cochlea	224
7.1.3.3 Cochlear width (the width of the basal turn)	225
7.1.3.4 Cochlear volume	226

7.1.3.5 Cochlear fenestrae	227
7.1.4 Shape analysis of the cochlea	230
7.1.4.1 Shape analysis by principal component analysis	230
7.1.4.2 Shape analysis after size correction	233
7.1.5 Phylogenetic signal in cochlear shape variation	235
7.1.6 The intermeatal distance and adaptations of the bony cochlea in adult mammals	236
7.2 Human developmental study	244
7.2.1 Size maturation of the bony cochlea	244
7.2.2 Shape maturation of the bony cochlea	248
7.3 Conclusions	250
References	253
Appendices	280
Appendix A: Procedures in Amira software (v. 5.2.2)	280
Appendix B: Module and NEXUS files	286
Appendix C: The phylogenetic tree for 45 mammalian species	290
Appendix D: Raw data and statistics	291
Appendix E: Abstracts for international conferences	304

List of figures

Figure 1.1	Anatomy of the mammalian ear (based on <i>Homo sapiens</i>).	2
Figure 1.2	Structures of the human cochlea.	4
Figure 1.3	The sound conducting pathway in the mammalian ear.	8
Figure 1.4	Sound localization in the horizontal plane using comparisons between left and right ears: A) interaural time difference (ITD) and B) interaural level difference (ILD).	10
Figure 1.5	The relationships between sound frequency and wavelength ($v = f\lambda$), and between the intermeatal distance and maximum time delay ($v = s/t$).	11
Figure 1.6	The inner ears (membranous labyrinths) of representative vertebrates.	13
Figure 1.7	Basilar membrane and spiral laminae differences among Type I, Type II odontocetes, and Type M mysticete inner ears.	31
Figure 1.8	Typical structures of the ear drum in mammals	46
Figure 1.9	The rotatory axis of left auditory ossicles (malleus and incus). The crosses represent the positions of the centers of ossicular mass. A) The “microtype” ossicles; B) The hypertrophied ossicle type; C) The freely mobile type.	49
Figure 1.10	Head shadow effect on sound localization.	57
Figure 1.11	Development of the bony inner ear including the cochlea (in the woolly opossum).	66
Figure 1.12	Ontogeny of the human bony cochlea	72
Figure 2.1	Modification of a polychromatic beam by attenuation.	82

Figure 2.2 Four processes of X-ray attenuation: A) unmodified scattering; B) photoelectric absorption; C) Compton scattering; D) pair production.	83
Figure 2.3 CT data processing, from data acquisition to image display and storage.	89
Figure 2.4 A CT slice consisting of picture elements called “pixels” and their volume elements “voxels”.	90
Figure 2.5 Effects of the window width (WW) and the window level (WL) on CT image quality.	92
Figure 2.6 In-vitro micro-CT setup.	97
Figure 2.7 Maximum intensity projection (MIP).	101
Figure 3.1 The space of Procrustes-superimposed triangles.	110
Figure 3.2 The relationship between Kendall’s shape space and the space of aligned triangles scaled to centroid size of one.	112
Figure 3.3 The projection of points representing triangles onto a space tangent to the reference shape.	115
Figure 3.4 Graphical representation of the principles of PCA.	118
Figure 3.5 Ontogenetic shape variation visualized by Procrustes superimposition. The shape variation can be depicted in two styles: vectors of relative landmark displacement and a thin-plate spline deformation grid.	120
Figure 4.1 The slice was rotated 22.5 degrees each to put landmarks around the mid-modiolar axis.	132
Figure 4.2 Original landmarks (red) and semi-landmarks (blue).	133
Figure 4.3 Measurements of the cochlear height and width.	135
Figure 4.4 The vestibular apparatus was removed and the cochlear volume was measured.	137

Figure 4.5 Measurement of the surface areas of the oval window (OW) and round window (RW).	138
Figure 4.6 The example of mapping of the shape variation onto a known phylogenetic tree.	144
Figure 5.1 The inner ear of the guinea pig, coypu and bottlenose dolphin.	150
Figure 5.2 A bony structure protruding into the basal turn in the European otter.	151
Figure 5.3 A CT slice (inverted grey scale) through the midmodiolar plane of the beluga whale showing the enlarged spiral canal and cochlear aqueduct.	153
Figure 5.4 The inner ears of the two talpid moles, the European mole and the Spanish mole.	155
Figure 5.5 A CT slice through the coronal plane of the Spanish mole showing the connection between the bullae.	156
Figure 5.6 The ventral view of the whole skulls showing the auditory bullae in the rat and in the tuco-tuco.	157
Figure 5.7 Repeatability test in shape space. Shape variation of the mammalian cochlea represented by the scatter plot of PC1 vs PC2.	159
Figure 5.8 Bivariate plots showing the relationships between the cochlear variables and body mass.	161
Figure 5.9 Bivariate plots showing the relationships between the hearing parameters and body mass.	163
Figure 5.10 Bivariate plots of length, height and width.	165
Figure 5.11 Plot of the proportion of variance accounted for each PC. Only PC1 to PC4 described more than 5% of the total variance.	166

Figure 5.12 Shape variation of the cochlea in 45 mammalian species. Scatter plots of PC1 vs PC2 explained 67.8% of the total variance.	168
Figure 5.13 Shape variation of the cochlea in 45 mammalian species. Scatter plots of PC3 vs PC4 explained 18.6% of the total variance.	169
Figure 5.14 Shape variation of the cochlea on the first four PCs after minimising the allometric effects.	171
Figure 5.15 The ANCOVA plots with regression lines showed all cochlear variables statistically related to habitat differences at the $P < 0.001$ or 0.01 level.	174
Figure 5.16 The ANCOVA graph with regression lines showed the significant difference in OW area between solitary mammals and gregarious mammals at the $P < 0.01$ level.	178
Figure 5.17 The ANCOVA graphs with regression lines showed the two cochlear variables statistically related to the categorical variables of the high frequency limit of hearing at the $P < 0.001$ or 0.01 level.	180
Figure 5.18 The ANCOVA plots with regression lines showed the two cochlear variables statistically related to the categorical variables of the best hearing frequency at the $P < 0.001$ or 0.01 level.	183
Figure 5.19 Reconstruction of evolutionary changes in cochlear shape in 45 mammalian species. The phylogenetic tree was mapped into plots of the first 2 PC axes, using unweighted squared-change parsimony and weighted squared-change parsimony.	186
Figure 5.20 Reconstruction of evolutionary changes in cochlear shape in 15 rodent species. The phylogenetic tree was mapped into plots of the first 2 PC axes, using unweighted squared-change parsimony and	

weighted squared-change parsimony.	187
Figure 5.21 Reconstruction of evolutionary changes in cochlear shape in 8 primate species. The phylogenetic tree was mapped into plots of the first 2 PC axes, using unweighted squared-change parsimony and weighted squared-change parsimony.	188
Figure 6.1 A bivariate plot of log ₁₀ petrous length against log ₁₀ gestational age ($r = 0.91$, $P < 0.001$).	191
Figure 6.2 Development of the bony inner ear in human. The petrous bone length was used as developmental stages of the bony inner ear.	193
Figure 6.3 Repeatability test in shape space. Shape variation of the human cochlea represented by the scatter plot of PC1 vs PC2.	196
Figure 6.4 Plot of the proportion of variance accounted for each PC. Only PC1 to PC5 explained more than 5% of the total variance.	201
Figure 6.5 Shape variation of the fetal human cochleae described by the scatter plot of PC1 vs PC2.	202
Figure 6.6 Three-dimensional cochlear images of some human specimens along PC1 (S4 and S5) and PC2 (S1 and L5).	203
Figure 6.7 Shape variation of the fetal human cochleae described by the scatter plot of PC3 vs PC4.	204
Figure 6.8 Shape variation of the fetal human cochleae described by the scatter plot of PC4 vs PC5.	205
Figure 6.9 Plot of the proportion of variance accounted for each PC. Only PC1 to PC5 described more than 5% of the total variance.	209
Figure 6.10 Shape variation of the human cochlea described by the scatter plot of PC1 vs PC2.	210

Figure 6.11 Three-dimensional cochlear images of some human specimens along PC1 (A3 and S5) and PC2 (S1 and A1).	211
Figure 6.12 Shape variation of the human cochlea described by the scatter plot of PC3 vs PC4.	212
Figure 6.13 Shape variation of the human cochlea described by the scatter plot of PC4 vs PC5.	213
Figure 6.14 Shape variation of the human cochlea described by the scatter plot of residual PC1 vs PC2.	214
Figure 7.1 The number of cochlear whorls in the four species: the coypu, guinea pig, bottlenose dolphin and African manatee.	222
Figure 7.2 The inter-dependencies of cochlear dimensions and hearing frequency.	230
Figure 7.3 The auditory bullae in the rat and in the tuco-tuco. The auditory bullae and the cochleae are shown at the plane through the mid-modiolar axis.	241
Figure 7.4 The middle-ear ossicles and the inner ear of the Spanish mole (<i>Talpa occidentalis</i>). The stapedial artery enclosed by a bony tube passes through the stapedial foramen.	242
Appendix C The topology and dates of phylogenetic tree for 45 mammalian species.	290

List of tables

Table 4.1	Taxonomy of 45 mammalian species studied.	122
Table 4.2	Body mass and eco-behavioural traits of 45 mammalian species.	123
Table 4.3	Audiograms and intermeatal distances in 45 mammalian species.	124
Table 4.4	Categories of hearing variables.	125
Table 4.5	Categories of human specimens.	126
Table 4.6	Imaging information and specimen sources of the species studied.	127
Table 5.1	The repeatability of measurements and landmarking.	158
Table 5.2	Spearman's rank correlation and RMA regression of cochlear variables with body mass.	162
Table 5.3	Spearman's rank correlation and RMA regression of hearing parameters with body mass.	163
Table 5.4	Spearman's rank correlation and RMA regression of pairs of cochlear variables.	164
Table 5.5	Spearman's rank correlation and RMA regression of PCs with centroid size.	170
Table 5.6	Spearman's rank correlation and RMA regression of PCs with body mass.	170
Table 5.7	Univariate analyses of the cochlear variables in categorical data.	175
Table 5.8	Discriminant function analysis with permutation tests (10,000 iterations) of regression residuals across the whole shape space.	176
Table 5.9	Mann-Whitney U test of PC scores after removal of the allometric effects.	177

Table 5.10 Spearman's rank correlation and RMA regression of residual cochlear variables with high frequency limit.	179
Table 5.11 Spearman's rank correlation and RMA regression of residual cochlear variables with residual low frequency limit.	181
Table 5.12 Spearman's rank correlation and RMA regression of PC residuals with residual low frequency limit.	181
Table 5.13 Spearman's rank correlation and RMA regression of residual cochlear variables with best hearing frequency.	182
Table 5.14 Tree lengths and <i>P</i> values for the permutation test of phylogenetic signal.	185
Table 5.15 Reduced major axis (RMA) regression between the independent contrasts of PCs and of ln-transformed centroid size.	189
Table 5.16 Comparing slopes of two regression lines obtained from the plots of the PCs against the ln-transformed centroid size before and after the independent contrasts analysis.	190
Table 6.1 The repeatability of measurements and landmarking.	195
Table 6.2 Spearman's rank correlation and RMA regression of cochlear variables with petrous bone length.	198
Table 6.3 Summary statistics of cochlear variables in sample groups.	199
Table 6.4 Significance of Mann-Whitney U tests of cochlear morphology between sample groups.	199
Table 6.5 Spearman's rank correlation and RMA regression of PCs with centroid size.	206
Table 6.6 Spearman's rank correlation and RMA regression of PCs with petrous length.	206

Table 6.7 Discriminant function analysis with permutation tests (10,000 iterations) of PC scores across the whole shape space.	206
Table 6.8 Mann-Whitney U test of PC scores on PC1-PC5.	207
Table 6.9 Spearman's rank correlation and RMA regression of PCs with centroid size.	214
Table 6.10 Discriminant function analysis with permutation tests (10,000 iterations) of regression residuals across the whole shape space.	215
Table 6.11 Mann-Whitney U test of regression residuals on PC1, and original PC2-PC5 scores.	215
Appendix D Raw data and statistics	291

List of abbreviations

2D	=	2-dimensional
3D	=	3-dimensional
ANOVA	=	Analysis of variance
ANCOVA	=	Analysis of covariance
ASC	=	Anterior semicircular canal
C	=	Crepuscular species
CAT	=	Computerized axial tomography
CC	=	Common crus of the semicircular canals
CT	=	Computed tomography
CTA	=	Computed tomography angiography
D	=	Diurnal species
DAB	=	Days after birth
DFA	=	Discriminant function analysis
DICOM	=	Digital Imaging and Communications in Medicine
Fly	=	Flying species
Fos	=	Fossorial species
FOV	=	Field of view
FWHM	=	Full width at half maximum
G	=	Gregarious species
GPA	=	Generalized Procrustes Analysis
H	=	Cochlear height
HU	=	Hounsfield unit
IHC	=	Inner hair cell

ILD	=	Interaural level difference
ITD	=	Interaural time difference
L	=	Cochlear length
LSC	=	Lateral semicircular canal
Mar	=	Marine species
MIP	=	Maximum intensity projection
MPR	=	Multiplanar reformatting
N	=	Nocturnal species
OHC	=	Outer hair cell
OPA	=	Ordinary Procrustes Analysis
OW	=	Oval window
PCA	=	Principal component analysis
PSC	=	Posterior semicircular canal
RMA	=	Reduced major axis
RW	=	Round window
S	=	Solitary species
Sem	=	Semi-aquatic species
Sub	=	Subterranean species
Ter	=	Terrestrial species
V	=	Cochlear volume
W	=	Cochlear width

Chapter 1 Introduction

Perception and interpretation of auditory cues are the two sensory systems most prominent in the majority of animals (Feldhamer et al., 2004). Hearing signals are particularly important for survival and reproduction. These are used for a variety of purposes including predator detection, finding food and communication. Significant proportion of all the sounds in nature originates from animals' activities, either by vocalization or moving through their environment (Heffner, 2004). The organ of hearing, the cochlea, is thus critical to an individual's and species survival. This thesis examines changes in bone morphology of the cochlea across extant mammals and during human development. Key factors such as evolution of hearing from fishes through to mammals and ontogeny of the mammalian bony cochlea are reviewed and considered in this chapter. Chapter 2 and 3 review technical aspects to the methodological approach. The materials and methods are presented in Chapter 4, and the results are presented in Chapters 5 and 6. Finally, the discussion and overall conclusion are given in the last chapter.

1.1 Basic anatomy of the mammalian ear

1.1.1 The outer (external) ear

The mammalian ear is composed of three portions: the outer, middle and inner ear (Kardong, 2006). The outer ear, or pinna, is unique to mammals (Feldhamer et al., 2004; Fig. 1.1). It primarily evolved to focus and direct sound toward the ear canal as well as to help identify the source of sound using the time of flight principle (Kardong, 2006). Pinnae have been lost secondarily in cetaceans, phocid seals, fossorial species and some insectivores (Feldhamer et al., 2004). Several mammalian groups,

including for example ungulates and bats, possess movable pinnae, these improve the ability to determine the direction of a sound source. The size and shape of the pinna can be indicative of functional hearing differences as well as to distinguish species in a taxon; for example, the presence of the tragus in echolocating bats and the much larger pinna in African elephants compared with Asian elephants (Feldhamer et al., 2004). Mammals can detect a wide range of wavelengths and intensities of sound; hearing frequency ranges extend from infrasonic wave (frequencies less than 20 Hz) in elephants (West, 1985) to ultrasonic wave (frequencies greater than 20000 Hz) in bats and cetaceans (Gould, 1983).

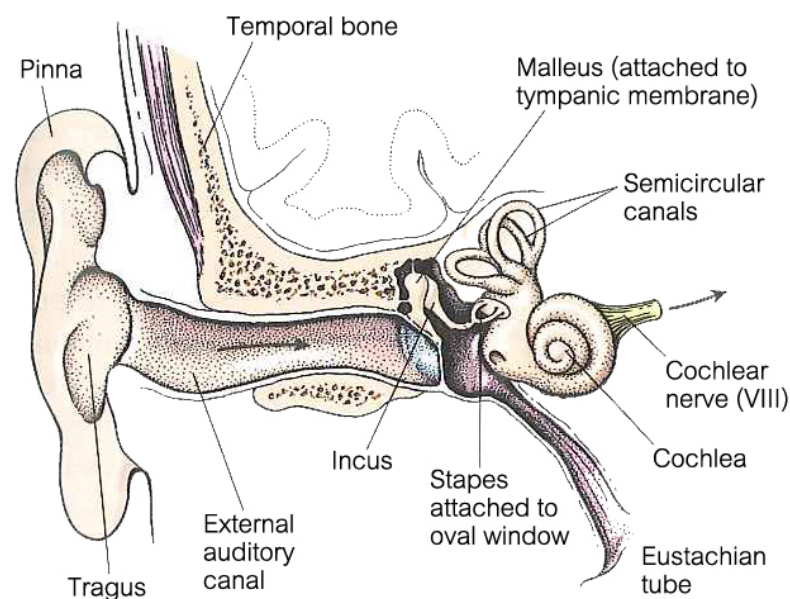


Figure 1.1 Anatomy of the mammalian ear (based on *Homo sapiens*)
(Randall et al., 2002; pg. 243).

1.1.2 The middle ear

The middle ear in mammals consists of three parts: the tympanum (tympanic membrane), an air-filled cavity (the tympanic cavity) and an articulated chain of three bones (ossicles), namely the malleus, incus and stapes (Kardong, 2006; Fig. 1.1).

These three ossicles are arranged as the bridge between the tympanum and the inner ear. The malleus and incus are unique to mammals (Feldhamer et al., 2004). The stapes, derived from the hyomandibular bone in fishes and only found in tetrapods, is attached to the oval window, a membrane-covered opening leading to the inner ear (Manley, 2010). Although the mammalian ossicles show some interspecific variation in shape, they are similar in terms of scaling relationships (Nummela, 1995). Sound pressure waves impinging on the tympanum at the bottom of the external auditory canal are transmitted through the three minute ossicles to the inner-ear fluid. Previous studies have demonstrated that the characteristics of the middle ear structures influence the shape of mammalian audiograms, particularly the frequency range of hearing (Nummela, 1995; Hemila et al., 2001; Mason, 2001).

1.1.3 The inner ear

The inner ear (Fig. 1.1) consists of two main functional parts: the vestibular apparatus and the cochlea (Liem et al., 2001; Kardong, 2006). The vestibular apparatus includes the semicircular canals, utricle and saccule, which function together as part of the body's balance control, whereas the cochlea responds to sound waves. The cochlea is a spiral-shaped structure, encircling a conical-shaped central bony axis called the modiolus. The interior of the cochlea is divided into three fluid-filled channels: the scala vestibuli, the scala media (cochlear duct) and the scala tympani (Fig. 1.2).

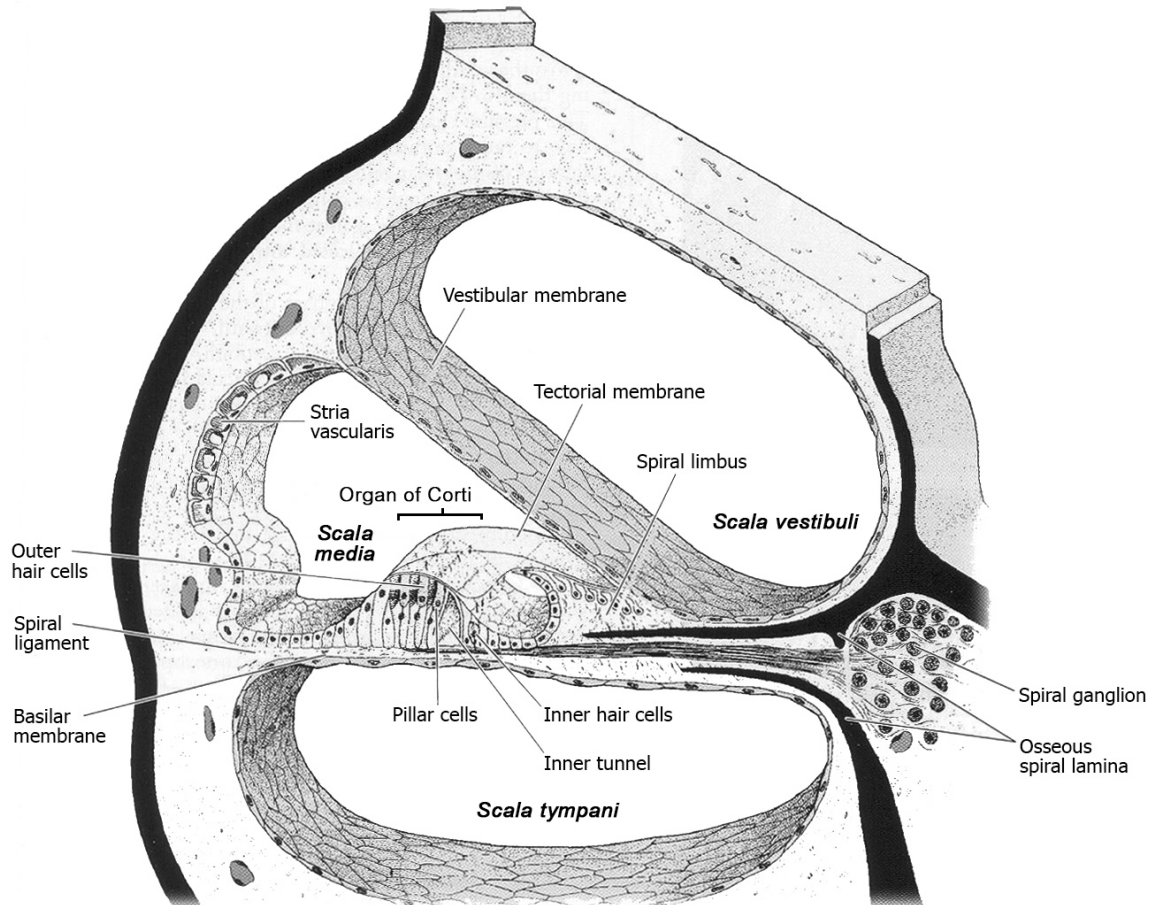


Figure 1.2 Structures of the human cochlea (adapted from Junqueira and Carneiro, 2005; pg. 473).

The cochlear duct is the middle cavity, separated from the scala vestibuli above by the vestibular membrane and from the scala tympani underneath by the basilar membrane (Junqueira and Carneiro, 2005). The receptor organ called the organ of Corti is housed along the length of the basilar membrane. The basilar membrane extends from bony-ledged projections of the modiulus, the inner (primary) osseous spiral lamina, to the outer wall of the cochlea. The inner osseous lamina consists of two plates separated by a space that is a passage for nerve fibers from the organ of Corti to the modiulus. In addition, in the basal region of the cochlea the outer (secondary) lamina can be visible as a projection inward from the outer cochlea wall.

These laminae provide a supporting frame for attachment of the basilar membrane in order to maintain its shape (Meng and Fox, 1995b). The mammalian laminae are different from those in other amniotes; reptiles and birds possess cartilaginous laminae (Rosowski and Graybeal, 1991; Meng and Fox, 1995b). On the lateral wall of the cochlear duct, there is a layer of highly vascularized pigmented cells called the stria vascularis. Its function is the maintenance of the ion concentrations of the endolymph, generating an endocochlear potential that is essential for hair-cell functions (Steel and Barkway, 1989).

The organ of Corti is the receptor organ of hearing and is anchored to the surface of the basilar membrane (Kardong, 2006; Fig. 1.2). It is made up of two cell populations: hair cells and supporting cells. Hair cells are classified into two types, inner hair cells (IHCs) and outer hair cells (OHCs), which are a uniquely mammalian characteristic (Vater and Kossl, 2010). In therians, there are three rows of OHCs and a single row of IHCs, while in the monotremes the number of the rows is much greater (Fernandez and Schmidt, 1963; Ladhams and Pickles, 1996). More than three rows of the therian OHCs are only found in the apical area of some species including humans and rats (Vater and Kossl, 2010). The OHCs and IHCs differ in morphological and functional aspects. Morphologically, the OHCs are tube-shaped and its stereocilia are arrayed in a W shape, whereas the IHCs are flask-shaped and its stereocilia are in a linear arrangement (Chen and Anderson, 1985). Due to concentrated afferent innervation, the IHCs directly contribute to the auditory perception. The OHCs help boost the IHCs' function, thereby improving sensitivity and sharp frequency resolution of cochlear mechanics (Randall et al., 2002; Vater and Kossl, 2010). The tips of the stereocilia are embedded in a glycoprotein-rich

substance appearing an awning-like projection overhanging the organ of Corti, termed the tectorial membrane.

The cochlea is connected to the middle ear cavity via two openings (Kardong, 2006). The scala vestibuli abuts on the oval window, of which the margin attaches to the circumference of the stapedial footplate by the annular ligament. The scala tympani is connected to the round window, which is in contact with the middle ear cavity. The round window is covered by a flexible three-layered membrane called the round window membrane or the secondary tympanic membrane (Goycoolea, 2001). The functions of the secondary tympanic membrane are proposed to play roles in releasing mechanical energies and conducting sound waves to the scala tympani (Scarpa, 1962; Goycoolea and Lundman, 1997, Goycoolea, 2001). Also, the membrane is thought to participate in absorption and secretion of the inner ear substances, and even as a defense against infection (Goycoolea, 2001).

1.1.4 Pathway of sound perception

Vibratory sound waves transmitted to the oval window by the ear ossicles causes vibration of fluid contained in the scala vestibuli. This wave in the scala vestibuli is transferred through the vestibular membrane, into the cochlear duct, through the basilar membrane into the scala tympani. The wave then causes the basilar membrane to vibrate, resulting in activation of auditory hair-cell receptors in the organ of Corti. The wave also vibrates the round window to dissipate compressive forces that would otherwise gradually build-up along the cochlea length and diminish lower frequency sensitivity (Randall et al., 2002; Sherwood et al., 2005). Once the basilar membrane is deflected in relation to the stationary tectorial membrane, the

stereocilia of hair cells are mechanically warped. This warping triggers the IHCs to release a neurotransmitter, causing the production of action potentials in bipolar neurons of the spiral ganglion lying in the modiolus (Sherwood et al., 2005). Voltage pulses are sent through nerve fibers of the spiral ganglion, then via the auditory nerve (cranial nerve VIII) to travel to the auditory cortex in the temporal lobe of the brain for interpretation.

Different regions of the cochlea respond maximally to different sound frequencies (Fig. 1.3). The apical segment of the cochlea is stimulated best by low frequency sounds, while regions nearer the cochlear base responds to higher frequency sounds (Bekesy, 1960; Dallos, 1973; Echteler et al., 1989; Rubsamen, 1992). This tonotopic localization is proposed to be correlated with the basilar membrane stiffness and the OHC characteristics. A narrow and thickened basilar membrane in combination with short cell bodies and stereovilli of the OHCs at the cochlear base responds maximally to higher frequency sounds (Muller, 1991; Echteler et al., 1994).

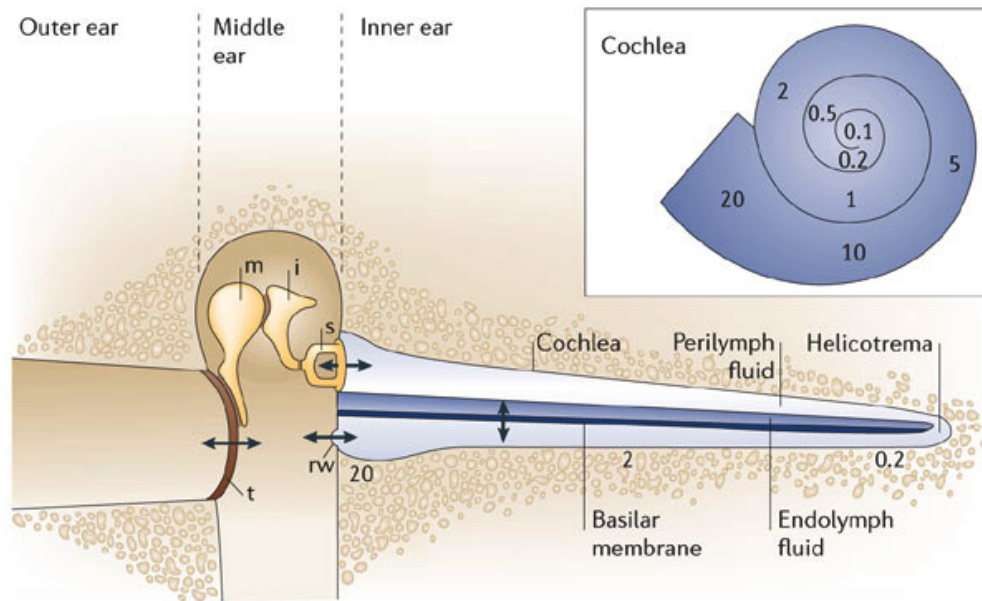


Figure 1.3 The sound conducting pathway in the mammalian ear. The cochlea is revealed out to illustrate its internal structures. High frequency sounds excite the basal part of the cochlea while lower frequencies excite the apical part: here 20 kHz at the base and 0.2 kHz near the apex. i, incus; m, malleus; rw, round window; s, stapes; t, tympanum (Fettiplace and Hackney, 2006; pg. 20).

1.2 Evolution of vertebrate hearing

There are two main selection pressures that have been assumed to shape the sense of hearing among vertebrates. The first is auditory function as part of a communication system (Hauser, 1997). The environment may constrain and determine the sorts of sounds that are transmitted effectively with minimal distortion. The auditory system, as a communication system, is thus assumed to adapt to environment constraints (Stebbins and Sommers, 1992). The second selective pressure is auditory scene analysis (Bregman, 1990), which describes the animals' ability to determine the actual sound source in the usual environment containing multiple sources, scattering and noise. The capacity for segregating the relevant

source from the irrelevant one(s) is the same basic problem all animals must solve, and is a state of primary adaptive value (Fay and Popper, 2000).

The ability to localize sound source is present in all vertebrate taxa examined so far (Fay and Popper, 2000). Sound localization in the horizontal plane depends primarily on two basic cues, which need comparisons between two ears: the interaural time difference (ITD) and interaural level difference (ILD) (Fay and Popper, 2000). They are the differences in the arrival time and in the frequency-intensity spectrum of a sound between two ears, respectively (Fig. 1.4). A third cue, only found in mammals, is the pinna cue provided by the directional frequency-filtering properties of the pinna orientation (Heffner, 2004). The efficiency of ITD and ILD depends on how far apart the ears are and the frequency of sound. At low frequencies, the evaluation of ITD is useful so long as the ear distance is smaller than half the wavelength as this allows for the analysis of phase differences (Feddersen et al., 1957). Level differences (ILD) are harder to differentiate at low frequencies. At higher frequencies the ILD cue improves as ITD diminishes (head wider than half the wavelength and phase differences cannot be resolved). An added complication is that the maximum time difference that can be actually perceived is also dependent on head size ($t = \text{distance/velocity}$) (Fig. 1.5). Smaller heads make it cognitively challenging to resolve differences on a very small time scale. Hence, for ITD to work effectively at low frequencies, the head needs to be smaller than half the wavelength but not too small as to make the time difference indeterminable. As a result of these factors, small mammals tend to rely on higher frequencies (ILD), large mammals rely on low frequencies (ITD) and intermediate sized mammals can mix ILD and ITD across a mid range of frequencies to localize sounds in the horizontal plane (Feddersen et al.,

1957; Heffner, 2004). For sound localization in the vertical plane in which ITD and ILD contribute little, animals solve the problem using two strategies: asymmetrical ears and/or movements of the head and ear (or pinnae in mammals) (Fay and Popper, 2000). These mechanisms will modify the sound spectrum reaching the tympanum, helping animals to pick out sounds of interest.

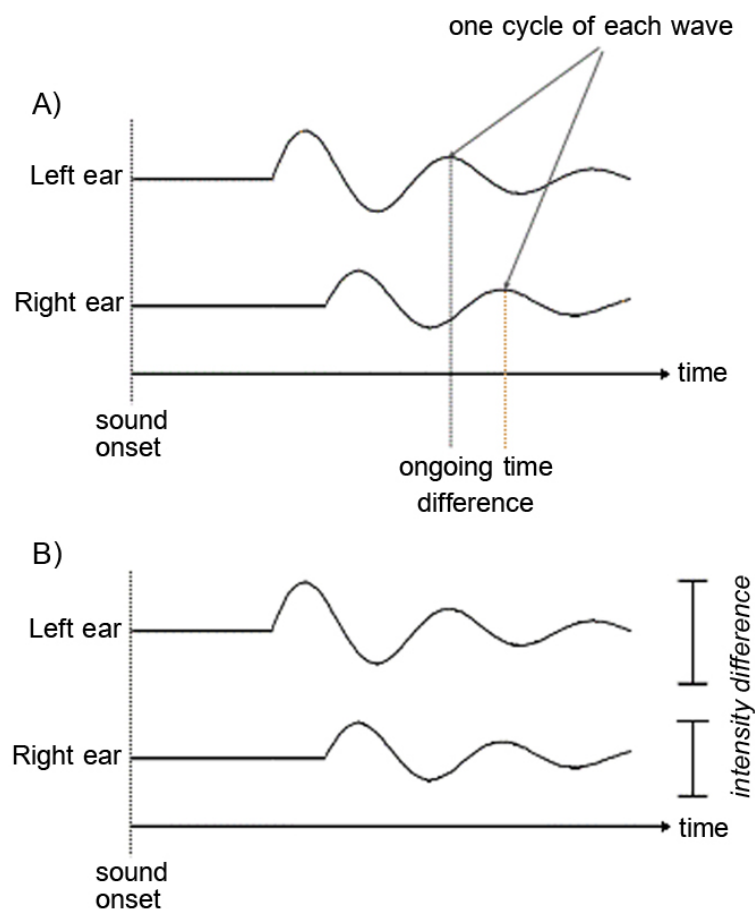


Figure 1.4 Sound localization in the horizontal plane using comparisons between left and right ears: A) interaural time difference (ITD) and B) interaural level difference (ILD) (Scottish Sensory Centre, 2010 [www.ssc.education.ed.ac.uk/courses/deaf/dnov10i.html]).

Frequency (Hz)	Half wavelength (cm)	Intermeatal distance (cm)	Maximum time delay (μ s)
150000	0.115	30	874.13
130000	0.132	25	728.44
120000	0.143	20	582.75
90000	0.191	15	437.06
60000	0.286	10	291.38
30000	0.572	9	262.24
15000	1.144	8	233.10
5000	3.432	7	203.96
1000	17.16	5	145.69
500	34.32	4	116.55
200	85.80	3	87.41
100	171.6	2.4	69.93
75	228.8	1.8	52.45
40	429.0	1.4	40.79
20	858.0	1.2	34.97
10	1716.0	0.7	20.40

Figure 1.5 The relationships between sound frequency and wavelength ($v = f\lambda$), and between the intermeatal distance and maximum time delay ($v = s/t$). The speed of sound in air at 20 °C (v) is 343.2 m/s.

Predator and prey detection are presumably two of the earliest and most fundamental of auditory functions (Gans, 1992). They require both sound detection and source determination components. Therefore, success in detection and sound source determination is driving forces in initially defining and maintaining the sense of hearing throughout vertebrate evolution (Fay and Popper, 2000). As a result, the ear structures in each group of vertebrates have been changed throughout evolutionary history. One of the major evolutionary changes in the auditory system occurred during the transition from water to land (Christensen-Dalsgaard and Carr, 2008). This transition involves the appearance or enhancement of the middle ear

and external ear (Kardong, 2006; Christensen-Dalsgaard and Carr, 2008). It also includes morphological and functional adjustments of hearing receptor organs in the inner ear as well as in the sensory hair cells (Fay and Popper, 2000; Kardong, 2006). The bony structures of receptor organs are changed in form and orientation for efficiently receiving sound signals from other peripheral parts. In addition, though the hair cell has similar morphology in general from the most primitive vertebrates, the lamprey and hagfish to the cochlea of mammals, it shows specializations for auditory signal processing in diverse species (Fay and Popper, 2000). Overall, from the early stages of vertebrate evolution, there has obviously been a need for changes that reflect adaptations of hearing structures to perform a variety of auditory processing tasks appropriately. The following is a review of the major transitions in the evolutionary history of the cochlea.

1.2.1 Fish

Fish hearing generally involves the sacculus, the lagena and the utriculus (Fig. 1.6), although sometimes one of them is more functionally dominant than the others (Fay and Popper, 2000; Kardong, 2006). Large patches of hair cells overlain by calcium carbonate concretions (otoliths), termed the maculae, within the sacculus, utriculus and lagena act as sound receptors. Most fish can detect sounds from below 50 Hz to over 800 Hz (Popper and Higgs, 2009). For example, some ostariophysan fish can detect sounds at 5,000 Hz (Liem et al., 2001). Many species have adaptations in their auditory system to extend the frequency range they can detect to improve their sense of hearing (Popper and Higgs, 2009).

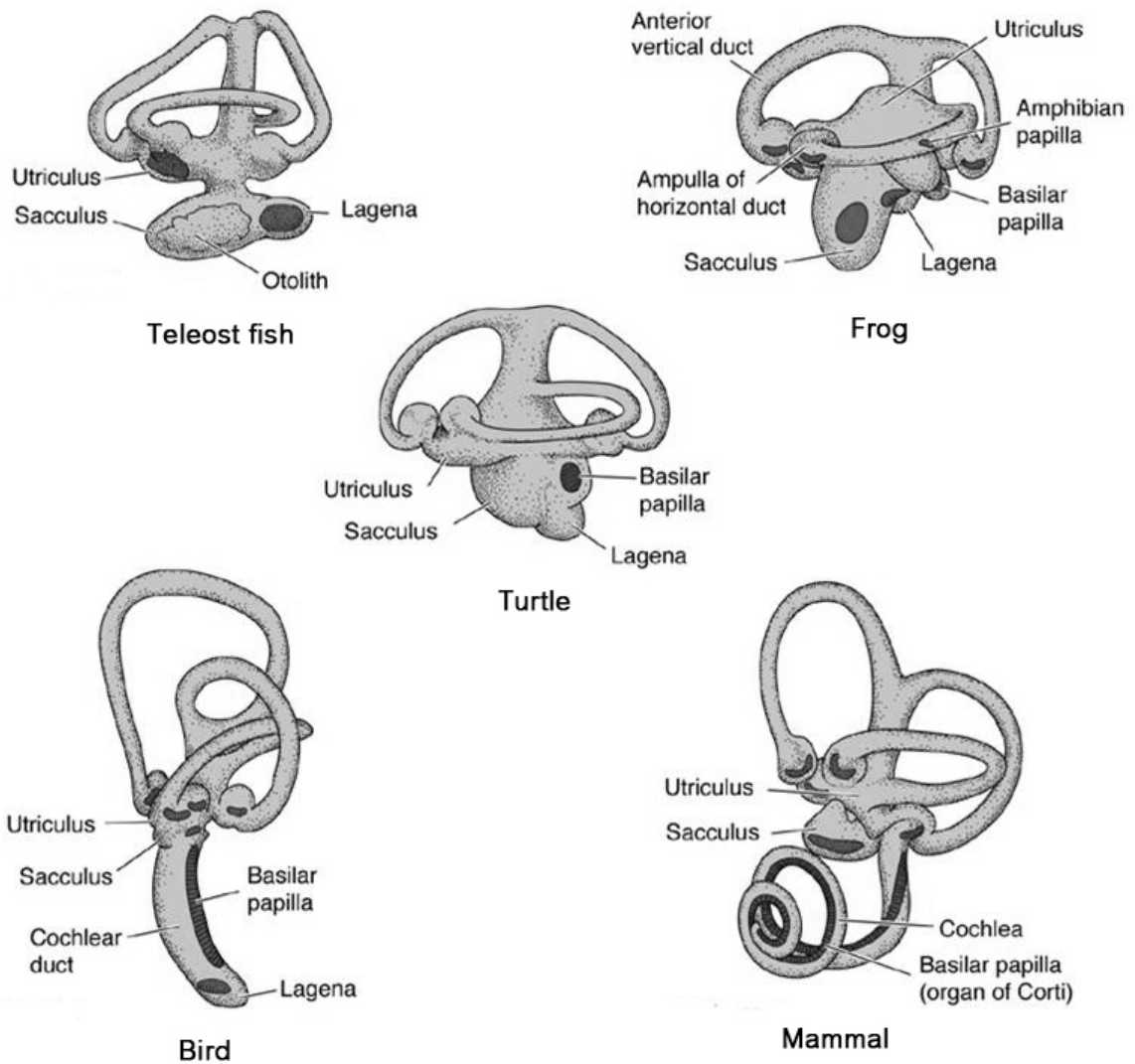


Figure 1.6 The inner ears (membranous labyrinths) of representative vertebrates. The coiled lagena forms the cochlear duct in mammals (adapted from Liem, 2001; pg. 414).

Sounds are transmitted into the inner ear of fish via many routes. Fish tissues primarily consist of water, and due to the similar acoustic properties of its environment, sound waves can therefore pass directly from water, through fish tissues, to the inner ear to induce hair cell movement (Kardong, 2006). A gas-filled space above the digestive tract called the swim bladder is also utilized for hearing by bony fish as well as for buoyancy control (Liem et al., 2001; Kardong, 2006). In some species, extensions of the swim bladder called 'bullae' come into contact with the

inner ear. Sound pressure waves passing through the body compress the air in the swim bladder, producing vibrations at its wall that are then conveyed via the bullae to the sound-detection apparatus (Kardong, 2006). In other species, the swim bladder is connected to the inner ear via a series of small bones called the Weberian ossicles, which are derived from ribs. The bladder vibrations are transferred by the Weberian apparatus to hair cells within the sacculus and lagena (Liem et al., 2001; Kardong, 2006).

Another hair-cell receptor organ called the neuromast in the lateral line system is found in fish and larval amphibians. Hair cells in the lateral line system are analogous to those present in the inner ear of all vertebrates (Hernandez et al., 2006). In sharks and skates, the lateral line organ is assumed to detect a range of low frequencies with maximum sensitivity between 50-150 Hz (Liem et al., 2001). Displacement waves may be conveyed to the inner ear by passing through the skin and jelly-filled parietal fossa (Liem et al., 2001), or by conducting through the swim-bladder bullae from the lateral line at the head (McCormick, 1999). The sound detection from the lateral line system is sent to the macula neglecta within the utricle.

Due to the slender fish shape, sound source localization of most fish by the cues of ITD and ILD at the two ears is absent (van Bergeijk, 1967). However, several species are reported to have restricted localization acuity (Fay and Popper, 2000).

1.2.2 Tetrapods

Tetrapods are animals having four limbs and have moved from an aquatic to terrestrial lifestyle. Ears adapted for hearing in aquatic environment are brought to an air environment during the water-land transition. Therefore, these animals encounter a basic physical problem in delivering sound energy traveling by air to the fluid filled spaces of the inner ear. Air has a much lower density than water, meaning that less sound energy is needed to propagate the wave, leading to impedance effects when sound travels from one medium (air) into another (water) (Nummela et al., 2007). The structures of the middle and inner ear have evolved to solve this problem. The functional combination of the tympanum and the middle-ear ossicles is necessary to amplify and transmit air-borne sounds to the inner ear at a sufficient level of energy to vibrate the inner-ear fluid. The perilymphatic duct receives displacement waves from the ossicles at the oval window and the waves pass receptor organs to the round window where they are dissipated. The energy boosted by the middle-ear components enables the sound vibrations to overcome the inertia, or impedance, of the perilymphatic fluid and set up the displacement waves within (Kardong, 2006; Nummela et al., 2007). Therefore the middle ear can be regarded as an impedance-matching device.

The selective pressures present during tetrapod evolution likely to have caused structural and functional changes of the middle-ear and inner-ear structures include an increased significance of air-borne sound detection in terms of predator-prey interaction or vocalization, leading to the necessity of improved hearing sensitivity (Manley, 1972; Fay and Popper, 2000; Christensen-Dalsgaard and Carr, 2008). The tympanic membrane and a middle-ear ossicle (stapes or columella) are first

observed among amphibians in the phylogenetic tree. The early eardrum is thought to be formed by closure of the spiracular opening with a layer of tissue (Christensen-Dalsgaard and Carr, 2008). The tympanic ear in all tetrapod lineages, however, is thought to have evolved independently and is considered to be an example of convergent evolution (Christensen-Dalsgaard and Carr, 2008). In mammals, the remaining ossicles, the malleus and incus, are derived from bones in the ancestral reptile made redundant by the selection of a more efficient jaw articulation system (Manley, 1972) that predates many inner-ear modifications (Meng and Fox, 1995b).

With regards to inner-ear evolution, selective pressures have driven development of higher endocochlear potentials and elongation of the sound receptor surface, resulting in improved frequency analysis (Manley, 1972). The phylogeny of the mammalian cochlea is independent of that in birds and reptiles (Fay and Popper, 2000). The elongation of the mammalian receptor surface, the basilar membrane, is accompanied by coiling of the cochlea. The fully coiled cochlea is established in therian mammals after diverging from the monotremes (Manley, 1972) during the Early Cretaceous period (Meng and Fox, 1995b).

1.2.3 Mammals

Mammalian evolution has a long history. Mammals evolved from the cynodonts, a taxon of synapsids (mammal-like reptiles) about 200 million years ago (Vater and Kossel, 2010; Manley, 2012). True mammals emerged in the early Jurassic period and branched out into a variety of groups. After the Cretaceous-Tertiary extinction, however, several mammalian groups were wiped out together with the non-avian dinosaurs. The remaining taxa diversified later into extant species. At present these

can be divided into three taxa: the monotremes, marsupials and placental mammals (Feldhamer et al., 2004). The latter two groups are collectively known as therian mammals, subdivided into metatherians and eutherians respectively (Feldhamer et al., 2004; Manley, 2012). Mammals are the only vertebrate group showing a widespread distribution of the species across land, water and air.

Regarding hearing capabilities, there are three major events thought to have occurred during the mammalian evolutionary pathway. The first key event is the appearance of three middle-ear ossicles, incorporating elements of the jaw-joint and jaw-supports into the sound-conducting apparatus. The malleus, incus and stapes are derived from the quadrate, articular and columella, respectively. It had been previously suggested that the quadrate and articular were included into the middle ear sometime in the Jurassic period, subsequent to a single-ossicle system (Fernandez and Schmidt, 1963). It is now believed that the three bones migrated to the middle ear simultaneously. Therefore, the mammalian middle ear is not an improved single-ossicle stage but constructed from three bones (Manley, 2010). It has also been suggested that the three-ossicle middle ear arises more than once and may have evolved independently in the monotreme and therian lineages (Rich et al., 2005).

The three-ossicle system is more efficient than the single-columella middle ear in transmitting high frequency sounds, due to less energy being lost along the articulating chain. In the single-ossicle system, the ossicle remains partly cartilaginous, meaning sound energy is lost during bending of the ossicle (Manley, 2010). In the three-ossicle system, all three bones are fully ossified and do not bend

during sound transmission (Manley, 2010). Recently, it has been suggested that the tympanic membrane may be co-adapted in terms of its configuration and ultrastructure with the ear-ossicle morphology to allow for appropriate ossicular motion to transmit high frequency sound (Puria and Steele, 2010). Based on the evidence of fossil investigations, a middle ear compatible with high frequency sounds predates a high-frequency inner ear (Meng and Fox, 1995b). Therefore, the middle ear is thought to serve as a pre-adaptation for the evolution of higher frequency hearing in mammals, which gives an advantage in sound localization (Heffner, 2004; Manley, 2010, 2012).

Manley (2010) and Heffner et al. (2001) suggested that a key driving force in favoring high-frequency hearing is the sound localization using neural computation, not the tri-ossicular system in the middle ear. In early mammals, the tri-ossicular system is pre-adapted for transmitting high-frequency sounds, although such sounds are merely enabled to be used (Manley, 2010). Furthermore, the sound localization using neural processing is proposed to be one factor driving the increase in brain size (Manley, 2010). Increased brain size correlates development of various auditory nuclei for better binaural neural processing for localizing sounds. Due to brain enlargement, connections between the oral cavity and the middle ear space have been confined and reduced to the eustachian tubes. Secondary palate development is also likely to have heavily influenced this process (Manley, 2010). Transformation of the middle ear into a purely pressure-receiver system for high sound frequencies is a corollary of middle ear isolation. This system differs from the pressure-gradient receiver system mechanism in non-mammals, whereby sound origins are detected by means of low frequencies without binaural neural computation (Christensen-

Dalsgaard and Carr, 2008). High-frequency sensitivity in sound localization is enhanced by the appearance of movable pinnae, which is unique to therian mammals (Heffner, 2004; Manley, 2010).

Since the mammalian middle-ear cavity is a near-closed environment having only restricted connection with the oral cavity, the stapedia artery can produce noise that disturbs hearing because the artery runs through the stapedia foramen. The earliest therians have adapted their hearing to a high-frequency range with little sensitivity at the low frequencies of arterial noise (Packer, 1987). This leads to reduced hearing disturbance from arterial sounds.

Another key event is the elongation of the sound receptor surface; the receptor membrane in mammals is longer than that in other vertebrates. Manley (1972) has shown that elongation of receptor membranes occurs many times in evolution, with a selective pressure for developing raised frequency analysis. The longer the membrane is, the higher the frequency to which animals respond. The increased membrane length correlates with the frequency space constant (the basilar membrane length/octave). The average space constant of mammals is higher than those of other amniotes (Manley, 2000). The space constant is closely related to the mechanism of frequency selectivity in hair cells and micromechanical tuning, by which responses to higher frequencies are mediated.

The configuration of the mammalian basilar membrane is related to the osseous spiral lamina. The lamina serves as a firm supporting frame for the membrane attachment, as well as the shape maintenance. Only mammals have this bony

supporting structure; reptiles and birds possess a cartilaginous lamina (Rosowski and Graybeal, 1991; Meng and Fox, 1995b). It has been proposed that the change from a cartilaginous to a bony lamina is associated with an increased sensitivity to higher frequencies (Fleischer, 1976; Ketten, 1984; Vater and Kossl, 2010). Compared to other amniotes, mammals show an improvement in the audible frequency range, including an increase in the upper limit of hearing (Manley, 1972; Manley, 2010).

A further key mammalian feature is the development of the IHCs and OHCs. These two cell populations evolved convergently with the short and tall hair cells in avian cochleae (Vater and Kossl, 2010). The main difference between the mammalian and avian hair cells is OHC motility. Mammalian OHC motility is responsible for an increased sensitivity to a wide hearing range and high frequency sound (Ladhams and Pickles, 1996; Vater and Kossl, 2010).

Adaptations in auditory hair cells occurred from the very early stages of vertebrate history (Fay and Popper, 2000). The number of hair cells has been linked with sound sensitivity (Begall et al., 2007). Along with the elongation of auditory receptor surface from amphibians to mammals, the number of hair cells apparently increases (Wever, 1974). In addition, mammals show a uniquely evolved feature; a well-developed link between its hair cells and basilar membrane. This link leads to an intimate involvement of the basilar membrane in frequency selectivity, for which the IHCs are responsible (Manley, 2000). These adaptations may explain why mammals are more sensitive to sound than others.

1.2.3.1 Monotremes

Monotremes consist of three extant genera, two of which belong to terrestrial echidnas: *Tachyglossus* and *Zaglossus*. The last genus is *Ornithorhynchus*, comprising a single species of semi-aquatic platypus, *O. anatinus*. Living monotremes are all indigenous to Australia and New Guinea. They are the survivors of an early branch that separates from the evolutionary tree of the therians about 163-191 million years ago (Vater and Kossl, 2010). A recent study indicated that *Teinolophos* is the oldest known monotreme, which lived in Australia 121-112.5 million years ago (Phillips et al., 2009). It is also suggested that echidnas split away from the platypus lineage 19-48 million years ago when they evolved from semi-aquatic to terrestrial lifestyle (Phillips et al., 2009).

Concerning the auditory organ, the external appearance of the monotreme cochlea is similar to that of the reptilian and avian cochleae (Ladhams and Pickles, 1996; Manley, 2012). The monotreme cochlea is slightly curved and does not achieve even one turn. The oval window in the echidna is round like that in birds and many reptiles (Chen and Anderson, 1985). The internal structure of the monotreme cochlea, however, has a distinctly mammalian structure, with a well-defined mammalian organ of Corti (Gates et al., 1974; Ladhams and Pickles, 1996). As in other mammals, the OHCs and IHCs, as well as the stria vascularis, are visible, although there is the difference in the number of hair-cell rows. In terms of an evolutionary aspect, the monotreme auditory system is placed in the transitional position between the systems of therapsid reptiles and therian mammals (Gates et al., 1974).

Some morphological aspects of the monotreme ear imply that the monotremes have been adapted to the detection of ground-borne vibration. The middle-ear ossicles are much less efficient in transmitting air-borne vibrations than those of other mammals (Gates et al., 1974). This is explained by the stiff middle ear, which is moved in low amplitude when driven by an air pressure stimulus. This ear type will transmit better the ground-borne vibration because sounds are conveyed via a high-impedance medium (Ladhams and Pickles, 1996). Its sensitivity to the ground vibration is also proposed by evidence of OHC features, which are less regularly arranged in the stereocilia and fewer in number than those of eutherians (Chen and Anderson, 1985; Ladhams and Pickles, 1996). These features are regarded as a possible example of reversals in evolution. Another remarkable character is the lack of the osseous spiral lamina, which is different from other mammals (Meng and Fox, 1995b; Luo et al., 2011). These features support the lower upper hearing limit and more restricted hearing range of the monotremes compared to most other mammals. It also supports the habit of favouring ground-borne sound vibration detection, as vibrations from the ground cannot transmit high-frequency stimuli (Ladhams and Pickles, 1996).

1.2.3.2 Therians

Theria is a mammalian group consisting of metatherians (marsupials) and eutherians (placentals). Based on evidence from the fossil record, marsupials diverged from the eutherian lineage no later than 125 million years ago in the Early Cretaceous period (Reimer, 1996; Luo et al., 2003). The earliest known members of the metatherian and eutherian lineages are *Synodelphys* and *Eomaia*, respectively (Luo et al., 2003). Marsupials occupy a narrower range of ecological niches and a more limited

structural diversity than eutherians; it is estimated that 94% of the world's mammalian fauna are eutherian species (Luo et al., 2003; Feldhamer et al., 2004).

Despite separation of the two mammalian lineages for over 100 million years, the otic anatomy and physiology in extant metatherians show considerable similarities to those of placentals (Fernandez and Schmidt, 1963; Meng and Fox, 1995a). To date, no clear differences in auditory development and function between marsupials and placentals have been found (Reimer, 1996).

The fully coiled cochlea, including its innervations, is a key evolutionary innovation in the inner ear of therian mammals (Meng and Fox, 1995a; Manley, 2012). Evidence from Jurassic fossils suggests that the state of the incomplete turn ($< 360^\circ$) and the partly-developed osseous spiral lamina happen before the fully spiral turn and the elongated osseous lamina (Meng and Fox, 1995b; Luo et al., 2011). The fully coiled cochlea and the developed bony spiral lamina are presumed to have been established during the Early Cretaceous (Meng and Fox, 1995a, b; Manley, 2000, 2012). The earliest radial innervation pattern of the cochlea is documented in Late Cretaceous therians, evolving along with the coiled cochlea and the bony spiral lamina (Meng and Fox, 1995a). This innervation pattern provides an efficient innervation of the elongated and coiled basilar membrane. Moreover, the discovery of the bony spiral laminae in fossils corroborates the assumption that the ability of high-frequency hearing has been present since early therian species and is a distinguishing character of modern therians (Meng and Fox, 1995b; Luo et al., 2011).

Though the basic pattern of the inner-ear structures in therians was probably achieved during the Early Cretaceous, differences in structures exist between early therians and their extant relatives (Meng and Fox, 1995b). Basal therians have fewer cochlear turns and a shorter basilar membrane. Thereafter, the cochlear coiling and the architecture inside the basilar membrane gradually evolved, leading to an increased hearing sensitivity to air-borne sounds and a huge diversity in hearing abilities among living therians (Meng and Fox, 1995b; Manley, 2012).

The auditory system of therians and monotremes also differs due to the varying degree of brain development present. A greater capacity of auditory nuclei for binaural neural processing is developed in therians for sound localization. Also, movable pinnae evolve in therians. These cause the selective pressure for the increased capability of high-frequency hearing in therian mammals (Heffner, 2004; Christensen-Dalsgaard and Carr, 2008; Manley, 2010).

1.3 Evolution of hearing with reference to example eutherian groups with differing habitats or behaviours

Living animals are more or less adapted to suit the current environments where they live. Environmental constraints can determine many adaptation designs. Some groups evolve in habitats that differ from those of other members of their taxon leading to distinct structures. Conversely, environmental constraints can force species from different taxa in similar habitats to evolve similar morphological features to satisfy similar biological demands. Mammals show a widespread distribution of species across land, underground, in the water and sky, as well as a large diversity

in morphological adaptation. One of the major systems necessarily modified is the sensory system, which includes hearing. Here, the adaptation of hearing to fit the environments is exemplified in some groups of mammals.

1.3.1 Aquatic or semi-aquatic eutherians (Cetacea, Sirenia and Pinnipedia)

1.3.1.1 Cetacea

Besides sea cows (Order Sirenia), whales (Order Cetacea) are the only group of mammals that are fully aquatic. They are highly adapted for life in the water, and are not capable of activity on land. Unlike fish, however, whose evolutionary history occurred wholly in the water, cetacean adaptations for living underwater are secondary. Cetaceans evolved from terrestrial artiodactyls about 50 million years ago (Nummela et al., 2007; Uhen, 2007). Their closest living relatives are likely to be hippopotamids (Feldhamer et al., 2004; Nummela et al., 2007; Uhen, 2007). The fossil record indicates that the evolutionary transition from land to water occurred during the Eocene and lasted less than 10 million years (Nummela et al., 2004; Nummela et al., 2007). Extant whales are divided into two suborders, the Odontoceti (toothed whales) and the Mysticeti (baleen whales). It is proposed that the split of the Odontoceti and Mysticeti possibly occurred at either the Eocene-Oligocene boundary or the late Eocene (Uhen, 2007). There are many differences between the two suborders, mainly in skull morphology, including ear structures.

Evolution of hearing mechanism in the Odontoceti

Based on fossil evidence, the earliest known cetaceans are the pakicetids (Nummela et al., 2007; Uhen, 2007). These lived about 50 million years ago. Evidence from fossils indicates that pakicetids have a link with shallow, fresh water (Uhen, 2007).

They are adapted for aquatic life to some extent. Although the overall ear morphology is of land mammal type, there are some derived characters of the hearing structures. These are the reduced periotic-tympanic contact and the thickened medial part of the tympanic, the involucrum (Nummela et al., 2004). The latter results in improved transmission of waterborne sound via bone conduction compared to generalized land mammals (Nummela et al., 2004).

The modern whale hearing mechanism first appears in basilosauroids. These lived about 35-40 million years ago in North America. Their postcranial skeletons reveal an incapacity for terrestrial locomotion with modified characters for a fully aquatic life (Uhen, 2007). Isolation of the tympanoperiotic complex from the skull by air-filled sinuses is considered a key characteristic change. The ear region is located in a cavity formed by evolutionarily removing the small, pneumatized mastoid spaces common in land mammals (Wartzok and Ketten, 1999). The condition of having the ear region isolated from the skull is proposed to be adaptive for aquatic echolocation (Ketten, 1997; Nummela et al., 2007). Based on fossil evidence, however, Eocene whales do not show the ability to echolocate (Fleischer, 1976; Uhen, 1998). Fleischer (1976) further suggested that echolocation evolved first among fossil odontocetes during the Oligocene, and by the Miocene the odontocetes already had fully-developed echolocation ability.

Other modifications in basilosauroids are the presence of a large mandibular foramen containing a fat pad and the strongly reduced periotic-tympanic contact (Nummela et al., 2004, 2007). This reduced bone contact improves sound transmission from the lower jaw to the middle-ear ossicles. Also, the orientation of

the ossicular chain is similar to that in modern odontocetes. Unlike modern whales, however, basilosauroids still have a large external acoustic meatus and a relatively larger incus (Nummela et al., 2004, 2007). Nevertheless, the modified ear structures suggest that underwater hearing had become the main function and hearing in air is no longer necessary, consistent with an obligate marine lifestyle in these whales (Nummela et al., 2007).

Basilosauroids gave rise to both living cetacean suborders. In modern odontocetes, additional adaptations for aquatic hearing are the thinner periotic-tympanic contact and the enlarged air sinuses around the ear region (Nummela et al., 2007). Large air cushions between the ear complex and skull cause the hearing mechanism from bone conduction to absolutely disappear (Wartzok and Ketten, 1999; Nummela et al., 2007). In addition, the external ear canal is exceptionally narrow and completely occluded by dense wax and debris, hence has lost of all acoustic function. In the middle ear, the incus is smaller, and joint movements along the ossicular chain are innovated. The malleus-incus joint, acting as a pivot in cooperation with the stapes, acts as an impedance matching device, improving the ability to hear in water. Accompanied by the adaptation of echolocation during the Oligocene, the bones of the elongated rostrum are modified in odontocetes. This enhances focusing on the ultrasonic outgoing sound and protecting the hearing apparatus from the emitted pulses (Fleischer, 1976).

The capability of echolocation is a primary character to distinguish the Odontoceti from the Mysticeti. Aquatic echolocation is proposed to appear first during the Oligocene (Fleischer, 1976; Uhen, 2007). Along with the evolution of underwater

hearing, odontocetes have several morphological adaptations to achieve echolocation. One of the key adaptations is a complete isolation of the ear from the skull that evolves gradually through the Eocene-Oligocene period (Nummela et al., 2007). Another adaptation is development of a thinner and smaller tympanic plate. Decrease in the tympanic mass enables vibration and transmission of higher sound frequencies collected through the mandibular foramen. Inside the inner ear, the dimension of the basilar membrane and its accessories are adapted for echolocation sounds as well (Fig. 1.7). The odontocete basilar membrane thickness to width ratio is associated with encoding ultrasonic signals. When compared with a mysticete membrane, the odontocete ratio is significantly higher in the basal region (Ketten, 1994; Wartzok and Ketten, 1999). In addition to the basilar membrane, the outer spiral lamina is a distinctive characteristic of ultrasonic ears. Unlike the mysticete membrane, the odontocete membrane is firmly stiffened by attachments to the bony lamina at the basal cochlear turn (Ketten, 1994; Wartzok and Ketten, 1999).

Evolution of hearing mechanism in the Mysticeti

As in odontocetes, mysticetes follow the evolutionary line of underwater hearing from pakicetids to basilosauroids during the Eocene. Thereafter a separation from the Odontoceti occurs and the Mysticeti develop their own distinctive features, especially in feeding ecology and auditory adaptation. The earliest known mystecete is a toothed whale from the Late Oligocene, *Janjucetus*, which is a macrophagous predator (Fitzgerald, 2006). The evolution of bulk filter-feeding is gradual and baleen is present in only around the Mid-Oligocene (Fitzgerald, 2006; Uhen, 2007). Pertaining to their auditory adaptations, extant mysticetes hear low frequency sounds, probably infrasonic ranges, which differ from the perception of ultrasonic

sounds in odontocetes. Echolocation has never been evolved in mysticetes (Fleischer, 1976; Fitzgerald, 2006; Steeman, 2009).

Many structures inside the skull are adapted for low-frequency hearing. Unlike odontocetes, baleen whales possess ears that are not completely decoupled from the skull. There are extensive bony flanges wedging the periotic against the skull, and contact of the middle ear capsule with a cartilaginous head of the mandible (Ketten, 1994; Wartzok and Ketten, 1999). These features suggest that the capacity for bony sound conduction in mysticetes remains from their ancestors (Wartzok and Ketten, 1999), and the ability to echolocate has hardly developed. In the forehead, mysticetes have a small mass of fats homologous with the hypertrophied melon that is associated with echolocation in odontocetes. The mysticete fat is proposed to be the vestigial melon (Fitzgerald, 2006).

Inside the mysticete ear, some structures suggest a capability for low-frequency hearing. Like odontocetes, the external acoustic meatus is narrow and occluded (Ketten, 1994). Extant mysticetes, however, have no enlarged mandibular foramen, which acted as a sound path to the middle ear in their ancestor (Fitzgerald, 2006). It is reasoned that an increased use of lower sound frequencies for communication causes the mandibular foramen to become a redundant structure (Steeman, 2009). A thick lateral wall of the mandible is used to receive incoming low-frequency sounds instead without much energy loss (Steeman, 2009). Baleen whales also have a substantially larger middle ear cavity than that of odontocetes. The ear ossicles are massive but loosely connected and not fused to the middle ear cavity (Ketten, 1994). These middle-ear features are typical of mammals with low-frequency audition as in

subterranean species (Mason, 2001, 2006). Within the cochlea, the basilar membrane thickness-to-width ratio is exceptionally low, consistent with the membrane configuration that can encode infrasonic sounds (Ketten, 1994; Wartzok and Ketten, 1999). The osseous spiral laminae in baleen whales differ morphologically and functionally from that of odontocetes. The inner lamina is spongy, fragile and the outer lamina is a narrow spicule that does not attach to the basilar membrane (Ketten, 1994; Wartzok and Ketten, 1999; Fig. 1.7). The membrane is supported only by a flexible spiral ligament. It is plausible that this outer lamina characteristic is a remnant of an ancestral condition rather than an adaptation of becoming infrasonic specialists (Wartzok and Ketten, 1999).

Overview of evolutionary differences between cetacean and land mammal hearing

There are three key events occurring in evolutionary history of cetacean hearing. The first is the isolation of the tympanoperiotic complex from the skull, which is fully developed in odontocetes but to a lesser extent in mysticetes. The second is the thick involucrum that is an apomorphic character among mammals involved in aquatic hearing function (Nummela et al., 2007). The next is existence of the mandibular foramen with a fat pad inside. Because the density of this oily substance is close to that of sea water, the foramen can function as a channel for receiving waterborne sounds, analogous to the external ear canal of land mammals. However, the foramen is reduced in size and in hearing function in all extant mysticetes. It seems that evolutionary history of underwater hearing in cetaceans is mainly concerned with the reorganization of the outer and middle ear structures, keeping the inner ear relatively unchanged (Nummela et al., 2004; Nummela et al., 2007). On

the other hand, the modification of the middle and inner ear plays a major role in adaptation of echolocation.

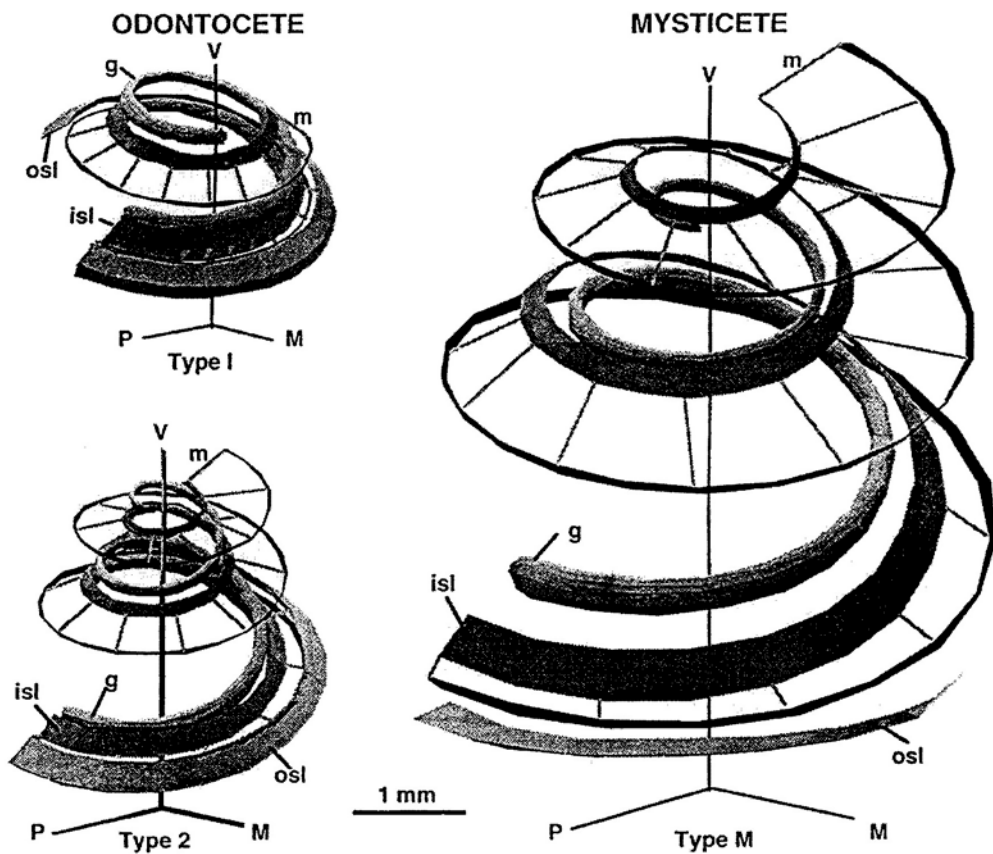


Figure 1.7 Basilar membrane and spiral laminae differences among Type I and Type II odontocetes and Type M mysticete inner ears (see page 60). g, spiral ganglion; isl, inner osseous spiral lamina; m, basilar membrane; osl, outer osseous spiral lamina; M, medial; P, posterior; V, ventral (Ketten, 1994; pg. 268).

1.3.1.2 Sirenia

Both Sirenia and Cetacea originate around the same time and have adaptations for fully underwater life by the end of the Eocene. Unlike cetaceans, sirenians belong to the only mammalian order that is composed exclusively of marine herbivores. They are restricted to relatively shallow coastal areas in tropical regions, feeding on

submerged and floating plants. Sirenians are part of a mammalian clade known as the Tethytheria, which also include elephants (Proboscidea) and extinct desmostylians (Desmostylia). Tethytheria evolved from the Condylarthra, an order of primitive hoofed mammals that arose in the early Paleocene epoch about 65 million years ago (Feldhamer et al., 2004). Tethytheres diverged from their common ancestor to form the various orders by the early Eocene epoch (Uhen, 2007). Besides elephants, hyraxes have also been posited as close living relatives and sharing the common ancestor with sirenians (Feldhamer et al., 2004; Reep et al., 2011). Most scientists, however, support the idea that elephants have a closer phylogenetic affinity with sirenians (Ketten et al., 1992; Wartzok and Ketten, 1999; Uhen, 2007).

The earliest sirenians, prorastomids, lived in the early Eocene; they are four-footed and have a capacity for terrestrial locomotion (Uhen, 2007). Another early sirenian fossil in the Eocene, *Pezosiren*, also has four well-developed legs but it spent most of the time in the water (Feldhamer et al., 2004; Uhen, 2007). Before the late Eocene, sirenians reduced their hindlimbs to be adapted for a fully aquatic lifestyle. It still remains unclear when the tails evolved but it is proposed to appear first in the late Eocene (Uhen, 2007). Extant sirenians are now represented by two families, the Dugongidae and the Trichechidae, which split evolutionarily in the late Eocene (Ketten et al., 1992; Wartzok and Ketten, 1999).

Evolution of hearing mechanism in sirenians

The sirenian ear is structurally and functionally different from the odontocete ear. Most studies of sirenian ears have been done on manatees and only a little

information about dugong hearing is available. The external ear canal is narrow, occluded by cellular debris and disconnected from the tympanic membrane by fatty tissues. In other mammals, canals are used together with pinnae for sound localization by the ITD cue. Ketten et al. (1992) proposed that if manatees use this localization cue, manatees need to have an upper frequency limit of 50 to 90 kHz. However, its audiogram shows an upper limit of functional hearing under 50 kHz (Gerstein et al., 1999). This implies that manatees are unable to use this localization cue and the external canal is not a direct path for sound reception.

Unlike cetaceans, the manatee tympanoperiotic complex is intracranial and attached to the inner wall of the skull (Ketten et al., 1992). The dorsal part of the periotic is joined to the inner surface of the squamosal connecting to the inflated zygomatic process. When observed microscopically the zygomatic process is a highly convoluted cartilaginous labyrinth filled with blood vessels and lipids giving it a lower density than other equivalent bones (Wartzok and Ketten, 1999; Ames et al., 2002). The relationship of the zygomatic process with the squamosal and periotic is reminiscent of the mandible-tympanoperiotic relationship seen in odontocetes. Therefore the zygomatic process is suggested to play a role in manatee sound reception, analogous to the odontocete fat channel (Ketten et al., 1992; Wartzok and Ketten, 1999; Chapla et al., 2007). As the squamosal is closely associated with the tympanic membrane and ear bones, sound waves along the zygomatic process may stimulate the tympanic membrane directly and sound vibrations are transmitted through the ossicles to the inner ear (Chapla et al., 2007). Further investigation is needed to clarify the hearing function (if any) of the manatee zygomatic process.

Scientists have proposed other sound transmission pathways in manatees, including pathways via head soft tissues (Chapla et al., 2007; Au and Hastings, 2008), as well as via the vertebral column and respiratory system (Chapla et al., 2007). It has been demonstrated that sound waves orientated at certain angles to the head may pass through only the skin and the adipose tissue, and reach the tympanic membrane directly without reflecting off of the skull. In manatees, the lungs are long and extend horizontally along most of the body length. Its two pleural cavities are floored by disjoined diaphragms (hemidiaphragms), which connect with upper ribs and about 50% of the vertebral column. Chapla et al. (2007) suggested that sound stimulation at the hemidiaphragms and ribs may be relayed through the vertebral column to the skull and ear bones. In addition, the separation of the hemidiaphragms is thought to be helpful in sound localization.

Concerning the manatee audiogram, the dimensions of the middle ear and cochlea play a major role in frequency and sensitivity of hearing. The middle ear cavity is large, and the ossicles are massive and loosely articulated. The shape of the stapes is columnar, resembling the reptilian columella (Wartzok and Ketten, 1999). Within the cochlea, the basilar membrane has a small gradient of its thickness and width from base to apex. Moreover, no outer bony spiral lamina is visible and the inner lamina is thin. Based on these characteristics of the middle and inner ear, it has been concluded that manatees have a low-frequency ear and a narrow frequency range of hearing without ultra- and infrasonic capabilities (Ketten et al., 1992; Wartzok and Ketten, 1999). Behavioural audiometric data, however, reveal that manatees have a hearing range from 0.4 to 46 kHz, indicating that they can hear ultrasonic sound (Gerstein et al., 1999). Other factors are suggested to partly shape

manatee hearing abilities, such as the vibratory pattern of the tympanic bone and tympanic membrane in sound transmission, and airspaces inside and surrounding the ear (Chapla et al., 2007).

Sirenians have inhabited shallow waters in tropical regions, feeding on seagrass or marine angiosperms, since the Eocene. They evolved in a relatively stable environment with few predators and limited competition from other mammals within their ecological niche (Ketten et al., 1992; Wartzok and Ketten, 1999; Feldhamer et al., 2004; Reep et al., 2011). In addition, modern manatee ears hold structural characteristics in common with fossil manatee ears (Ketten et al., 1992; Wartzok and Ketten, 1999). For most mammals, sounds associated with predators, mates and food sources are important for survival. Therefore, it is proposed that acoustic cues in sirenians have little survival value. Hearing in sirenians has not seen much evolutionary change since the Eocene, leading to their low frequency detection and poor sensitivity of hearing (Ketten et al., 1992; Wartzok and Ketten, 1999). However, Gerstein et al. (1999) reported that manatees have a higher range of hearing and greater sensitivity than those predicted from the previous anatomical studies. As manatees inhabit shallow coastal zones, they are affected by the 'Lloyd Mirror Effect', which can considerably attenuate propagation of sound near the surface and can effectively cancel low frequencies (Gerstein et al., 1999). This effect might be a selective pressure for manatees to evolve hearing sensitivity at higher frequencies (Gerstein et al., 1999). It reveals the influence of physical properties in the marine environment on the shape of hearing ability.

1.3.1.3 Pinnipedia

Pinnipedia refers to a group of fin-footed carnivorous mammals, based on the modification of their limbs into flippers for an aquatic existence. It comprises three families: Phocidae (earless or true seals), Otariidae (eared seals), and Odobenidae (walrus). Formerly, pinnipeds were classified either as their own separate order or as a suborder within the Order Carnivora. There has been some debate about their phylogenetic relationship to other carnivores. The traditional idea supports a diphyletic origin; i.e., odobenids and otariids derived from ursids, and phocids derived from mustelids. The current view, however, based on both morphological and molecular analyses, confirms a monophyletic origin of pinnipeds from ursids (Uhen, 2007; Berta, 2009).

The earliest known pinniped is *Enaliarctos*, from the late Oligocene and early Miocene (27-18 million years ago) of Oregon and California (Feldhamer et al., 2004; Uhen, 2007; Berta, 2009). *Enaliarctos* is a coastally aquatic dweller with limbs modified into flippers, although capable of moving on land as well (Berta, 2009). Pinnipeds from the North Pacific origin have now diversified throughout the world's oceans.

Evolution of hearing mechanism in pinnipeds

Herein, the literature review of pinniped hearing is mainly focused on phocids and otariids. Unlike cetaceans and sirenians, pinnipeds are not entirely adapted for underwater life but an amphibious condition. Pinnipeds search for food in the water but must occasionally return to land or ice floes where they breed, give birth, rear their young and rest (Kastak and Schusterman, 1999; Feldhamer et al., 2004).

Therefore, pinnipeds are adapted to cope with this amphibious life in the aspects of both overall morphology and sensory perception (Schusterman, 1981). With regard to hearing, it is vital for pinnipeds to have special adaptations of the auditory structures for efficient operation in two very different media: water and air. The pinniped ear is homologous to the ear of land mammals (Au and Hastings, 2008) and has the same hearing mechanism for air-borne sounds as in other terrestrial species. However, water-borne sound must take a different path to the inner ear. Because their underwater hearing plays important roles in predator avoidance, prey detection and navigation, selection for water-borne sound perception is just as, if not more significant than for airborne sound (Schusterman et al., 2000).

Although having a similarly amphibious lifestyle, phocids and otariids differ to some extent in ear anatomy, which affects their hearing frequency and sensitivity. For the outer ear, the external pinnae in phocids are absent whereas the reduced pinnae are still found in otariids (Feldhamer et al., 2004; Au and Hastings, 2008). The absence or rudimentary pinnae not only reduce hydrodynamic resistance but also reduce hydrodynamic flow noise as they swim through the water (Au and Hastings, 2008). The reduced pinnae of otariids also function to close off the outer ear canal while they are in the water (Hemila et al., 2006; Au and Hastings, 2008). The characteristics of the pinniped pinnae, however, result in reduced localization ability and reduced sensitivity to surrounding noise in the air (Au and Hastings, 2008).

The external auditory canal of pinnipeds is narrow, long, tortuous, and contains ceruminous mass and waxy hair (Au and Hastings, 2008). Otariids have a tendency to possess a wider external canal than that of phocids (Wartzok and Ketten, 1999).

The modified anatomy of the external canal is mainly attributed to a decreased sensitivity to air-borne sounds (Kastak and Schusterman, 1999). The distal part of the pinniped external meatus has a voluntary muscle to provide the closure of the ear canal during diving. Moreover, the inner surface of the meatus is lined with a layer of cavernous epithelium or corpus cavernosum, which is associated with the meatal closure (Møhl, 1968; Repenning, 1972). Based on anatomy, it seems water is blocked from entering the canal and an air-filled canal condition still exists (Møhl, 1968; Au and Hastings, 2008). The presence of the air-filled canal poses an impedance mismatch problem, making the conventional sound conduction pathway to the middle and inner ear difficult when pinnipeds are submerged (Nummela, 1995; Wartzok and Ketten, 1999). Therefore other modes of underwater hearing are required, the most parsimonious mode being bone conduction (Møhl and Ronald, 1975; Au and Hastings, 2008). This is supported by a study of underwater sound conduction of the harp seal. Møhl and Ronald (1975) found that the head areas having the highest sensitivity to water-borne sounds are located below the auditory canal, providing strong evidence of hearing by bone conduction in the seal.

The pinniped middle ear resembles terrestrial mammals with only a few differing characteristics (Repenning, 1972; Au and Hastings, 2008). There are many distinctive differences in the middle ear structures between phocids and otariids. First, the ossicles of phocids are denser and larger than those of otariids (Wartzok and Ketten, 1999; Au and Hastings, 2008). The ossicles of phocids are much larger than those of terrestrial mammals with a comparable skull size, especially the enlarged incus (Nummela, 1995; Hemila et al., 2006; Au and Hastings, 2008). By comparison, the size of the otariid ossicles is within the range of terrestrial carnivores

(Hemila et al., 2006). The enlarged ossicles can enhance bone-conducted underwater hearing by shifting the centre of the ossicular mass away from the rotational axis, as found in some subterranean species (Nummela et al., 2007). This could indicate that phocids respond to lower frequencies of air-borne sound than otariids (Wartzok and Ketten, 1999), and that phocid auditory system is more specialized for underwater hearing (Hemila et al., 2006). Second, the middle ear cavity of phocids is more voluminous than that of otariids (Hemila et al., 2006; Au and Hastings, 2008). Moreover, the eardrum of phocids is larger than that of otariids (Hemila et al., 2006; Au and Hastings, 2008). However, the eardrum size is not significantly different from that of terrestrial mammals with similar body mass (Wartzok and Ketten, 1999). In pinnipeds, the area of the oval window is about one-half to one-third of the round window area (Wartzok and Ketten, 1999).

The middle ear, as well as the external meatus, contains a corpus cavernosum, although this is less developed than that of cetaceans (Møhl, 1968; Repenning, 1972). The swelling of the cavernous tissue is suggested to function in controlling and equalizing air pressures during diving because it blocks the eustachian tube and disconnects it from the middle ear (Møhl, 1968; Repenning, 1972). Furthermore, at depth from 70 to 100 m, swelling of the cavernous epithelium may cause its close contact with both sides of the eardrum so that impedance matching between the ear and the water occurs. This means that conventional sound conduction via the tympanic-ossicular route may take place underwater (Repenning, 1972). The presence of the cavernous epithelium, in combination with a greatly reduced external canal, can enhance underwater sound detection and seems a morphological adaptation for underwater life. This hearing route is presumably particularly important

in some phocid species such as the northern elephant seal, which has a deep diving skill and spends an inordinate amount of time in water (Kastak and Schusterman, 1999).

Little work on the pinniped inner ear has been published and the current data available are largely descriptive (Wartzok and Ketten, 1999; Au and Hastings, 2008). The pinniped cochlea possesses several turn whorls with partial laminar support (Wartzok and Ketten, 1999). In phocids, the cochlea has two and one-half turns and the basal turn is much enlarged when compared to that in most mammals including otariids (Au and Hastings, 2008). Interestingly, the basal turn of the phocid cochlea is placed across the orientation of the skull, different from a posterolateral direction as found in otariids and other carnivores (Repenning, 1972). The basal turn is assumed to be an effective adaptation for sound reception from either side of the head by means of bone conduction (Repenning, 1972). Møhl (1968) reported that pinnipeds have a large cochlear aqueduct that may facilitate bone conduction in pinnipeds.

The ear morphology mentioned above, together with behavioural capabilities, influences the shape of pinniped hearing. Under water, phocids have better sensitivity and hear higher frequencies than otariids do, and vice versa for air-borne sounds (Schusterman, 1981; Kastak and Schusterman, 1999; Hemila et al., 2006). However, all pinnipeds hear better in water than in air and phocids show relatively large difference between underwater and in-air audiograms (Schusterman, 1981; Schusterman et al., 2000). From an anatomical viewpoint, the large difference between the two audiograms of phocids is unlikely to be linked to the cochlear

morphology. It is more likely to be associated with differences in sound transmission between the two media and different mechanisms by which sounds reach the cochlea (Hemila et al., 2006). On the other hand, the cochlear constraints are thought to play a major role in otariid hearing (Hemila et al., 2006). That phocids hear better in water than otariids is supported by a behavioural trait that phocids have more vocalization under water (Kastak and Schusterman, 1999; Schusterman et al., 2000), dive deeper, and are submerged for longer (Feldhamer et al., 2004). It is also suggested that phocids are generally adapted for amphibious hearing, whereas otariids have remained essentially adapted to hear in air after evolving from their ancestor (Kastak and Schusterman, 1999; Schusterman et al., 2000; Hemila et al., 2006).

The acquisition of echolocating capabilities depends on the evolution of specialized sound production, sound reception and neural processing in the brain (Schusterman et al., 2000). All pinnipeds can produce sound under water, which is especially obvious in phocids (Kastak and Schusterman, 1999; Schusterman et al., 2000). Moreover, like odontocetes, pinnipeds forage at times in relatively murky waters where vision is often limited (Schusterman et al., 2000). From these behaviours, pinnipeds were previously proposed to evolve a sophisticated sonar system (Repenning, 1972). To date, no strong evidence supports their echolocation capability. Scientists currently believe that pinnipeds have neither evolved the sort of sound productions nor underwater hearing mechanism that matches the biosonar capability (Schusterman et al., 2000; Hanke and Dehnhardt, 2013).

There are several factors that preclude the acquisition of underwater echolocation in pinnipeds. With regard to the ear anatomy, the conservation of the basic terrestrial carnivore ear is apparent in pinnipeds (Schusterman et al., 2000). The bony isolation between the ear and the skull is considered as an indicator of having biosonar activities (Nummela et al., 2007). Unlike odontocetes that achieve echolocation, however, the tympanoperiotic complex of pinnipeds is not acoustically isolated from the skull but has partly or completely ossified articulations with the skull (Wartzok and Ketten, 1999; Au and Hastings, 2008). Concerning their behaviours, pinnipeds are evolutionarily constrained to have breeding and social activities on land apart from foraging in water. These are selective pressures for pinnipeds to maintain auditory sensitivity in air as well as limiting factors to evolve a sophisticated sonar system meanwhile (Schusterman et al., 2000).

In addition, the evolutionary refinement of sensory systems permits pinnipeds to inhabit underwater efficiently despite the absence of the echolocation ability. In a noisy underwater environment, they are capable of tonal signals that stand out from background noise over a range of frequencies (Schusterman et al., 2000). Pinniped eyes are primarily adapted for vision under water rather than in air. The eye structures are developed to suit foraging in dim aquatic conditions at the expense of the decreased quality of their in-air vision (Schusterman, 1981; Schusterman et al., 2000; Feldhamer et al., 2004). For tactile sense, the vibrissae and facial structures of pinnipeds are modified for short-range prey capture and object detection in poor visual conditions (Schusterman et al., 2000; Hanke and Dehnhardt, 2013). These efficient sensory systems may be the factors that offset the pressures to evolve echolocation capability.

1.3.2 Subterranean and fossorial eutherians (Rodentia and Insectivora)

Subterranean mammals are a group of mammals spending most of their time or entire lives underground: examples include subterranean rodents—Order Rodentia, true moles (Talpidae) and golden moles (Chrysochloridae)—Order Insectivora, as well as marsupial moles (*Notoryctes* sp.)—Metatheria. These mammals often dig to create tunnels using the limbs, head or even anterior teeth. Characteristic adaptations for this activity include enlarged structures and muscles of the limbs, the highly developed musculature of the head, and increased strength in muscles associated with using large incisors (Feldhamer et al., 2004).

Because of low light levels in burrows, the visual sense often becomes reduced in importance. Many subterranean species possess minute eyes, or even non-functional vestigial eyes as found in golden moles and blind mole rats (*Spalax* spp.) (Nevo et al., 1991; Mason, 2003). To compensate for the visual restrictions, the sense of hearing is predominant and plays the major role in communication and alertness of subterranean species (Mason, 2003; Begall et al., 2007).

Evolution of hearing mechanism in subterranean mammals

The acoustic characteristics in tunnels are different from those above-ground. It has been demonstrated that both air-borne sounds along the burrows and substrate-borne vibrations are transmitted best in the range of low frequencies, 100-800 Hz (Nevo et al., 1991; Begall et al., 2007; Lange et al., 2007). The amplitude of these frequencies may also be amplified like in a stethoscope, known as the 'stethoscope effect' (Lange et al., 2007). Higher frequencies are likely to be absorbed by the tunnel walls, whereas lower frequencies are reflected by the walls (Lange et al.,

2004). Surprisingly, evidence suggests that the acoustic properties of various tunnels inhabited by diverse subterranean mammals are similar (Lange et al., 2007). There are no significant differences in sound propagation among tunnels with different diameters, depths, and soils, and in different habitats. It is thus not surprising that the audiograms of various subterranean species are also similar; hearing in subterranean mammals is tuned towards low frequencies and has decreased sensitivity. Low-frequency hearing is an adaptation to transmit sounds with low attenuation in the tunnel, and low-sensitivity hearing is an adaptation to avoid overstimulation of the ear from the stethoscope effect. These similar hearing abilities in several species of unrelated subterranean mammals provide an example of convergent evolution, which many authors consider as progressive specializations (Mason, 2001, 2006; Schleich and Busch, 2004; Begall et al., 2007; Lange et al., 2007).

Subterranean mammals have morphological adaptations of the ear that favor low-frequency hearing. The pinnae of most subterranean species are reduced or missing, accounting for poor binaural sound localization due to little use in one-dimensional underground burrows (Schleich and Busch, 2004; Lange et al., 2007). There is no selective pressure to maintain the pinna in highly fossorial mammals (Lange et al., 2007). In addition, the external ear canal is likely to be tight and filled with ceruminous plugs (Burda et al., 1989, 1992; Wilkins et al., 1999), which are supposed to reduce sensitivity to air-borne sounds (Burda et al., 1989, 1992).

Characteristics of the middle ear have been widely investigated in adaptations to low-frequency hearing capability among subterranean mammals. The volume of the

middle ear cavity of subterranean species is relatively large in comparison with surface-dwelling generalists (Schleich and Vassallo, 2003). The enlarged cavity contributes to increased middle-ear compliance which is related to improvement in low-frequency response (Relkin, 1988). Of all mammals, only subterranean species of true moles and golden moles have a direct connection between left and right middle ear cavities (Mason, 2001, 2003, 2006). This interbullar connection is proposed to improve sound localization at low frequencies. Sound reaches both sides of the eardrum with phase differences depending on the direction of the sound origin. Subterranean species can localize sounds by detecting these phase differences (Coles et al., 1982).

Although the area of the pars tensa of the eardrum is not significantly different from that in non-fossorial mammals (Mason, 2001; Fig. 1.8), the pars flaccida appears reduced or not present in subterranean mammals (Burda et al., 1992). It is proposed that shunting of low-frequency sounds through the pars flaccida lessens the sound pressure difference across the pars tensa, leading to a loss of low-frequency transmissions (Mason, 2006). The lack of the pars flaccida also increases middle-ear compliance (Schleich and Busch, 2004). Therefore, the loss of the pars flaccida may be adaptive for low-frequency hearing.

Subterranean mammals possess the loosely connected middle-ear ossicles characterized by a reduced gonial (small bone fused with the central part of the malleus) and a loose articulation between the malleoincudal complex and the tympanic bone (Mason, 2001, 2003). The malleoincudal complex is weakly attached to the bulla wall via ligaments, permitting the complex to swing freely around the

rotational axis (Mason, 2001, 2003). This freely mobile type is a feature derived from the ancestral type in which the bony gonial connects the malleoincudal complex to the bulla wall firmly (Mason, 2001, 2003; Schleich and Busch, 2004). The derived type suggests a broader hearing range with a biased response towards low-frequency sound (Mason, 2001). Although they are commonly found in exclusively subterranean species, the freely mobile ossicles are not unique to subterranean species and also found in many small terrestrial mammals (Mason, 2001).

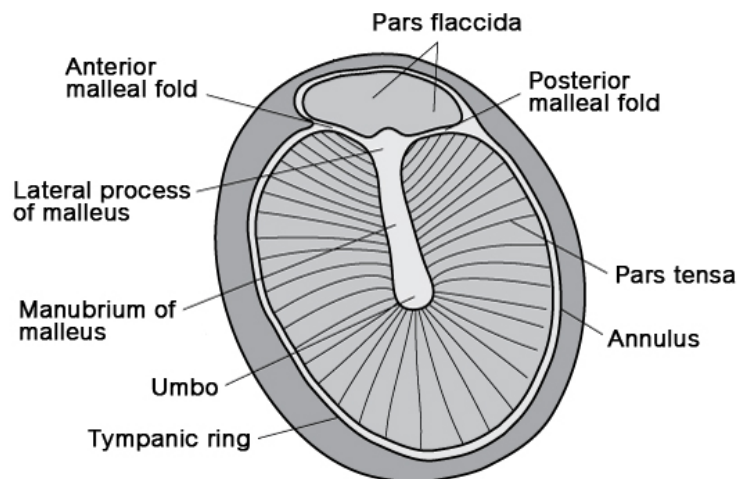


Figure 1.8 Typical structures of the eardrum in mammals. The eardrum has two general parts: the pars tensa (most of the area) and the pars flaccida (adapted from Lalwani, 2007; pg. 579).

Impedance matching is one of the key functions of the middle ear. The efficiency of this function is presumably explained by the area ratio of the eardrum and stapedial footplate, and the ratio of lengths of the malleus and incus lever arms (Relkin, 1988). Lower eardrum/footplate and lever ratios are commonly found in fossorial and subterranean mammals when compared to non-fossorial species (Burda et al., 1992; Mason, 2001, 2006). The lower eardrum/footplate and lever ratios are not caused by

a reduced pars tensa of the eardrum or a reduced malleus. In fact, enlarged stapedia footplate and an enlarged incus contribute to lower eardrum/footplate and lever ratios, respectively (Mason, 2001). These low ratios imply that subterranean mammals have less efficient sound transmission from the eardrum to the inner ear, resulting in poor sensitivity to air-borne sound (Wilkins et al., 1999; Mason, 2001, 2006).

Mammals with auditory systems turned to low frequencies are susceptible to low-frequency noises from bone conduction and arterial pulsation within the middle ear that may interfere with their normal hearing (Packer, 1987). Some subterranean species, such as golden moles and true moles, possess a stapedia artery that passes through the stapedia foramen. To attenuate the effect of unwanted arterial noises, there is a bony tube enclosing the artery. Such an adaptation reduces noise and improves low-frequency hearing (Packer, 1987; Mason, 2003, 2006).

Typically at least one of the middle-ear muscles, either the tensor tympani or the stapedius, is reduced or lost in underground species (Mason, 2001). Contraction of the middle-ear muscles has an effect on attenuating low-frequency transmission to the cochlea. The reduction or absence of the muscles leads to reduced stiffness (Begall et al., 2007) and is indicative of the decreased ecological importance of high-frequency hearing (Mason, 2001). Muscle degeneration, however, is not restricted to underground mammals, and is not always related to low-frequency hearing; several heteromyid rodents and tree shrews lack one of the two muscles but still retain good hearing ability of high frequencies (Mason, 2001, 2006).

Low-frequency substrate-borne vibrations are important in the non-visual communication among subterranean mammals (Nevo et al., 1991; Begall et al., 2007). Seismic vibrations are produced by thumping of the head against the tunnel roof, digging, chewing and vocalizing (Nevo et al., 1991). The vibrations from sound sources are transmitted through the soil and cause the recipient's skull to vibrate. Skull vibrations are in turn transmitted through the inner ear to the brain by means of bone conduction. In the case of the freely mobile ossicles, the centre of mass of the ossicles is much closer to the rotational axis of the ossicles (Fig. 1.9C). This allows bone-conducted vibration transmission to the inner ear by the ossicular inertial path to be minimized (Mason, 2006). It is proposed that underground mammals may exploit other routes to transmit seismic stimuli to the brain. Nevo et al. (1991) demonstrated that seismic vibrations in subterranean mammals are perceived by the somatosensory system and transmitted directly to the brain independent of the auditory mechanism. Moreover, these somatosensory functions were reported in blind mole rats, which use their paws to detect seismic stimuli (Kimchi et al., 2005). Seismic somatosensory perception is presumed to evolve as a channel of long-distance communication for life underground (Nevo et al., 1991).

Some golden moles have an additional adaptation for the detection of seismic vibrations; they have hypertrophied mallei, resulting in the displacement of the centre of the ossicular mass far from the rotational axis (Mason, 2003, 2006; Fig. 1.9B). These ossicular characteristics are adaptations towards the improved detection of seismic vibrations through inertial bone conduction (Mason, 2001, 2003, 2006).

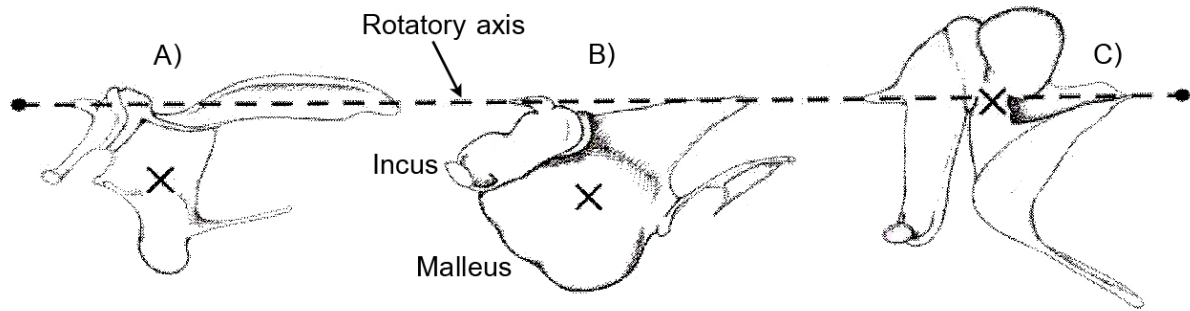


Figure 1.9 The rotatory axis of left auditory ossicles (malleus and incus). The crosses represent the positions of the centers of ossicular mass. A) The “microtype” ossicles suited for high frequencies. B) The hypertrophied ossicle type - the hypertrophied malleus results in the displacement of the center of mass far from the rotatory axis. C) The freely mobile type - the centre of mass is much closer to the rotatory axis (Mason, 2006; pg. 691).

The inner ear characteristics also reflect low-frequency hearing in subterranean mammals. The shape of the cochleae in underground species looks like a tower, and is likely to have more turns than that found in their aboveground relatives (Begall et al., 2007). In addition, compared to skull size, the length of the basilar membrane is longer in subterranean species (Burda et al., 1989; Begall et al., 2007). In *Spalax* mole rats and fossorial voles, hair cell densities are reported showing an increase from the basal turn towards the apex. This is opposite to those in most other mammals in which the density maximum is in the middle flanked by minima at the base and the apex (Burda et al., 1989; Lange et al., 2004). A higher density of receptors at the apex may be associated with the best sensitivity of hearing tuned to low frequencies (Burda et al., 1989). Furthermore, immature OHCs are found throughout most of the cochlear coil in contrast to those in other mammals found only in the apical turn (Begall et al., 2007). Information about the cochlear tuning and auditory brain centres in subterranean mammals, however, is still scarce and further investigations in various species are warranted.

1.4 Summary of functional anatomy of the bony mammalian cochlea and potential correlates

The above review of hearing in mammals shows that several features of the bony cochlea are indicative of specific functions. Below, the potentially most informative features are summarized, potential functional determinants are outlined and key hypotheses for testing in this thesis are listed.

1.4.1 The gross dimensions of the bony cochlea

The gross dimensions of the cochlea and its components are associated with the range of frequencies that animals can detect. The significance of the spiral form of the cochlea in mammals is not entirely clear. It may enable the packing a long cochlea into the confines of the petrous bone. Meng and Fox (1995b) also suggested that a coiled cochlea may allow acoustic nerve fibres to innervate an elongated basilar membrane with the minimum, and roughly equivalent, of wiring lengths. Bekesy (1960) argued that the cochlear curvature appears to have very little effect on the hearing sensitivity in most mammals. However, it has been suggested that the cochlea with a small height-to-diameter ratio (as found in cetaceans) favors very high frequency perception, whereas species having a greater ratio develop a greater sensitivity for lower frequencies, as in for example the chinchilla (Fleischer, 1976). Recently, Manoussaki et al. (2008) reported that the ratio of the radii of curvature from the outermost and innermost turns of the cochlear spiral is strongly correlated with the low-frequency limit of hearing among both land and marine mammalian generalists. Mammals with greater radii ratio tend to have lower low-frequency limit of hearing.

The number of cochlear turns is also thought to have an influence on mammalian hearing. Except for monotremes, which have a hooked cochlea (as in avians), most therian mammals have between two and four turns (Gray, 1951). Mammals that have fewer than two turns are found in some cetacean and sirenian species (Gray, 1951; Fleischer, 1976; Ketten et al., 1992; Ketten, 1997; Wartzok and Ketten, 1999), as well as in the hedgehog and certain marsupials, such as the marsupial mole and the common wombat (Gray, 1907; Sanchez-Villagra and Schmelzle, 2007). Cetacea and Sirenia are considered as the mammalian orders with the smallest number of turns (Fleischer, 1976). Mammals that possess more than four turns can be found in some rodents, for example in the guinea pig, the coypu and the capybara (Gray, 1951; West, 1985; Solntseva, 2010). Wysocki (2005), however, reports that there are only 3.5-3.75 turns in the guinea pig cochlea.

Fleischer (1976) concluded from his study of cetaceans that the number of turns reflects phylogeny and is mostly independent of function. This is the opposite of Gray's (1951) view that the number of turns is influenced more by function than phylogeny. West (1985) reported a positive correlation between the number of spiral turns and the octave range of audible frequencies in ground dwelling species independent of the basilar membrane length. Lange et al. (2004) and Begall et al. (2007) have stated that there is a tendency for higher coiling in subterranean mammals with limited hearing capabilities when compared to their aboveground relatives. Nevertheless, Solntseva (2010) has argued that there is no link between the number of turns and the perceived frequency range, based on her observation that dolphins with only 1.5-2 turns and some bats with 3.5 turns share the same ability to echolocate.

Recently, Kirk and Gosselin-Ildari (2009) used the cochlear labyrinth volume as an estimator of hearing abilities in primates. A close link between the cochlear volume and the basilar membrane length was found. The data also showed a strong negative correlation of the cochlear volume with high-frequency limit of hearing independent of body mass and phylogeny. Therefore a functional relationship between cochlear size and audible frequency ranges is thought to exist. A similar argument is reported and proposed for early hominids, with a smaller cochlea linked to better hearing of high frequencies when compared with modern humans (Moggi-Cecchi and Collard, 2002). These results contradict Heffner's (2004) claim that the physical geometry of the cochlea is not associated with high-frequency hearing. Moreover, an influence of cochlear size (diameter of the basal turn in particular) on hearing has been reported among echolocating bat species (Habersetzer and Storch, 1992). Echolocating bats possess a larger cochlea than that of non-echolocating bats, and within Microchiroptera, small bats with a smaller cochlea produce higher frequency echolocation calls.

Irrespective of its physiology, the length of the basilar membrane appears to have an impact on hearing sensitivity and can be approximated by the length of the cochlea (Coleman and Colbert, 2010). Greater coiling could be considered as a means of permitting storage of a longer basilar membrane. However, there does not appear to be any significant correlation between the number of spiral turns and basilar membrane length (West, 1985). West (1985) reported that the length of the basilar membrane is significantly negatively correlated with the upper and lower limits of hearing in ground dwelling mammals. Species with long basilar membranes are good lower-frequency detectors, whereas species with short basilar membranes

have good high-frequency hearing. This is corroborated by the work of Burda et al. (1989) and Begall et al. (2007), reporting a relationship between a long basilar membrane and a low frequency range in rodents. Furthermore, a comparative study of diverse mammalian species proposes that mammals with a short basilar membrane would be expected to be sensitive to high-frequency sounds (Rosowski and Graybeal, 1991). Manoussaki et al. (2008) updated West's (1985) research and argued that the basilar membrane length is only weakly correlated with low-frequency hearing limits when compared with the radii ratio of cochlear curvature. In a recent study in non-human primate hearing, Coleman and Colbert (2010) reported that the basilar membrane length shows a strongly positive relationship with low-frequency sensitivity, resembling the results from West (1985) and Burda et al. (1989). A significant relationship, however, is not detected between the cochlear length and variables of high-frequency sensitivity, contrasting with the results from West (1985) and Rosowski and Graybeal (1991).

Another structure of the bony cochlea that is linked to hearing frequencies is the outer osseous spiral lamina. The outer lamina is suggested to be a specialized feature of ultrasonic ears (Solntseva, 2010; Vater and Kossl, 2010). In odontocetes and bats, the outer spiral lamina is thick and present throughout almost all of the cochlear length (Wartzok and Ketten, 1999; Solntseva, 2010; Vater and Kossl, 2010). Also, the outer bony lamina is found in land mammals with ultrasonic hearing but is reduced or absent in species with a lower frequency ear (Ketten, 1994). The extent of the ossified outer lamina increases the stiffness of the basilar membrane, resulting in good high frequency hearing (Wartzok and Ketten, 1999; Vater and Kossl, 2010).

The eardrum and cochlear fenestrae play a major role in transmission of sound energy between the middle ear and the inner ear. A difference between the relatively larger size of the tympanum and the size of the stapedial footplate (tympanum to footplate ratio) is believed to be associated with a pressure-amplification mechanism of sound waves to the inner ear (Huangfu and Saunders, 1983; Cohen et al., 1992; Liem et al., 2001). This ratio can represent the ratio of the tympanum to the oval window because the size of the oval window is related to the diameter of the stapedial footplate (Meng, 1992), and is occasionally used to directly estimate the size of the footplate (Ladeveze et al., 2010). Mason (2001) demonstrated that many fossorial mammals have lower ratios because of their large footplate areas relative to non-fossorial mammals. Additional works on area ratios in fossorial and subterranean herbivorous rodents are consistent with Mason's data (Burda et al., 1989; Wilkins et al., 1999; Schleich and Busch, 2004). It is presumed that the low tympanum/footplate ratio may be related to poor sensitivity to airborne sounds in species with borrowing lifestyle by virtue of reduced energy transmission to the inner ear (Wilkins et al., 1999; Mason, 2001; Schleich and Busch, 2004). These data correspond to the studies in non-fossorial rodents, the ratios of which are relatively high (Huangfu and Saunders, 1983; Cohen et al., 1992). Among mammals hearing waterborne sounds, the sirenian manatee has a rather low mean area ratio compared to fossorial species (Ketten et al., 1992; Wartzok and Ketten, 1999).

Although the ratio of the tympanum to the stapedial footplate (or the oval window) has been cited frequently as a factor in middle ear gain, this association is not altogether clear and still debated (Rosowski, 1994; Mason, 2004). Coleman and Colbert (2010) revealed that hearing sensitivity does not relate to the area ratio, and

when considered in each individual area, both areas show strong correlations only with measures of low-frequency sensitivity. This suggests that increased eardrum and footplate size enhances sensitivity of low audible frequencies. However, Rosowski and Graybeal (1991) reported negative correlations of both areas with low-frequency limit, high-frequency limit and centre frequency. The round window size is proposed as an additional factor for sound amplification (Scarpa, 1962; Wartzok and Ketten, 1999). The oval and round window areas in terrestrial mammals are reported to be of approximately the same size, whereas the oval window is one-half to one-third of the round window size in pinnipeds (Wartzok and Ketten, 1999). The significance of the ratio between the oval window and round window on mammalian hearing mechanism, however, has not yet been established.

1.4.2 Interaural distance

Masterton et al. (1969) were the first to propose that mammals with small heads or close-set ears typically rely on higher frequencies than larger species because of the relative size of the head and pinnae compared with the sound wavelength. Listening to high frequencies enables small mammals to improve sound localization ability because sound intensity differences at the two ears are increased due to the greater shadow effect (i.e., low frequency sound can pass around the head whereas high frequency sounds are blocked by the head; Fig. 1.10). Similarly, low frequencies are not readily reflected into the ear by the components of small pinnae (Heffner, 2004). Hence it has been concluded that the smaller the mammals are, the higher the hearing frequencies they use (Heffner et al., 2001; Heffner, 2004). The above, however, is specific to sound localisation. Where just detection is selectively more important than detection and localization, there will be pressure to extend the range

into the lower frequencies generated by, for example, predator movement. A group that includes small species particularly good at low-frequency hearing is the rodents (Webster and Webster, 1972; Heffner et al., 2001); examples include rodents that have evolved independently in a desert environment (e.g., chinchilla, kangaroo rats and gerbils; Webster and Webster, 1972). Other rodents that are reported as good low-frequency detectors are subterranean mole rats, prairie dogs and guinea pigs (Heffner et al., 2001; Schleich and Vassallo, 2003). Heffner et al (2001) suggest that, among rodents, the interaural distance, or functional head size, is negatively correlated with high-frequency hearing limit but not correlated with low-frequency hearing limit.

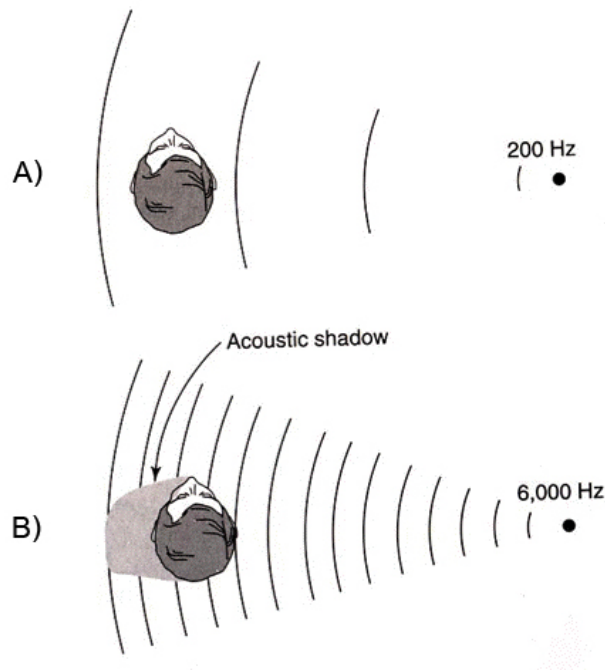


Figure 1.10 Head shadow effect on sound localization. A) Low-frequency sound can bend or diffract around the head so intensity between two ears is almost equal. B) For high frequencies, sound energy is absorbed by the head, hence a significantly higher intensity in one ear than the other ear (Scottish Sensory Centre, 2010 [www.ssc.education.ed.ac.uk/courses/deaf/dnov10i.html]).

In predator avoidance behaviour of kangaroo rats, detection is considered more important than precise sound localization ability (Webster and Webster, 1972). The width of the field of best vision is related to sound-localization acuity; mammals with broad fields of best vision are poorer sound localizers (Heffner, 2004; Heffner et al., 2007). Kangaroo rats possess large and protruding eyes that are helpful adjuncts to hearing (Webster and Webster, 1972). As a result, the necessity of localizing sounds may be decreased in kangaroo rats. The capability of hearing high frequencies that is, in turn, useful for sound localization, is essential only if those sounds are more important for the animals' survival (Webster and Webster, 1972). In kangaroo rats, detection of low-frequency predator-generated sounds is more important, hence the

ear morphology has evolved primarily for low frequency hearing (Webster and Webster, 1972). Similarly, there is no selective pressure to require high frequencies for localizing sounds in subterranean mammals. This is because subterranean mammals live exclusively in long narrow tunnels in which their directional responses to sounds are restricted (Heffner et al., 2001; Heffner, 2004), and low-frequency sensitivity is more important in their seismic communication (Mason, 2003, 2006).

Small mammals have many adaptations of the ear morphology to improve low-frequency hearing. For instance, many surface-dwelling rodents possess enlarged middle ear cavity; e.g., kangaroo rats, gerbils, guinea pigs and chinchillas (Webster and Webster, 1972; Schleich and Vassallo, 2003). Bullar size of some subterranean rodents (e.g., the tuco-tuco) is also relatively large when compared to aboveground generalists (Schleich and Vassallo, 2003). The enlarged cavity contributes to increased middle-ear compliance, which is related to improvement in low-frequency sensitivity (Relkin, 1988). In subterranean mole rats, although the enlarged bullae are not apparent, cochlear specializations in the OHC innervation have evolved instead (Heffner and Heffner, 1993). Moreover, several species (e.g., kangaroo rats, gerbils, guinea pigs, chinchillas and subterranean moles) have freely mobile ossicles, potentially improving low-frequency transmission (Heffner et al., 2001; Mason, 2003, 2006). Contrary to the morphological specializations observed in these mammals, prairie dogs (fossorial rodents that favor low-frequency hearing) have no structural specializations in the auditory apparatus (Heffner et al., 1994). It is suggested that morphological and neural mechanisms that promote low-frequency hearing in prairie dogs may not yet be completely understood (Heffner et al., 1994).

1.4.3 Ecology and behavioural influences

It is believed that ecological and behavioural factors, such as habitat, predation, diet and sound localization, may also influence interspecific variation in hearing abilities and thus cochlear morphology. Examples below are evidence that differences in auditory abilities are related to these factors.

Subterranean mammals spending their entire lives underground in long narrow tunnels have limited high-frequency hearing and rely primarily on low frequency ranges. They have no selective pressure for sound localization to hear high frequencies (Heffner et al., 1994; Heffner, 2004). Prairie dogs, a rodent species that spend much time underground but forage above ground, show intermediate adaptations; they have good low-frequency hearing (more sensitive than subterranean rodents) but have limited high-frequency hearing and poorer sensitivity than surface-dwelling species specialized for high-frequency hearing (Heffner et al., 1994). It has also been pointed out that species that spend more time foraging above ground and that socially interact vocally are more likely to retain more sensitive high-frequency hearing (Lange et al., 2004; Mason, 2004).

Bats, the only mammals capable of true flight, are good high-frequency detectors (Heffner et al., 2006; Jones and Teeling, 2006). Bats using laryngeal echolocation pulses for detecting insects hear higher frequencies than non-echolocating bats and even bats that use tongue clicks (Heffner et al., 2006; Jones and Teeling, 2006). Insectivorous bats are thought to be subject to selective pressure from laryngeal echolocation to extend their high-frequency hearing (Heffner, 2006). Moreover, the echolocation system of bats shows adaptation to many kinds of ecological factors.

Frequency characteristics of echolocation calls can vary among species or within a population in response to changes in vegetation, climate and topography (Kalko, 1995; Xu et al., 2008; Teeling, 2009). This implies that the systems and morphology are not wholly canalised to a specific frequency and that there is sufficient flexibility to allow for inter-individual adaptation to new environments.

Nocturnal primates (e.g., bushbabies and tarsiers) that feed on insects appear to rely on low- to mid-frequency hearing for tracking prey; it is an adaptation to roughly localize the type of low frequency sounds produced by the beating wings of nocturnal insects (Packer, 1987). They then use eye-hand coordination to pin-point and capture the prey (Niemitz, 1984). Hence such species are typified by enlarged eyes and visual cortex of the brain (Packer, 1987).

Pinnipeds exploit the aquatic environment but remain tied to the shore. Hence, their inner ears resemble terrestrial high-frequency generalists (Wartzok and Ketten, 1999). All pinnipeds adapt their hearing to be more sensitive to underwater sounds than to airborne sounds (Schusterman, 1981; Schusterman et al., 2000). The phocid species, which spend the majority of time at sea and dive deeply, are more sensitive to high-frequency underwater sounds than the otariid species (Schusterman et al., 2000; Feldhamer et al., 2004). On the other hand, the otariids, which spend more time on land and engage in more communication above water, are more sensitive to high-frequency airborne sounds than the phocids (Schusterman, 1981; Kastak and Schusterman, 1999; Hemila et al., 2006). The high frequency limit of airborne hearing in the otariids is approximately 32-36 kHz, higher than that of the phocids (Schusterman, 1981).

There are only two mammalian orders with a completely aquatic lifestyle: Cetacea and Sirenia. In Cetacea, the skull and the cochlea in odontocetes differ significantly from those of other mammals (Ketten, 1997; Wartzok and Ketten, 1999; Nummela et al., 2007), reflecting the perception of ultrasonic echolocation signals. The odontocete echolocators are categorized according to the cochlear types into higher-range ultrasonic Type I and lower-range ultrasonic Type II odontocetes (Ketten, 1994, 1997; Fig. 1.7). In contrast, mysticetes or baleen whales can detect frequencies in the infrasonic sound spectrum. These frequency ranges coincide with habitats and feeding behaviours - the higher the frequency is used, the smaller the object that can be detected over shorter distances. Type I odontocetes live in turbid water close to the shore so ultrahigh frequency and short wavelength signals are useful to identify details of nearby objects (Ketten, 1997). Type II species, living in offshore and pelagic areas, use lower-frequency ultrasonic signals to detect larger prey and predators at greater distances (Fleischer, 1976; Ketten, 1997). In large and pelagic mysticetes, a specific use for infrasonic frequencies remains unclear - it has been assumed that they use low frequencies for long-range communications during migrations and to aid offshore navigation by identifying topographical features such as cliffs (Fleischer, 1976; Ketten, 1994; Ketten, 1997).

In contrast to cetaceans, there are no obvious features relating to echolocation ability and infrasonic hearing in the sirenian cochlea (Ketten et al., 1992; Wartzok and Ketten, 1999). The basilar membrane structures are closer to those of pinnipeds and some land mammals than to those of cetaceans (Wartzok and Ketten, 1999). Manatees possess low frequency hearing with a relatively narrow range, poor sensitivity and poor localization. It is presumed that there is no selective pressure for

adaptation to effective hearing abilities because of their evolution in a relatively stable environment with few predators and limited competition (Ketten et al., 1992; Wartzok and Ketten, 1999; Feldhamer et al., 2004; Reep et al., 2011). However, manatees have better than expected high frequency hearing, both in terms of range and sensitivity. They live in shallow coastal areas where low frequency sounds are attenuated by the properties of marine acoustic physics. This might be a selective pressure to evolve better sensitivity at higher frequencies (Gerstein et al., 1999).

As mentioned above, it can be seen that the cochlear dimensions are associated with hearing abilities and vocalization. Both hearing and vocalization can provide information about ecological and behavioural patterns that animals occupy. Walsh et al. (2009) demonstrated that it is possible to predict ecological and behavioural traits from information of the cochlear dimensions in reptiles and birds. As yet, this sort of work has not been conducted on mammals in general. It is feasible that cochlear anatomy in mammals may carry important information with regards to the ecological and behavioural adaptations of species.

1.4.4 Hypotheses: the adult interspecific mammalian cochlea

Hypothesis regarding size and shape of the adult mammalian bony cochlea in relation to hearing frequency

It has been reported that the cochlear size has no functional influence on hearing frequency (Masterton et al., 1969; Heffner, 2004). Other studies, however, do not support this idea. Kirk and Gosselin-Ildari (2009) revealed a strong correlation of the cochlear size with the high-frequency limit in primates; another primate study shows a strong correlation with low rather than high frequency hearing (Coleman and

Colbert, 2010). The influence of the cochlear size on echolocation frequency is found among bat species as well (Habersetzer and Storch, 1992). In addition to this discrepancy in the interpretation of cochlear size, to date there is little information on the relationship between the cochlear shape and hearing frequency. Published data are largely descriptive and are not tested by statistical methods (Fleischer, 1976; Begall et al., 2007). To clarify the above, the hypothesis is tested that the bony cochlear morphology in mammals is tightly constrained by functional requirements, i.e., frequency sensitivity. The parameters of hearing frequency will include the high- and low-frequency limit of hearing and the best hearing frequency.

Hypothesis regarding the interaural distance and adaptations of the bony cochlea in adult mammals

Masterton et al. (1969) emphasized the importance of sound localization in mammalian hearing and proposed it as a selective pressure for high frequency hearing, especially in mammals with a short interaural distance (small head size). Many species with a short interaural distance, however, are good low-frequency detectors. Specializations for low-frequency hearing in small mammals can be found in the middle ear region (e.g., the enlarged bulla and freely mobile ossicles; e.g., Mason, 2003; Schleich and Vassallo, 2003). Few data, however, are available on the adaptations of the bony cochlea. It is possible that small mammals that rely on low-frequency hearing may also show adaptive features of the bony cochlea size and, in particular, shape. Thus, it is hypothesised that mammals with a short interaural distance and that rely on localization as well as sound detection have distinct cochlea in comparison to a) larger mammals and b) small mammals that primarily rely on sound detection.

Hypothesis regarding the relationship between ecology and the bony cochlear morphology in adult mammals

The morphology of the bony cochlea is related to the capabilities of hearing, which, in turn, is closely linked to eco-behavioural traits. It is therefore hypothesised that species exhibiting unusual traits, such as echolocation (e.g., Cetacea and Chiroptera), and/or distinct habitat usage, such as subterranean (e.g., rodents and moles) or semi-aquatic (e.g., pinnipeds), will demonstrate significant differences of the cochlea morphology reflecting the varied selective pressures on hearing. Pairwise comparisons between groups of species representing different eco-behavioral categories should reveal significant differences of the cochlear size and shape, including the oval and round windows. Categories will include habitat, active period and sociality. Specific predictions of the cochlea that will be tested include 1) habitual marine and semi-aquatic mammals will be morphologically distinct from other mammals; 2) habitual subterranean mammals will be morphologically distinct from other mammals; 3) habitually solitary mammals will be morphologically distinct from gregarious species.

1.5 Ontogeny of the cochlea and auditory frequency mapping

The above sections mention the auditory structures and functions in terms of adaptive evolution, gradual change in the characteristics of a population during successive generations, due to natural selection acting on heritable variation among individuals. Ontogeny, on the other hand, is the progressive changes in form and function through the life cycle of an individual organism by which its genotype is translated into the phenotype. Ontogeny plays the major role in linking the heritable

genotypes, passed from one generation to the next, to the phenotypes that are made available for natural selection (Cheverud, 2007). Considering the role of ontogeny in structuring variation and, through its effects on variation, structuring evolution will provide a better understanding of the evolutionary process. Below, size (growth) and time (development) dependent ontogenetic changes in morphology and function of the mammalian cochlea are summarized, the human bony cochlea is discussed, and key hypotheses for testing are devised.

1.5.1 Ontogenetic changes of the mammalian cochlea

Whereas formation of the cochlea is tightly regulated and conserved, its subsequent size and shape maturation does not appear to follow a standard mammalian pattern nor trajectory. In some mammalian species, the process of cochlea growth occurs mostly before birth, particularly in the basal and intermediate segments (Nemzek et al., 1996; Mu et al., 1997; Fig. 1.11). In other species, like the felids and lagomorphs, the bony labyrinth attains its final dimensions at birth (Harris and Dallos, 1984). Moreover, a complete formation of the last apical turn during prenatal life is reported in cetaceans, pinnipeds, ungulates, suids, and some rodents (*Rattus* and *Cavia*) (Solntseva, 2010). The cochlear labyrinth in humans is completely ossified during fetal life and it has been suggested that it does not change in size after birth (Purcell et al., 2003; Jeffery and Spoor, 2004). In contrast, the bony labyrinth in marsupials attains their mature form, including the number of complete turns, during post-natal life (Sanchez-Villagra and Schmelzle, 2007; Fig. 1.11). Harris et al. (1990) reported that the growth of the cochlear capsule in Mongolian gerbils, in terms of the midmodiolar axial length and the radii of spiral turns, approaches an adult dimension at 10 days after birth (DAB). Solntseva (2010) suggested that the anatomical

formation of the mammalian cochlea generally completes in early prenatal life, whereas cell differentiation of the sensory epithelium inside the cochlea continues up to the early stages of postnatal period.

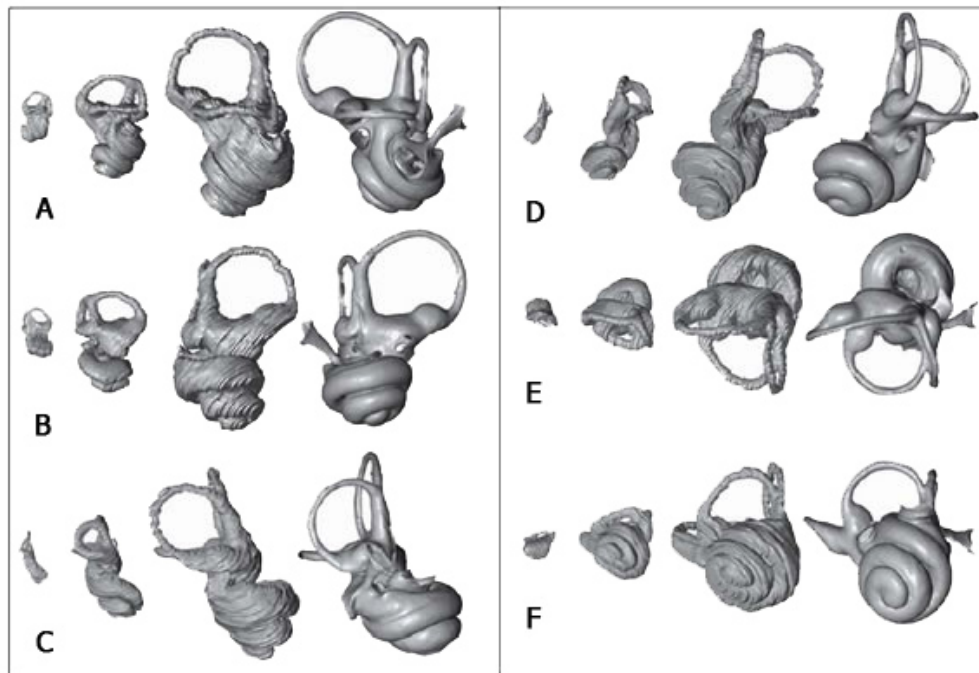


Figure 1.11 Development of the bony inner ear including the cochlea in the woolly opossum (from left to right, a crown-rump length of 11.5, 20 and 25 mm, and adult). A, lateral; B, medial; C, posterior; D, anterior; E, dorsal; F, ventral side (Sanchez-Villagra and Schmelzle, 2007; pg. 57).

The oval and round windows are the two openings on the surface of the otic capsule connecting between the middle ear and the cochlea (Kardong, 2006). Their developmental changes in some example species are given as follows. In Mongolian gerbils and mice, the oval windows reach their adult size after birth at the first postnatal week (Huangfu and Saunders, 1983; Cohen et al., 1992). Although there are no data available on its development, the round window in rodents is supposed to be immature at birth, based on Woolf and Ryan's (1988) data, indicating

completion of the middle-ear and inner-ear development after the 2nd postnatal week. In humans, the oval and round windows have reached their mature states at birth (Su et al., 1982; Bonaldi et al., 1997). Both cochlear fenestrae stop their growth at the 4th month of intrauterine life (Bonaldi et al., 1997). In contrast, Toth et al. (2006) noted that the round window is complete at the eighth fetal month. An average surface area of the human round window is $2.70 \pm 0.43 \text{ mm}^2$ (Takahashi et al., 1989). No significant changes in the form of round window as a function of age are reported (Su et al., 1982; Toth et al., 2006).

Together with the bony labyrinth growth, the basilar membrane, on which the organ of Corti resides, grows in length, width and thickness (Muller, 1991, 1996). Its development has been studied in a few species. The basilar membrane length in humans attains its maximum length during the fetal period and shows sexual dimorphism (Sato et al., 1991). The membrane length is about 8.5 mm in rats (Muller, 1996) and about 11 mm in Mongolian gerbils (Tarnowski et al., 1991; Muller, 1996). The adult width is established by five DAB in Mongolian gerbils (Harris and Dallos, 1984). An increase in the thickness may be found during development when the width is constant (Muller, 1991). In the mature state in most species, the membrane tapers with a basoapical gradient of increasing in width and decreasing thickness towards the apex (Vater and Kossel, 2010). Mu et al. (1997) demonstrated that the final numbers of inner and outer hair cells (IHC & OHC, respectively) along the membrane in rats are reached at the same time (three DAB) and remain constant through adulthood; OHCs reach their adult-like sizes at seven DAB before the IHCs reach the mature sizes at 14 DAB. That the hair cells have the capability of converting sound into an electrical stimulus is partially associated with the presence

of the endocochlear potential (Steel and Barkway, 1989). In mice, the endocochlear potential rises steadily from six DAB onwards to reach mature levels at around 13-16 DAB (Steel and Barkway, 1989), matching up with the onset of hearing. From observing the developing rodent cochlea from young to old age, Tarnowski et al. (1991) reported that aged animals show a remarkable range of OHC loss at the extreme ends of the cochlea, corresponding in lower sensitivities in auditory functions. The work of Keithley et al. (1989, 1991) also showed that a decreased number of spiral ganglion cells and degeneration of the stria vascularis are observed as a function of age at both basal and apical cochlear ends.

1.5.2 Ontogenetic changes in sound frequency analysis

Auditory capabilities vary in different mammalian species at birth (e.g., Rubsamen, 1992). Audition in some mammals is exemplified as follows: among primates, human auditory responsiveness can be detected during the 25-28th week in the uterus (Birnholtz and Benacerraf, 1983), whereas macaque auditory responsiveness is detected immediately after birth (Winter et al., 1973). In Rodentia, the precocial guinea pig has an auditory function before birth (Horner et al., 1987), while Mongolian gerbils, mice and rats are deaf until 12-14 DAB (Finck et al., 1972; Harris and Dallos, 1984; Echteler et al., 1989; Muller, 1991, 1996; Rubsamen, 1992). The adult-like audition appears between the 2nd -3rd postnasal week in gerbils (Harris and Dallos, 1984; Echteler et al., 1989; Weaver and Schweitzer, 1994), at the 4th week in mice (Rubsamen, 1992), and at the 5th week in rats (Muller, 1991). Cats have the onset of hearing between 2-4 DAB, before reaching the adult-like audition at about the 3rd -4th postnasal week (Aitkin and Moore, 1975). In Chiroptera, some bats can hear at birth but in some species it can take a few postnatal weeks (Rubsamen,

1992). After seven weeks, young bats typically attain their adult auditory ranges (Rubsamen, 1992). In manatees, the auditory system is reported as having structural maturity, and presumably full function, at birth (Ketten et al., 1992; Au and Hastings, 2008). The differences in the onset of hearing found among mammals are associated with the developmental pattern of the auditory nervous system, in particular formation of the auditory cortices, and the innervation of cochlear hair cells in each species (Hepper and Shahidullah, 1994).

One of the common properties of the auditory system that is studied most is the sound frequency analysis (Hyson and Rudy, 1987). The fundamental discovery in this area is von Bekesy's (1960) observation that the mammalian cochlea represents different frequencies at different locations along the cochlear duct. He found that in adults, high frequency sounds activate the basal part of the cochlea, whereas low frequency sounds activate the apical portion. Morphologically, the maturation of the cochlea progresses from the basal end towards its apex (Pujol and Marty, 1970; Rubel, 1978). This might lead one to expect that developing animals hear high frequency sounds first. However, physiological studies show that the development of hearing begins with low-to-mid frequency ranges and expands to high frequencies (Rubel, 1978; Romand, 1983). Therefore, development of cochlear morphology appears to progress in the opposite direction from that of cochlear physiology. From this discrepancy, Rubel and Ryals (1983) formulated a hypothesis suggesting that cochlear place-frequency code is not stable during development. It starts to function only at the midbasal cochlea with low-to-mid frequency ranges. During subsequent development, the basal cochlea changes to respond to higher frequencies, while the low frequency representation shifts progressively towards the apex.

Rubel's hypothesis generates both supportive (Ryan and Woolf, 1988; Sanes et al., 1989) and contradictory (e.g., Manley et al., 1987; Arjmand et al., 1988) discussion. Manley et al. (1987) studied chickens and found that the cochlear frequency map remains stable throughout development. In addition, Arjmand et al. (1988) showed that frequency shifts towards high frequencies are restricted to the basal region, while no significant shifts occur in the second cochlea turn. Furthermore, from a study of frequency representation in the rat cochlea, it is apparent that the cochlear function emerges in the middle of the cochlea rather than at the base (Muller, 1991). Ryan and Woolf (1988) also suggested that, in gerbils, the entire cochlea (not only in the basal turn) is capable of responding to acoustic stimulation at the onset of hearing. In some of the species studied, hearing range was observed to expand towards lower frequencies during development, coinciding with the major expansion towards higher frequencies (Reimer, 1996). It is now obvious, however, that the existence of the place-frequency shift during ontogenesis is confirmed by many studies with different approaches in different mammalian species (e.g., Rubel, 1978; Romand, 1983; Ryan and Woolf, 1988; Reimer, 1996).

There are many reasons proposed with regards to why auditory responsiveness firstly emerges in low-to-mid frequency ranges rather than in high frequencies. Woolf and Ryan (1988) suggested this might be due to middle ear transmission capabilities; at the inception of hearing when frequency mapping is first established, the middle ear is still partly filled with fluid and mesenchyme, and the ossicles are not fully ossified. This agrees with Finck et al. (1972) and Relkin and Saunders (1980), who identified the middle ear processes as considerable determiners of the postnatal response to sound. Spatial and temporal variations in the morphological and

physiological development of the hair cells also affect frequency distributions (Pujol et al., 1978; Lenoir et al., 1980, 1987; Muller, 1991; Weaver and Schweitzer, 1994).

1.5.3 Ontogenetic changes of the human bony cochlea

The embryonic development of human auditory apparatus starts at 20 days of gestation (the stage of 1-3 pairs of somites) when a thickening of the ectoderm on the side of the head called the otic placode develops (O'Rahilly, 1983). Later, at 24 days of gestation, the otic placode has invaginated to form the otic pit. At about 28 days of gestation, the otic pit pinches off from the surface ectoderm to become a hollow sphere called the otic vesicle. The otic vesicle is divided into the upper and lower portions. The lower segment elongates to form the cochlear duct (O'Rahilly, 1983). The basal cochlear turn is apparently formed and curved before the middle and apical turns (Solntseva, 2010). The formation of the cochlear whorls coincides with the development of the cochlear nerve (Moore and Linthicum, 2007). Nerve cells separating from the otic vesicle migrate to the modiolus to form the spiral ganglion, the axons of which are bundled to form the cochlear nerve. The cochlear duct continues its spiral growth and shows almost two and a half turns by 8 weeks of gestation (O'Rahilly, 1983; Moore and Linthicum, 2007). After the apical cochlear turn is formed, cell differentiation of the organ of Corti begins at the basal turn and extends gradually to the upward turn. During the same period, the tectorial membrane starts to form above the developing organ of Corti (Pansky, 1982; Moore and Linthicum, 2007). At around 12 weeks of gestation, a shell of cartilage encloses the cochlea and fluid-filled spaces are seen between the cartilage wall and the curled cochlear duct (Moore and Linthicum, 2007; Fig. 1.12).

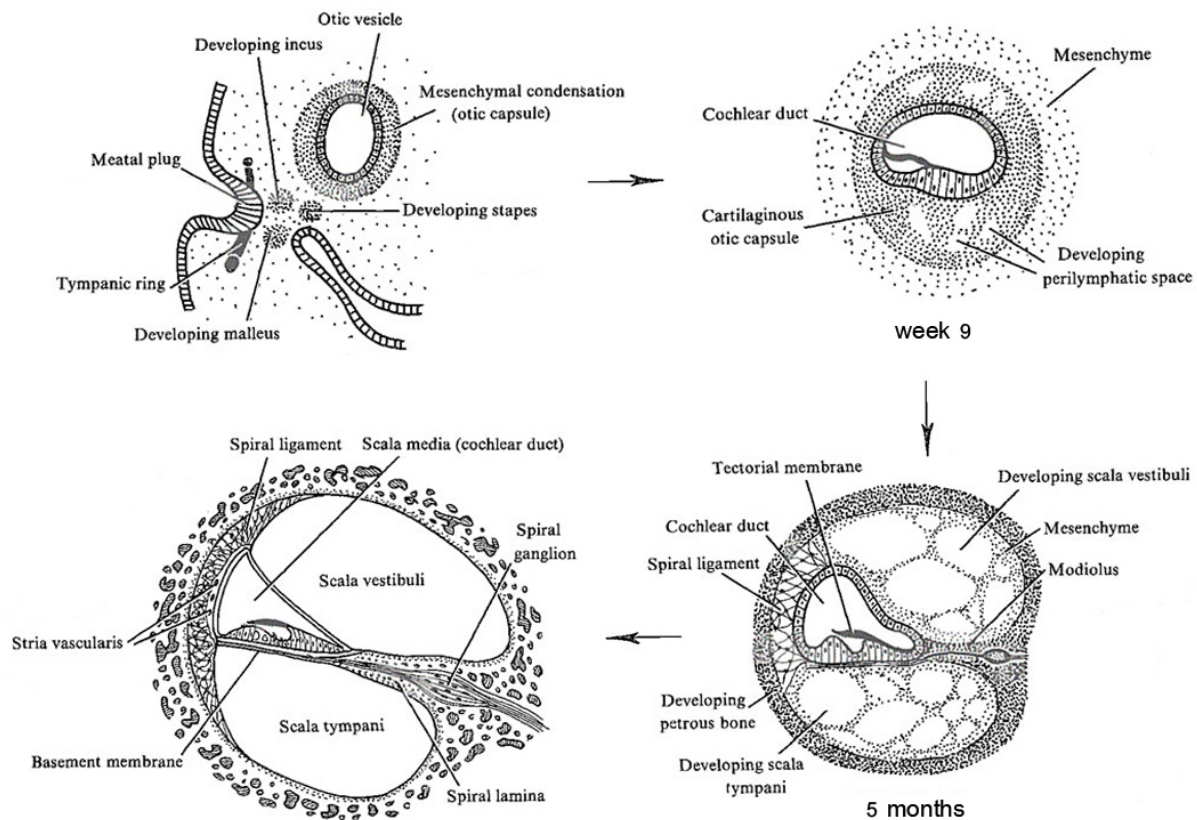


Figure 1.12 Ontogeny of the human bony cochlea (adapted from Pansky, 1982; pg. 172-173).

Discrepancies in the literature exist with regards to development of the human bony cochlea during the second and third trimesters of intrauterine period (e.g., Bonaldi et al., 1997; Toth et al., 2006). Whether the bony cochlea reaches its adult morphology before birth is still debatable. The following summarises some of conflicting information concerning the development of the fetal bony cochlea from previous studies.

After the membranous labyrinth reaches adult dimensions at around 16 weeks of gestation, ossification of the otic capsule to replace the cartilaginous framework commences, beginning at the basal turn of the cochlea (Nemzek et al., 1996). The

spiral bony partition between the cochlear turns begins to be partially ossified at 18 weeks of gestation. At gestational age of 21 weeks, the cochlea is fully ossified and all of its spiral turns are seen (Nemzek et al., 1996). These results are similar to those reported by Jeffery and Spoor (2004), demonstrating that the fetal cochlea attains its adult size at around 16-17 weeks of gestation, at least a week before the cochlea is fully ossified. The completed ossification of the cochlea is observed during the sixth month in the uterus by others too (Bast, 1930; Richard et al., 2010). No significant changes in cochlear size and shape are observed during the late fetal and postnatal period (Nemzek et al., 1996; Jeffery and Spoor, 2004). Studies also suggest that there is little change in the microstructure of the cochlea after birth (Eby and Nadol, 1986; Sato et al., 1991). Despite the presence of sexual dimorphism, the cochlear length in each sex does not appear to change with age postnatally (Sato et al., 1991). From the above, it could be reasonably concluded that the cochlea achieves its maximum size during prenatal life. Some authors, however, report postnatal changes in the bony cochlear morphology. Turkewitsch (1930), for instance, found a small increase in cochlear size. Hardy (1938) reported the observation of a longer cochlea in humans over 20 years old compared with under 20 years old. Sercer (1958) proposed that the cochlea in adults is more rolled-up when compared with that in neonates. Moreover, Richard et al. (2010) demonstrated that, although the cochlea is fully embedded in bone, the bone density in each part is still not equal at the end of gestation; the basal turn has a higher density than the apex, suggesting that the mineralization process continues after birth.

Pertaining to the cochlear fenestrae, their development is still unclear as well, especially in regards to the round window. Su et al. (1982) reported that there are no

differences in the round window dimensions among postnatal specimens, suggesting that it reaches a mature state at birth. Indeed, the round window is assumed to cease its growth after the fourth month in the uterus (Bonaldi et al., 1997). Toth et al. (2006) reported that the round window starts to be ossified at 16 weeks of gestation and attains its adult configurations at around the eighth fetal month. During this period, the round window niche can change the shape of the entrance, which is due to the uneven growth of its different walls. Toth's findings are inconsistent with the recent study by Richard et al. (2010), showing that the adult size of the round window is achieved during the second (23rd week gestation) rather than third trimester. The exact timing of maturation of the oval window is not clear. It is suggested that formation of the oval window is closely related to development of the stapedial footplate (Zeifer et al., 2000). Since the stapes is assumed to attain adult dimensions at the second trimester of gestation (Nemzek et al., 1996), it is likely that the oval window matures in size during this period as well. If correct, it will correspond with Bonaldi et al.'s (1997) study, reporting that the oval window is mature by the fourth month of intrauterine life. By contrast, Richard et al. (2010) reported that an adult state is achieved at 35 weeks of gestation, some 19 weeks later. The discrepancies with regard to Richard et al.'s work warrants further investigation.

In addition to the morphology of the bony cochlea itself, a few studies have also examined its spatial orientation in the cranium during ontogeny. Bossy and Gaillard de Collogny (1965) found the reorientation of the long axis of the cochlea between 11 weeks and 9 months of gestation. Based on CT imaging, Spoor (1993) reported a small but statistically significant difference in the orientation of the fetal and adult

cochleae relative to the vestibule. Jeffery and Spoor (2004) used magnetic resonance imaging and found that the orientation of the fetal cochlea relative to the vertical semicircular canals changes after the cochlea attains adult size and is completely ossified, although not significantly different from that found in adults. Recently, a study using CT scans of the temporal bones in patients aged from 9 months to 85 years reveals that there is a significant reduction in the angle of the basal cochlear turn relative to the midsagittal plane with increasing age (Lloyd et al., 2010). It is proposed that the orientation of the cochlea during fetal life and postnatal period is not associated with remodeling of the otic capsule but results from changes in the surrounding petrosal morphology (Jeffery and Spoor, 2004; Lloyd et al., 2010). The otic capsule is thought to cease its development once it is fully ossified in order to maintain normal hearing (Zehnder et al., 2006; Lloyd et al., 2010). Changes in the orientation of the whole unit within the skull then give rise to changes in the spatial relationships of the enclosed cochlea.

1.5.4 Hypotheses regarding development of the bony cochlear morphology in human

Few data are available for the development of bony cochlear morphology in mammals, including humans. Also, there are still some discrepancies in published data on the development of the human cochlea. In particular, there remains some debate as to when cochlear form ceases to change during development relative to its adult form. Some papers reported that the cochlea attains its mature form prior to birth (Jeffery and Spoor, 2004) whilst others have reported that postnatal changes in the bony cochlea (Turkewitsch, 1930; Sercer, 1958). Therefore this investigation tests the hypothesis that the bony cochlear morphology reaches the adult form prior

to birth, with the continued development of bony cochlear morphology observed after birth to be used as evidence to reject the null hypothesis.

Pertaining to the cochlear fenestrae in particular, most papers concur that the oval and round windows cease their growth during intrauterine gestation. There are, however, some discrepancies in the exact timing. The oval window is reported to mature in size at the second trimester of gestation (Nemzek et al., 1996; Bonaldi et al., 1997) or at the last month before birth (Richard et al., 2010). The fenestrae are critical to the propagation of sound and therefore considering when they mature in size and shape, and whether this occurs before, after or at the same time as the cochlea in general, is an important consideration. It may provide a better understanding of the form-function relationship over developmental time and infer whether hearing capability is comparable with adults. Therefore, an aim of this study is to determine what time during gestation period the cochlear fenestrae reach their mature size. In particular, it is hypothesized that maturation of the round window is contemporaneous with that of cochlea in general, whereas maturation of the oval window differs, reflecting growth of the stapes.

Chapter 2 Review: capturing the cochlear morphology

2.1 Early methods versus computed tomography

The bony labyrinth, including the cochlea, is one of the most difficult structures of the body to study, since its complex three-dimensional (3D) geometry is concealed within the dense otic capsule of the petrous bone (Spoor and Zonneveld, 1995). The earliest studies of the bony labyrinth were primarily descriptive and based on casts or dissection; casting involves the filling the air-filled cavities of the macerated temporal bone under vacuum with metal alloys (Hyrtl, 1845 [quoted in Gray, 1951]), paraffin (Gray, 1907; West, 1985) or plastics (Wilbrand and Rauschnig, 1986; Spoor and Zonneveld, 1995). Afterward, the bone tissues are removed from the cast using a highly concentrated acid, such as hydrochloric acid or nitric acid. With the aid of a dental drill or a stereomicroscope, the cast of the bony labyrinth can be freed from debris and then photographed. The casting technique can provide reliable information about the surface features of the labyrinth and the dimensions of the cochlea; e.g., the number of spiral turns (Gray, 1907; West, 1985). Numerous species representing the major mammalian orders have been thus investigated so far (Gray, 1951). The technique, however, has several major disadvantages: 1) it is destructive and now prohibited for museum specimens; 2) the method is laborious, time consuming and prone to error (e.g., air-pockets); 3) errors can occur due to shrinkage during the solidification process of casting (Spoor and Zonneveld, 1995).

One of the most famous works by Gray (1907) used stereoscopic photographs of casts. He made an extensive study of the labyrinth of diverse avian and mammalian species. Watt (1917) subsequently made a further study of the mammalian cochlea

using Gray's photographs. Because of Gray's wonderful photographs, the length of the basilar membrane could be approximately measured from the outer edge of the cochlea whorls (Watt, 1917).

The bony labyrinth can also be examined microscopically by microdissections and serial sections from tissue-embedding techniques. Here, the cochlea is dissected away from the temporal bone and immersed in the fixative. The dehydrated cochlea is then infiltrated with the embedding materials, generally paraffin or celloidin for light microscopy and plastic resin for advanced microscopic examinations (e.g., Hashimoto et al., 1990; Sato et al., 1999). Sections are serially cut and then photographed to perform 2D or 3D image reconstruction. The microscopic techniques give the opportunity to study tiny structures at the tissue and cellular levels. However, these techniques are time-consuming and require considerable skill for their preparation (Spoor and Zonneveld, 1995; Hardie et al. 2004). The delicate labyrinthine structures may be damaged or shrink during tissue processing and sectioning (Hashimoto et al., 1990; Spoor and Zonneveld, 1995). In addition, the co-registration of sections to create 3D volumes is cumbersome and time consuming (Hardie et al., 2004; Hashimoto et al., 1990; Sato et al., 1999). Recent advances in episcopic and micro-grinding microscopy (e.g., Rau et al., 2013; Shen et al., 2013) may bring considerable improvements and insights at the microscopic level but will remain prohibitive for large comparative studies due to their destructive nature. A potential solution to this problem is to employ non-invasive imaging techniques.

Since the 1970s, technologies of X-ray imaging have been highly developed, and computed tomography (CT) is well established as a technique scientific research. In

contrast to the above earlier methods, CT is a nondestructive technique, and the process of making CT scans of the petrous bone is relatively easy and fast to do (Spoor and Zonneveld, 1995). Although producing lower resolution than that achieved with microscopy, the measurements taken from CT scans are sufficiently accurate to permit the morphometric analysis of the form of the bony labyrinth (Spoor and Zonneveld, 1995). Also, unlike reconstructions from histological sections, CT images are already in a co-registered space, so 3D reconstruction is easier and higher in quality. Consequently, CT allows the inner ear structures to be visualized in detail, providing useful data for a better understanding of its functional morphology, ontogeny and evolutionary history. Hence, CT and its successors (e.g., micro-CT) now dominate studies of large samples and of rare paleontological specimens (Spoor and Zonneveld, 1995; Spoor et al., 2000).

2.2 Basic principles of X-ray physics in CT

Computed tomography is based on the properties of X-rays, which are a form of electromagnetic radiation, and their interactions with matter. A basic understanding of these properties and interactions is essential for the appropriate and effective application of the method. The following is a brief review.

2.2.1 Quality and quantity of X-ray beam

The quality of an X-ray beam is a measure of its penetrating power, which is determined by the photon energy or wavelength (Hay and Hughes, 1988). In general, beams of radiation may be monochromatic or polychromatic. If radiation is monochromatic, it means that all the photons in the beam have the same energy

(i.e., a single wavelength). The beam from an X-ray tube, however, is nearly always polychromatic; that is, the photons have a range of wavelengths or energies (Ball et al., 2008). With regard to the quantity, this is a measure of the number of photons in the beam. In other words, it refers to the intensity of the beam and is defined as the amount of energy flowing per unit time through a unit area (Hay and Hughes, 1988).

There are many factors that determine X-ray quality and intensity (quantity). The first key factor is the voltage applied across the X-ray tube. Tube voltage affects both quality and intensity. If the applied voltage is increased, the kinetic energy of electrons from the X-ray tube filament (cathode) will be increased when they reach the target (anode) in the tube (Graham and Cloke, 2003). As a result, both the quality and quantity of the X-ray beam produced from the target are increased. The voltage also affects the presence or absence of line spectra. If the tube voltage generates electrons with energy equal to or greater than the binding energy of electrons in the anode's atomic shells (typically k-shell), electrons are knocked-out or excited and the anode emits x-rays characteristic of those energy states (Graham and Cloke, 2003; Ball et al., 2008). These are represented by as sharp lines (k-lines) on the spectral graph. The second key factor is the X-ray tube current. The value of tube current (mA) affects only the beam intensity. If the current is increased, the number of electrons flowing across the tube and the number of x-rays produced increase per unit time (Graham and Cloke, 2003). However, no changes in the maximum photon energy and the position of the characteristic line spectra are observed, indicating that the beam quality is not influenced by the tube current (Hay and Hughes, 1988; Graham and Cloke, 2003; Ball et al., 2008).

Filtration is another factor that can be used to modify X-ray properties. Filters are routinely employed to improve the quality of the beam and/or to reduce the total intensity (e.g., to prevent damage to sensitive detectors) (Hay and Hughes, 1988). A filter is typically a thin sheet of metal made of copper, aluminum or brass (Hsieh, 2003). The filter is inserted into the X-ray beam to absorb most of the low-energy (long-wavelength) photons. Different metals of different thickness are used to cut off the bottom end of the spectrum by differing amounts. The filtered beam has an increased average of photon energy (higher quality) because it contains a higher proportion of the high-energy photons that are more penetrating (Hay and Hughes, 1988). Also, because the spread of photon energies is reduced, the filtered beam becomes less polychromatic. Other practical applications of filtration are to reduce unwanted radiation dose to patients' skin (Seeram, 2001; Ball et. al, 2008), and to correct beam hardening artifacts (Hsieh, 2003). Beam hardening results from the polychromatic nature of x-ray production (Hsieh, 2003). The polychromatic beam can be considered as a combination of many superimposed homogeneous beams (Fig. 2.1). In this case, when the beam passes through a medium, the lower-energy component of the beam is attenuated to a greater extent than the high-energy component because the low-energy photons are mostly absorbed and scattered from the beam (Ball et al., 2008). Accordingly, the emergent beam contains a larger proportion of high-energy photons than did the original beam (Fig. 2.1). The beam therefore becomes more monochromatic and more penetrating, although its intensity reduces (Hay and Hughes, 1988; Ball et al., 2008). Since the lowest energy x-rays are typically attenuated within a short distance, at the periphery of an object, even a homogenous block of material can appear denser towards the edges (see section

2.3.2 further details). Filtering reduces the lower end of the spectrum and therefore the effects of beam hardening.

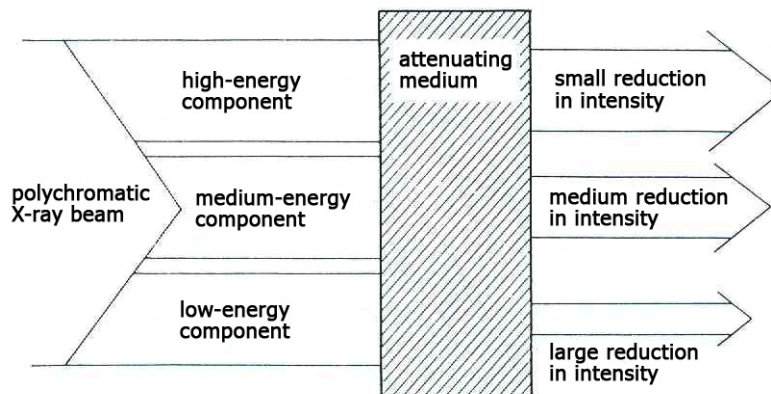


Figure 2.1 Modification of a polychromatic beam by attenuation. The low-energy component is more attenuated by the photoelectric and Compton processes than is the high-energy component (adapted from Ball et al., 2008; pg. 282).

2.2.2 X-ray interaction with matter

When a monochromatic beam of X-rays passes through a medium, there are many possible processes that cause X-rays to be attenuated (reduced in intensity) by the processes of absorption and scattering.

Classical or unmodified scattering - This process (Fig. 2.2A) takes place when the energy of photons in the beam is less than the ionization energy of the atoms of the attenuating medium; i.e., it occurs mainly with low-energy X-rays (Hay and Hughes, 1988; Graham and Cloke, 2003; Ball et al., 2008). In this process, the incident photon interacts with an electron but does not have enough energy to release the electron from its shell, so none of the photon energy is transferred to the electron. The photon does not lose energy but changes direction, hence the term *unmodified*

scattering. In radiography, unmodified scattering usually makes only a small contribution to the overall attenuation because the X-ray energies used are normally too high for this process to occur (Hay and Hughes, 1988; Graham and Cloke, 2003; Ball et al., 2008).

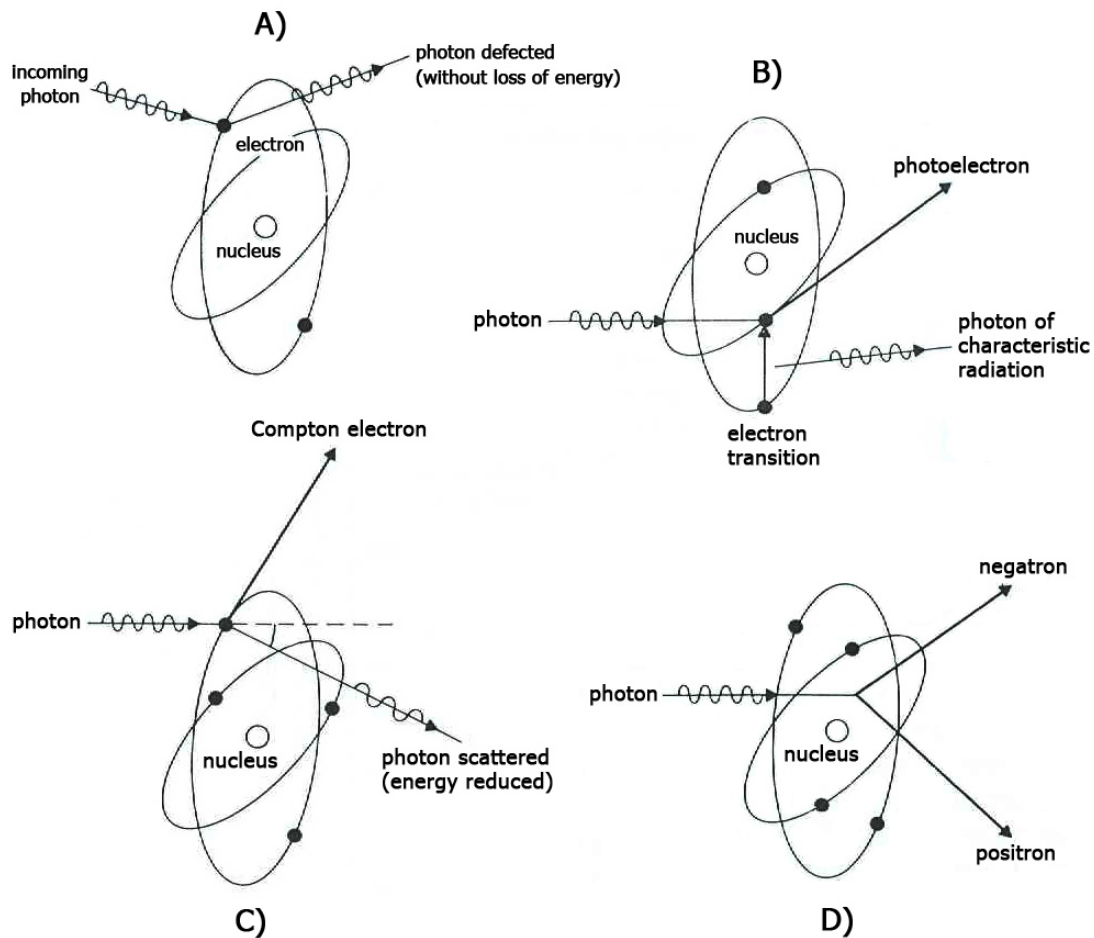


Figure 2.2 Four processes of X-ray attenuation: A) unmodified scattering; B) photoelectric absorption; C) Compton scattering; D) pair production (adapted from Ball et al., 2008; pg. 270, 276 and 277).

Photoelectric absorption - This process (Fig. 2.2B) can occur when the incoming photon has energy equal to or not much greater than the ionization energy of the atoms of the medium (Hay and Hughes, 1988; Graham and Cloke, 2003; Ball et al.,

2008). In this case, the photon gives up all its energy to an electron. Some of its energy is used in overcoming the ionization energy to eject the electron from a shell of the atom, and the rest is given to the electron as kinetic energy. The electron ejected is known as the photo-electron. Since the photon gives up all its energy, it no longer exists, hence the complete absorption (Ball et al., 2008). The vacant site in the shell is then filled by an electron jumping from another shell farther away from the nucleus, leading to the emission of excess energy in the form of characteristic radiation. The photon of radiation emitted has an energy that depends on the difference between the ionization energies of the two shells involved in the electron transition (Hay and Hughes, 1988). The photon energy also depends on the proton number of the atom in the medium because it partly determines the energy levels of the electron shells. Because most of the elements in tissues consist of carbon, oxygen and hydrogen, which have low proton numbers, the photon energy of characteristic radiation is generally very low and is in the range of infrared spectrum (Graham and Cloke, 2003). This characteristic low-energy radiation itself is quickly absorbed by ionizing other nearby atoms and generating heat (Ball et al., 2008). In contrast, if the photoelectric absorption occurs in medium with high proton numbers, electrons are occasionally ejected from the K-shell, nearest to the nucleus and whose ionization energy is greatest. The subsequent transition of an electron down to the K-shell usually emits the characteristic radiation in the X-ray part of the electromagnetic spectrum (Hay and Hughes, 1988; Ball et al., 2008). This characteristic X-radiation is identical in nature to that generated in the target of an X-ray tube (Hay and Hughes, 1988; Ball et al., 2008). In the photoelectric absorption, no scattering occurs because the incident photon disappears after transferring all its energy to the atom and its electrons.

Compton or modified scattering - This process (Fig. 2.2C) can occur if the incident photon has very much greater energy than the ionization energy of the electron with which it interacts (Hay and Hughes, 1988; Graham and Cloke, 2003; Ball et al., 2008). On colliding with the electron, the photon transfers part of its energy to the electron, causing the electron to recoil and to be ejected from the atom. The recoil electron is termed as the Compton electron. Like the photoelectron in the process of photoelectric absorption, the Compton electron, given kinetic energy by the photon, moves through the medium giving up its energy by ionizing nearby atoms. Meanwhile, the photon is deflected and continues with reduced energy (increased wavelength), hence the term *modified* scattering (Ball et al., 2008). The loss of the photon energy depends on the angle through which it is scattered. The photon loses most energy when the angle is 180° (i.e., when it is scattered back towards the source) (Hay and Hughes, 1988; Ball et al., 2008). The deflection is independent of the photon's original wavelength and the attenuating medium, but is dependent on the photon's original energy. The photon with high energy tends to have the smaller angle as it is less likely to be deflected off course by the collision with the electron (Ball et al., 2008). The incidence of Compton scattering decreases as the photon energy of the beam increases (Hay and Hughes, 1988; Graham and Cloke, 2003; Ball et al., 2008).

Pair production - This process (Fig. 2.2D) can occur only when the energy of the incident photon is equal to or exceeds 1.02 MeV (Hay and Hughes, 1988; Graham and Cloke, 2003; Ball et al., 2008). While the photon passes close to the nucleus of an atom of the medium, it interacts with the strong electric force around the nucleus. This leads to the creation of two charged particles, hence the process is called *pair*

production. One of the particles is the “negatron”, carrying a negative electric charge like a normal electron, whereas the other is the “positron”, having the same mass as that of the negatron but carrying a positive electric charge (Ball et al., 2008). If the photon has more energy than 1.02 MeV, the excess energy is converted into kinetic energy in the negatron and positron equally. The negatron and positron can move through the medium to impart their kinetic energies by ionizing other atoms. When the negatron slows down, it is captured by a nearby atom. However, when the positron comes to rest, it combines with a normal electron and they annihilate each other (Ball et al., 2008). The annihilation is the process which the combined mass of the positron and electron is converted into energy in the form of two photons. The two photons have the same energy and travel at 180 degrees to each other; i.e., in opposite directions (Ball et al., 2008). Pair production has no scattering because the incident photon transfers all its energy and then no longer exists.

For the range of X-ray energies usually used in CT and micro-CT, the photoelectric and Compton processes predominate (Hay and Hughes, 1988; Ball et al., 2008). Both photoelectric absorption and Compton scattering depend on the photon energy; both processes are less likely as the photon energy increases (Hay and Hughes, 1988; Graham and Cloke, 2003; Ball et al., 2008). At a given photon energy, the photoelectric attenuation is directly proportional to the atomic number of the medium while the Compton process is approximately the same for all media (Hay and Hughes, 1988; Graham and Cloke, 2003).

2.3 Computed tomography

Within a year after the discovery of X-rays in 1895, radiography, the technique of using X-ray radiography was being used in scientific research (Spoor et al., 2000). Conventional or plain-film radiography involves the process in which X-rays are directed at the object, and then pass through it to form an image on a film that represents differences of attenuation (Smith, 1997). A basic problem in plain-film radiography is that all structures appear superimposed onto one image (2D) plane and cannot be readily differentiated from each other (Spoor et al., 2000). This problem, however, was solved in the early 1970s with the introduction of CT imaging.

Computed tomography, also called Computerized Axial Tomography (CAT), is a non-destructive technique using X-rays for creating cross-sectional slice images of an object in digital form (Seeram, 2001, 2009). The object tested is placed between an X-ray source (tube) and a detector system, both of which are linked to a computer so that X-ray images collected can be correlated to the position of the object (Kalender, 2005). A CT image is created by directing X-rays through the slice plane from multiple orientations and measuring the decrease in intensity of X-rays (attenuation) when passing through the sample. Digital cross-sectional images, which map the different degrees of attenuation in the slice, are shown on a computer monitor using a grey scale. Structures with higher density and atomic number (such as bones and teeth) block more of X-rays, leading to a lower signal (white in image), compared to structures with low density and atomic number (such as soft tissues), which appear black in the image (e.g., Seeram, 2001; Kalender, 2005). To produce a three-dimensional CT image, a series of slice images need to be acquired.

2.3.1 Technical background of CT data processing

When X-rays emitted from the source pass through a scanned object, *raw data* (not an image) are produced by the detectors (Seeram, 2001; Fig. 2.3). These data represent the attenuation through the sample at that particular orientation, slice and point in time and are subject to three stages of processing. Firstly, corrections and some reformatting of the data are made, for example in corrections to errors from beam hardening, and adjustments for bad detector readings or scattered radiation (Seeram, 2001). These improve image quality and reduce the incidence of image artifacts. After preprocessing, the second step is image reconstruction. This step is the mathematical process of converting raw data into two-dimensional slice images, using reconstruction algorithm to convert attenuation coefficients of the data into a digital image characterized by CT values. The image reconstruction algorithm used by current CT scanners is the filtered back projection (Seeram, 2001; Kalender, 2005). Raw data are first convolved with a filter or kernel to get rid of blur, resulting in higher image quality. Then, convoluted data are back-projected into the image matrix to derive attenuation coefficients for subregions and create CT images (image data) displayed on a computer monitor (Seeram, 2001; Fig. 2.3).

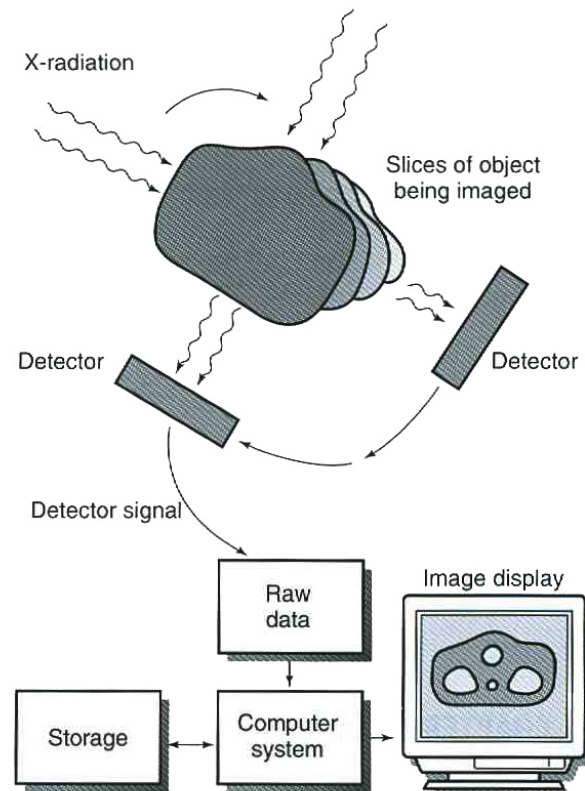


Figure 2.3 CT data processing, from data acquisition to image display and storage (Seeram, 2001; pg. 2).

A CT image is typically called a slice because it corresponds to a two-dimensional plane with thickness, like a slice from a loaf of bread. Like any digital image, a CT slice consists of an array of a limited number of picture elements called pixels (Spoor et al., 2000). Since each slice has a certain thickness of the object being scanned, each pixel also represents a cubic volume element called voxel (Fig. 2.4). Pixels are arranged in rows and columns to create the image matrix (Fig. 2.4). In medical CT, the typical matrices used are 256×256 , 320×320 and 512×512 pixels (Henwood, 1999). Pixel resolution depends on the field of view (FOV) represented by the image matrix (Spoor et al., 2000). For instance, a scan with a matrix size of 320×320 pixels and a FOV of 240×240 mm has a pixel size of 0.75 mm (Henwood, 1999). Hence, there is a trade-off between the size of the structure that can be imaged and

the resolution that can be achieved. The slice thickness can be also selected, but has a minimum of between 1.0 and 2.0 mm in general for clinical scanners (Spoor et al., 2000).

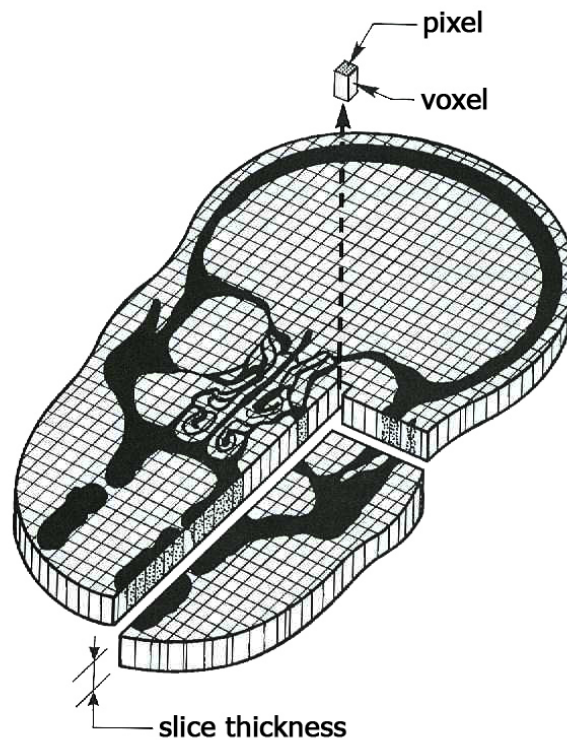


Figure 2.4 A CT slice consisting of picture elements called “pixels” and their volume elements “voxels”. Pixels arrange in rows and columns to make up a fixed matrix (adapted from Spoor et al., 2000; pg. 128).

Each voxel in a CT slice is given one CT number (value) which is a measure of the average density (the attenuation coefficient) in that volume. The attenuation coefficients are displayed as a CT value scale of typically 4096 Hounsfield units (HU), ranging from -1024 HU to $+3071$ HU (Kalender, 2005). That corresponds to 4096 grey levels in a CT slice. On this scale, water has a CT value of 0 HU and air has a value of -1000 HU (Spoor et al., 2000). Most soft tissues have values ranging

from – 100 to 100 HU, whereas values for bones range from 600 to over 2000 HU (Zatz, 1981). The human eye can typically discriminate up to a maximum of 60 to 80 grey levels (Kalender, 2005). To help the viewer discern subtle variations among the 4096 greys or determine more general patterns across the 4096 greys, the greys represented on the computer screen can be adjusted by altering the window level and the window width. The window level is chosen to correspond with the mean CT value of the structure(s) of interest, whereas the window width is adjusted to determine the CT value range over which shades of grey are to be represented (Spoor et al., 2000; Seeram, 2009). Tissues with CT values above the chosen window range will be displayed as white, while tissues with values under the range will appear black. When tissues with little attenuation difference are to be discriminated (e.g., between grey and white matter of the brain) a narrow window width is selected as well as a suitable window level (Spoor et al., 2000; Kalender, 2005). On the other hand, for tissues with large attenuation differences, for example between the lung and skeleton, a wide window width is chosen (Kalender, 2005). The effects of changing these settings are illustrated in Figure 2.5.

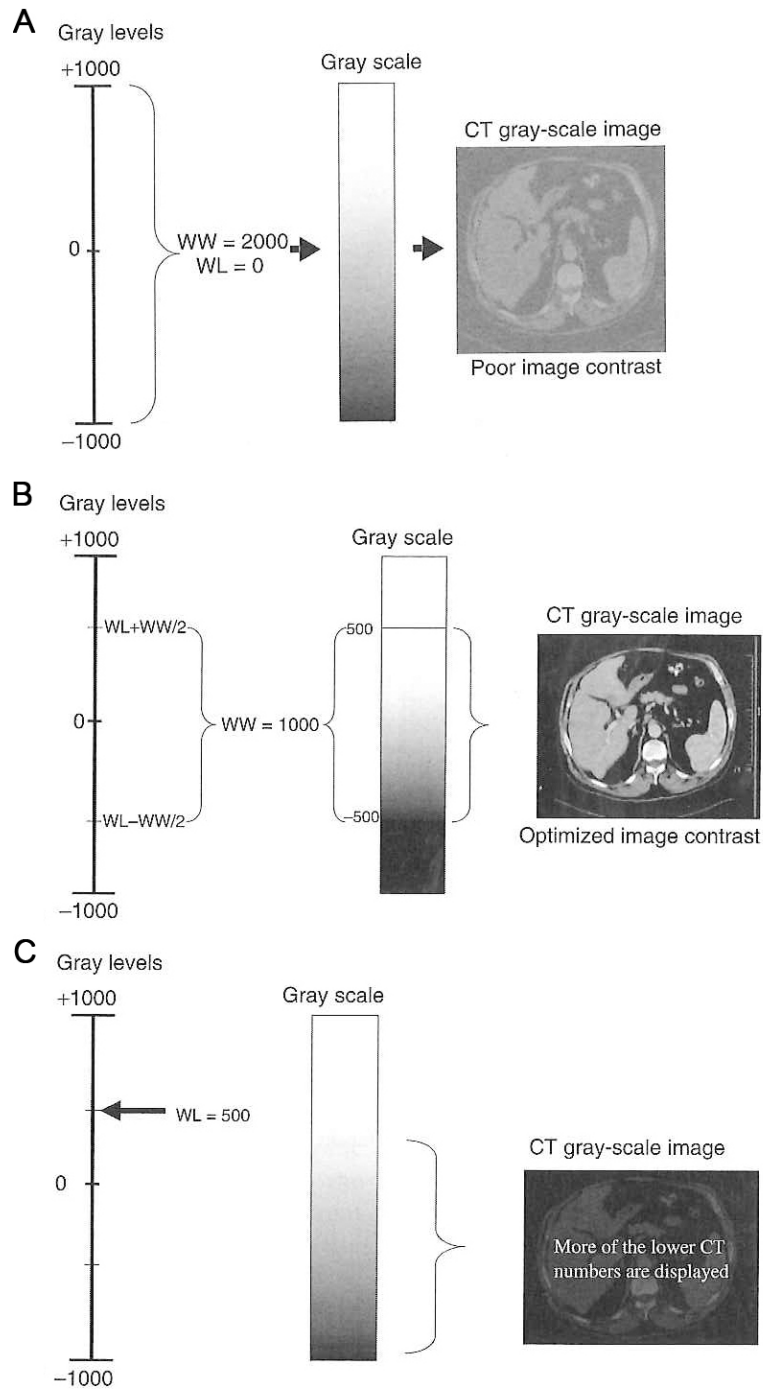


Figure 2.5 Effects of the window width (WW) and the window level (WL) on CT image quality. As the WW decreases, the contrast increases (A and B). While the WL increases, the image becomes darker (B and C) (adapted from Seeram, 2009; pg. 172-173).

The last step in data processing is storage of the reconstructed digital images. The digital images are stored as computer files in devices such as optical disks, optical tapes and hard drives (Spoor et al., 2000; Seeram, 2001). The raw data, can be also stored, subsequently retrieved and reprocessed with different parameters, such as FOV, convolution filter or CT-image bit scale, for example (Spoor et al., 2000). Care should be taken to save the files in an appropriate format that preserves the image integrity and grey scale. For instance, saving data as 8 bit (256 greys) will potentially lose approximately 94% of the data. Lossy compression formats (e.g., jpeg) are also to be avoided. The current standard image format of Digital Imaging and Communications in Medicine (DICOM) is 12 bit (4096 greys) and has an option for lossless compression. Alternatively, the digital images on the screen can be saved as files or printed as hardcopies. However, this way is not appropriate for scientific research because the window levels are set and cannot be altered to optimize the visualizations and quantification of different features (Spoor et al., 2000).

2.3.2 CT image artifacts

A CT image artifact is defined as any discrepancy between the reconstructed CT values in the image and the true attenuation coefficients of the object (Hsieh, 1995). Anything that causes an incorrect measurement of readings by detectors will result in incorrect CT values, leading to an image artifact. Artifacts appear in the image as anomalous structures not present in the scanned object. These errors can lower image quality and obscure details. Here, examples of common artifacts and possible solutions are given.

Beam hardening artifacts - Beam hardening is one of the most commonly encountered artifacts in CT scanning. The name is derived from its underlying cause: the increase in the mean energy, or “hardening”, of the X-ray beam as it passes through the scanned object. A radiation beam used in CT scanning is a polychromatic (heterogeneous) beam, the photons of which have different energies (Fig. 2.1). Beam hardening can occur when the radiation beams have different path lengths. For instance, in objects with roughly circular cross sections, the radiation path is shorter at the edge and longer across the center of the circle. There is relatively greater attenuation of the lower energy x-rays along the long path and therefore the average X-ray energy at the center of the object is higher than that at the edge (represented as lower CT values at the center and higher values at the edge of the reconstructed image). This can cause the edge to appear denser, brighter than the centre of the object irrespective of its material properties (Seeram, 2001; Barrett and Keat, 2004). There are many possible solutions to beam hardening artifacts, ranging from scanning preparation to data processing (Seeram, 2001; Castele, 2004). A popular method is to pre-harden the X-ray beam by passing it through an attenuating filter (see Section 2.2.1 and Castele, 2004).

Partial volume artifacts - Recall that a single CT value is assigned to a pixel corresponding to the X-ray attenuation within its volume element, the voxel. If the voxel contains only one tissue type, its CT value will be representative of the attenuation coefficient of that tissue. If the voxel, however, is composed of more than one tissue type with varying densities and atomic numbers, the resulting CT value will be an average (Seeram, 2001; Barrett and Keat, 2004). This is termed as “partial volume averaging”. This averaging effect is most pronounced if a small proportion of

the tissue representing the voxel is particularly dense or particularly radiotranslucent. For instance, a voxel containing 70% water and 30% enamel can appear to be bone, giving the appearance of ectopic tissues or altering the boundary between neighbouring tissues (Barrett and Keat, 2004). The artifacts may also appear as bands and streaks in the image (Seeram, 2001; Barrett and Keat 2004), reducing image sharpness (Spoor et al., 2000) and making the CT data more problematic to interpret quantitatively (Ketcham and Carlson, 2001). Partial volume artifacts can be diminished with thinner slices and smaller pixels (Barrett and Keat, 2004; Seeram, 2009) as the likelihood of encompassing more than one tissue type diminishes with improvements in spatial resolution. Improved pixel resolution can be achieved by reducing the FOV. Slice thickness can be determined by varying the thickness of linear apertures in front of the detectors (Seeram, 2009). Nevertheless, decreasing slice thickness reduces the X-ray flux on detectors, so long scanning time is desirable to improve signal-to-noise (Ketcham and Carlson, 2001).

2.3.3 Micro-computed tomography (micro-CT)

Typically the spatial-resolutions achievable with conventional CT are in the 100s of microns (Engelke et al., 1993). This is not always sufficient for the examination of small specimens or small features (e.g., trabecular bone). The development of micro-CT in the 1980s (Elliott and Dover, 1982) produced pixels in one micrometer. This technique has been developed to access small samples, for example to study small animals, microfossils, biomedical samples, and other studies for which delicate detail is desired (Kuhn et al., 1990; Shibata and Nagano, 1996; Thomson and Illerhaus, 1998).

Commercial micro-CT scanners are categorized into in-vitro and in-vivo systems (Kalender, 2005). In in-vitro imaging, the X-ray source and area detector are kept stationary, whereas the non-living sample rotates (Fig. 2.6). On the other hand, in-vivo imaging sets the X-ray source and detector to rotate around the specimen. That way the animal can be supplied with anesthetizing gas, electrodes, etc. and remain stationary during the examination (Kalender, 2005). Similar to clinical imaging, monitoring exposure time and radiation dose are important to avoid suffering from acute radiation damage. Unlike medical scanners, micro-CT scanners can produce isometric voxels (i.e., the slice thickness is equal to the pixel size) at a much higher spatial resolution, typically at 1 to 200 μm (Spoor et al., 2000; Kalender, 2005). Because of the high resolution, partial volume artifacts are less likely to occur in micro-CT. The smaller voxel sizes are reflected in the smaller anode focal-spots used in micro-CT to generate x-rays (Kalender, 2005). The downside to this is that x-ray energy levels are generally lower for a given voltage when generated from smaller focal spot compared with a large one. This can decrease the signal-to-noise and as a consequence imaging times are increased to compensate (Ketcham and Carlson, 2001; Kalender, 2005). Prolonged scan times are not desirable, but not a problem in principle if the scanned objects are not alive. The scan time per slice is typically minutes with micro-CT, while it takes only a few seconds with a medical CT instrument (Spoor et al., 2000). Micro-CT has been particularly useful for imaging matrix-filled fossils. Fossil material will often fall above the normal Hounsfield range for which medical systems are designed, resulting in lower image quality with low contrast between the mineralized bone and the matrix (Spoor et al., 2000). Micro-CT is designed to accommodate a greater range and can even be used to study rock samples (Stevenson et al., 2010).

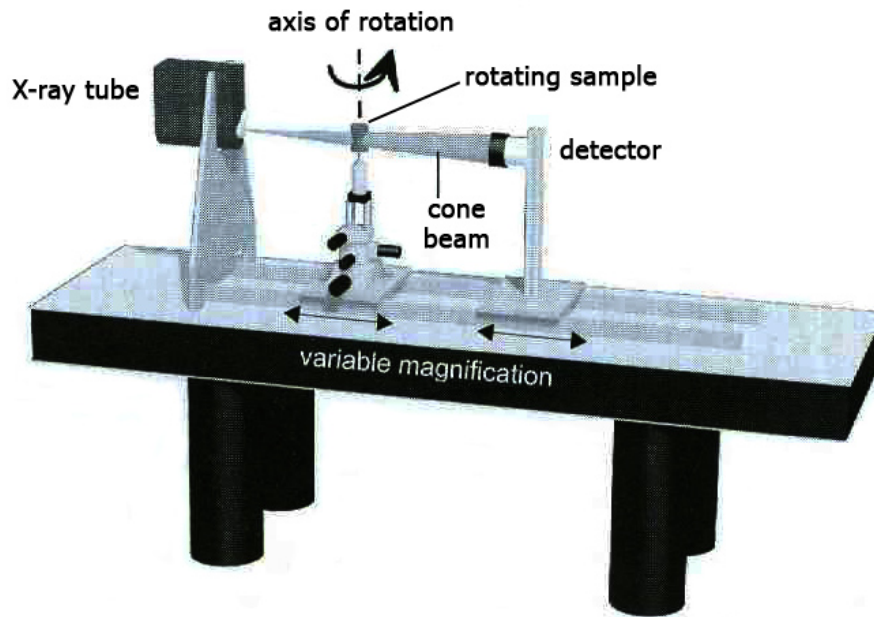


Figure 2.6 In-vitro micro-CT setup (adapted from Kalender, 2005; pg. 228).

2.3.4 Processing and visualization of images

After CT slices are produced by X-ray scanning, a series of contiguous slice images is stacked to provide a 3D data set of the scanned object, using computer graphic techniques. The 3D stack of data can be analyzed and visualized using a variety of methods. The following section reviews some of the most common methods for representing a stack in a 3D space.

Multiplanar reformatting (MPR) - This is one of the most popular techniques to create images for display on a computer screen (Hsieh, 2003). This technique is used to generate images in planes other than the original stack; e.g., the creation of coronal, sagittal or oblique images from an original stack of transverse data set of images. The image generated is either perpendicular (called orthogonal reslicing) or placed at an angle to the original image plane. The quality of reformatted images depends on the quality of the original images. If the planes are thick, it will lead to blurring and

loss of structural detail (Seeram, 2009). In micro-CT imaging, isometric voxels of the image stack can be generated, hence a good spatial resolution of reformatted images, as in the original images, can be achieved (Spoor et al., 2000; Seeram, 2009).

Surface rendering - This technique transforms the 3D data set into a 3D simulated image displayed on a computer monitor. The 3D reconstruction provides a better and more realistic detailed description of the overall morphology (Spoor et al., 2000). Surface rendering generally consists of three steps. The first step, segmentation, is used to determine the tissue of interest to be viewed in the 3D reconstruction. The segmentation process is performed discretely in each CT slice, commonly by thresholding for the range of CT values characterizing the relevant material (Spoor et al., 2000; Seeram, 2001). To improve segmentation, manual drawing and specialized edge detection algorithms are used to determine specific parts of interest and to exclude unwanted regions from the 3D reconstruction (Spoor et al., 2000). In the second step, the boundary lines of the chosen tissues in each slice are combined to form a 3D surface image of that tissue (Spoor et al., 2000). The last step is to add photorealism and create the illusion of depth in the image, improving its appearance in three dimensions and bringing out surface details (Spoor et al., 2000; Seeram, 2001). Typically, a simulated light source can be positioned to direct the light toward the surface of the image at different locations. For shaded surface display, the computation is based on how much light emitted by the source is reflected by each surface point toward the observer. A brighter surface point means that more light is reflected toward the eyes of the observer, compared with a darker point (Seeram, 2001).

Surface rendering has the advantage that it does not require a lot of computing power, since it does not use all the voxel information in the 3D data set; i.e., typically less than 10% of the data set (Heath et al., 1995). Only contour information is used to create the 3D image. This, however, leads to poor image information content because no information about structures inside or behind the surface is displayed. In addition, partial volume averaging artifacts can occur in segmentation (Spoor et al., 2000; Seeram, 2001). This results in incorrect CT values of the tissue to be imaged, not corresponding to the range of CT values selected in segmentation. Therefore, the process of thresholding is important to determine which range yields the most accurate depiction of the actual anatomical structures (Kalender, 2005).

Volume rendering - Another display technique that generates a 3D image on the monitor from the slice data is volume rendering. In this method, up to 100% of the data volume can contribute to the reconstruction (Heath et al., 1995). Different brightness levels and different degrees of opacity are assigned to each voxel according to its CT value. Subsequently, image projection is used to render the data volume description by way of ray-casting. A simulated ray is sent through the data volume along the viewing orientation. All CT values of the voxels through which the ray travels are calculated to determine the intensity or colour of a pixel on the screen for that ray. The 3D image produced by volume rendering has a better quality and provides more information than surface rendering because it allows the observer to examine both external and internal morphologies. However, volume rendering requires more computing power, hence more expense and more time for its operation (Heath et al., 1995; Spoor et al., 2000; Seeram, 2001). Additionally, interfaces and surfaces in volume rendering are fuzzy and are not suitable for

defining the exact boundaries between, for example, bone and air (Spoor et al., 2000).

Maximum intensity projection (MIP) - MIP is a special case of the volume rendering, which is now used frequently in computed tomography angiography, or CTA (Seeram, 2001; Hsieh, 2003). Like surface rendering, MIP makes use of less than 10% of the 3D data set (Heath et al., 1995). The MIP program displays a 2D image on a computer screen. A mathematical ray is projected from the observer's eye and passes through a set of voxels in the data volume along its path. Only the voxel with the maximum intensity (brightest or greatest value) is chosen by the MIP program (Seeram, 2001). This selected voxel intensity is displayed directly in the corresponding pixel of the MIP image (Fig. 2.7). To enhance 3D impression, a series of MIP images that varies only slightly in viewing angles can be generated and viewed in a cine loop (Seeram, 2001).

A limitation of the MIP technique is its inability to differentiate superimposed structures because only one voxel in the set of voxels encountered by the ray is used in the MIP image display. However, MIP has the considerable advantage of analyzing the vascular structures and has become the most popular rendering technique in CTA (Seeram, 2001), since vessels containing contrast medium are clearly seen. Moreover, because it uses less than 10% of the 3D data set, its computational cost is lower and the time to produce the images is considerably less than volume rendering (Heath et al., 1995; Seeram, 2001). Continued advances in desktop computing power now allow for volume rendering of large micro-CT datasets

in the laboratory, though surface renderings as still preferred due to the greater surface and boundary fidelity.

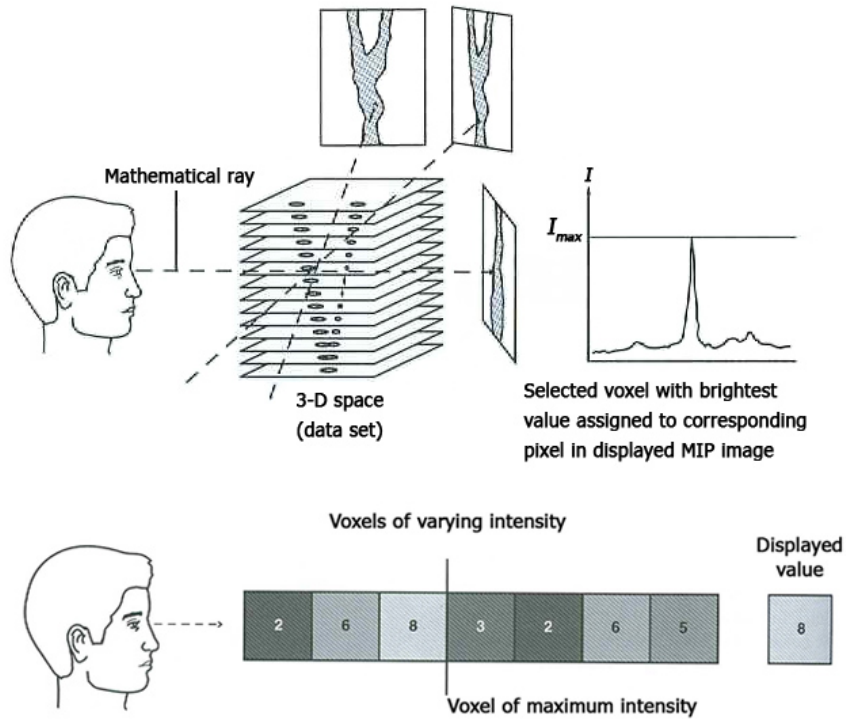


Figure 2.7 Maximum intensity projection (MIP). The voxel with the maximum intensity found along each ray path is used directly for display (adapted from Seeram, 2001; pg. 293-294).

Chapter 3 Review: analyzing the cochlear form

Comparing the anatomical traits of organisms has been a fundamental part of biological research for centuries. Studies of both taxonomic classification and biodiversity of organisms are traditionally based on descriptions of morphological forms (Richtsmeier et al., 2002; Adams et al., 2004). Conventional morphological approaches are typically qualitative literature with detailed descriptions or pictures. During the early twentieth century, biological sciences transitioned from a purely descriptive approach to a more quantitative one (Bookstein, 1998). Morphological analyses included data for measurable traits, which were displayed as tables and compared across groups. By the mid-twentieth century, the development of statistical methods allowed researchers to improve the rigour and repeatability of their comparisons within and among groups, and the modern area of morphometrics commenced (Adams et al., 2004).

3.1 Traditional morphometrics

Morphometrics aims to examine shape variation and covariation with other variables (Adams et al., 2004). Traditional morphometrics is the application of multivariate statistical analyses to collections of morphological variables that are measurements of linear distances, angles, areas and ratios (Rohlf, 1999; Adams et al., 2004). The traditional scheme could be considered a measurement of size rather than shape since linear distance measurements are usually highly correlated with size (Bookstein et al., 1985). These data sets hold relatively little information about shape and some of that information is fairly ambiguous. As a result, attempts were made to develop methods for separating information about shape from size, typically

involving ratios of different measures. These are not wholly effective for several reasons. First, several different methods have emerged giving different answers and it is not always clear which is the most appropriate for any given question (Parsons et al., 2003; Adams et al., 2004). Second, the measurements may not sample homologous features of organisms, so the linear distances measured (e.g., maximum body width) might not be comparable anatomically from species to species, or even from specimen to specimen (Adams et al., 2004; Zelditch et al., 2004). Lastly, it is feasible that two objects with different shapes can produce the same set of ratios, for example in values of maximum length and maximum width measured on both an oval and a teardrop (Adams et al., 2004). In effect, linear distances measured in traditional morphometrics convey no information about the geometry of the original object (Adams et al., 2004; Zelditch et al., 2004). Therefore, it is impossible to generate graphical representations of shape from these linear distances. Nonetheless, these approaches remain useful in cases where linear and angular data are provided, and can detect change, though not how (Richtsmeier et al., 2002). For the analyses of more subtle patterns of change, a new series of methods was required.

3.2 Geometric morphometrics

Owing to the problems in traditional morphometrics, researchers explored alternative methods to analyze and depict shape differences (e.g., Rohlf and Marcus, 1993; Bookstein, 1998). Data that preserve the geometry of biological structures are highly desirable, and methods to analyze such data have gradually developed with improvements in the theoretical ideas and more importantly with improvements in

computers that allow these ideas to be put into practice. The result is a rigorous statistical theory for shape analysis, which opens an opportunity to combine the use of multivariate statistics and methods for visualizing statistical relationships in biological form. This is the basis to a collection of methods referred to as geometric morphometrics (Rohlf and Marcus, 1993).

Capturing geometry by way of landmark data is a widespread method used in studies for morphometric analysis (Richtsmeier et al., 2002). Landmarks are precise locations on biological forms that contain some developmental, functional, structural, or evolutionary significance (O'Higgins, 2000; Richtsmeier et al., 2002). Landmarks are located as two- or three-dimensional coordinates, and must be present correspondingly on all specimens studied. There are three types of landmarks (Bookstein, 1991; O'Higgins, 2000): type I landmarks- landmarks whose claimed homology from case to case is supported by strong evidence of structure or histology, etc.; type II landmarks- landmarks defined by relative locations, for example the tooth tip. This type includes landmarks which are not homologous in a developmental or evolutionary aspect but which are equivalent functionally; e.g., wing tips (O'Higgins, 2000); and type III landmarks- landmarks that characterize more than one location of the form, not a specific location, such as tip of a rounded bump. Type III includes landmarks defined relative to other landmarks; e.g., the midpoint between landmarks X and Y (Bookstein, 1991). In terms of utility, the third type leads to greater error in data than the others, and is often weighted against in analyses (O'Higgins, 2000). Consideration should also be given to the limited availability of type II and particularly type I landmarks in comparison to type III when selecting which set of landmarks to use.

Once collected, the landmarks coordinates cannot be directly analyzed as variables because the effects of variation in position, scale and orientation of the configurations (specimens) still exist (Adams et al., 2004). This non-shape variation must be removed so that the coordinates of the final configurations can be used to statistically analyze shape differences between objects. Superimposition is a technique developed to eliminate non-shape variation in landmark configurations. Many superimposition methods have been proposed but the most widely-used method is Generalized Procrustes Analysis, or GPA (Zelditch et al., 2004; Slice, 2007). GPA superimposes configurations of landmarks using least-squares estimates for translation and rotation parameters (Adams et al., 2004; Slice, 2007). First, the location of the center of configurations, called the centroid, is determined, and the centroid of each configuration is translated to the same position, resulting in removal of position differences. Then, the centroid size of each configuration is calculated and used to scale the configurations to the same unit size to remove differences in scale. Lastly, each configuration is optimally rotated to align with others so that the squared differences between corresponding landmarks are minimized. After superimposition, the entire landmark configuration of each specimen, not individual landmarks, is usable as a shape variable, and the differences in coordinates of corresponding landmarks between specimens are used as data in multivariate analyses of comparing shape variation (Adams et al., 2004; Zelditch et al., 2004).

Using landmarks has become the most widely accepted approach, since landmarks are reputable and give geometric information in terms of the relative location of points, and since various methods are developed for their analysis (Richtsmeier et

al., 2002). Nevertheless, landmark-based geometric morphometrics do not solve all the problems in traditional morphometrics. One remaining problem is that the analysis discretizes a continuum and therefore the overall and relative density of landmarks sampled is an important consideration. Too many landmarks and the bias will tend towards type III and the analysis will be computational demanding. Too few and potentially salient features of morphology are ignored (Adams et al., 2004). Landmarks are particularly poor at conveying information on the curves, spaces or surfaces between them (Richtsmeier et al., 2002; Zelditch et al., 2004). Consequently, the accurate information concerning form changes occurring between landmarks cannot be acquired. An alternative solution is the sliding semi-landmark method (Adams et al., 2004). The semi-landmarks are placed equidistantly in sequence along an outline or midline curve. Importantly, like general landmarks, it has to be ensured that the semi-landmarks are present correspondingly across the entire samples (Adams et al., 2004).

3.2.1 Procrustes superimposition and morphometric spaces

The generalized Procrustes superimposition is the generally favored superimposition method. Today, almost all landmark-based morphometric studies analyze shape with procedures based on the Procrustes approach (Adams et al., 2004; Slice, 2007). Comprehension of GPA principles allows researchers to understand the data form used in studies based on ordination methods, such as principal components analysis, or in studies using multivariate statistics. The basics of GPA and morphometric spaces concerned with it are described as follows.

3.2.1.1 Configuration matrix and configuration space

An entire configuration of landmarks is represented as a configuration matrix. It is a $k \times m$ matrix of Cartesian coordinates, where k is the number of landmarks and m is the number of coordinates (Dryden and Mardia, 1998). Every configuration of k landmarks having m coordinates can be thought of as a point in a space with $k \times m$ dimensions called configuration space or figure space (Rohlf, 1999; Zelditch et al., 2004). Therefore, the configuration space encompasses all matrices representing landmark configurations with the same number of k landmarks and m coordinates. The location of a configuration matrix is at the centroid of that matrix. In geometric morphometrics, the most widely-used size measure is the centroid size (Zelditch et al., 2004). For each configuration, the centroid size is the square root of the sum of the squared distances of the landmarks from the centroid (Bookstein, 1991). In configuration space, configuration matrices can be different in position, size and orientation, as well as shape.

3.2.1.2 Pre-shape space

The next step is to move configuration matrices from the configuration space to the pre-shape space. It is the surface of a hypersphere of radius one, on which all $k \times m$ configurations are arrayed. There are two restrictions placed on each configuration: 1) each is centered at the origin, and 2) each centroid size is scaled to be unit size of one (Dryden and Mardia, 1998; Rohlf, 1999). These are the operations of translation and scaling, used to eliminate the effects of differences in location and scale, but those do not alter shape. The effects of rotation, however, have not yet removed. Thus, it has not yet attained Kendall's (1977) definition of shape, where all three effects are filtered out from each configuration. Because of the centering and the

scaling, the number of dimensions in pre-shape space has $m+1$ fewer dimensions than the configuration space. In other words, it is $km-(m+1)$ dimensions (m dimensions are lost due to the centering and one dimension is lost due to the scaling) (Zelditch et al., 2004). For the simplest case, triangles in the plane ($k = 3$ and $m = 2$), the pre-shape space for triangles has three dimensions. Points representing individual configurations of landmarks are ranged on the three-dimensional surface of a four-dimensional hypersphere (Rohlf, 1999; Zelditch et al., 2004). In pre-shape space, configurations may be different in rotation, in shape or in a combination of the two. Landmark configurations that are different only in rotation are located at different points, as are configurations that differ only in shape (Zelditch et al., 2004).

Zelditch et al. (2004) have proposed the concept of a fiber that is a circular arc lying on the surface of a hypersphere. All points in pre-shape space representing all possible rotations of a landmark configuration lie along the same fiber (Zelditch et al., 2004). In other words, configurations that have the same shape but differ only in rotation are located along the same fiber. The shortest distance of an arc crossing the surface from one fiber to the other is used for defining the distance between configurations in space. This distance is also the distance between shapes in pre-shape space since configurations in different fibers are different in shape. The length of this shortest arc is known as the Procrustes distance (Rohlf, 1999; Zelditch et al., 2004). Because the hypersphere is one in radius, the length of the arc is the value in radians of the angles subtended (ρ).

3.2.1.3 Shape spaces

In the shape space, one configuration on each fiber is selected, eliminating differences in rotation. Hence, each point in the shape space represents the shape of a landmark configuration, which is irrespective of position, size and rotation. The shape space has fewer dimensions than the pre-shape space from which it develops. In the transition between the two spaces, $m(m-1)/2$ dimensions are lost. The lost dimensions are differences in rotation that are removed, reflecting the number of axes on which a configuration can be rotated around its centroid (Zelditch et al., 2004). In the case of triangles, the lost dimension is one, and therefore its shape space is two dimensions; i.e., the two-dimensional surface of a three-dimensional sphere with a radius of one (Rohlf, 1999; Zelditch et al., 2004; Fig. 3.1). The lower half of the sphere is a reflection of the upper. Because shape spaces in other cases are more complex, namely the higher dimensionality of a shape space that is not on a ball-shaped sphere, triangles represent a logically simple geometry to demonstrate as follows.

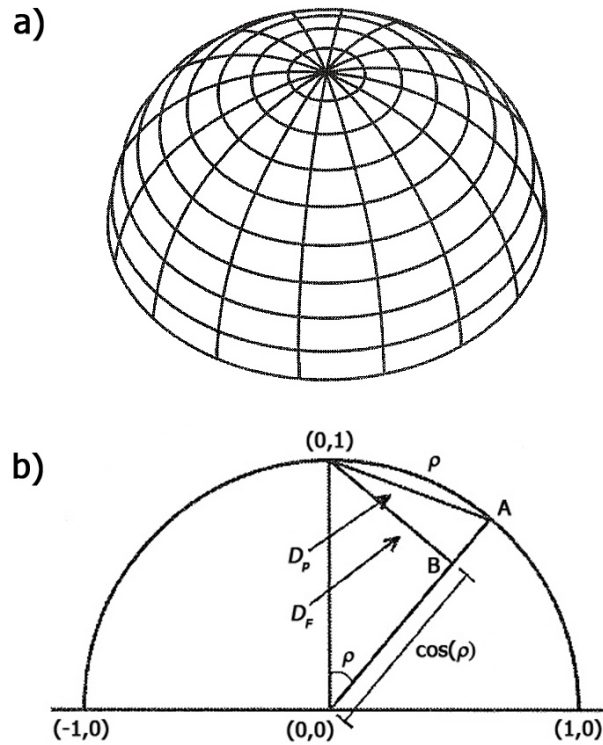


Figure 3.1 The space of Procrustes-superimposed triangles. a) The hemisphere of the space of triangles that have been centered and scaled to centroid size of one. The space is oriented so that the point representing the reference configuration is located at the north pole. The lower hemisphere (not shown) is a reflection of the upper. b) A slice through the polar axis of the space of aligned triangles, showing the distances between the reference and shape A. The arc length is the Procrustes distance (ρ), the length of the chord within the hemisphere is the partial Procrustes distance (D_p), and the shortest possible distance is the full Procrustes distance (D_f), producing the configuration B (adapted from Zelditch et al., 2004; pg. 84-85).

To construct a shape space, firstly, one shape in a convenient orientation is chosen from a pre-shape fiber to serve as the reference configuration. Every other shape called a target configuration is chosen as the rotation corresponding to the point of closest approach of its fiber to the reference (Zelditch et al., 2004). This means that the orientation is selected to minimize the Procrustes distance between the

reference and the target. Using the criterion of the point of closest approach, each pre-shape fiber is reduced to a single point (a shape), and configurations in the shape space are thus different only in shape (Zelditch et al., 2004). The Procrustes distance (arc length), however, is not the shortest possible distance between shapes (Fig. 3.1). The chord of the arc connecting fibers and passing through the inside of the hemisphere is shorter. The length of the cord is called the partial Procrustes distance (Fig. 3.1). Accordingly, at the points of closest approach, it appears that the square root of the summed squared distances between the coordinates of corresponding landmarks is minimized. Configurations that conform to this condition are considered to be in partial Procrustes superimposition (Rohlf, 1999; Zelditch et al., 2004).

Nonetheless, the partial Procrustes distance is still not the shortest possible distance between configurations. The square root of the summed squared distances between corresponding landmarks can be further reduced by changing the constraint on the centroid sizes of configurations. Traditionally, the centroid size of the reference is still maintained at one, but the centroid size of the target is rescaled to centroid size of $\cos(\rho)$ instead of one (Slice, 2001; Zelditch et al., 2004). The resulting distance between configurations (shapes) is $\sin(\rho)$ and is termed the full Procrustes distance (Fig. 3.1). Configurations that meet this condition are considered to be in full Procrustes superimposition (Rohlf, 1999; Slice, 2001; Zelditch et al., 2004).

The set of shapes of triangles in full Procrustes superimposition consists of a new shape space (sphere) with a radius of one-half, within the larger hemisphere of shapes in partial Procrustes superimposition, and tangent to the larger hemisphere

at the reference shape (Rohlf, 1999; Slice, 2001; Zelditch et al., 2004). This new smaller, inner sphere is Kendall's shape space (Fig. 3.2). It is the set of centered shapes where each is at the size and orientation that have the shortest distance from the reference (Zelditch et al., 2004).

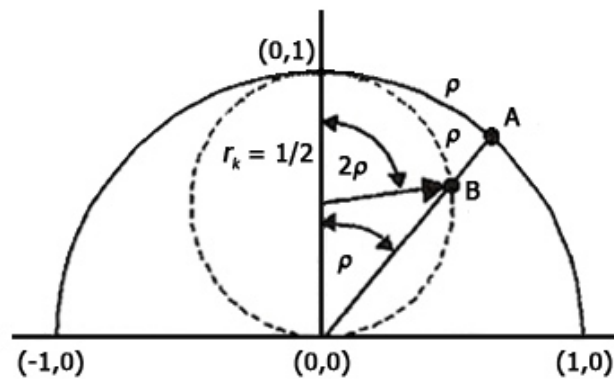


Figure 3.2 The relationship between Kendall's shape space and the space of aligned triangles scaled to centroid size of one. The outer half circle is a cross-section of the space of aligned triangles scaled to centroid size of one. The inner circle is a cross-section of Kendall's shape space with a radius of $1/2$. The centroid size of triangles in Kendall's shape space is scaled to $\cos(\rho)$. Points A and B represent the same shape but differ in centroid size; i.e., A at centroid size of one in partial Procrustes superimposition and B at centroid size of $\cos(\rho)$ in full Procrustes superimposition (adapted from Rohlf, 1999 [pg. 204] and Zelditch et al., 2004 [pg. 86]).

For landmark configurations that are more complicated than triangles, the same set of processes to move from pre-shape space to partial Procrustes shape space and Kendall's shape space can be applied (Zelditch et al., 2004). Irrespective of the number of landmarks and the number of their coordinates, the transitions involve: 1) choosing the rotations located at the shortest distance from the reference in pre-shape space, and 2) rescaling the centroid sizes to adopt the value that completely

minimizes the distance from the reference (Zelditch et al., 2004). The higher dimensionality of hyperspheres cannot be converted into Kendall's shape space by simply making the centroid sizes equal to $\cos(\rho)$ (Rohlf, 1999; Slice, 2001). For higher dimensionality, the geometry of shape space and intuitive visualization are more complicated, so the conversion into Kendall's shape space needs processes of higher mathematics.

3.2.1.4 Tangent space

All the spaces mentioned above, including Kendall's shape space, are curved and non-Euclidean spaces. Therefore, standard Euclidean methods cannot be used to analyze shapes in Kendall's shape space (Slice, 2001; Zelditch et al., 2004). Representations must be transferred from the Kendall's shape space to a Euclidian space for any meaningful statistical analysis to proceed. The replacement of the curved space with a Euclidian approximation involves the projection of a tangent plane (Rohlf, 1999; Slice, 2001; Zelditch et al., 2004).

In the case of triangles, a Euclidian plane is a linear space tangent to both Kendall's shape space (the inner sphere) and the Procrustes hemisphere, at the reference shape (Rohlf, 1999; Slice, 2001; Zelditch et al., 2004; Fig. 3.3). There are two common ways of projecting from one space onto another (Slice, 2001; Zelditch et al., 2004). The first is the stereographic projection, which is the approach to projecting from the centroid of some reference space to the new space. The other is the orthogonal projection, in which the projection is done along lines that are perpendicular to the new space. The latter approach is the same way as the projection of a map of the earth onto a flat piece of paper by a cartographer (O'

Higgins, 2000). Distances between points in the linear tangent plane approximate the distances in the Procrustes methods between corresponding landmark configurations. In the stereographic projection, it is not important whether the projection to the tangent plane is from the hemisphere of shapes in partial Procrustes superimposition, or from the sphere of shapes in Kendall's shape space. The projection of both target configurations onto the tangent plane is the same position (Slice, 2001; Zelditch et al., 2004; Fig. 3.3). By contrast, in the orthogonal projection, the projection from partial Procrustes shape space and from Kendall's shape space gives different results. The projection from the Procrustes hemisphere generates distances closer to the partial Procrustes distance, and the projection from Kendall's shape space generates distances closer to the full Procrustes distance (Slice, 2001; Zelditch et al., 2004).

The usefulness of any projection depends on how accurately Procrustes distances are preserved in the tangent space (Slice, 2001). It is found that the orthogonal projection from the hemisphere of shapes in partial Procrustes superimposition is generally the preferred linearization (Slice, 2001). Such a projection more accurately approximates the Procrustes shape distances than either projection from Kendall's shape space (Rohlf, 1999; Slice, 2001). Moreover, it is more easily accessible with existing morphometric software (Slice, 2001). For a small amount of shape variation, however, any of these linearization methods should bring about similar results (Slice, 2001). At this stage of geometric morphometrics, the coordinates of points representing specimens are no longer located along curved spaces, but across a linear plane in which statistical analyses can be carried out.

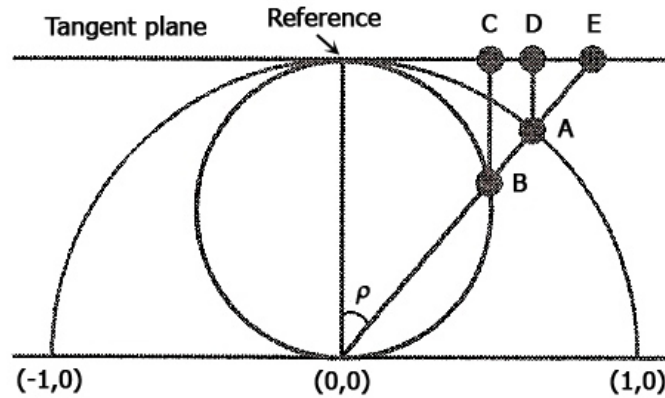


Figure 3.3 The projection of points representing triangles onto a space tangent to the reference shape. Point B represents a triangle scaled to centroid size of $\cos(\rho)$ in Kendall's shape space. Point A is the same shape as B but is scaled to unit centroid size in the Procrustes hemisphere. C is the orthogonal projection of B onto the tangent plane. D is the orthogonal projection of A onto the tangent plane. E is the stereographic projection of B onto the tangent plane (adapted from Slice, 2001 [pg. 146] and Zelditch et al., 2004 [pg. 95]).

3.2.1.5 Reference configuration

Many processes that place target configurations in shape spaces, or in the Euclidean space, are associated with a reference shape (Zelditch et al., 2004). As a result, selecting the reference shape is an important and fundamental operation. If it is a comparison of shapes between only two specimens, one configuration will be chosen to be the reference, and the second configuration is then rotated to minimize the partial Procrustes distance. This approach is referred to as Ordinary Procrustes Analysis, or OPA (Slice, 2001). Most research questions in the biological sciences, however, are associated with the analysis of more than two specimens and their landmark configurations. In such cases, one feasible reference is the average shape of all specimens (Zelditch et al., 2004). All configurations are rotated to optimal alignment on a trial reference configuration (probably the first configuration). Then,

the mean shape of these aligned specimens is estimated, and all configurations are rotated to optimal alignment on the mean shape, which is the new reference. At this step, the computation of the average shape is repeated. If it is different from the previous reference, calculation of the rotations will be repeated using this newest reference. The iterations continue until the newest reference is the same as the previous (Zelditch et al., 2004). This approach is referred to as Generalized Procrustes Analysis (GPA) and has the advantage that the average distance from the reference is minimized, which in turn minimizes the average distortions of inter-specimen distances projected to the Euclidean space (Rohlf, 1998; Zelditch et al., 2004).

Another consideration in choosing the reference shape is whether it symbolizes the starting point of some biological process of interest. The advantage of this approach is that the difference between target and reference can be construed as biological transformation in addition to mathematical transformation (Zelditch et al., 2004). Nevertheless, the reference is at the periphery of the observed distribution of shapes, and distortions of the distances among specimens are increased for points away from the reference (Slice, 2001). Hence, the risk of distortions of Euclidean distances in the tangent plane increases when changes in shape are large (Rohlf, 1998). Other references can be used, but it remains to be determined whether or not Euclidean distances in the tangent space are accurate approximations of the distances in shape space.

3.2.2 Analysis of shape differences

After GPA superimposition and the projection onto the Euclidian space, the coordinates of points representing specimens are converted to shape variables, which can be used as data in multivariate statistical analyses of shape variation (e.g., Slice, 2001; Zelditch et al., 2004). One of the most common tools used for describing the diversity of shapes among specimens is principal component analysis, or PCA (Fig. 3.4). The patterns of variation and covariation in shape variables are typically complicated and difficult to interpret (Zelditch et al., 2004). PCA can simplify those complex patterns and make them easier to understand by converting the original variables into a set of linearly uncorrelated variables called principal components (PCs). Another benefit of PCA is that most of the overall variation in a data set can typically be explained with only a few PCs (Parsons et al., 2003; Zelditch et al., 2004). Each projection of the shape space onto a tangent space is considered as two principal components of the shape (x,y) and the positions of the individual specimens on the PCs are determined in terms of PC scores. Each PC is then ordered according to the amount of variation represented within it, with those components describing the most shape variation given the lowest numbers (e.g., PC1). The scores of different PCs are then compared in bivariate plots. As the PCs plots intersect at the average shape of all specimens, the values of PC scores will indicate the distances of specimens from the average in the directions of the PCs (Zelditch et al., 2004). The pattern of clustering of individuals on PC plots represents similarities and differences in shapes among individuals. The differences found on the PCs, however, do not represent evidence of statistical significances. Testing the hypothesis for statistically significant differences can be carried out by other multivariate methods, depending on specific purposes; e.g., discriminant function

analysis for testing shape differences between groups, and permutation test for the presence of phylogenetic signals.

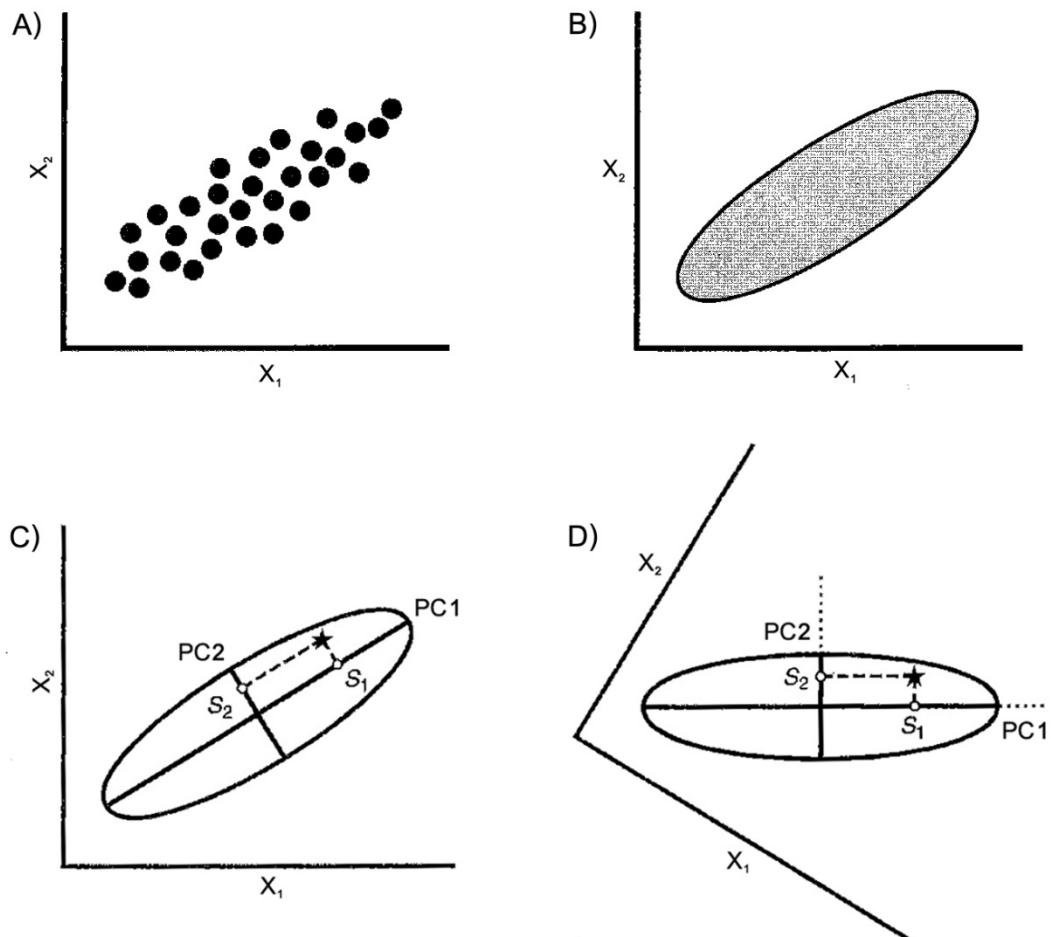


Figure 3.4 Graphical representation of the principles of PCA. A) Scatter plots of individuals on X_1 and X_2 axes. B) The distribution of points shown in A) is summarized by an ellipse. C) The star is the location of an individual in the sample. The distances of S_1 and S_2 from the intersection of PC1 and PC2 are the scores of the star on PC1 and PC2. D) The figure C) is rotated in order that PCs are aligned with the rims of the page. The scores on these axes are the position of the individual in the new coordinate system of PCs (adapted from Zelditch et al., 2004; pg. 157 and 160).

The last step of a morphometric analysis is graphical representations of the statistical results. Shape differences between landmark configurations can be depicted in two visual fashions: thin-plate spline deformation grids or vectors of relative landmark displacement (O'Higgins, 2000; Adams et al., 2004; Zelditch et al., 2004; Slice, 2007; Fig. 3.5). For the former deformation technique, the main principle is that the reference object, usually the mean shape, is deformed into the target object so that corresponding landmarks in the two objects are mapped to each other exactly (Richtsmeier et al., 2002; Adams et al., 2004). The amount of energy required to bend a theoretical thin plate of metal to map landmarks from the reference to the target is minimized (Richtsmeier et al., 2002). Shape differences between objects can be described using the change in the grid in terms of regions of expansion and bending (Rohlf, 1999). For the technique of vector displacement, vectors represented by arrows are drawn between a landmark in the initial configuration and the same landmark in the target configuration (Viscosi and Cardini, 2011). This technique depicts shape differences via the magnitude and direction by which a landmark is displaced relative to another. In contrast to the deformation method, the shape variation examined by this method depends on the type of superimposition used, possibly leading to different results of shape differences (Rohlf, 1999; Viscosi and Cardini, 2011). The thin-plate spline deformation grid seems more effective and commonly used in illustrating the overall shape differences between objects (Rohlf, 1999; Viscosi and Cardini, 2011). Both techniques, however, will produce the most accurate result of shape variation if changes at particular landmarks are interpreted in the context of the whole landmark configuration (Rohlf, 1999; Slice, 2007; Viscosi and Cardini, 2011).

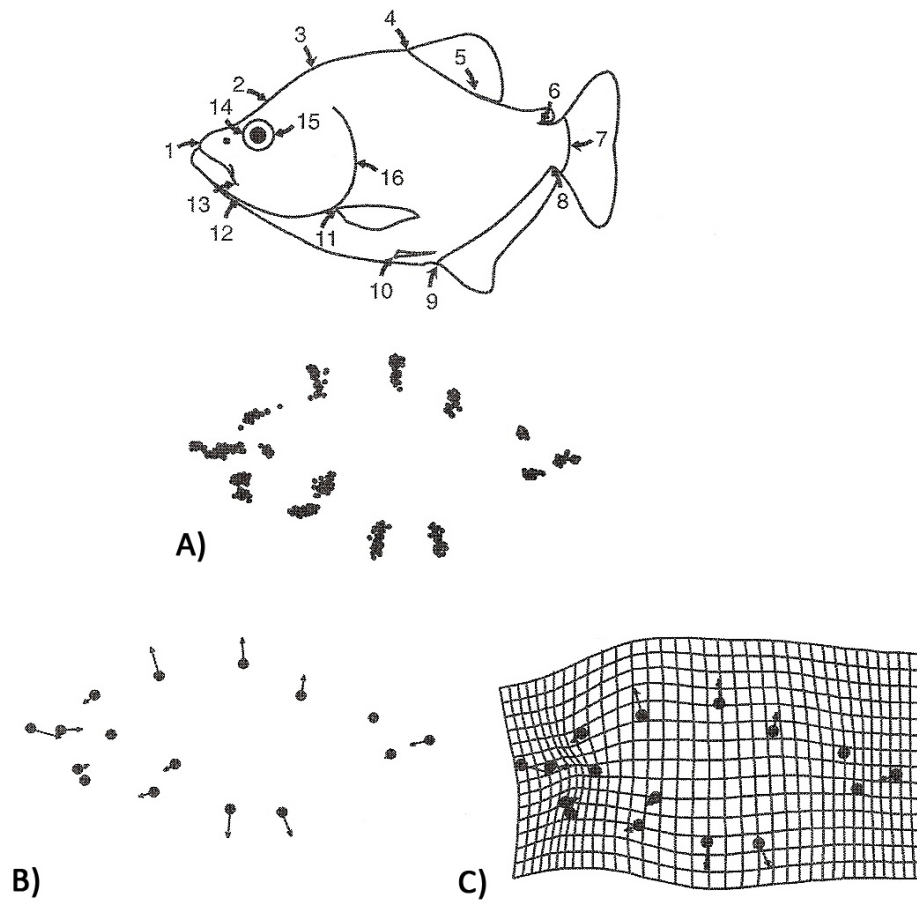


Figure 3.5 Ontogenetic shape variation visualized by Procrustes superimposition. A) Landmark configurations from which differences in position, scale and orientation have been eliminated. The shape variation can be depicted in two styles: B) vectors of relative landmark displacement, and C) a thin-plate spline deformation grid (Zelditch et al., 2004; pg. 8).

Chapter 4 Materials and methods

In the present thesis, there were two studies: an adult interspecific study and a human developmental study. Samples, 2D and 3D image processing, measurement protocols and statistical methods that were used in both studies are presented in this Chapter.

4.1 Samples

4.1.1 Adult interspecific study

The cochleae representing 45 extant eutherian mammals (one sample per species) were included in the study. Data on body mass were taken from Silva and Downing (1995). When sex was known, the average body mass for that sex was used. If sex was unknown, the average body mass was calculated from values for both sexes. Specific information concerning taxonomy and eco-behavioural traits was taken from Walker's Mammals of the World (Nowak, 1999; Table 4.1 and 4.2). The eco-behavioural characteristics included:

1. Habitat selection. It was categorized as terrestrial, fossorial, subterranean, flying, semi-aquatic, or marine.
2. Active time. It was classified according as diurnal, nocturnal or crepuscular.
3. Sociality. It was classified into two general categories: solitary and gregarious.

Audiograms of the species studied were obtained from many different sources (see Table 4.3). Images of the whole skulls from Takahashi (2005) were downloaded and used for calculating the intermeatal distance (distance between the left and right external auditory meatuses) with ImageJ software (v. 1.42q; Rasband, 2012).

Audiograms and intermeatal distances were classified into categories as shown in Table 4.4. These were categorized according to data intervals to represent discrete groups and to provide a similar number of specimens in each category.

Table 4.1 Taxonomy of 45 mammalian species studied.

Order	Species	Common name	ID
Artiodactyla	<i>Bos primigenius</i>	Aurochs	Bp
	<i>Camelus dromedarius</i>	Dromedary	Cd
	<i>Hippopotamus amphibius</i>	Hippopotamus	Ha
Carnivora	<i>Puma concolor</i>	Cougar	Pc
	<i>Felis catus</i>	Cat	Fc
	<i>Vulpes vulpes</i>	Red fox	Vv
	<i>Ailurus fulgens</i>	Red panda	Af
	<i>Mephitis</i> sp.	Skunk	Me
	<i>Procyon lotor</i>	Common raccoon	Pl
	<i>Taxidea taxus</i>	American badger	Tt
	<i>Lutra lutra</i>	Otter	Ll
Cetacea	<i>Tursiops truncatus</i>	Bottlenosed dolphin	Tu
	<i>Delphinapterus leucas</i>	Beluga whale	Dl
Chiroptera	<i>Eptesicus fuscus</i>	Big brown bat	Ef
Insectivora	<i>Talpa europaea</i>	European mole	Te
	<i>Talpa occidentalis</i>	Spanish mole	To
	<i>Neamblysomus</i> sp.	Golden mole	Ne
Perissodactyla	<i>Equus caballus</i>	Domestic horse	Ec
Pinnipedia	<i>Odobenus rosmarus divergens</i>	Walrus	Or
	<i>Mirounga angustirostris</i>	Northern elephant seal	Mi
Primates	<i>Arctocebus calabarensis</i>	Calabar potto	Ac
	<i>Tarsius bancanus</i>	Horsfield's tarsier	Tb
	<i>Aotus trivirgatus</i>	Northern night monkey	At
	<i>Daubentonia madagascariensis</i>	Aye-aye	Dm
	<i>Saimiri sciureus</i>	Common squirrel monkey	Ss
	<i>Cebus apella</i>	Brown capuchin	Ca
	<i>Homo sapiens</i>	Human	Hs
	<i>Galago senegalensis</i>	Senegal bushbaby	Gs
Proboscidea	<i>Loxodonta africana</i>	Savanna elephant	La
Rodentia	<i>Mus musculus</i>	Mouse	Mm
	<i>Glaucomys volans</i>	Southern flying squirrel	Gv
	<i>Rattus norvegicus</i>	Rat	Rn
	<i>Cavia porcellus</i>	Guinea pig	Cp
	<i>Cynomys ludovicianus</i>	Prairie Dog	Cl
	<i>Pedetes capensis</i>	Springhare	Pe
	<i>Lagostomus maximus</i>	Plains viscacha	Lm
	<i>Microtus pennsylvanicus</i>	Meadow vole	Mp
	<i>Marmota monax</i>	Woodchuck	Ma

Order	Species	Common name	ID
	<i>Xerus erythropus</i>	African ground squirrel	Xe
	<i>Ctenomys opimus</i>	Highland Tuco-tuco	Co
	<i>Cryptomys hottentotus</i>	Common mole rat	Ch
	<i>Cannomys badius</i>	Lesser bamboo rat	Cb
	<i>Castor canadensis</i>	American beaver	Cc
	<i>Myocastor coypus</i>	Coypu	Mc
Sirenia	<i>Trichechus senegalensis</i>	African manatee	Ts

Table 4.2 Body mass and eco-behavioural traits of 45 mammalian species.

Species	Body mass (kg)	Habitat	Active time	Sociality
<i>Bos primigenius</i>	269	Ter	D	G
<i>Camelus dromedarius</i>	415	Ter	D	G
<i>Hippopotamus amphibius</i>	1153	Sem	N	G
<i>Puma concolor</i>	43.14	Ter	N	S
<i>Felis catus</i>	3.231	Ter	N	S
<i>Vulpes vulpes</i>	4.294	Ter	N	S
<i>Ailurus fulgens</i>	5.267	Ter	C	G
<i>Mephitis sp.</i>	1.673	Ter	C	S
<i>Procyon lotor</i>	7.316	Ter	N	G
<i>Taxidea taxus</i>	6.612	Fos	N	S
<i>Lutra lutra</i>	7.428	Sem	N	S
<i>Tursiops truncatus</i>	179.5	Mar	D	G
<i>Delphinapterus leucas</i>	753.3	Mar	D	G
<i>Eptesicus fuscus</i>	0.017	Fly	N	G
<i>Talpa europaea</i>	0.084	Sub	N	S
<i>Talpa occidentalis</i>	0.093	Sub	N	S
<i>Neamblysomus sp.</i>	0.021	Sub	N	S
<i>Equus caballus</i>	250	Ter	D	G
<i>Odobenus rosmarus divergens</i>	850	Sem	unknown	G
<i>Mirounga angustirostris</i>	363	Sem	unknown	G
<i>Arctocebus calabarensis</i>	0.207	Ter	N	S
<i>Tarsius bancanus</i>	0.078	Ter	N	S
<i>Aotus trivirgatus</i>	0.848	Ter	N	G
<i>Daubentonia madagascariensis</i>	2.80	Ter	N	S
<i>Saimiri sciureus</i>	0.795	Ter	D	G
<i>Cebus apella</i>	2.766	Ter	D	G
<i>Homo sapiens</i>	63.5	Ter	D	G
<i>Galago senegalensis</i>	0.172	Ter	N	G
<i>Loxodonta africana</i>	2411	Ter	D	G
<i>Mus musculus</i>	0.015	Ter	N	G
<i>Glaucomys volans</i>	0.065	Ter	N	G
<i>Rattus norvegicus</i>	0.290	Ter	N	G
<i>Cavia porcellus</i>	0.728	Ter	C	G

Species	Body mass (kg)	Habitat	Active time	Sociality
<i>Cynomys ludovicianus</i>	0.780	Fos	D	G
<i>Pedetes capensis</i>	3.007	Fos	N	G
<i>Lagostomus maximus</i>	4.145	Fos	C	G
<i>Microtus pennsylvanicus</i>	0.036	Fos	N	S
<i>Marmota monax</i>	3.844	Fos	D	S
<i>Xerus erythropus</i>	0.383	Fos	D	G
<i>Ctenomys opimus</i>	0.400	Sub	D	S
<i>Cryptomys hottentotus</i>	0.082	Sub	N	G
<i>Cannomys badius</i>	0.650	Sub	N	S
<i>Castor canadensis</i>	24.35	Sem	N	G
<i>Myocastor coypus</i>	7.052	Sem	N	G
<i>Trichechus senegalensis</i>	408.5	Mar	unknown	G

Note: Fly, flying; Fos, fossorial; Mar, marine; Sem, semi-aquatic; Sub, subterranean; Ter, terrestrial; C, crepuscular; D, diurnal; N, nocturnal; G, gregarious; S, solitary.

Table 4.3 Audiograms and intermeatal distances in 45 mammalian species.

ID	High frequency limit (kHz)	Low frequency limit (kHz)	Best frequency (kHz) ^a	Intermeatal distance (mm) ^b	Audiogram source
Bp	37	0.017	8	230.06	Laboratory of Comparative Hearing*
Cd				133.16	
Ha				177.86	
Pc					
Fc	85	0.048	8	31.64	Laboratory of Comparative Hearing
Vv				38.81	
Af				56.92	
Me				33.06	
Pl	38	0.134	1	43.63	Laboratory of Comparative Hearing
Tt					
LI	35	0.450		61.67	Finneran and Jenkins, 2012 (in air)
Tu	150	0.200	65	173.66	Ketten, 1994
DI	130	0.040	70		Nedwell et al., 2004
Ef	110	2.600	20	7.73	Laboratory of Comparative Hearing
Te	15	0.100	0.5	12.00	Aitkin et al., 1982
To					
Ne					
Ec	35	0.042	2	82.42	Laboratory of Comparative Hearing
Or	32	0.125	12		Nedwell et al., 2004 (in water)**
Mi	63	0.075	6.4	156.00	Nedwell et al., 2004 (in water)**
Ac					
Tb	91	1.000	16	18.79	Ramsier et al., 2012
At	46	0.125	10	24.97	Beecher, 1974
Dm					
Ss	45	0.170	10	28.75	Laboratory of Comparative Hearing

ID	High frequency limit (kHz)	Low frequency limit (kHz)	Best frequency (kHz) ^a	Intermeatal distance (mm) ^b	Audiogram source
Ca				42.41	
Hs	18	0.023	4	91.87	Laboratory of Comparative Hearing
Gs	65	0.092	8	18.67	Laboratory of Comparative Hearing
La	12	0.017	1		Heffner and Heffner, 1980
Mm	89	2.000	16	7.90	Laboratory of Comparative Hearing
Gv					
Rn	70	0.290	32	16.94	Laboratory of Comparative Hearing
Cp	51	0.047	8	20.02	Laboratory of Comparative Hearing
Cl	28	0.013	4	27.03	Laboratory of Comparative Hearing
Pe				30.60	
Lm				53.57	
Mp	59	1.900	8		Lange et al., 2004
Ma	29.5	0.021	4	39.67	Laboratory of Comparative Hearing
Xe					
Co					
Ch	18	0.225	0.8	16.00	Bruckmann and Burda, 1997
Cb				23.54	
Cc				73.69	
Mc				51.19	
Ts	46	0.015	18	278.00	Nedwell et al., 2004

^aThe frequency with the lowest detection threshold

^bThe intermeatal distance was measured with ImageJ software.

*<http://laboratoryofcomparativehearing.com>

**The audiogram was measured in water.

Table 4.4 Categories of hearing variables.

Hearing variables	Criteria	Categories	Abbreviation
High frequency limit (kHz)	≥ 70	High value	HHL
	65-45	Medium value	MHL
	≤ 38	Low value	LHL
Low frequency limit (kHz)	≥ 0.2	High value	HLL
	0.17-0.075	Medium value	MLL
	≤ 0.048	Low value	LLL
Best frequency (kHz)	≥ 12	High value	HBF
	10-6.4	Medium value	MBF
	≤ 4	Low value	LBF
Intermeatal distance (mm)	> 61	High value	HID
	57-30	Medium value	MID
	< 29	Low value	LID

Note: categories were determined according to data gaps to represent discrete groups and to provide a similar number of specimens in each category.

4.1.2 Human developmental study

Seventeen human cochleae (5 adults and 12 fetuses) were included in the study. Micro-CT scans of the adult specimens were provided by the Max Planck Institute for Evolutionary Anthropology, Germany. The fetal specimens, ranging from approximately four to nine months of gestation, were taken from the Victorian Workhouse Osteology collection at the University of Liverpool. Not all fetal ages were accurately labeled, so fetal samples were classified into large and small fetus groups (n = 6/each) according to the length of the petrous bone (Table 4.5). The length of the bone was measured with a vernier caliper (to 0.1 mm, GPM Swiss, Switzerland) from the anteriormost point to posteriormost point of the bone.

Table 4.5 Categories of human specimens.

Specimen ID	Petrous length (mm)	Categories
A1		Adult
A2		Adult
A3		Adult
A4		Adult
A5		Adult
L1	34.5	Large fetus
L2	31	Large fetus
L3	28.25	Large fetus
L4	24.5	Large fetus
L5	22.75	Large fetus
L6	21.5	Large fetus
S1	21	Small fetus
S2	20.25	Small fetus
S3	20	Small fetus
S4	19.25	Small fetus
S5	17.5	Small fetus
S6	15	Small fetus

4.2 Micro-CT image processing

The skull of each specimen was non-invasively imaged with micro-computed tomography (micro-CT) using several different machines and locations (Table 4.6). The majority of the data were imaged for this thesis using the micro-CT facility at the University of Manchester. Image data were then post-processed with ImageJ. Contiguous series of slice images were stacked to produce the entire volume of a 3D CT image. Cropping the 3D image stack was done based on the rectangular selection to obtain only the cochlear part. This minimized the time taken to complete subsequent steps and the computational demands of the rendering. The grey-scale of the stack was inverted to make it easier to identify the void, representing the duct, rather than the surrounding bone. Then, image contrast was increased and detail in the image was accentuated.

Most specimens were scanned with isometric voxels. If not, the ImageJ plugin TransformJ was used to interpolate (B-spline function) the data and create isometric voxels (Meijering et al., 2001). For the final step, the image stack was saved as a 16bit TIFF file.

Table 4.6 Imaging information and specimen sources of the species studied.

ID	Specimen source	Imaging location	Parameters	Resolution* (mm)
Bp	University of Liverpool	University of Manchester	125 kV; 95 μ A	0.046
Cd	Northeast Ohio Medical University	Pennsylvania State University		0.070
Ha	Northeast Ohio Medical University	Pennsylvania State University		0.070
Pc	Natural History Museum, LA	University of Texas		0.277
Fc	Liverpool Museum	University of Manchester	125 kV; 95 μ A	0.033
Vv	Liverpool Museum	University of Manchester	125 kV; 95 μ A	0.036
Af	Liverpool Museum	University of Manchester	125 kV; 95 μ A	0.049
Me	Liverpool Museum	University of Manchester	125 kV; 95 μ A	0.038

ID	Specimen source	Imaging location	Parameters	Resolution* (mm)
Pl	Northeast Ohio Medical University	Pennsylvania State University		0.070
Tt	Northeast Ohio Medical University	Pennsylvania State University		0.039
Ll	Liverpool Museum	University of Manchester	125 kV; 95 μ A	0.043
Tu	Cambridge University	University of Manchester	200 kV; 105 μ A	0.019
Dl	Cambridge University	University of Manchester	200 kV; 105 μ A	0.017
Ef	University of Washington	University of Texas		0.044
Te	University College London	University of Texas		0.018
To	Sanchez-Villagra, M.R.	University of Manchester	80 kV; 80 μ A	0.023
Ne	Cambridge University	University of Manchester	90 kV; 95 μ A	0.016
Ec	University of Liverpool	University of Manchester	125 kV; 95 μ A	0.038
Or	University of California	University of Texas		0.272
Mi	University of California	University of Texas		0.261
Ac	Pennsylvania State University	Pennsylvania State University		0.032
Tb	University of Texas	University of Texas		0.078
At	University of Texas	University of Texas		0.083
Dm	Pennsylvania State University	Pennsylvania State University		0.027
Ss	Pennsylvania State University	Pennsylvania State University		0.078
Ca	University of Texas	University of Texas		0.042
Hs	University of Leipzig	Max Planck Institute		0.083
Gs	University of Texas	University of Texas		0.037
La	Liverpool Museum	University of Manchester	125 kV; 95 μ A	0.028
Mm	Texas Memorial Museum	University of Texas		0.025
Gv	Texas Memorial Museum	University of Texas		0.044
Rn	University of Liverpool	University of Manchester	125 kV; 95 μ A	0.051
Cp	University of Liverpool	University of Manchester	125 kV; 95 μ A	0.037
Cl	University of Michigan	University of Texas		0.094
Pe	Cambridge University	University of Manchester	125 kV; 95 μ A	0.037
Lm	Cambridge University	University of Manchester	125 kV; 95 μ A	0.044
Mp	Pennsylvania State University	Pennsylvania State University		0.024
Ma	Pennsylvania State University	Pennsylvania State University		0.027
Xe	Pennsylvania State University	Pennsylvania State University		0.021
Co	Cambridge University	University of Manchester	125 kV; 95 μ A	0.032
Ch	Cambridge University	University of Manchester	125 kV; 95 μ A	0.033
Cb	Cambridge University	University of Manchester	125 kV; 95 μ A	0.037
Cc	Cambridge University	University of Manchester	125 kV; 95 μ A	0.060
Mc	Cambridge University	University of Manchester	125 kV; 95 μ A	0.049
Ts	Cambridge University	University of Manchester	200 kV; 105 μ A	0.019

*Isometric resolution after interpolation

Note: image parameters were not available in some specimens.

4.3 Standardization and 3D reconstruction

The inverted TIFF file of an image stack was opened in Amira (v. 5.2.2; Visage Imaging, Germany). The standardization process was done to make image stacks of all specimens have the same plane for 3D reconstruction. The 3D image of the inner ear was then reconstructed for further investigation of the cochlear form.

4.3.1 Standardization

The orientation of the petrous bone in each specimen might be different during scanning. Therefore plane standardization was done in all species studied to provide the same plane for 3D reconstruction of the inner ear. The original inverted TIFF file of an image stack (the source field) was opened in Amira. A slice was obliquely oriented and translated to find the lateral semicircular canal. Then, the *fit to points* toggle was enabled to reset the plane to be parallel to the lateral canal. By clicking three times at different points on the lateral canal in the scene, the plane was automatically adjusted to match these points and reset to be parallel to the lateral canal (reference plane). Next, using the *ApplyTransform* module, a new field was created and its sampling planes were shown parallel to the lateral canal. The new field was saved to use for reconstructing a 3D image of the cochlea (see Amira commands given in Appendix A.1).

4.3.2 Reconstruction of 3D images of the inner ear

The image data after standardization were loaded into the Amira segmentation editor. The process of reconstructing 3D images has two operations—image segmentation and surface reconstruction (see Amira commands given in Appendix A.2). Image segmentation is the procedure of selecting voxels and then assigning

these voxels to a material of interest. Most of the segmentation was accomplished with a threshold on the basis of the Full Width at Half Maximum (FWHM) principle. Indistinct and/or complex boundaries (e.g., foramina) were determined by eye. For instance, the cochlea was separated from the tympanic cavity by linear boundaries created between two edges of the round window, and between two edges of the oval window. Boundaries were also created along the surfaces of the internal acoustic meatus and the modiolus to close off the numerous nerve foramina and to separate them from the cochlea. Next, polygonal surfaces of the inner ear were reconstructed and smoothed to generate 3D shells representing the cochlea. Three-dimensional reconstructions and the original TIFF data were maintained in the same spatial reference frame throughout. This allows for cross-checking, for example, of landmarks between 2D micro-CT images and the 3D surface rendering.

4.4 Landmark methods

A problem with landmarking the cochlea is its complex geometry. Any standard orthogonal plane will show only an oblique view of the duct's true cross section, thereby underestimating or overestimating width, etc. To address this problem the cochlea data were resliced around a central axis, creating a series of images (like the spokes of a wheel) that track the duct as its spirals. The following describes the method used.

The original inverted TIFF file of a stack of slice images was opened. The image slice was obliquely oriented and translated to find a plane for defining the rotation axis of the cochlea. This axis passed through the approximate mid-modiolar plane.

An axial line was drawn passing the mid-modiolar plane. Two landmarks were added on the axial line. A specially created module, *ReAlignObliqueSliceByLandmarks.scro* (see Appendix B.1), was used to set these two landmarks as the rotational axis with a rotation angle ranging from 0 to 360 degrees. It was decided that resliced planes every 22.5 degrees (16 per 360 degrees) would be sufficient for sampling the cochlea (Fig. 4.1, see Amira commands given in Appendix A.3). Once each plane was rotated 22.5 degrees, landmarks were placed at the centre of the cochlear cavity (Fig. 4.2). The start and end landmarks were standardized - the first landmark placed at the centre of the duct in the plane showing the initial appearance of the inner osseous spiral lamina (usually located between the oval and round windows). The end landmark was placed at the apex (Fig. 4.2). This method captures the complex geometry of the cochlea but the number of landmarks varies among specimens according to the number of spirals and there is a spatial bias in the landmark density (i.e., morphologies closest to the rotational axis are represented by more landmarks than those further away from the axis). To offset these, the original landmarks were used to create a set of 25 semi-landmarks at equidistant points from the start to end landmarks (Fig. 4.2). These equidistant landmarks were then used in subsequent calculations and the geometric morphometric analyses.

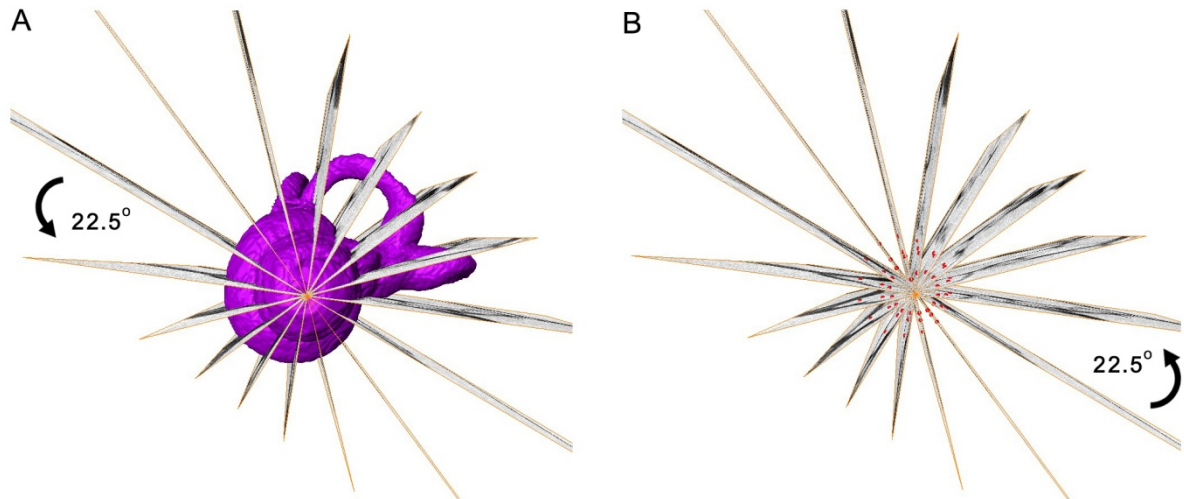


Figure 4.1 The slice was rotated 22.5 degrees each to put landmarks around the mid-modiolar axis. A, the cochlea with planes of rotation; B, landmarks (red) in each plane of rotation.

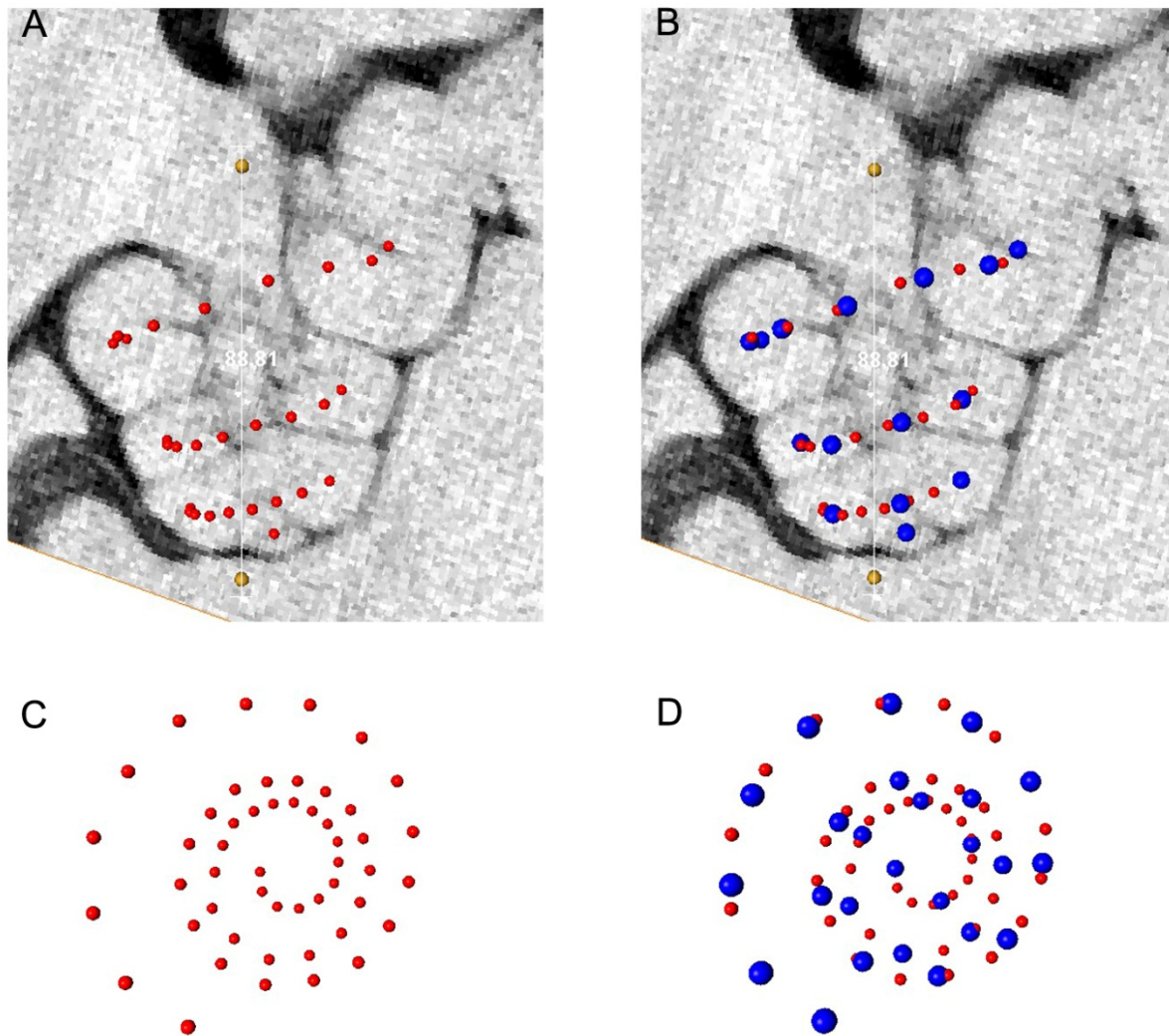


Figure 4.2 Original landmarks (red) and semi-landmarks (blue). A) original landmarks at the centre of the cochlear cavity around the mid-modiolar axis. B) 25 equidistant semi-landmarks calculated and placed among the original landmarks. C) and D), original landmarks and semi-landmarks viewed laterally, respectively.

4.5 Measurement protocols of the cochlear variables

The cochlear variables measured in this study included the number of cochlear turns, cochlear length, cochlear height, cochlear width, cochlear volume, and the surface area of the oval and round windows. The ratios of height to width and of the

oval window to the round window were also examined. This section presents step-by-step procedures for measuring or deriving these variables.

Number of the cochlear turns

The total number of original landmarks (not the equidistant set) from the first appearance of the inner bony lamina to the apex was used to calculate the number of the cochlear turns. Given n total landmarks, the number of intervals between adjacent landmarks was $n-1$. As the former landmark was 22.5 degrees distant from the next, the total degree of the cochlear spiral was $(n-1) \times 22.5$. To obtain the number of the cochlear turns, this total degree was divided by 360.

Length

The 3D length was computed as the sum of distances between adjacent original landmark co-ordinates $[(((x_2-x_1)^2 + (y_2-y_1)^2 + (z_2-z_1)^2)^{1/2}]$ (Deza and Deza, 2009) multiplied by voxel resolution.

Height

Cochlear height was calculated as the distance between the last landmark (at the apex) and the landmark (at the inferior edge of the round window) projected onto the mid-modiolar axis (axial line) of the cochlea (Fig. 4.3, see Amira commands given in Appendix A.4). The distance was multiplied by the voxel resolution to obtain cochlear height.

Width

Cochlear width was calculated as the distance from the landmark at the inferior edge of the round window to the opposite landmark. The distance was measured perpendicular to the mid-modiolar axis (axial line) of the cochlea (Fig. 4.3, see Amira commands given in Appendix A.5). The distance was multiplied by the voxel resolution to obtain cochlear width.

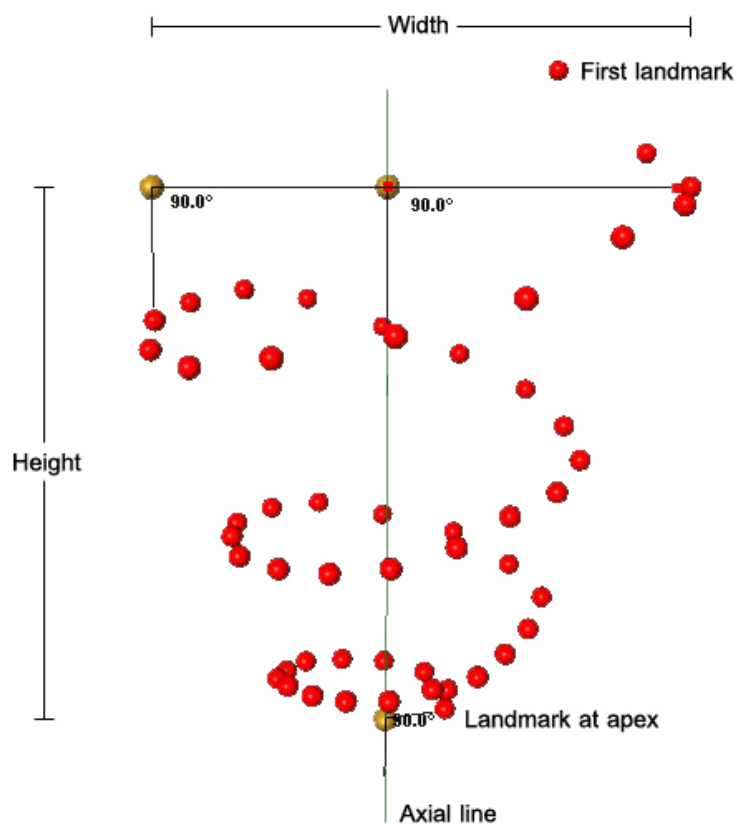


Figure 4.3 Measurements of the cochlear height and width. The height was measured from the distance between the last landmark (at the apex) and the landmark (at the inferior edge of the round window) projected onto the mid-modiolar axis (axial line). The width was measured from the distance between the landmark at the inferior edge of the round window and the opposite landmark. The distance was perpendicular to the axial axis.

Volume

All voxels of the inner-ear structures were loaded into the Segmentation Editor of Amira. The boundary between the cochlea and the vestibular apparatus was identified. The boundary passed parallel to the groove under the saccular protrusion, and passed the first clear point of the inner osseous lamina (Fig. 4.4). Voxels of the vestibular apparatus were then removed so that only voxels of the cochlea remained. Using the *MaterialStatistics* module, the volume value was calculated as numbers of voxels multiplied by the volume (mm^3) of a single voxel (see Amira commands given in Appendix A.6).

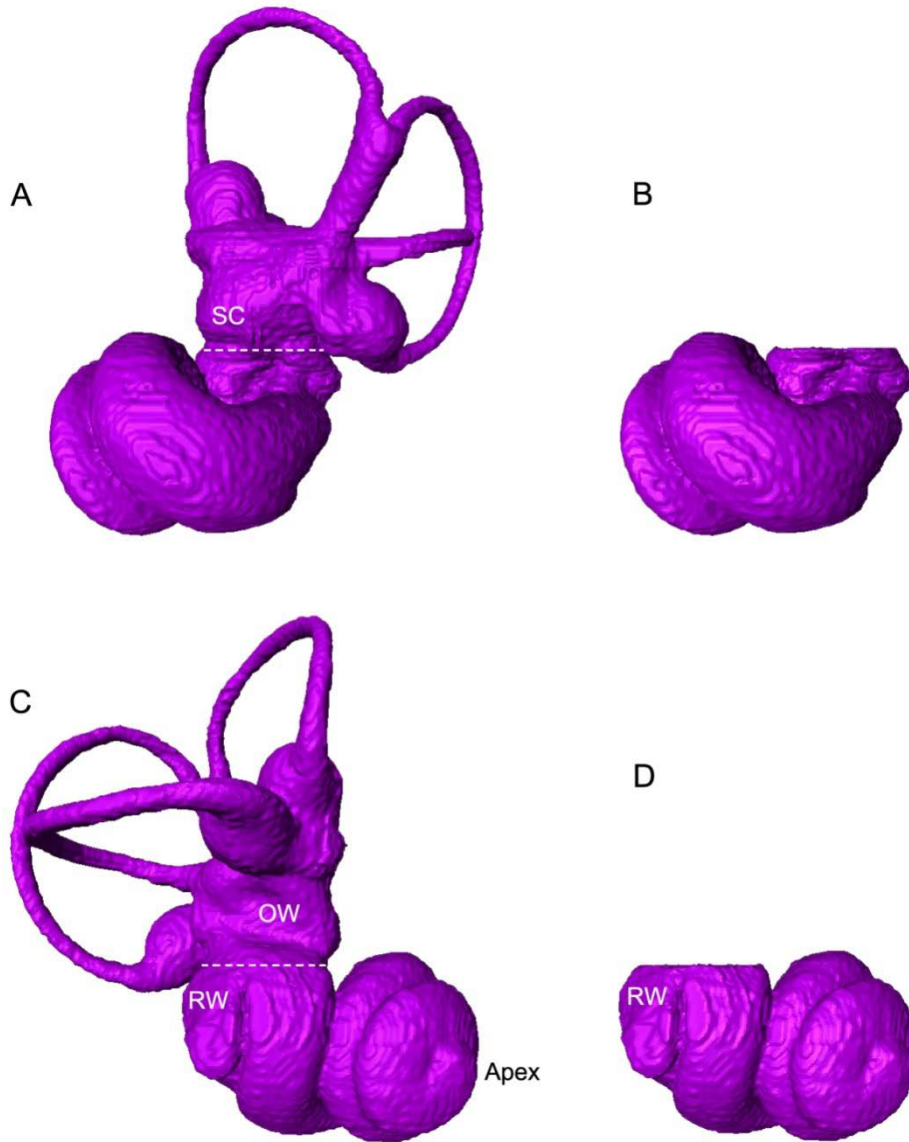


Figure 4.4 The vestibular apparatus was removed and the cochlear volume was measured in *Galago senegalensis*. The boundary passed parallel to the groove under the saccule (A and B), and passed the first appearance of the inner osseous spiral lamina. The inner lamina usually started between the oval and round windows (C and D). SC, saccule; OW, oval window; RW, round window.

Surface areas of the cochlear fenestrae

The reconstructed surface was first smoothed to reduce errors in the area measurements due to surface roughness (typically worse if the slice direction was perpendicular to the surface of interest). Triangles occupying the area of the oval and round windows were highlighted and the selection inverted. All other triangles were then removed from the buffer, leaving only triangles representing the oval and round windows (Fig. 4.5, see Amira commands given in Appendix A.7). Using the *SurfaceArea* module, the surface area of triangles of the window region was computed and multiplied by pixel resolution (mm²).

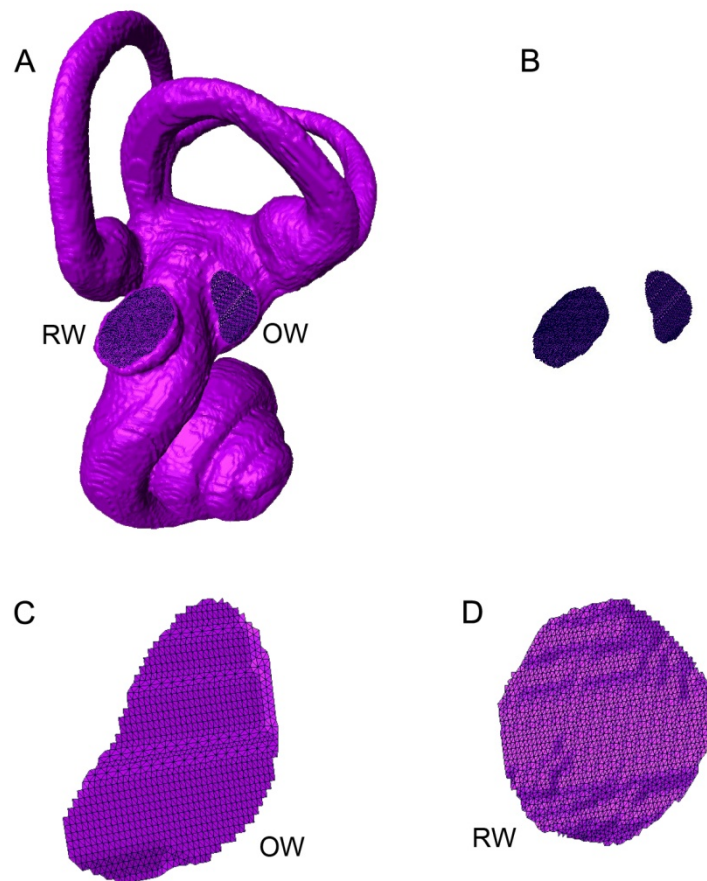


Figure 4.5 Measurement of the surface areas of the oval window (OW) and round window (RW) in *Cebus apella*. A, the regions of OW and RW were highlighted. B, other unwanted regions were removed. C and D, triangles of the OW and RW areas (magnified).

4.6 Data analyses of the adult interspecific study

4.6.1 Repeatability of Measurements

Three species (*Ctenomys opimus* (Co), *Glaucomys volans* (Gv) and *Homo sapiens* (Hs)) were chosen to represent the range of values found amongst mammals and assess the repeatability of measurements and landmarking of the cochlea. For the repeatability of measurement, the cochlear variables were measured on three separate occasions for each of the specimens. A one-way analysis of variance (ANOVA) was used to calculate the repeatability. The concept of ANOVA is that the total variance of measurements is partitioned into the variance within species (S^2) and the variance among species (S^2A). The statistic is the F-test, with degrees of freedom and the P value. The P value indicates whether there is a significant difference in measurement between the different species. In the present study, statistical significance of all tests was accepted if the P value was less than 0.05. Then, the ratio of the variance among species (S^2A) to the total phenotypic variance ($S^2 + S^2A$) was computed for the intraclass correlation coefficient (r), which is an estimate of repeatability (Lehtonen and Lindstrom, 2008). The r value represents the proportion of variation in a measurement that is caused by differences among species, not caused by differences within an individual species. The r value ranges from 0 to 1. For repeatability of shape analysis, a set of semi-landmarks were derived three times for each species. Each time, the start and end sites for creating a set of landmarks were determined independently. The repeatability of shape analysis can be determined from the location of the repeats in comparison with the distribution seen across all specimens studied in the principal component (PC) plots (Cucchi et al., 2011; Gunz et al., 2012).

4.6.2 Statistical analyses with body mass

The strength of the relationship between the cochlear variables and body mass, and between the hearing variables and body mass was examined using Spearman's rank correlation and reduced major axis (RMA) regression in PAST (v. 2.17b) (Hammer et al., 2001). All variables were log₁₀ transformed prior to analysis. If the cochlear variables and the hearing variables were significantly correlated with body mass, the residuals of these variables from RMA regression on body mass were calculated and used to reduce the effects of allometry. Afterward, the relationship between the cochlear and hearing variables after size-correction was examined. Spearman's rank correlation and RMA regression were also used for pairwise comparisons of the cochlear variables. The slope of a regression line was used to represent the rate of change in the y variable as the x variable changes.

To investigate the relationship between the bony cochlear morphology and ecological and hearing influences, analysis of covariance (ANCOVA) was used in PAST. The ANCOVA tests for equality of means between a dependent variable (cochlear variables) and a categorical independent variable (categories of ecology and hearing variables), while controlling for the effects of a covariate (body mass). The cochlear variables and body mass were log₁₀ transformed before analysis. In addition, descriptive statistics, such as the mean and standard deviation, were computed for each category.

4.6.3 Quantifying shape with geometric morphometrics and related statistics

The 3D coordinate data of the 25 semi-landmarks were transposed into the Morphologika file format and imported into MorphoJ (v. 2.0) (Klingenberg, 2011).

Data were subjected to a full Procrustes fit to minimise the effects of location, scale and rotation. All configurations were rotated to optimal alignment on the mean configuration. The resulting hyper-dimensional covariance matrix representing differences among configurations remaining after Procrustes was explored using Principal Component Analysis (PCA) and by comparing the Procrustes distances among configurations. A generally accepted cut off for examining PCs is 5% of the total variance (Zelditch et al., 2004). The mean shape corresponds to the PC score of zero on all PC axes and trends of cochlear shape changes in all specimens can be estimated from the comparison of differences in PC scores among individuals along each PC axis.

To examine whether shape change was associated with size differences, Spearman's rank correlation of scores on each PC against centroid size was performed. Natural log-transformed centroid size was calculated automatically in MorphoJ and used as a size measure to increase the fit of linear relationship (Viscosi and Cardini, 2011; Klingenberg et al., 2012). If the centroid size showed a significant correlation with PC scores, shape residuals (PC residuals) from RMA regression on centroid size were calculated and used for further analyses to minimise allometric effects. Shape residuals obtained from MorphoJ were computed across the whole shape space (full Procrustes distances; Zelditch et al., 2004). In addition, PAST was used for calculating the residuals in each PC to consider shape differences in detail (shape residuals based on ln-transformed centroid size are the same as those based on log₁₀ centroid size). Residuals obtained from PAST were also analyzed using PCA to explore the patterns of shape variation without the effects of size.

Discriminant function analysis (DFA) is a classical multivariate statistics that is most useful for comparison between two specific groups (Klingenberg, 2011). In the present study, DFA in MorphoJ was used to test for differences of the cochlear shape (full Procrustes distances) between mammalian groups with different eco-behavioural traits, or with different hearing characteristics. In the case of existing size effects on shape, PC residuals of the two groups were compared. The permutation test was included and 10,000 random permutations were run. A significant difference in shape was indicated by the *T*-square statistic of less than 0.05 and the reliability of the result was assessed by cross-validation (Klingenberg, 2011). DFA, however, looks at shape differences across the whole shape space, irrespective of portion of shape that is important. Potentially important shape events can be averaged out when examining across the whole space (Klingenberg, 2011). On the other hand, PCA resolves the shape space into PCs and allows for a more focused analysis of shape differences (Zelditch et al., 2004). Therefore, differences were also tested among PC scores with the Mann-Whitney U test in PAST. If there were the size effects on shape, PC residuals were used. The Mann-Whitney U test is a non-parametric statistic for comparing the medians of two independent samples. The results from DFA and Mann-Whitney U test were then compared each other.

4.6.4 Test of phylogenetic signal

One interesting question is whether or not the cochlear shape is significantly related to phylogeny. Strong background phylogenetic signals could generate false positive results in comparisons of variables against hypothesised functional determinants (e.g., frequency range). A strong phylogenetic signal means that shapes of closely related species have a tendency to be near each other in morphometric space,

whereas shapes of more remotely related species tend to be found in distant locations (Klingenberg and Gidaszewski, 2010) (Fig. 4.6). A method to test the presence of the phylogenetic signal in the morphometric data is mapping geometric morphometric data (shapes) onto a known phylogenetic tree, which is directly imagined as a projection of the tree into the morphometric space (Klingenberg, 2011). This involves using squared-change parsimony (Maddison, 1991) to reconstruct the locations (PC scores) of internal nodes of the tree. The topology and dates of the known phylogenetic tree were derived from Bininda-Emonds et al. (2007) (see Appendix C). The procedures were performed in MorphoJ software (Klingenberg, 2011).

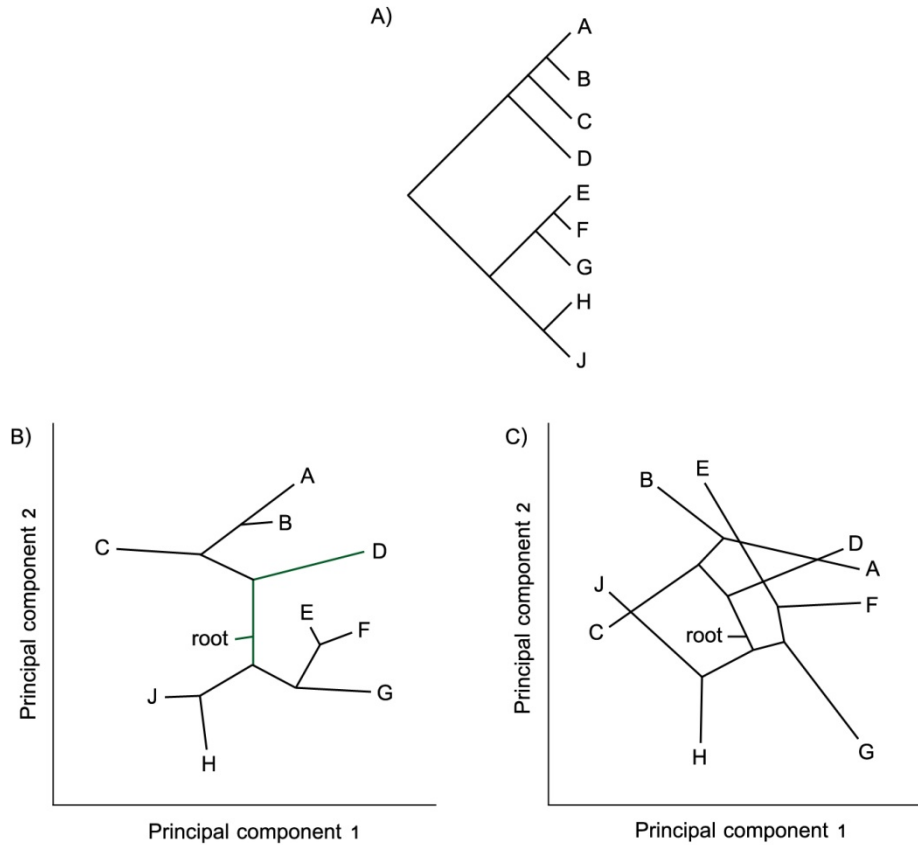


Figure 4.6 The example of mapping of the shape variation onto a known phylogenetic tree (A). B) The example of a result suggesting the presence of a phylogenetic signal in the data. It shows a clear divergence between the two main clades and closely related species are nearer in the morphometric space. C) The example of a result that is unlikely to have the signal. Closely related species are not close to each other and some remotely related species have similar shapes (modified from Klingenberg and Gidaszewski, 2010; pg. 253-254).

In principle, the amount of shape change on the entire tree can indicate the strength of the phylogenetic signal. If there is a strong phylogenetic component, then related species will be closer together in the shape space and shape differences will be smaller among closely related species compared with distantly related species (Klingenberg and Gidaszewski, 2010; Foth et al., 2012). A measure of this can be

mathematically described by the total tree length (Foth et al., 2012; Alvarez and Perez, 2013). The statistical significance of the tree length was evaluated using a permutation test that simulated the null hypothesis of the complete absence of the phylogenetic signal (Klingenberg, 2011). The permutation test randomly swapped the PC scores for each species (the branch tips of the tree) across the phylogenetic tree 10,000 times, and calculated the total tree length in units of morphometric distance. The *P* value for the test represents the proportion of permuted data sets in which the calculated tree length is equal or shorter than the tree length of the known original phylogeny. The null hypothesis will be rejected if fewer than 5% of permutations result in a calculated tree length that is equal or less than the tree length of the known phylogeny. Rejection of the null hypothesis implies that there is some phylogenetic structure in the data, and suggests that this phylogenetic structure should be taken into consideration in the comparative analyses.

It is important to note that the branches of the phylogeny are usually not independent of each other (Klingenberg, 2011). Also, data on shape changes along the branches of the phylogenetic tree should normally not be used in statistical tests (Klingenberg, 2011). Rejection of the null hypothesis does not necessarily imply that the phylogeny is tightly associated with the shape data. To confirm whether there were the effects of phylogeny on the results, independent contrasts analysis was performed in MorphoJ. The values of the independent contrasts for PC scores on each PC and for the natural log-transformed centroid size were calculated and used to minimise the influence of phylogenetic effects. Then, Spearman's rank correlation and RMA regression were used to investigate the relationship between independent contrasts. Afterward, pairwise comparisons (T-test) were performed between regression lines

obtained before and after the independent contrasts analysis. Non-significant difference between the regression slopes implied the non-existence of phylogenetic effects on shape changes, and vice versa.

4.7 Data analyses of the human developmental study

For the repeatability test, human specimens (A3, S1, and S6) were randomly selected and the test followed the protocols given in the adult interspecific study. The developmental study was divided into two sections: comparisons of the cochlear morphology 1) between adult and fetal groups, and 2) between large and small fetuses.

4.7.1 Comparison between adult and fetal cochleae

In this section, all human specimens were used and divided into adults and fetuses (large + small fetuses). Pairwise comparisons of the cochlear variables were examined using the Mann-Whitney U test in PAST to test whether the variables were different between adults and fetuses.

For quantifying shape with geometric morphometrics, the 3D coordinate data of 25 semi-landmarks of all specimens were imported in MorphoJ. The protocols were the same as those outlined in the adult interspecific study. Then, Spearman's rank correlation of scores on each PC against centroid size was performed. If the centroid size showed a significant correlation with PC scores, shape residuals (PC residuals) from RMA regression on centroid size were calculated and used for further analyses of shape variation to minimise the effects of allometry. Shape residuals were

computed using both MorphoJ and PAST. Residuals computed from PAST were also analyzed using PCA to explore the patterns of shape variation without the allometric effects.

Similar to the procedures in the adult interspecific study, DFA was performed with MorphoJ to examine differences of the cochlear shape (represented as PC scores) between adult and fetal populations. Also, the Mann-Whitney U test was performed with PAST to test the shape difference between two groups on each PC axis. In the event that there were the size effects on shape variation, PC residuals of the two groups were compared. The results from DFA and Mann-Whitney U test were then compared.

4.7.2 Comparison between large and small fetal cochleae

Fetal specimens were divided into large and small groups. Spearman's rank correlation and RMA regression in PAST were calculated to test the relationship between the cochlear variables and the length of the petrous bone. All variables were log₁₀ transformed prior to analysis.

Similar to the section 4.7.1, pairwise comparison of the cochlear variables was performed using the Mann-Whitney U test in PAST to test whether the variables are different between large fetuses and small fetuses.

In shape analysis with geometric morphometrics, the 3D coordinate data of 25 semi-landmarks of fetal specimens were imported in MorphoJ. The major features of shape variation of the cochlea could be displayed by PCA. Then, Spearman's rank

correlation of scores on each PC against centroid size was performed. The correlation of scores against the petrous bone length was also examined. Shape residuals (PC residuals) from RMA regression on centroid size were computed and used for DFA and Mann-Whitney U test if the effects of allometry were found in shape changes. The results of shape variation in fetal cochleae obtained from the two analyses were compared.

Chapter 5 Results: adult interspecific study

This chapter presents the results from the analyses of changes in the bony cochlear morphology in 45 mammalian species. The first section outlines the general observations of inner-ear morphology. Measurement repeatability is evaluated in the second section. The third section deals with scaling of the cochlear size variables with body mass whilst results for inter-measurement comparisons are given in the fourth section. The fifth and sixth sections document results concerning the relationships between cochlear form, ecology and hearing capabilities. Finally, the results of the phylogenetic tests are presented in last section.

5.1 Descriptive morphology of the inner ear

5.1.1 The number of spiral turns

The mean number of the cochlear turns in 45 mammalian species studied was 2.74 ± 0.60 turns. The bottlenose dolphin (*Tursiops truncatus*) and the African manatee (*Trichechus senegalensis*) had the least number of cochlear turns (1.75 turns), whereas the most number of cochlear whorls was found in the coypu (*Myocastor coypus*) and the guinea pig (*Cavia porcellus*) at 4.1875 turns (Fig. 5.1).

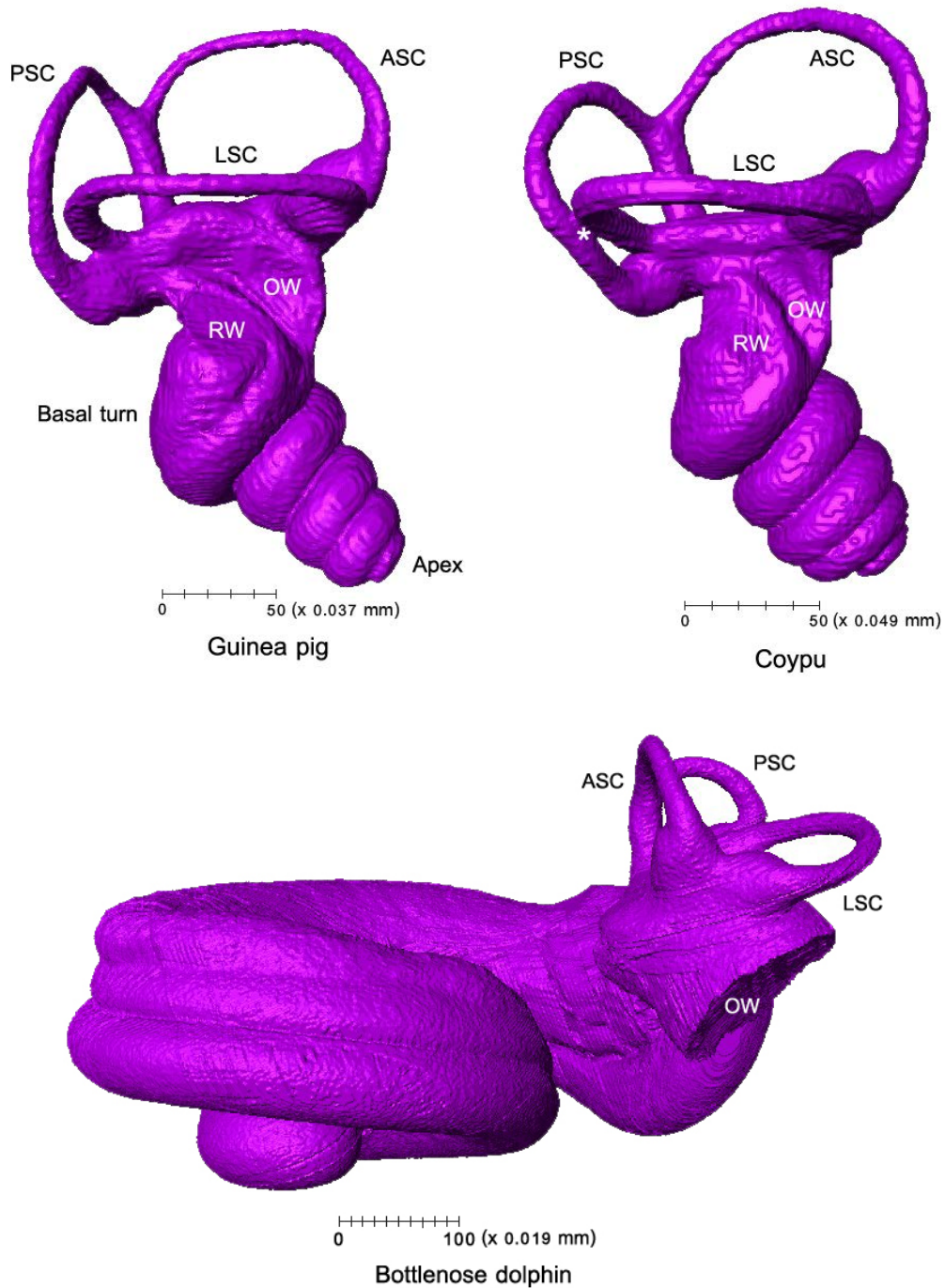


Figure 5.1 The inner ear of the guinea pig, coypu and bottlenose dolphin. The cochlea in the guinea pig and coypu had 4.1875 turns, whereas the cochlea in the bottlenose dolphin had 1.75 turns. The cup-shaped oval window and the reduced semicircular canals were also observed in the bottlenose dolphin. OW, oval window; RW, round window; ASC, anterior semicircular canal; asterisk (*), bony connection between the lateral and posterior semicircular canals (LSC, PSC).

5.1.2 The general appearance of the bony cochlea

The general appearance of the cochlea among mammals was varied. Its overall shape ranged from the wide-based cochlea with a rounded apex in odontocetes (e.g., bottlenose dolphin) to the sharp-pointed cone-shaped cochlea in the coypu and the guinea pig. The spiral ascent from the most basal turn to the upward turn was rather steep in some subterranean species, such as the tuco-tuco (*Ctenomys opimus*) and moles (Fig. 5.4). A greatly enlarged basal turn with an enlarged scala tympani was observed in pinnipeds (e.g., *Mirounga angustirostris*) when compared to most other mammals. In the European otter (*Lutra lutra*), there was a bony structure protruding into the basal turn of the cochlea (Fig. 5.2).

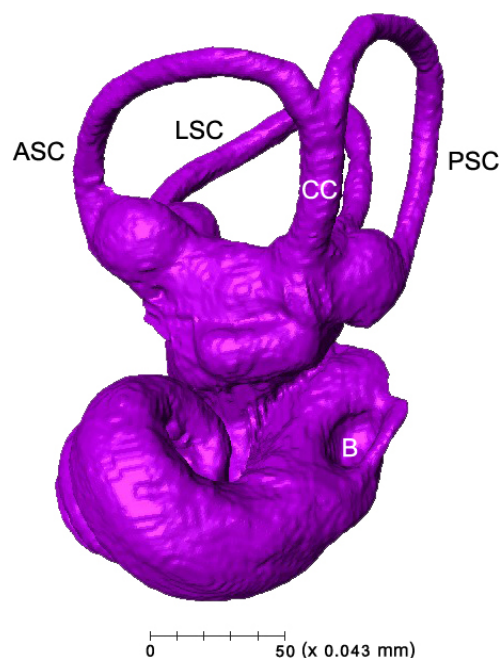


Figure 5.2 A bony structure (B) protruding into the basal turn in the European otter. ASC, anterior semicircular canal; LSC, lateral semicircular canal; PSC, posterior semicircular canal; CC, common crus.

5.1.3 The internal architecture of the bony cochlea

In the dolphin and the beluga whale (*Delphinapterus leucas*), a cross sectional areal ratio of the scala tympani to the scala vestibuli differed from that in other species. At the basal turn, the scala tympani was relatively larger than the scala vestibuli. The size of the scala tympani decreased gradually toward the apex, whereas the size of the scala vestibuli appeared constant throughout the cochlear length. Both scalae were nearly equal in size at the apex. Also, at the basal and middle turns, the spiral canal where it housed the spiral ganglion of the acoustic nerve was enlarged and protruded into the cavity of the scala tympani (Fig. 5.3).

Most mammals lacked a complete outer osseous spiral lamina that anchors and stiffens the basilar membrane. Some species, however, possessed the ossified outer lamina at the basal cochlear turn, e.g., the cat (*Felis catus*), horse (*Equus caballus*), red fox (*Vulpes vulpes*), skunk (*Mephitis* sp.), rat (*Rattus norvegicus*), springhare (*Pedetes capensis*), bushbaby (*Galago senegalensis*), Calabar potto (*Arctocebus calabarensis*), American beaver (*Castor canadensis*) and European otter. Only a few species had an extended outer lamina; its presence occupied up to 80% of the entire cochlear length in odontocetes (Fig. 5.3) and up to 50% in the big brown bat (*Eptesicus fuscus*).

A greatly enlarged cochlear aqueduct was observed in pinnipeds and odontocetes (Fig. 5.3). The cochlear aqueduct in most mammals, however, was typically narrow. The cochlear aqueduct opened into the cochlea via two main routes. In general, it entered the cochlea at the scala tympani of the basal turn next to the round window. The other entrance into the cochlea was through the posteromedial edge of the

round window (RW), for example in the bushbaby, brown capuchin (*Cebus apella*), human (*Homo sapiens*) and red fox.

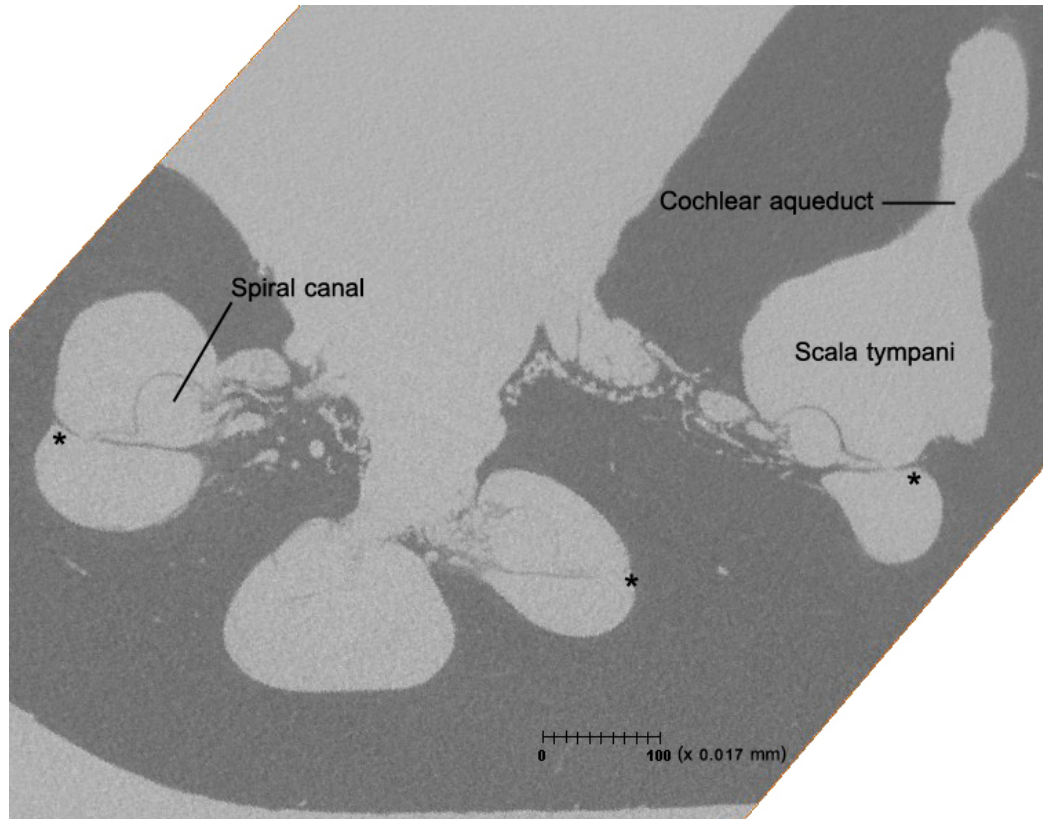


Figure 5.3 A CT slice (inverted grey scale) through the mid-modiolar plane of the beluga whale showing the enlarged spiral canal and cochlear aqueduct. The large spiral canals were found at the basal and middle cochlear turns. The cochlear aqueduct connected with the scala tympani at the basal turn. The outer bony spiral laminae, present along almost entire length of the cochlea, were marked with asterisks (*).

5.1.4 Semicircular canals

The semicircular canals in most mammals studied conformed to the general trend: 1) the lateral semicircular canal was relatively smaller than the vertical canals; 2) the anterior and posterior canals joined to form a common crus; and 3) the anterior

ampulla was located alongside the lateral ampulla but the posterior ampulla was independent. Though marine mammals followed the general trend, the semicircular canals were considerably reduced in size and much smaller in volume than the cochlear component, particularly in the odontocetes (Fig. 5.1).

Distinct morphological adaptations of the canals were noted in some species. In the European otter, the radius of the lateral canal was larger than that of the anterior canal. In talpid moles and three rodents (the coypu, plains viscacha [*Lagostomus maximus*] and meadow vole [*Microtus pennsylvanicus*]), there was a bony connection between the lateral and posterior canals about one-third along the curvature from the posterior ampulla (Fig. 5.1 and 5.4). Moreover, an additional common crus between the lateral and posterior canal was seen in the red fox, prairie dog (*Cynomys ludovicianus*), woodchuck (*Marmota monax*) and African ground squirrel (*Xerus erythropus*).

5.1.5 The cochlear fenestrae

The shape of the oval window (OW) surface was constant throughout all species studied, forming an elongated ellipse. The oval window in odontocetes projected from the vestibule like a cup-shaped structure (Fig. 5.1). This was different from other mammals, in which the OW opening was continuous with the surface of the vestibule and the basal cochlear turn. In subterranean moles, the stapedial footplate was medially convex and bulged extensively into the OW (Fig. 5.4). In contrast to the OW, the RW surface was rather diverse in shape. An elliptical shape was commonly present, with a variable diameter, in 58% of specimens. Other shapes found in the study were circular, bean and irregular or undefined (see Appendix D.1).

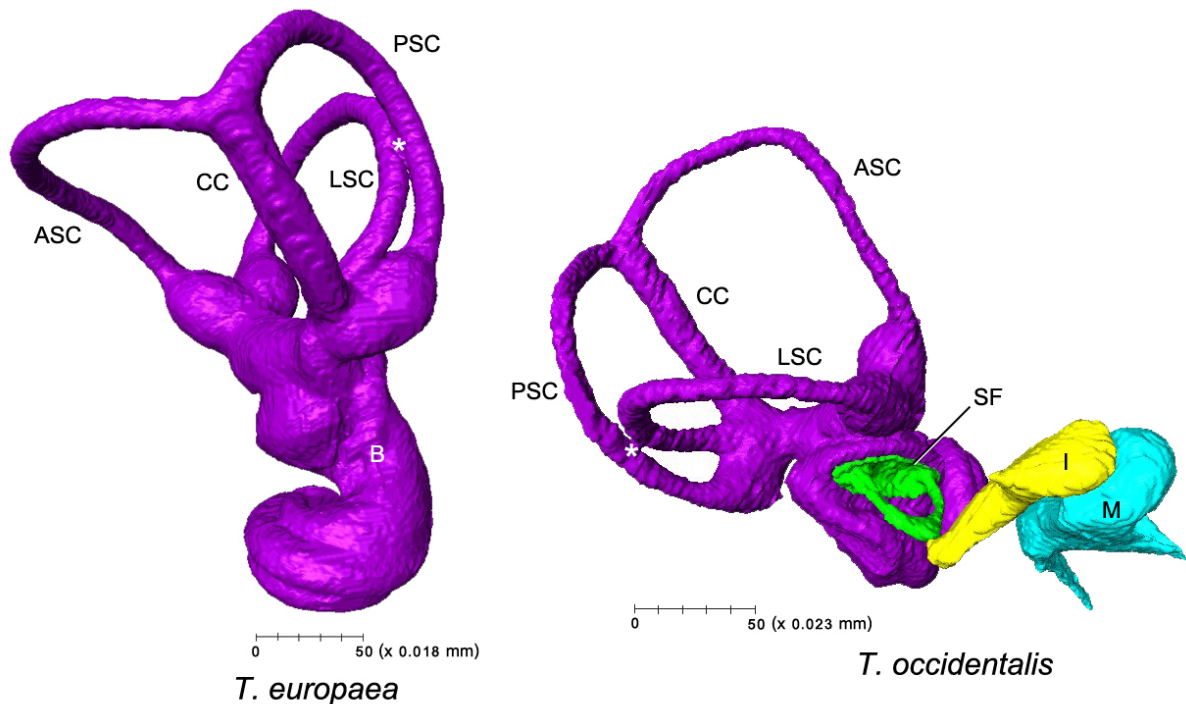


Figure 5.4 The inner ears of the two talpid moles, the European mole (left) and the Spanish mole (right). A steep ascent of the basal turn (B) to the middle turn and a bulging stapedia footplate (SF) into the oval window could be seen. The bony connection between the lateral and posterior semicircular canals (LSC, PSC) was marked with asterisks (*). ASC, anterior semicircular canal; CC, common crus; I, incus; M; malleus.

5.1.6 Variation of the auditory bullae

The inflated auditory bulla was found in many rodents: the lesser bamboo rat (*Cannomys badius*), tuco-tuco, coypu, woodchuck, plains viscacha, prairie dog, African ground squirrel and guinea pig. It was also seen in the primates, including the bushbaby and tarsier (*Tarsius bancanus*). In the tuco-tuco, the auditory bulla was divided into numerous air compartments. In species with inflated bullae the cochlea tended to protrude into the bulla. By contrast, a flat bulla was present in anthropoid primates (monkeys and human), horse and dromedary (*Camelus dromedarius*). In general, the air-filled cavity of the bulla in most mammals in this study was not

divided into compartments. Also, the cochlea was relatively firmly fused with the bullar wall, compared to the species with inflated bullae. It was interesting to note that a connection between the left and right bullae medially to the cochlea was present in only the talpid moles and the golden mole (*Neamblysomus* sp.) (Fig. 5.5).

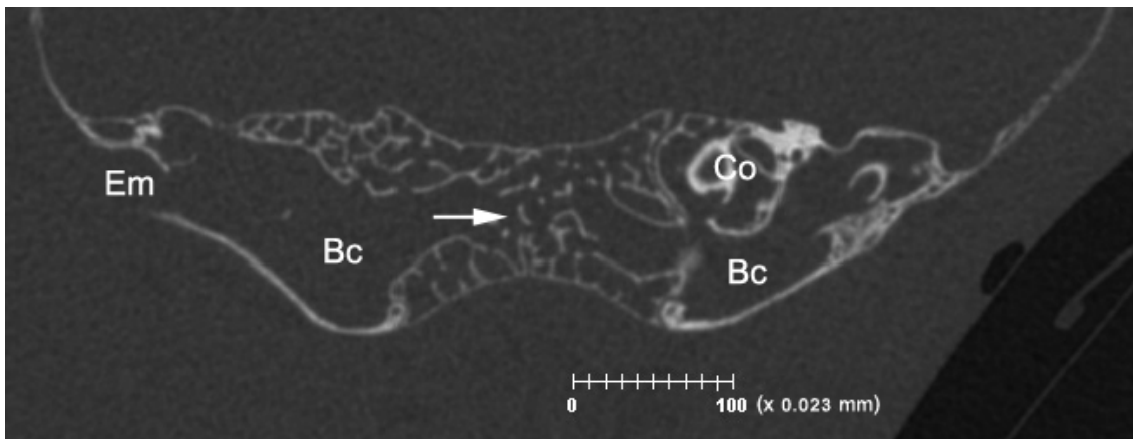


Figure 5.5 A CT slice through the coronal plane of the Spanish mole showing the connection between the bullae (arrow). Em, external auditory meatus; Bc, bullar cavity; Co, cochlea.

Figure 5.6 showed the example of comparison of bulla size between two species that had similar body size. The tuco-tuco possessed a highly inflated bulla, whereas the rat had a relatively flatter bulla. In the tuco-tuco, the bullar length (longest axis of the bulla) was 8.03 mm; the bullar width (the axis perpendicular to the longest axis) was 4.44 mm. The bullar depth (dorsal surface of the acoustic meatus to ventral bullar surface) was 4.96 mm. Calculated based on the formula reported by Schleich and Vassalo (2003), bullar volume in the tuco-tuco was about 46.28 mm³. In the rat, the bullar length, width and depth were 7.00, 3.31 and 5.04 mm, respectively, and bullar volume was 30.52 mm³.

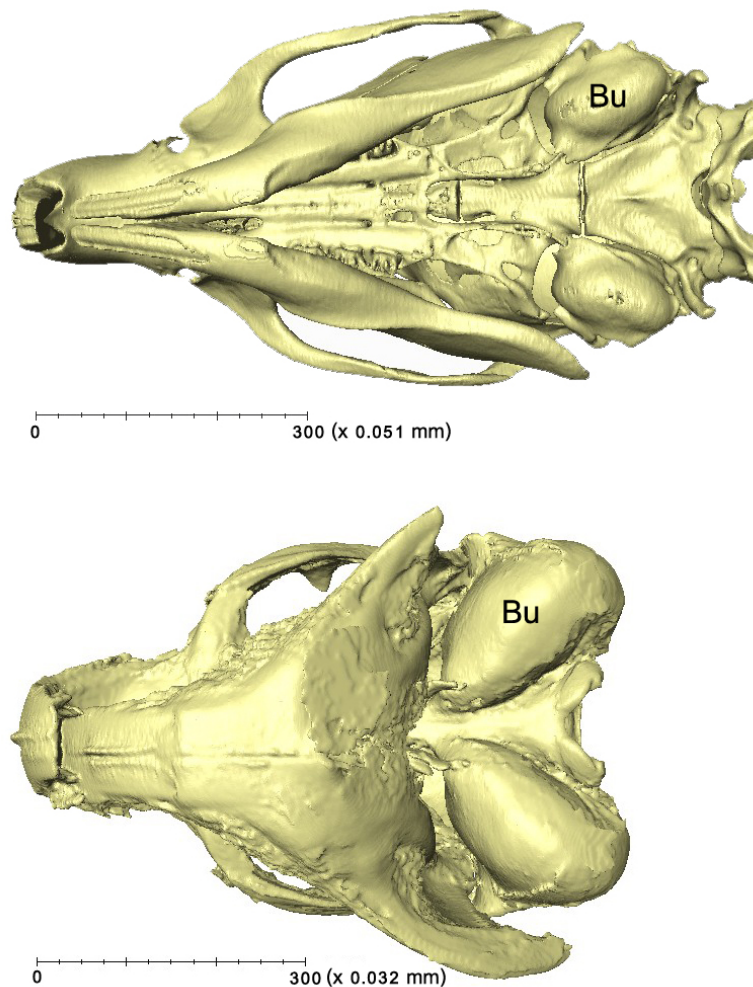


Figure 5.6 The ventral view of the whole skulls showing the auditory bullae (Bu) in the rat (the upper) and in the tuco-tuco (the lower). The bulla in the tuco-tuco was relatively inflated.

5.2 Repeatability of measurements of the cochlear form analyses

The intra-observer repeatability of the landmarking and measurements were assessed by repeating the measures three times for three randomly selected specimens (Co, Gv and Hs). The smaller the variance within species (S^2) was, the better the repeatability. For measurements of each cochlear parameter (Table 5.1), S^2 was very small and the P value was less than 0.001, indicating that differences in

measurement between different species were strongly significant compared with error among repeated measurements. In addition, the intraclass correlation coefficient (r) was almost equal to one (> 0.97). This suggested that more than 97% of the variation was due to differences among the different species and measurements of individual species were relatively constant. All standard cochlear metrics were considered repeatable.

Table 5.1 The repeatability of measurements and landmarking.

Parameters	ANOVA						Repeatability		
	Variance	Sum of sqrs	df	Mean square	F	Sig.	S ²	S ² A	r
Length	Between sp.	631.97	2	315.985	44560	***	0.00709	105.33	0.9999
	Within sp.	0.0425	6	0.0071					
Height	Between sp.	4.9948	2	2.4974	537.30	***	0.00465	0.8309	0.9944
	Within sp.	0.0279	6	0.0046					
Width	Between sp.	62.9367	2	31.4683	31510	***	0.00100	10.4891	0.9999
	Within sp.	0.0060	6	0.0010					
Volume	Between sp.	18417.6	2	9208.8	43490	***	0.21173	3069.53	0.9999
	Within sp.	1.2704	6	0.2117					
OW	Between sp.	11.2058	2	5.6029	3161	***	0.00177	1.8670	0.9991
	Within sp.	0.0106	6	0.0018					
RW	Between sp.	3.9422	2	1.9711	2524	***	0.00078	0.6568	0.9988
	Within sp.	0.0047	6	0.0008					
OW/RW	Between sp.	0.4572	2	0.2286	119	***	0.00192	0.0756	0.9752
	Within sp.	0.0115	6	0.0019					
H/W	Between sp.	2.1012	2	1.0506	341	***	0.00308	0.3492	0.9913
	Within sp.	0.0185	6	0.0031					
PC1	Between sp.	0.6411	2	0.3205	17280	***	0.00002	0.1068	0.9998
	Within sp.	0.0001	6	0.00002					
PC2	Between sp.	0.4735	2	0.2367	7777	***	0.00003	0.0789	0.9996
	Within sp.	0.0002	6	0.00003					
PC3	Between sp.	0.0030	2	0.0015	65.13	***	0.00002	0.0005	0.9553
	Within sp.	0.0001	6	0.00002					
PC4	Between sp.	0.0188	2	0.0094	1424	***	0.00001	0.0031	0.9979
	Within sp.	0.00004	6	0.000007					

*** $P < 0.001$; df = degrees of freedom

In shape space, the repeated shape variables were close to each other in the PCA plot (Fig. 5.7). Shape differences among repeated shape variables of the same specimen were significantly less than shape differences between that specimen and the nearest neighbour. These findings suggest that the landmarking and shape analyses were reliable.

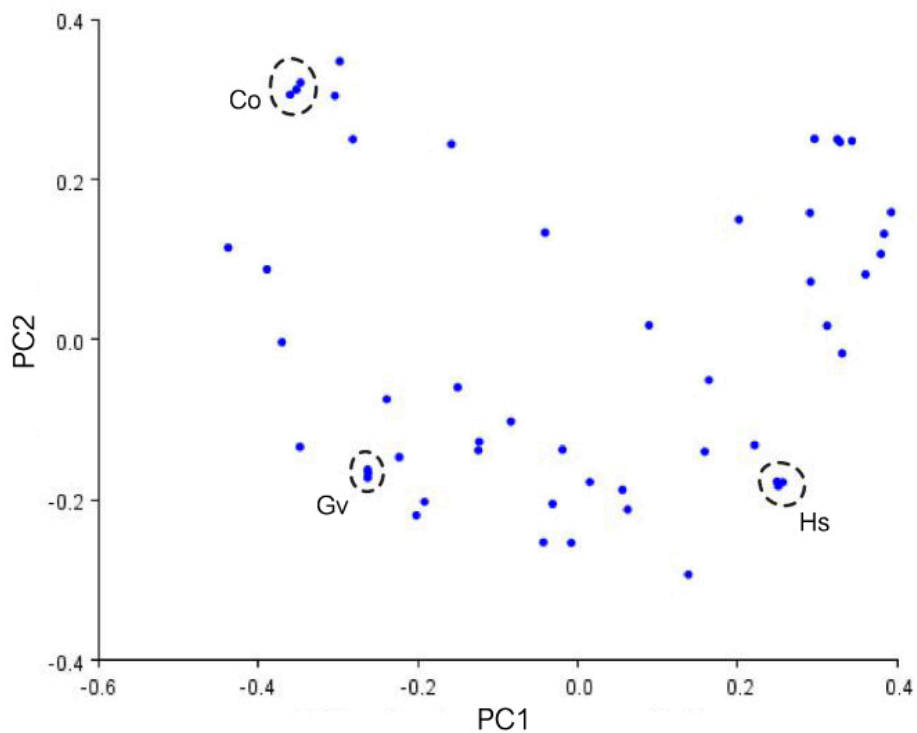


Figure 5.7 Repeatability test in shape space. Shape variation of the mammalian cochlea represented by the scatter plot of PC1 vs PC2. Three specimens (Co, Gv and Hs) chosen randomly were measured three times; repeated shape variables plotted closely together in shape space (dashed circles).

5.3 Bivariate analysis—allometry with body mass

Except for the number of spiral turns, all cochlear dimensions in the study were significantly correlated with body mass ($P < 0.01$ for OW/RW area; $P < 0.001$ for the others) (Table 5.2). Positive correlations with body mass were found in L, H, W, V, OW area and RW area, whereas negative correlations were found in the ratios of OW area/RW area and H/W. These strong correlations were examined by bivariate plots of log₁₀ body mass and the log₁₀ of each cochlear variable for the 45 mammalian species (Fig. 5.8). Reduced major axis (RMA) regression showed that these cochlear variables exhibited strong negative allometry with respect to body mass (expected slope for isometry = 0.33; observed slope < 0.33, $P < 0.001$). In other words, cochlea dimensions and ratios did not keep pace with increases of body size. When the relationships between the cochlear variables and body mass were examined without logarithmic transformations, the cochlear variables showed a curvilinear trend with positive allometry in mammals with small body sizes and negative allometry in larger mammals.

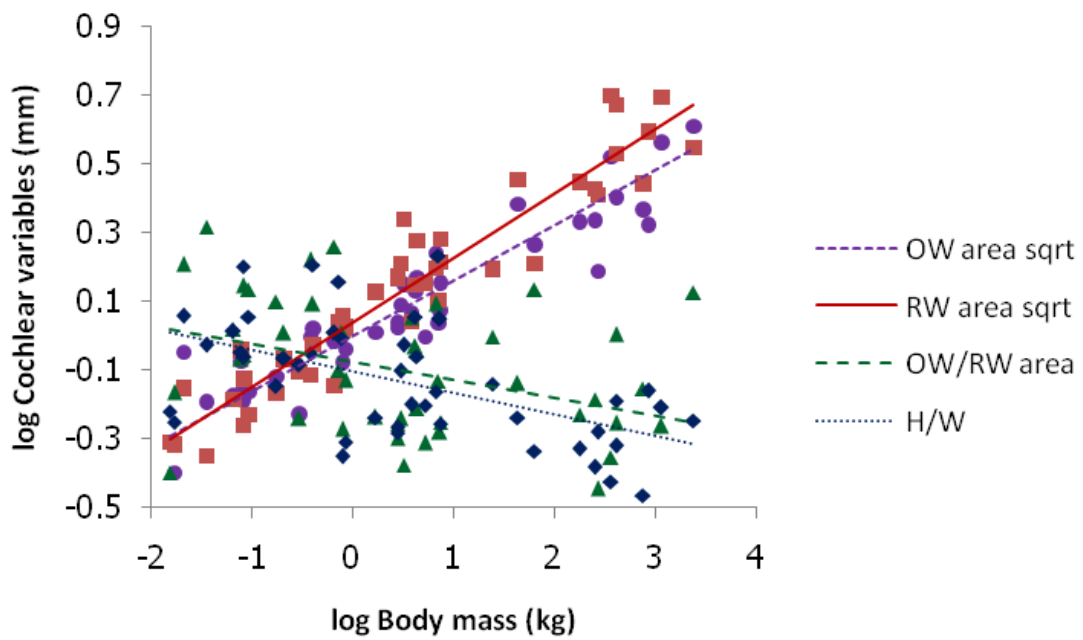
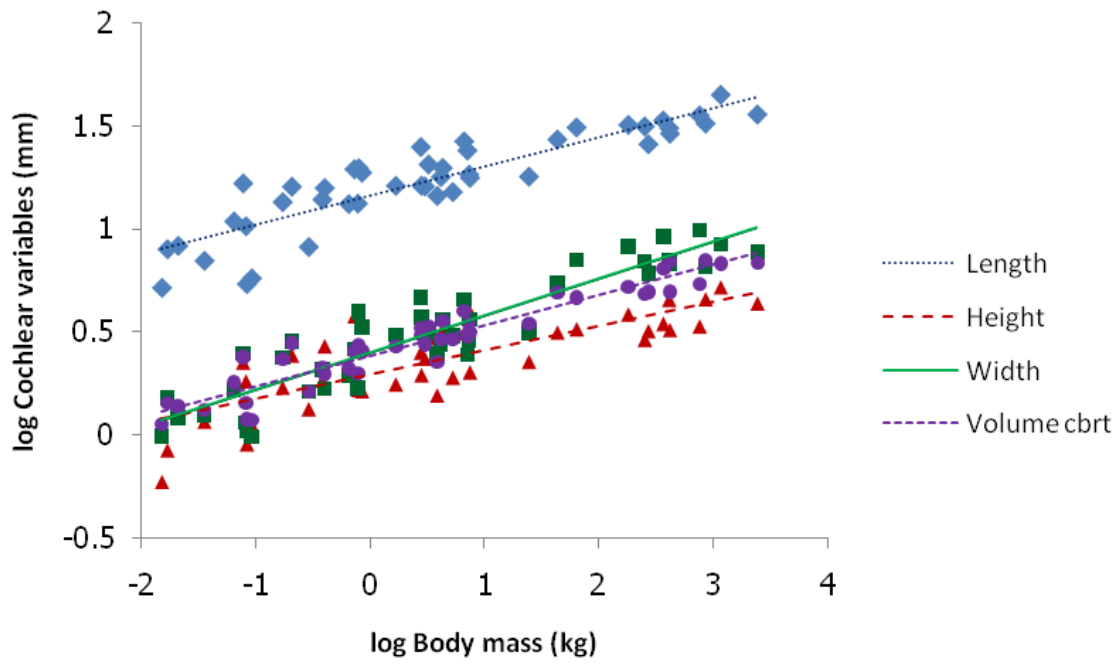


Figure 5.8 Bivariate plots showing the relationships between the cochlear variables and body mass. cbprt, cube root; H, height; OW, oval window; RW, round window; sqrt, square root; W, width.

Table 5.2 Spearman's rank correlation and RMA regression of cochlear variables with body mass.

Log body mass vs	r	Sig.	RMA regression		
			Slope	95% CI	Intercept
Log Length	0.8954	***	0.1589	0.1331-0.1849	1.1520
Log Height	0.8241	***	0.1437	0.1167-0.1703	0.2800
Log Width	0.8906	***	0.1949	0.172-0.2151	0.3888
Log Volume cbt	0.9427	***	0.1553	0.1405-0.1704	0.3791
Log (No. of turns)	-0.2142	ns			
Log OW area sqrt	0.9462	***	0.1730	0.1493-0.1977	-0.0065
Log RW area sqrt	0.9505	***	0.1967	0.1761-0.2152	0.0332
Log (OW/RW area)	-0.3871	**	-0.1389	(-0.168)-(-0.1091)	-0.0293
Log (H/W)	-0.5078	***	-0.1176	(-0.1447)-(-0.0859)	-0.0728

*** $P < 0.001$; ** $P < 0.01$; ns = not significant

Strong significant correlations with body mass were also found with the low frequency limit of hearing and the intermeatal distance ($P < 0.001$), with a negative correlation for the low frequency limit and a positive correlation for the intermeatal distance (Table 5.3, Fig. 5.9). Reduced major axis regression demonstrated that the intermeatal distance was strongly negatively allometric with respect to body mass (expected slope for isometry = 0.33; observed slope < 0.33, $P < 0.05$) and the low frequency limit had a negative scaling. When the data were examined without logarithmic transformations, the intermeatal distance had positive allometry in small mammals but negative allometry in large species. The low frequency limit had a faster scaling with body mass in small mammals than in large mammals. In contrast, no significant correlations with body mass were observed with the high frequency limit of hearing and the best hearing frequency.

For variables correlated with body size, residuals were calculated from the RMA regressions to minimise the effects of size scaling in some of the subsequent analyses (see sections of 5.6.4-5.6.7).

Table 5.3 Spearman's rank correlation and RMA regression of hearing parameters with body mass.

Log body mass vs	r	Sig.	RMA regression		
			Slope	95% CI	Intercept
Log high limit of hearing	-0.2467	ns			
Log low limit of hearing	-0.6383	***	-0.4115	(-0.504)-(-0.3087)	-0.6892
Log best frequency	-0.0337	ns			
Log intermeatal distance	0.9740	***	0.3046	0.2725-0.3373	1.4461

*** $P < 0.001$; ns = not significant

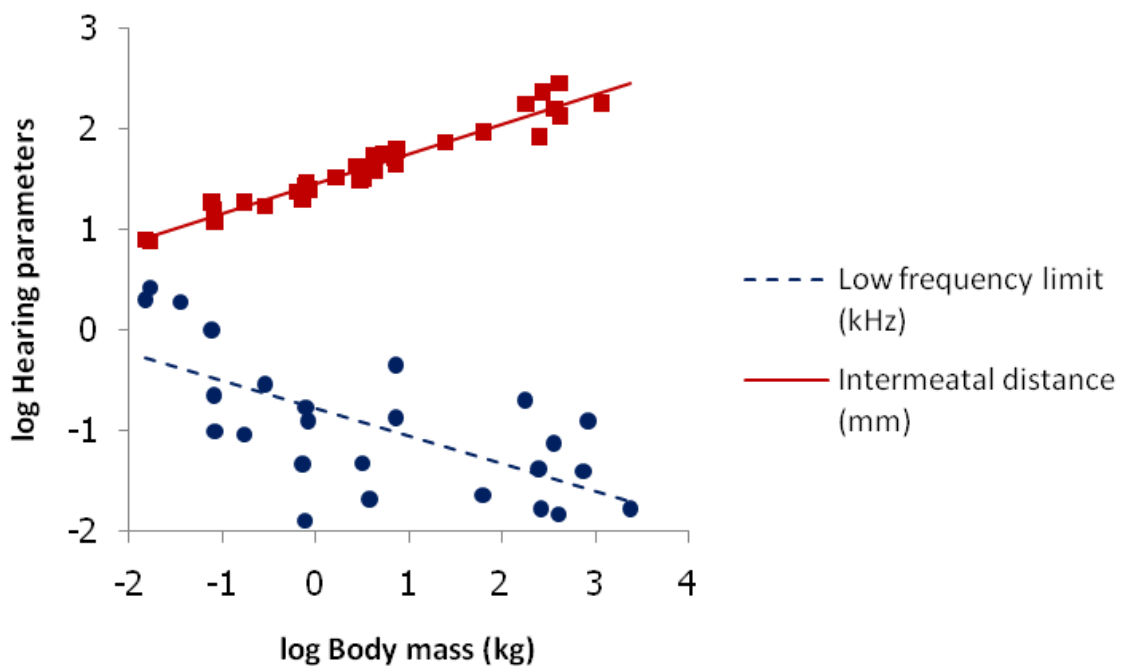


Figure 5.9 Bivariate plots showing the relationships between the hearing parameters and body mass.

5.4 Bivariate analysis—pairwise measurement comparisons

For pairwise comparisons of the cochlear variables, there were strong significant relationships between pairs of the cochlear variables (P value < 0.001; Table. 5.4). These results revealed that as expected increases in the individual linear cochlear measures (L, H and W) were associated with an increase in the cochlear volume (V). Based on the regression slope, it showed that as L increased, H and W increased more gradually in proportion (Fig. 5.10). The rate of increase in W was greater than H. The OW area was also positively correlated with the RW area. The regression slope indicated that the rate of increase in RW area was higher than that in OW area. The number of the cochlear turns, however, had no significant correlation with any other variable.

Table 5.4 Spearman's rank correlation and RMA regression of pairs of cochlear variables.

Plot	r	Sig.	RMA regression		
			Slope	95% CI	Intercept
Length vs height	0.8908	***	0.1168	0.1017-0.1305	0.2355
Length vs width	0.9452	***	0.2616	0.2244-0.2959	-1.3107
Height vs width	0.7711	***	2.2392	1.704-2.683	-1.8381
Volume cbt vs length	0.9501	***	5.4836	4.679-6.188	1.4811
Volume cbt vs height	0.8808	***	0.6405	0.5419-0.7157	0.4085
Volume cbt vs width	0.9473	***	1.4342	1.169-1.649	-0.9234
OW vs RW area	0.9499	***	1.3984	0.5999-1.818	0.1748

*** P < 0.001

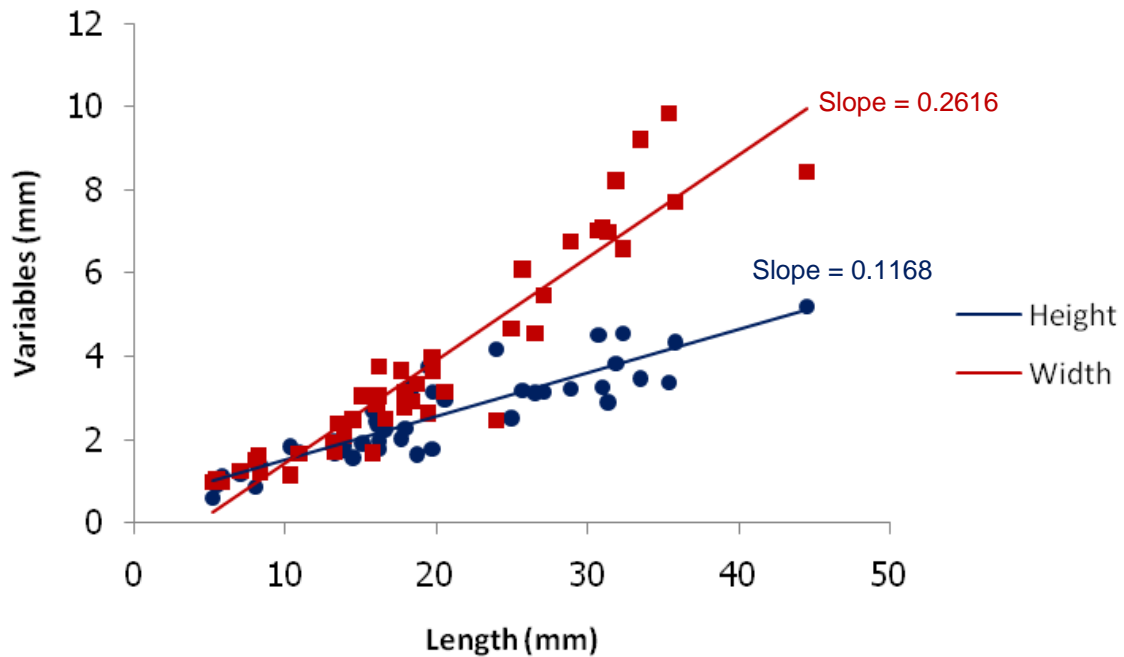


Figure 5.10 Bivariate plots of length, height and width. As length increased, height and width increased more gradually in proportion.

5.5 General geometric morphometrics

For shape analysis of the bony cochlea, principal components (PC) 1 through 4 met the criterion that each one described 5% or more of the variance. All four components accounted for 86.3% of the variance in total (Fig. 5.11, 5.12 and 5.13). The majority of shape variation of the cochlea across 45 species was summarized by the first two PC axes, which together explained 67.8% of the total variance. Specimens could be classified into two distinct clusters on the plot of PC1 vs PC2. The first cluster, including most of the species studied, had a bell-shaped scatter; the other cluster, comprising six species, was located at the positive extreme of PC2 (Fig. 5.12).

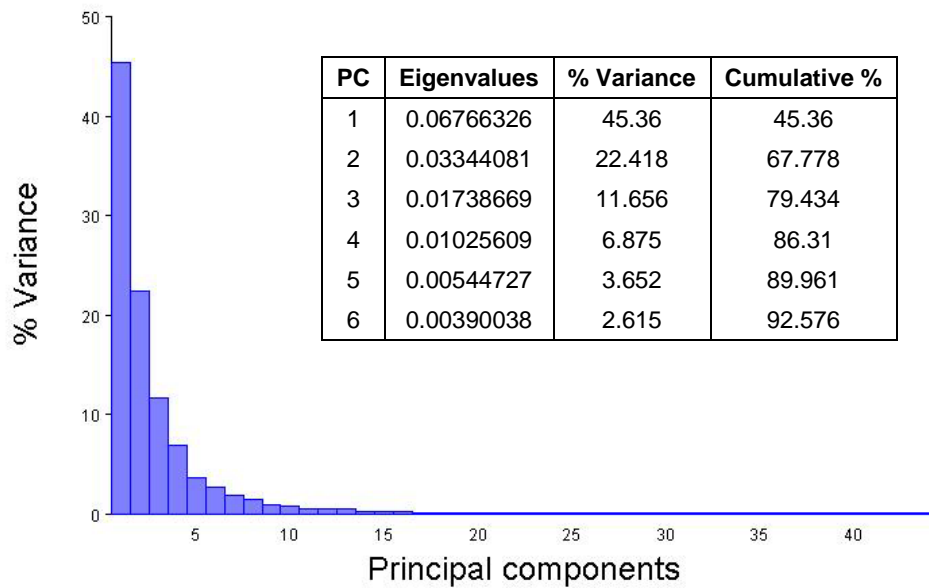


Figure 5.11 Plot of the proportion of variance accounted for each PC. Only PC1 to PC4 described more than 5% of the total variance.

The pattern of shape variability described by each PC was visualised by warping the mean shape along each axis. Shape variations on PC1 primarily represented changes in the number of spiral turns and the radius of curvature at the basal cochlear part. The positive extreme of PC1 was characterized by fewer spiral turns and a larger radius of curvature at the basal turn than at the negative extreme. The most representative species of the positive extreme were obligate aquatic species (Fig. 5.12, dashed circle) and large terrestrial species. Variations on PC2 principally represented the twisting pattern of the middle turn with changes in its slope and angle. The positive extreme of PC2 indicated a more tightly packed middle turn and more tapered cochlear shape. Species presenting these patterns formed a distinct cluster consisting of five rodents (prairie dog, plains viscacha, tuco-tuco, guinea pig and coypu) and a single primate (tarsier). PC3 primarily described variation in the radii ratio of curvature of the basal turn relative to the middle turn. The larger ratio of

curvature corresponded to the positive extreme of the axis and was represented in obligate aquatic species and some primates. The low ratio at the negative extreme was represented by some rodents (e.g., the coypu and guinea pig). Shape variation on PC4 was related to changes in the elongation and diameter of coiling. The negative extreme showed an elongated cochlea. Also, the diameter of coiling became increasingly uniform and spring-like. The most representative species of this negative extreme were the coypu and guinea pig, which were clearly separated from other species (Fig. 5.13, solid circles). The positive extreme of PC4 was characterized by a more spiral-shaped cochlea. It was noteworthy that obligate aquatic species remained tightly clustered on PC1 through to PC4 (Fig. 5.12 and 5.13). Based on the overview of constructed cochlear wireframes from all 4 PCs, many landmark coordinates at the middle part and the apex of the cochlea had obviously large shifts in position. In contrast, landmark positions relative to the basal turn, particularly the most basal, seemed rather constant in comparison with the middle turn and the apex.

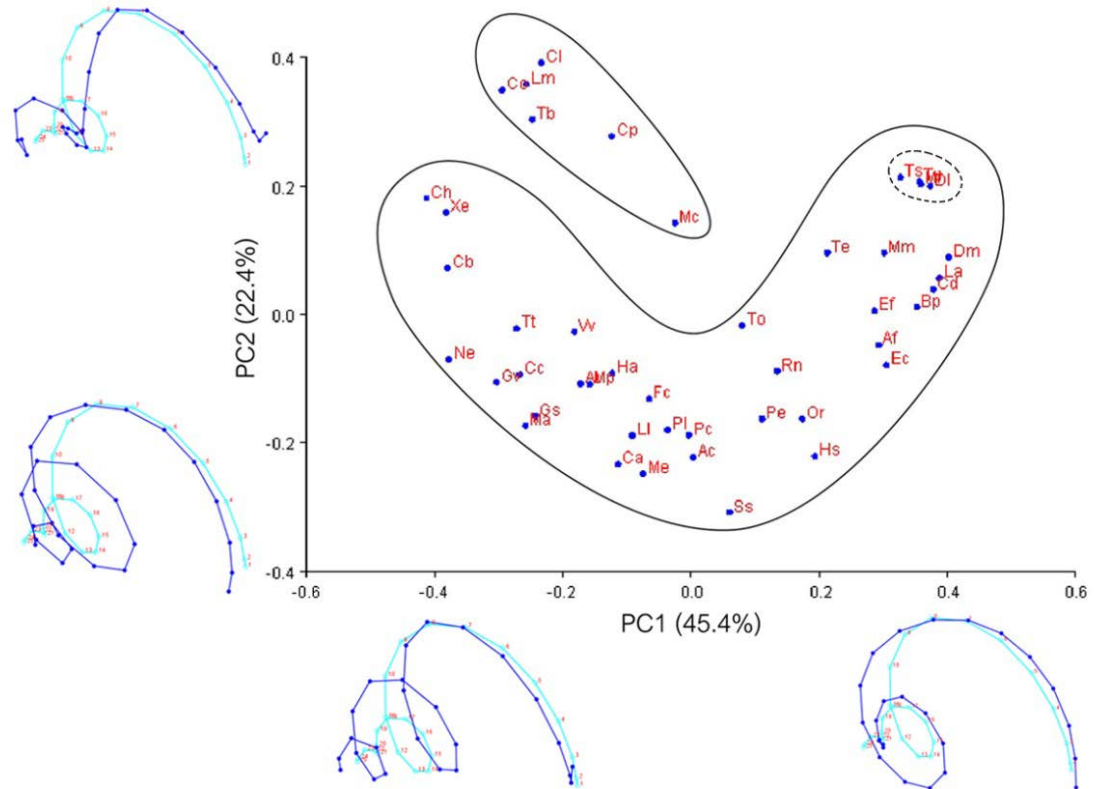


Figure 5.12 Shape variation of the cochlea in 45 mammalian species. Scatter plots of PC1 vs PC2 together explained 67.8% of the total variance. The pattern of shape variability represented by each PC was indicated by the constructed cochlear wireframes. The light blue lines indicated the mean shape (the coordinate (0.0, 0.0)) and the dark blue lines showed the shape at the extreme of each axis. Specimens were divided into two clusters (solid circles), and the dashed circle included obligate aquatic species.

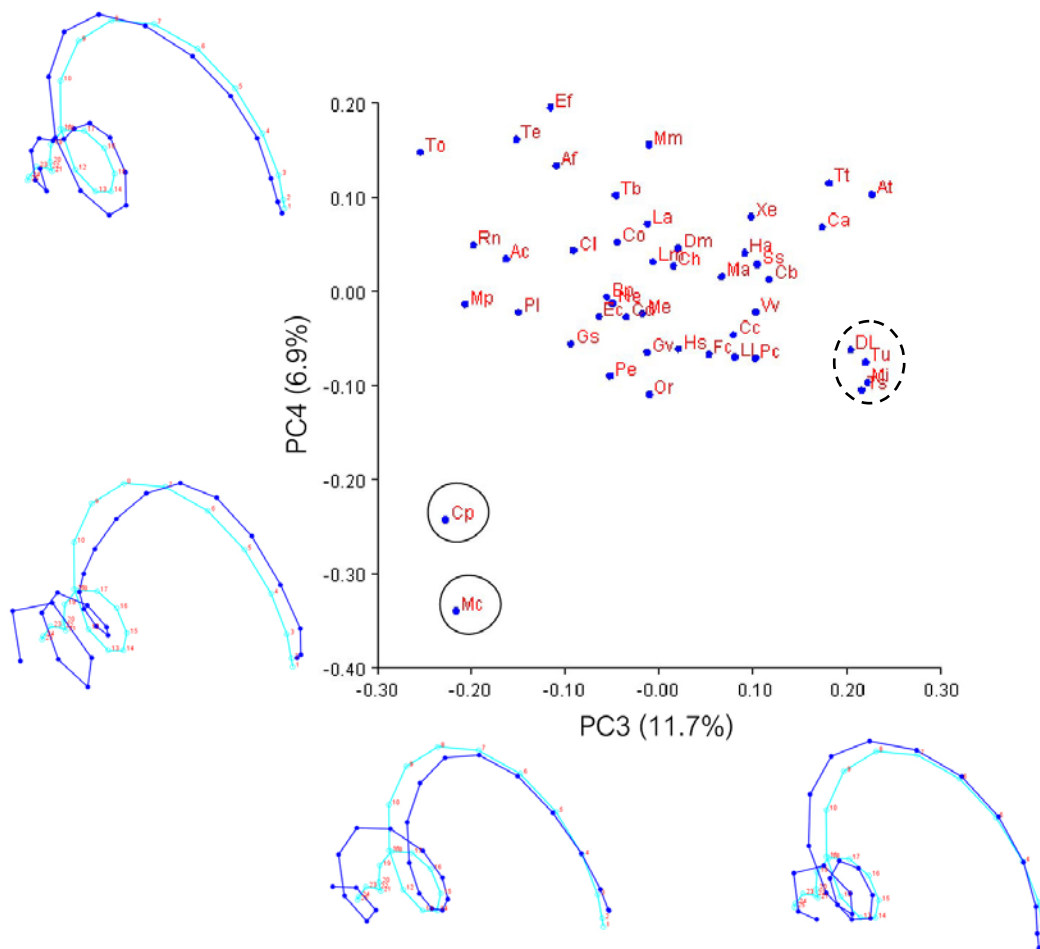


Figure 5.13 Shape variation of the cochlea in 45 mammalian species. Scatter plots of PC3 vs PC4 together explained 18.6% of the total variance. The dashed circle was obligate aquatic species and the solid circles were the guinea pig (Cp) and coypu (Mc).

Reduced major axis regression analysis of the PC scores against the natural log-transformed centroid size was performed to examine the effects of size on shape variation. The result showed that scores on the PC1, PC3 and PC4 axes were significantly correlated with centroid size ($P < 0.001$; Table 5.5). This was consistent with the findings of strong correlations of the PC scores and body mass ($P < 0.01$; Table 5.6). These results indicated that size differences of the cochlea played a significant role in determining the cochlear shape. Therefore, shape residuals (on

PC1, PC3 and PC4) from the regression on centroid size were calculated and were used in subsequent analyses to minimise the effect of allometric scaling in the shape space.

Table 5.5 Spearman's rank correlation and RMA regression of PCs with centroid size.

Ln centroid size vs	r	Sig.	RMA regression		
			Slope	95% CI	Intercept
PC1	0.4951	***	0.45152	0.3669-0.5193	-0.91846
PC2	-0.0557	ns			
PC3	0.4862	***	0.22888	0.1769-0.2706	-0.46558
PC4	-0.4991	***	-0.17579	(-0.2279)-(-0.1091)	0.35758

*** $P < 0.001$; ns = not significant

Table 5.6 Spearman's rank correlation and RMA regression of PCs with body mass.

Log body mass vs	r	Sig.	RMA regression		
			Slope	95% CI	Intercept
PC1	0.4708	**	0.17806	0.1471-0.2039	-0.09651
PC2	-0.0447	ns			
PC3	0.4169	**	0.09026	0.06698-0.1092	-0.04892
PC4	-0.4642	**	-0.06932	(-0.08974)-(-0.04361)	0.03757

** $P < 0.01$; ns = not significant

When shape variation after minimising the allometric effects was considered, no species or groups were clearly separated from others on the first two PCs (Fig. 5.14). Four obligate aquatic mammals, however, remained closely clustered on PC axes, although were not completely separate from others. Five of six species in the second cluster on PC1 vs PC2 in Figure 5.12 were still clustered on residual PC1 vs PC2, except for the coypu. On residual PC3 and residual PC4, the guinea pig and coypu still had different cochlear shapes from other species.

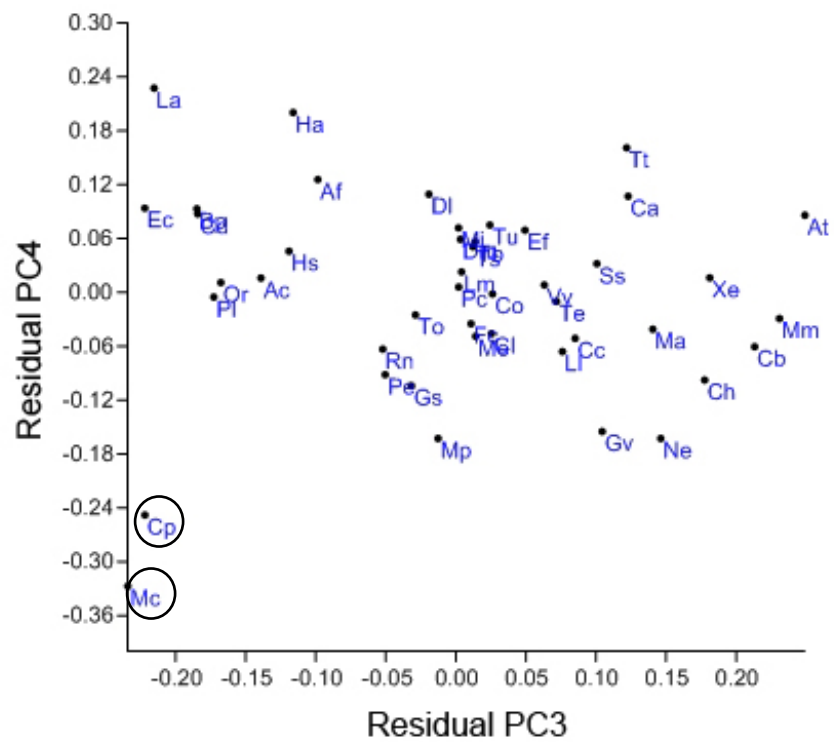
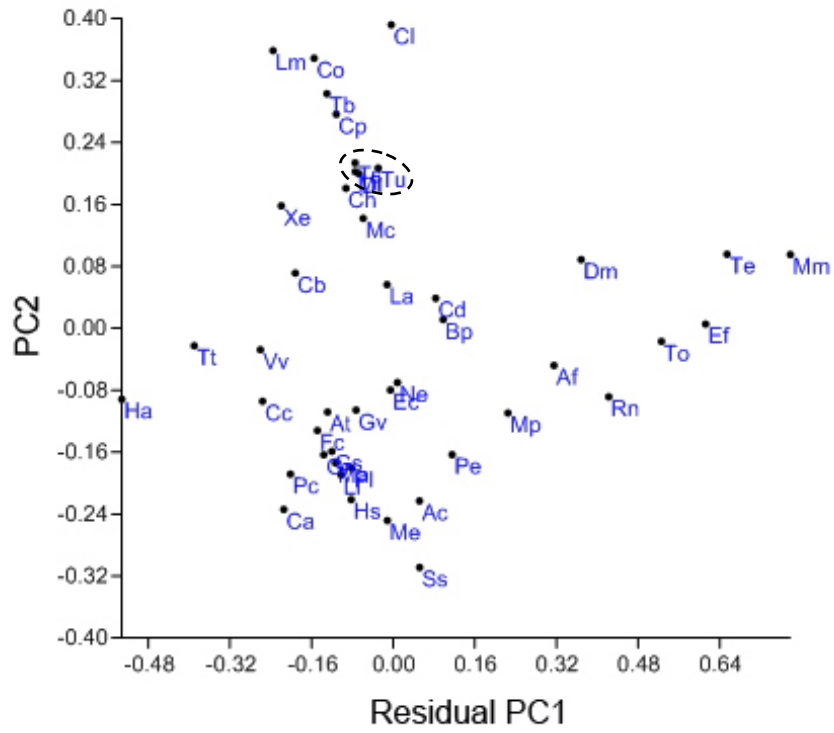


Figure 5.14 Shape variation of the cochlea on the first four PCs after minimising the allometric effects. The dashed circle was obligate aquatic species and the circled species were the guinea pig (Cp) and coypu (Mc).

5.6 Relationships between the bony cochlear morphology and ecological and hearing influences

This section presents comparisons between groups of species representing different hearing parameter categories and different eco-behavioral categories, including habitat, active period and sociality. Categories of hearing parameters included the high-frequency limit of hearing, low-frequency limit of hearing, best hearing frequency and intermeatal distance.

5.6.1 Habitat selection

In general, the univariate analyses (Table 5.7) suggested that marine mammals possessed larger cochleae and cochlear fenestrae than any other group. The averaged number of spiral turns in marine species was almost exactly two turns. The means of L, H and W were highest in marine species, corresponding with a greatly enlarged cochlear volume. This was in contrast to subterranean mammals that had the lowest means of L, H, W, V and the cochlear fenestrae.

After using ANCOVA to control for the effects of body mass, several significant differences in cochlear variables were found in pairwise comparisons between terrestrial and subterranean groups (Fig. 5.15). Values of W and V showed strongly significant differences ($P < 0.001$) and the size-adjusted means were higher in aboveground species than in underground species (see Appendix D.4). In addition, the OW/RW and H/W ratios showed moderately significant differences at the $P < 0.01$ level. Unlike W and V, the size-adjusted means of these ratios in underground species were higher than those in aboveground species.

Between terrestrial and fossorial mammals, the OW/RW ratio and W showed significant differences at the $P < 0.01$ (Fig. 5.15) and $P < 0.05$ levels, respectively. Fossorial species had a higher size-adjusted mean of the OW/RW ratio, whereas terrestrial species had a higher size-adjusted mean of W.

Concerning the number of cochlear turns, marine mammals were significantly different from fossorial species at the $P < 0.01$ level (Fig. 5.15), and from ground dwellers at $P < 0.05$ level. The adjusted means in marine mammals were less than those in fossorial and terrestrial species.

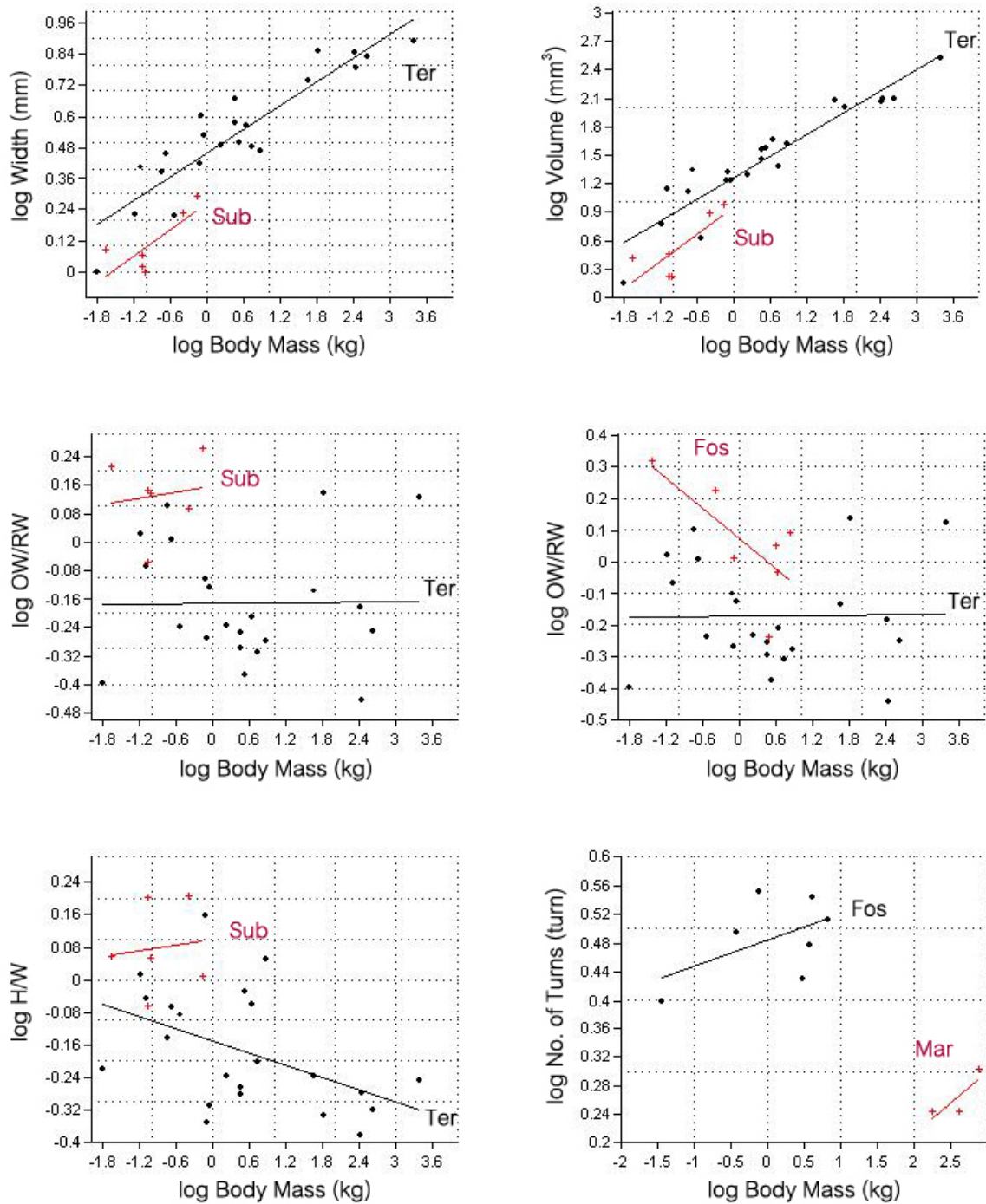


Figure 5.15 The ANCOVA plots with regression lines showed all cochlear variables statistically significantly related to habitat differences at the $P < 0.001$ or 0.01 level. Ter, terrestrial; Sub, subterranean; Fos, fossorial; Mar, marine.

Table 5.7 Univariate analyses of the cochlear variables in categorical data.

Classifier	Group	n	Length (mm)		Height (mm)		Width (mm)		Volume (mm ³)		No. of turns		OW area (mm ²)		RW area (mm ²)		OW/RW area		H/W ratio	
			mean	SD	mean	SD	mean	SD	mean	SD	mean	SD	mean	SD	mean	SD	mean	SD	mean	SD
Habitat	Ter	22	19.975	7.724	2.490	0.904	3.921	1.941	56.742	72.653	2.708	0.531	2.477	3.579	3.381	3.550	0.722	0.300	0.704	0.261
	Fos	7	15.605	5.887	2.120	0.775	2.542	1.073	20.193	20.986	3.089	0.395	1.464	0.828	1.446	0.927	1.232	0.493	0.863	0.175
	Sub	6	9.820	4.133	1.651	0.654	1.337	0.382	4.276	3.323	2.875	0.648	0.703	0.282	0.518	0.209	1.385	0.321	1.225	0.303
	Sem	6	28.327	10.435	3.616	1.272	5.577	2.887	172.669	155.343	2.865	0.784	5.727	5.134	12.044	10.928	0.594	0.245	0.778	0.471
	Mar	3	32.664	2.443	3.911	0.583	8.352	1.406	214.061	111.267	1.833	0.144	10.773	9.980	12.547	8.274	0.767	0.217	0.485	0.152
Active period	D	13	24.788	8.399	2.784	0.878	5.326	2.739	90.492	90.436	2.688	0.591	3.827	4.259	4.842	4.196	0.900	0.410	0.641	0.342
	N	25	15.846	8.738	2.180	1.083	2.744	1.676	34.933	64.379	2.788	0.532	1.741	2.702	2.622	4.897	0.926	0.451	0.869	0.306
	C	4	17.168	1.912	2.642	0.971	2.873	0.213	21.252	4.012	3.141	0.896	1.202	0.420	1.747	0.373	0.697	0.201	0.943	0.414
Sociality	S	16	21.955	10.041	2.765	1.194	4.445	2.732	92.384	116.001	2.681	0.661	3.844	5.374	5.706	7.411	0.784	0.352	0.750	0.357
	G	29	15.429	6.494	2.101	0.762	2.700	1.316	26.078	30.504	2.844	0.482	1.520	1.371	2.018	2.117	1.039	0.492	0.863	0.283
High freq. limit	H	7	17.986	11.993	2.171	1.275	3.977	3.545	51.413	68.632	2.420	0.721	1.907	2.230	3.172	3.513	0.604	0.161	0.661	0.228
	M	7	20.383	9.197	2.577	1.310	4.257	2.834	96.715	143.657	2.714	0.830	5.250	8.435	7.306	11.039	0.977	0.552	0.720	0.368
	L	11	21.437	10.249	2.680	1.177	4.307	2.606	100.976	125.622	2.660	0.489	3.470	4.545	4.877	5.046	0.864	0.410	0.762	0.351
Low freq. limit	H	8	13.130	8.804	1.737	1.026	2.614	2.427	25.017	48.342	2.578	0.705	1.101	1.547	1.736	2.720	0.890	0.563	0.803	0.361
	M	7	20.231	9.941	2.469	1.299	4.207	2.778	101.781	144.724	2.509	0.464	2.777	3.873	6.616	9.612	0.667	0.324	0.671	0.261
	L	10	25.775	8.340	3.154	0.978	5.466	2.755	123.503	121.998	2.701	0.750	6.002	7.329	6.678	6.522	0.878	0.350	0.693	0.333
Best hearing freq.	H	8	21.054	12.817	2.665	1.621	4.786	3.496	127.129	150.074	2.273	0.661	4.760	7.431	6.875	8.200	0.638	0.232	0.628	0.180
	M	8	19.778	7.803	2.457	0.993	4.004	2.525	61.918	91.020	2.805	0.707	2.353	3.554	5.046	8.268	0.827	0.578	0.732	0.357
	L	8	20.005	11.227	2.465	1.151	3.881	2.869	75.537	109.424	2.720	0.547	3.666	5.372	3.499	4.200	1.037	0.330	0.827	0.395
Intermeatal distance	H	10	29.317	7.753	3.391	0.957	6.657	1.948	160.023	109.924	2.358	0.483	7.246	6.499	11.295	9.023	0.707	0.312	0.526	0.108
	M	10	18.735	3.587	2.676	0.811	3.113	0.640	29.014	10.960	2.988	0.563	1.471	0.410	2.438	1.043	0.655	0.218	0.892	0.357
	L	12	12.651	5.264	1.691	0.819	2.069	0.934	9.135	6.642	2.927	0.725	0.612	0.319	0.707	0.391	0.913	0.405	0.868	0.355

Note: Ter, terrestrial; Sub, subterranean; Fos, fossorial; Mar, marine; C, crepuscular; D, diurnal; N, nocturnal; G, gregarious; S, solitary;

H, high value; M, medium value; L, low value; SD, standard deviation.

In shape analysis, results differ between the discriminant function analysis (DFA) and Mann-Whitney U test. In DFA, a significant difference in cochlear shape was only present between fossorial and marine mammals at the $P < 0.01$ level (Table 5.8). This is a very conservative test, however, as it spans the whole shape space, many parts of which will be unrelated or spurious shape changes. The Mann-Whitney test indicated that the shape of the cochlea in marine species was slightly significantly different from that in terrestrial and subterranean species as defined by principal components ($P < 0.05$; Table 5.9). Cochlear shape was also weakly significantly different between terrestrial and underground species ($P < 0.05$; Table 5.9).

Table 5.8 Discriminant function analysis with permutation tests (10,000 iterations) of regression residuals across the whole shape space.

Classifier	Group 1	Group 2	Procrustes dis.	T ² (Sig.)	DFA (%)		Cross-validation (%)	
					Group 1	Group 2	Group 1	Group 2
Habitat	Fos	Mar	0.0414	**	100	100	86	100
Habitat	Fos	Sem	0.5069	ns	86	83	43	17
Habitat	Fos	Sub	0.5880	ns	100	100	71	67
Habitat	Fos	Ter	0.0345	ns	86	100	14	77
Habitat	Mar	Sem	0.0249	ns	100	83	100	100
Habitat	Mar	Sub	0.2403	ns	100	83	67	67
Habitat	Mar	Ter	0.0103	ns	100	100	100	77
Habitat	Sem	Sub	0.4990	ns	100	100	67	67
Habitat	Sem	Ter	0.2326	ns	100	95	17	59
Habitat	Sub	Ter	0.1006	ns	100	100	67	82
Active period	C	D	0.6675	ns	100	92	0	23
Active period	C	N	0.5081	ns	100	100	0	48
Active period	D	N	0.4756	*	92	100	31	52
Sociality	G	S	0.4374	ns	100	100	55	44
High freq. limit	H	L	0.1295	ns	100	91	29	36
High freq. limit	H	M	0.2180	ns	86	100	43	43
High freq. limit	L	M	0.6440	ns	91	100	45	29
Low freq. limit	H	L	0.8613	ns	88	90	38	30
Low freq. limit	H	M	0.4727	ns	75	100	50	29
Low freq. limit	L	M	0.4487	ns	90	86	40	29

Classifier	Group 1	Group 2	Procrustes dis.	T ² (Sig.)	DFA (%)		Cross-validation (%)	
					Group 1	Group 2	Group 1	Group 2
Best freq.	H	L	0.1497	**	100	100	88	100
Best freq.	H	M	0.0388	ns	88	88	63	50
Best freq.	L	M	0.7789	ns	88	100	25	50
Intermeatal dis.	H	L	0.8454	ns	100	100	20	8
Intermeatal dis.	H	M	0.3308	ns	100	100	20	10
Intermeatal dis.	L	M	0.2918	ns	100	90	17	10

** $P < 0.01$; * $P < 0.05$; ns = not significant; Abbreviations are the same as Table 7.

Table 5.9 Mann-Whitney U test of PC scores after removal of the allometric effects.

Classifier	Pairs	PC1	PC2	PC3	PC4
Habitat	Fos-Mar	ns	ns	ns	ns
Habitat	Fos-Sem	ns	ns	ns	ns
Habitat	Fos-Sub	ns	ns	ns	ns
Habitat	Fos-Ter	ns	ns	ns	ns
Habitat	Mar-Sem	ns	ns	ns	ns
Habitat	Mar-Sub	ns	ns	ns	*
Habitat	Mar-Ter	ns	*	ns	ns
Habitat	Sem-Sub	ns	ns	ns	ns
Habitat	Sem-Ter	ns	ns	ns	ns
Habitat	Sub-Ter	ns	*	*	*
Active period	C-D	ns	ns	ns	ns
Active period	C-N	ns	ns	ns	ns
Active period	D-N	ns	ns	ns	*
Sociality	G-S	ns	ns	ns	ns
High freq. limit	H-L	ns	ns	ns	ns
High freq. limit	H-M	ns	ns	ns	ns
High freq. limit	L-M	ns	ns	ns	ns
Low freq. limit	H-L	ns	ns	ns	ns
Low freq. limit	H-M	ns	ns	ns	ns
Low freq. limit	L-M	ns	ns	ns	ns
Best freq.	H-L	ns	ns	ns	ns
Best freq.	H-M	ns	ns	ns	ns
Best freq.	L-M	ns	ns	ns	ns
Intermeatal dis.	H-L	ns	ns	ns	*
Intermeatal dis.	H-M	ns	ns	ns	ns
Intermeatal dis.	L-M	ns	ns	ns	ns

* $P < 0.05$; ns = not significant. Abbreviations are the same as Table 5.7.

5.6.2 Activity period

Results of the ANCOVA showed that the period of the day during which a mammal is active was unrelated to cochlear dimensions. In the shape analysis, DFA showed a shape difference between diurnal and nocturnal species ($P < 0.05$; Table 5.8). Similarly, the Mann-Whitney U test showed a shape difference between diurnal and nocturnal species across PC4 ($P < 0.05$; Table 5.9). An overview of the shape variations along PC4 are given in above in section 5.5.

5.6.3 Sociality

Regarding the pattern of sociality in relation to the cochlear dimensions, only the area of OW showed a statistically significant difference between solitary mammals and gregarious mammals ($P < 0.01$) whilst controlling for the effects of body mass (Fig. 5.16). The adjusted mean of the OW surface area in solitary species was higher than that in gregarious species (see Appendix D.5). In the analysis of shape variation, no significant differences in the cochlear shape were documented between solitary and sociable mammals in both DFA and Mann-Whitney U test.

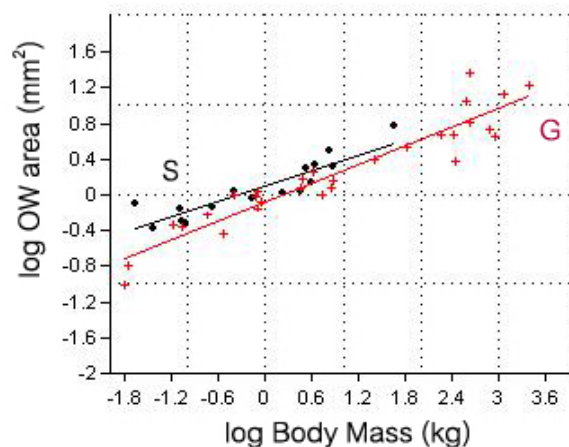


Figure 5.16 The ANCOVA graph with regression lines showed the significant difference in OW area between solitary mammals (S) and gregarious mammals (G) at the $P < 0.01$ level.

5.6.4 High frequency limit of hearing

When the high frequency limit was compared with the residual cochlear variables using RMA regression, the results showed that W and V were significantly related to the high frequency limit. The strength of the relationship was weaker for V ($r = 0.41$; $P < 0.05$) than for W ($r < 0.61$; $P < 0.01$; Table 5.10).

In comparisons between categories using ANCOVA, the results demonstrated that mammals with a medium value of the high frequency limit were significantly different from mammals with a low value of the limit in terms of L ($P < 0.05$), W ($P < 0.01$) and V ($P < 0.001$) (Fig. 5.17). The adjusted means of these cochlear variables were higher in mammals with a medium value of the limit (see Appendix D.6). Moreover, W in the group having a high value of the limit was significantly different from the group with a low value of the limit ($P < 0.05$). The adjusted mean of W was higher in the group with the highest high-frequency limit.

Table 5.10 Spearman's rank correlation and RMA regression of residual cochlear variables with high frequency limit.

Log high frequency limit vs	r	Sig.	RMA regression		
			Slope	95% CI	Intercept
Residual log length	0.2578	ns			
Residual log height	0.1697	ns			
Residual log width	0.6138	**	2.4464	1.626-3.124	1.6513
Residual log volume cbrt	0.4102	*	3.8673	2.238-11.25	1.6862
Residual log OW area sqrt	-0.0889	ns			
Residual log RW area sqrt	0.2578	ns			
Residual log (OW/RW area)	-0.3529	ns			
Residual log (H/W)	-0.3633	ns			
Log (No. of turns)	-0.2482	ns			

** $P < 0.01$; * $P < 0.05$; ns = not significant.

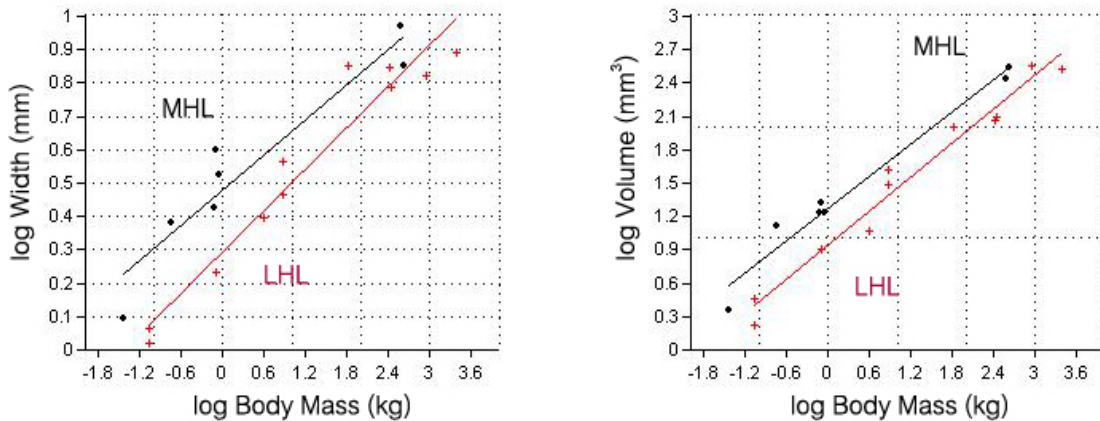


Figure 5.17 The ANCOVA graphs with regression lines showed the two cochlear variables statistically related to the categorical variables of the high frequency limit of hearing at the $P < 0.001$ or 0.01 level. MHL, medium high frequency limit; LHL, low high frequency limit.

In shape analysis of the cochlea using RMA regression, no significant relationships existed between the upper frequency limit and size-corrected shape variables. In addition, DFA and Mann-Whitney U test did not show statistically significant differences between categorical variables of the upper frequency limit and size-corrected shape variables.

5.6.5 Low frequency limit of hearing

The results showed that the low frequency limit was significantly related to the number of spiral turns at the $P < 0.01$ level (Table 5.11).

Independent of body mass using ANCOVA, the number of the spiral turns showed only a marginally significant difference between the group with a high value and the group with a low value of the low frequency limit ($P < 0.05$). Based on the adjusted means, there were fewer cochlear whorls in mammals with a high value of the low frequency limit (see Appendix D.7).

Table 5.11 Spearman's rank correlation and RMA regression of residual cochlear variables with residual low frequency limit.

Residual log low frequency limit vs	r	Sig.	RMA regression		
			Slope	95% CI	Intercept
Residual log length	-0.2238	ns			
Residual log height	-0.1877	ns			
Residual log width	0.1154	ns			
Residual log volume cbrrt	0.0262	ns			
Residual log OW area sqrt	-0.26	ns			
Residual log RW area sqrt	-0.0315	ns			
Residual log (OW/RW area)	0.0962	ns			
Residual log (H/W)	0.0331	ns			
Log (No. of turns)	-0.557	**	-5.3681	(-6.867)-(-3.443)	2.1688

** $P < 0.01$; ns = not significant.

In shape analysis of the cochlea, when compared using RMA regression, a significant relationship was present between the low frequency limit of hearing and the PC4 residuals ($P < 0.05$; Table 5.12). No significant differences in cochlear shape in relation to the low hearing limit, however, were found in both DFA and Mann-Whitney U test.

Table 5.12 Spearman's rank correlation and RMA regression of PC residuals with residual low frequency limit.

Residual log low frequency limit vs	r	Sig.	RMA regression		
			Slope	95% CI	Intercept
Residual PC1	0.1092	ns			
PC2	-0.0238	ns			
Residual PC3	-0.1769	ns			
Residual PC4	0.4292	*	5.6796	2.248-7.629	-0.0259

* $P < 0.05$; ns = not significant.

5.6.6 Best frequency of hearing

In comparisons between the best hearing frequency and the residual cochlear variables using RMA regression, results showed that W was significantly related to the best frequency at the $P < 0.05$ level (Table 5.13).

Table 5.13 Spearman's rank correlation and RMA regression of residual cochlear variables with best hearing frequency.

Log best hearing frequency vs	r	Sig.	RMA regression		
			Slope	95% CI	Intercept
Residual log length	0.0748	ns			
Residual log height	0.0267	ns			
Residual log width	0.4793	*	4.6494	2.823-6.083	0.8261
Residual log volume cbrt	0.2943	ns			
Residual log OW area sqrt	-0.2755	ns			
Residual log RW area sqrt	0.1233	ns			
Residual log (OW/RW area)	-0.2664	ns			
Residual log (H/W)	-0.3158	ns			
Log (No. of turns)	-0.2935	ns			

* $P < 0.05$; ns = not significant.

In comparisons between categories using ANCOVA, W and V in mammals with a medium value of the best frequency were significantly different from those in mammals with lower best hearing frequency ($P < 0.01$; Fig. 5.18). The adjusted means of W and V were higher in the group with a medium best frequency than the group with a low best frequency (see Appendix D.8). Also, the OW/RW areal ratio showed a significant difference between mammals with high and low best hearing frequency ($P < 0.05$). The adjusted mean of the ratio in the group with low best frequency was higher than that in the other.

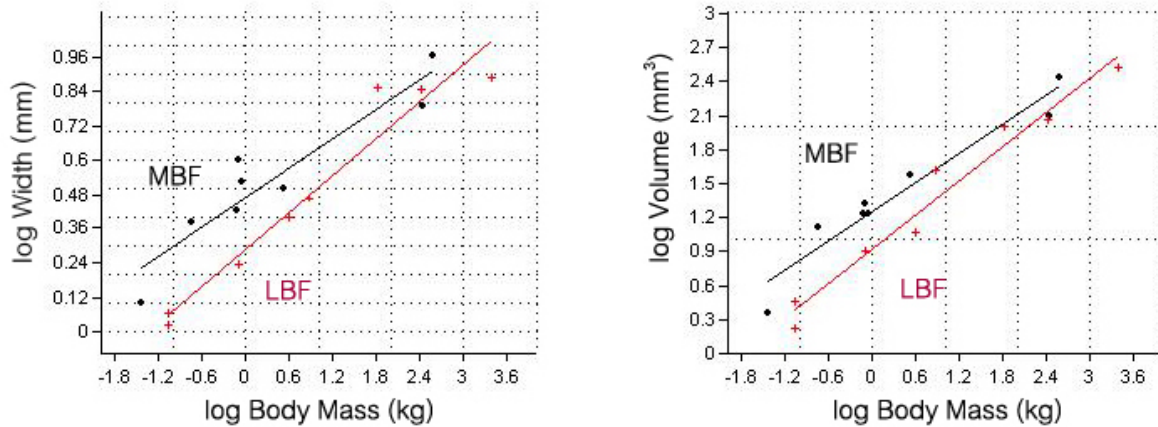


Figure 5.18 The ANCOVA plots with regression lines showed the two cochlear variables statistically related to the categorical variables of the best hearing frequency at the $P < 0.001$ or 0.01 level. MBF, medium best frequency; LBF, low best frequency.

When testing cochlear shape variation via RMA regression, the best hearing frequency was not statistically related to size-corrected shapes. There was a discrepancy between the results from DFA and Mann-Whitney U test. A significant difference was found between the group with a high best frequency and the group with a low best frequency ($P < 0.01$; Table 5.8) in DFA, whereas no significant difference in cochlear shape was found in the equivalent Mann-Whitney U test.

5.6.7 Intermeatal distance

After RMA regression analysis of the residuals, no relationship was discovered between the intermeatal distance and the cochlear dimensions. Also, in comparisons between categories using ANCOVA, the cochlear dimensions were not significantly different among mammalian groups with different intermeatal distances. In other words, the intermeatal distance showed no considerable influence on the cochlear parameters.

In the analysis of shape variation via RMA regression, no significant relationships were noted between the intermeatal distance and size-corrected shape variables. The Mann-Whitney U test, however, indicated that mammals with a high value of the distance had a different cochlear shape from mammals with short intermeatal distances as represented along PC4 ($P < 0.05$; Table 5.9).

5.7 Test of phylogenetic signal

When the phylogeny of all 45 mammalian species was subjected to the permutation test, it showed that the cochlear shape was significantly correlated with phylogeny for both weighted and unweighted squared-change parsimony (Table 5.14). Nevertheless, when this correlation within individual subclades (i.e., primates and rodents) was tested, different results were obtained. There was no phylogenetic signal in shape variation of the cochlea in primates, whereas the cochlear shape in rodents exhibited a significant correlation with phylogeny for unweighted as well as weighted squared-change parsimony (Table 5.14). Obviously, although the phylogenies of the whole sample and at the level of rodent subclade were correlated with variation in cochlear shape, distances in morphometric spaces seemed unlikely to be congruent with phylogenetic distances. Closely related species did not necessarily fall closely together in morphometric space, and some distantly related species resembled one another in cochlear shape. Hence, criss-cross long branches were found in the graph (Fig. 5.19, 5.20 and 5.21). The tree from morphometric data on cochlear shape was therefore inconsistent with the phylogeny of mammals.

Table 5.14 Tree lengths and *P* values for the permutation test of phylogenetic signal.

Phylogeny	n	Unweighted		Weighted	
		Tree length	Sig.	Tree length	Sig.
All	45	2.99071	***	3.66427	***
Rodents	15	1.22443	*	1.39603	*
Primates	8	0.52800	ns	0.66560	ns

****P* < 0.001; **P* < 0.05; ns = not significant.

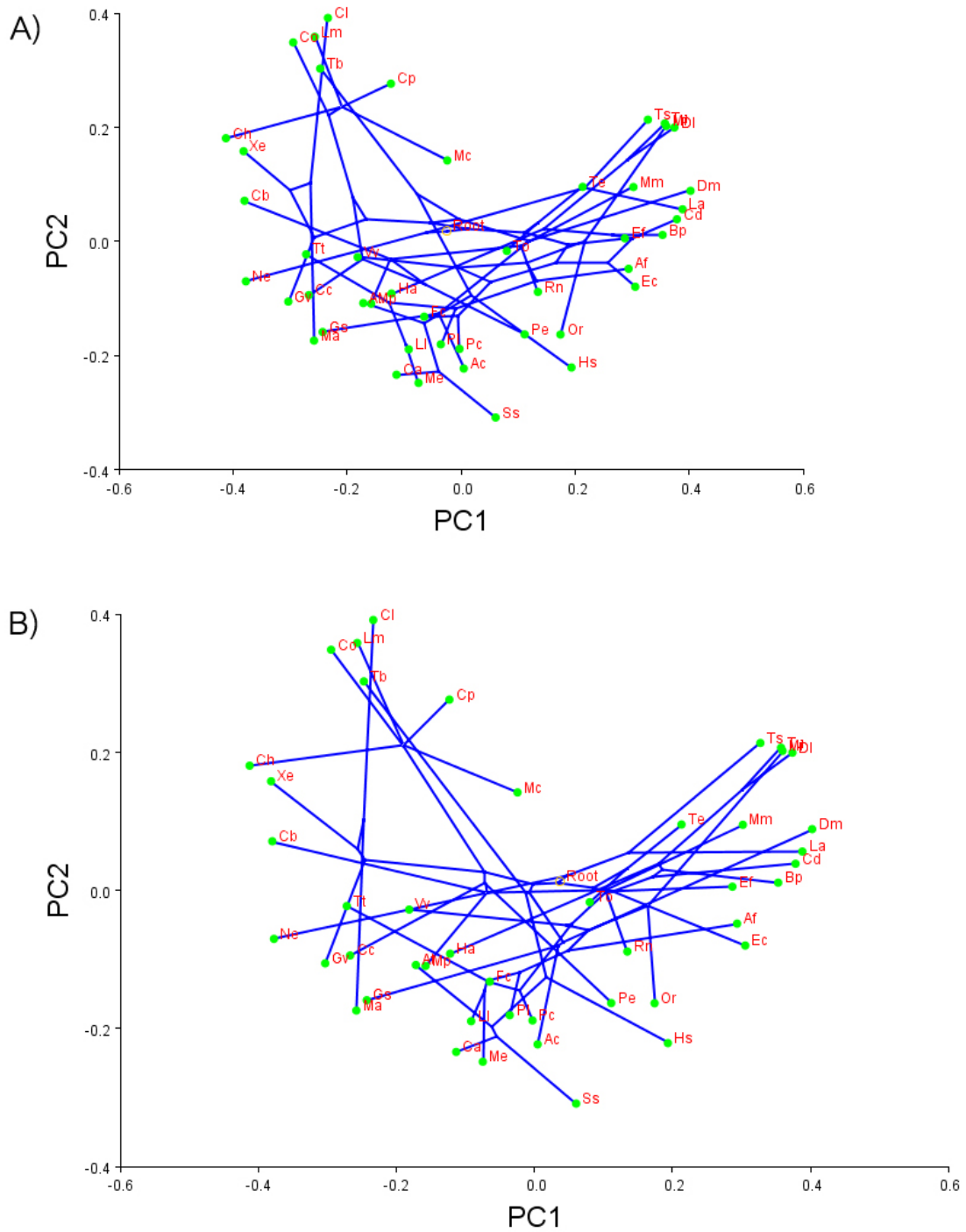


Figure 5.19 Reconstruction of evolutionary changes in cochlear shape in 45 mammalian species. The phylogenetic tree was mapped into plots of the first two PC axes, using unweighted squared-change parsimony (A), and weighted squared-change parsimony (B).

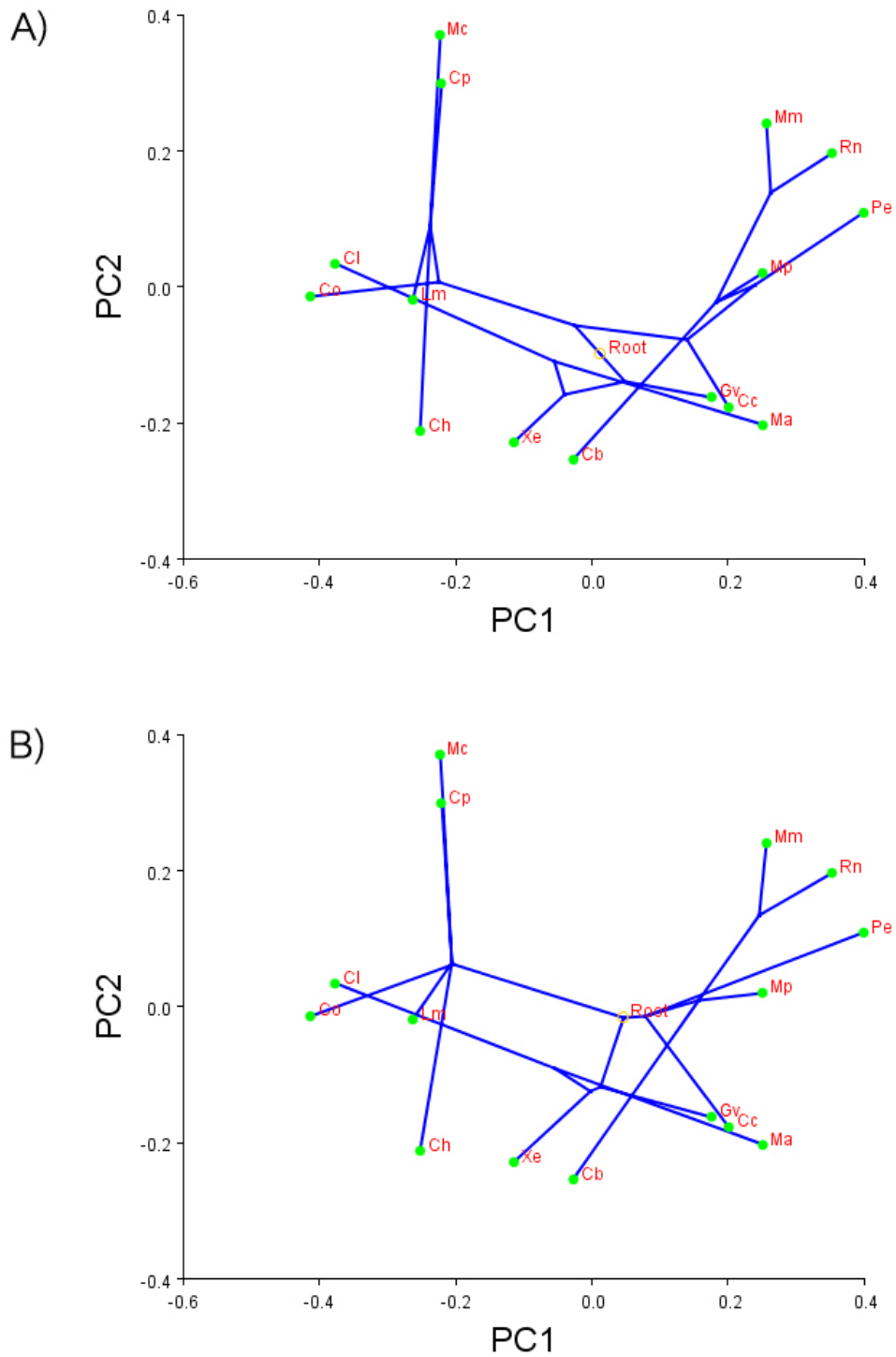


Figure 5.20 Reconstruction of evolutionary changes in cochlear shape in 15 rodent species. The phylogenetic tree was mapped into plots of the first two PC axes, using unweighted squared-change parsimony (A), and weighted squared-change parsimony (B).

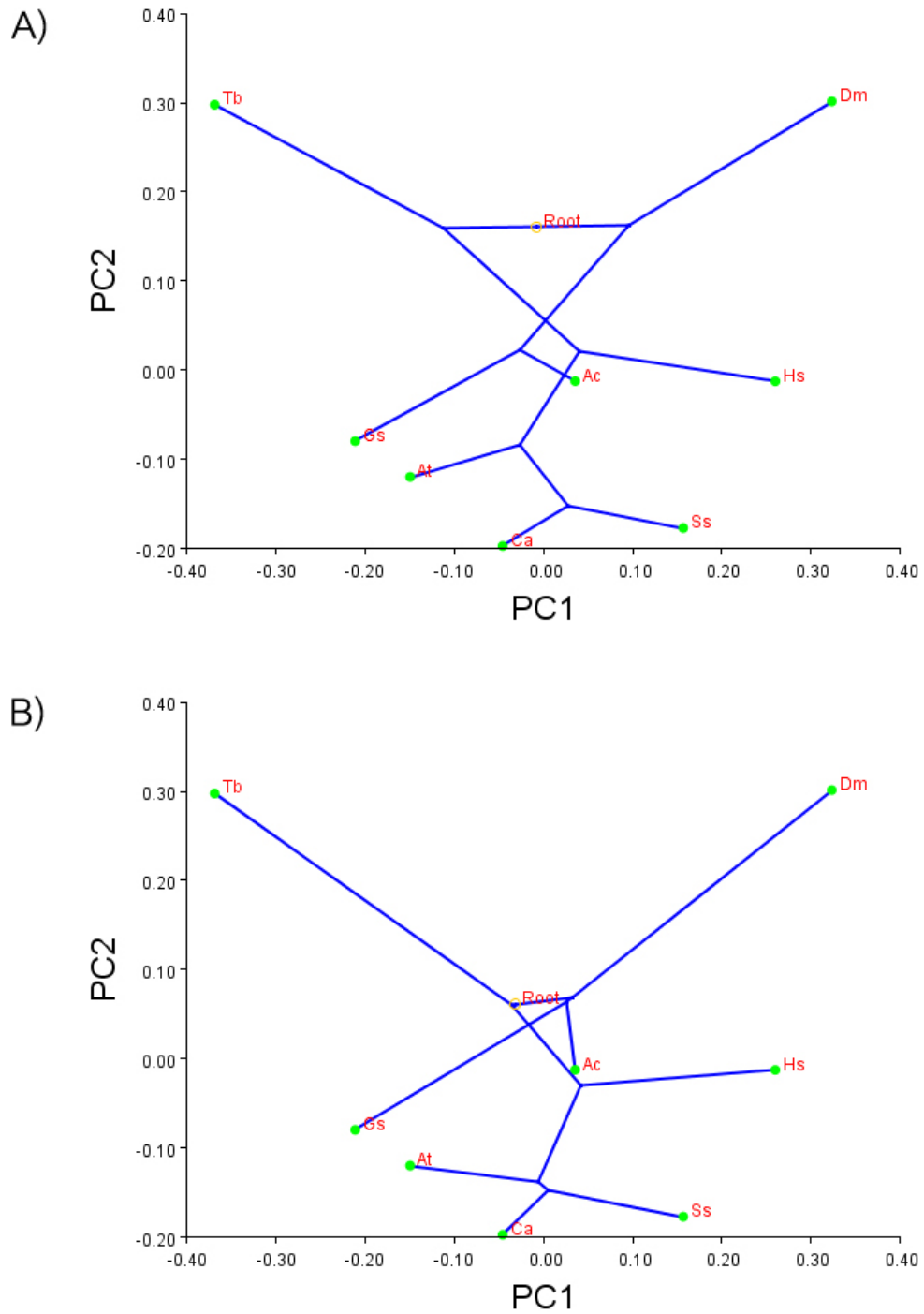


Figure 5.21 Reconstruction of evolutionary changes in cochlear shape in eight primate species. The phylogenetic tree was mapped into plots of the first two PC axes, using unweighted squared-change parsimony (A), and weighted squared-change parsimony (B).

In the independent contrasts analysis, contrasts were obtained from the first four Procrustes PC axes and from the natural log-transformed centroid sizes of each species. Then, RMA regression of the contrasts of each PC axis on the contrasts of the natural log-transformed centroid sizes was performed. The contrasts of the centroid sizes showed a significant correlation with the contrasts of PC1 and PC3 ($P < 0.05$), and with the contrasts of PC4 ($P < 0.01$; Table 5.15). These correlations found on the three PC axes were similar to the correlations found before the independent contrasts analysis (compared to Table 5.5). When the pairwise regression lines obtained before and after the independent contrasts analysis were compared, the slopes were not significantly different (Table 5.16). The results indicated that phylogenetic scenario had relatively little influence on the cochlear shape. These results also suggested that the evolution of morphological variation of the cochlear shape described by the PC1, PC3 and PC4 was size-related, and that the cochlear shape co-evolved with the size change along mammalian lineages.

Table 5.15 Reduced major axis (RMA) regression between the independent contrasts of PCs and of ln-transformed centroid size.

Contrasts	r	Sig.	RMA regression		
			Slope	95% CI	Intercept
PC1 - ln centroid size	0.3023	*	0.54133	0.3428-0.6952	0.00807
PC2 - ln centroid size	0.0326	ns			
PC3 - ln centroid size	0.3325	*	0.31864	0.1845-0.4035	1.060E-06
PC4 - ln centroid size	-0.3906	**	-0.23682	(-0.2994)-(-0.1372)	0.00127

** $P < 0.01$; * $P < 0.05$; ns = not significant.

Table 5.16 Comparing slopes of two regression lines obtained from the plots of the PCs against the ln-transformed centroid size before and after the independent contrasts analysis.

On PC	SE_{diff}	t	Sig.
1	0.4922	0.0485	ns
2	0.3928	-0.0281	ns
3	0.2417	0.0441	ns
4	0.1961	0.0940	ns

ns = not significant.

Chapter 6 Results: human developmental study

This chapter presents the results of developmental study. The first section deals with the general description of the cochlear development observed from micro-CT images. The repeatability of measurements is presented in the second section. Finally, comparisons of the bony cochlea among fetuses, and between adults and fetuses are documented in the third and fourth sections, respectively. Throughout these sections, petrous length is used as a proxy for fetal age and body size to minimise the impact of erroneous gestation ages on the specimen tins (refer to Materials & Methods chapter for details). Figure 6.1 shows a plot of petrous length against the gestational ages given on the tins. Generally there is a good fit with a correlation of 0.91 ($P < 0.001$). The recorded ages of some individual specimens, however, do not fit the curve.

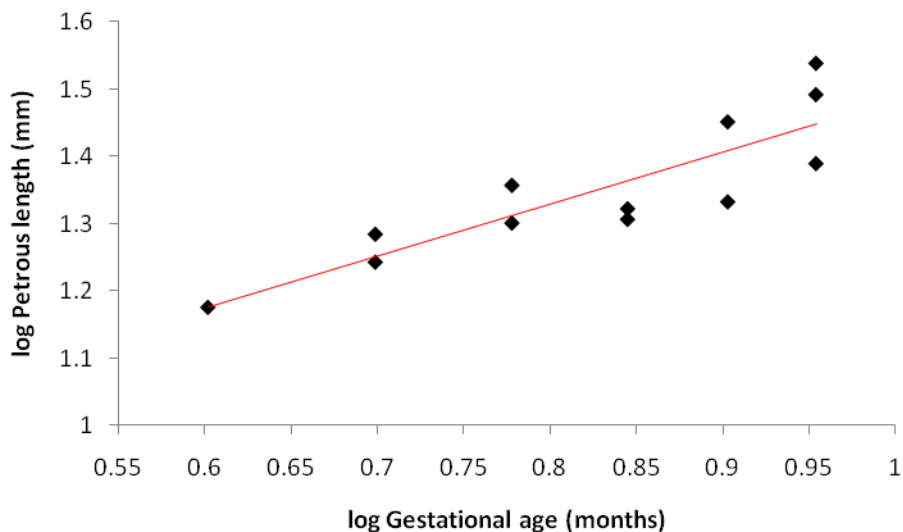


Figure 6.1 A bivariate plot of log₁₀ petrous length against log₁₀ gestational age ($r = 0.91$, $P < 0.001$).

6.1 Cochlear development from micro-CT images

The fetus of 15-mm petrous length (approximately four months gestation) showed the early ossification process of the osseous labyrinth. The interscalar septum between the cochlear turns was not clearly visible. The inner bony spiral lamina, spiral ganglion and cochlear aqueduct were not apparent. A bony border of the openings of the cochlear fenestrae was rather thin. The number of spiral turns, however, was equivalent to the adult cochlea. Apart from the cochlea, the bony margins of the vestibular apparatus were still poorly demarcated, as well. The capsule surrounding the anterior semicircular canal was only partially ossified, and not at all for the borders of the lateral and posterior canals. The bony tubes through which the vestibular nerves pass to innervate the ampullae of the anterior and posterior semicircular canals were not clearly defined. Moreover, a short internal acoustic meatus existed with a poorly-demarcated facial nerve canal.

At the stage of 17.5-mm petrous length (approximately early five months gestation), the fetus showed an obvious interscalar septum at the basal turn and the initial part of the middle turn. The inner bony spiral lamina and spiral ganglion were visible at the most basal turn. The cochlear aqueduct could be identified as a narrow bony canal at the posteromedial margin of the round window (RW). The fetus showed more advanced ossification of the vestibule and the semicircular canals than the smaller petrous stage. There was a confluence of ossification between the vestibule and the cochlea. The anterior canal was completely ossified, whereas the lateral and posterior canals were partly ossified. The common crus was enclosed by a thin bone layer and was visible. The bony tubes of the vestibular nerves were still difficult to detect, but the facial nerve canal was well developed.

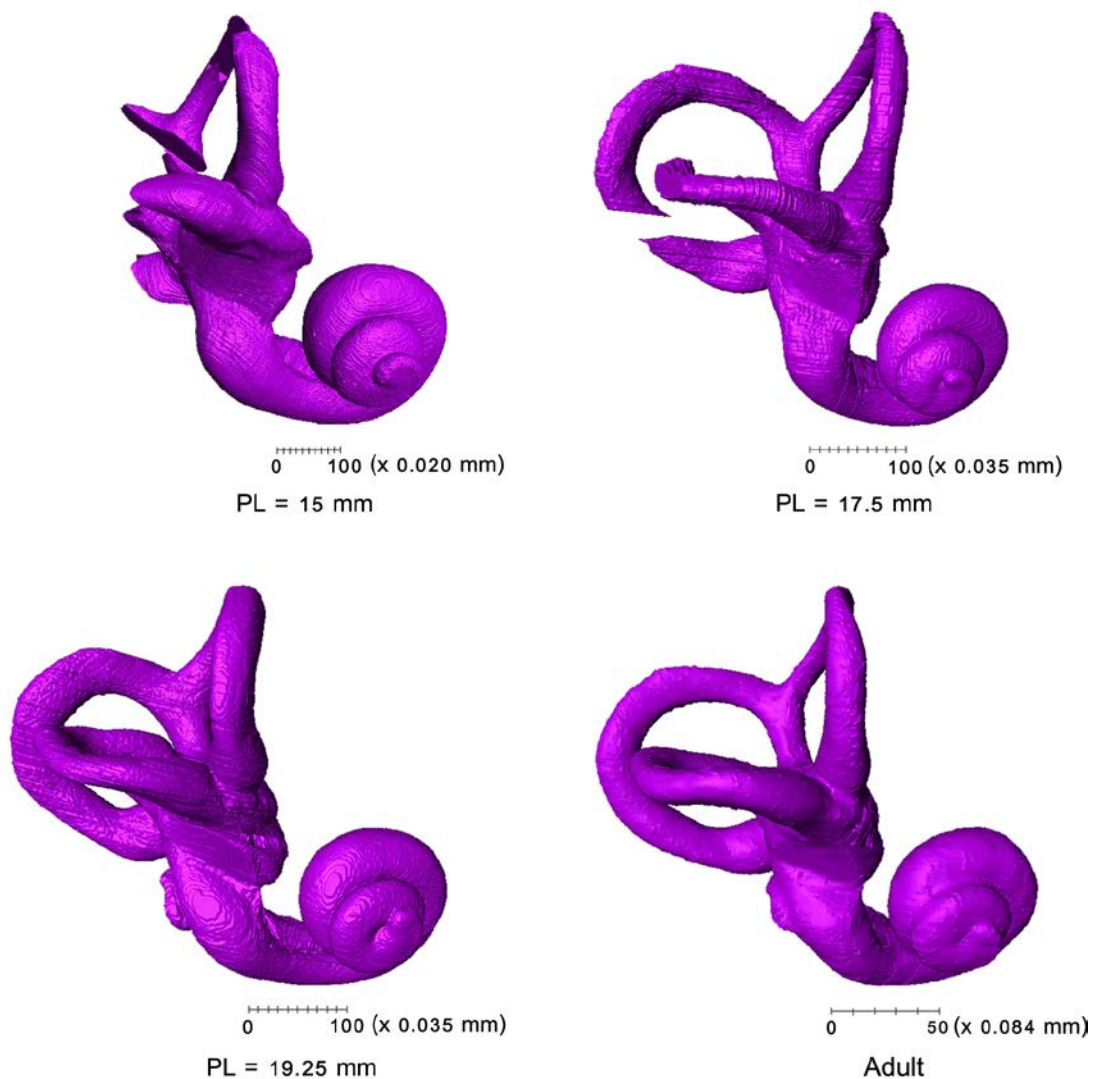


Figure 6.2 Development of the bony inner ear in human. Petrous bone length (PL) was used as a proxy for developmental stages of the bony inner ear. From the stage of 19.25-mm petrous length, the interscalar septum and all semicircular canals were fully ossified.

At the stage of 19.25-mm petrous length (approximately late five months gestation), the bony partition between the cochlear whorls was fully ossified, providing a clearer separation of each turn. The lateral bony wall of the cochlea was denser than that in younger fetuses. The spiral ganglion was more clearly seen and the inner osseous lamina was well-developed towards the apical turn, while there was no trace of the

outer osseous lamina. The micro-CT images also showed the ossification of the modiolus in the center of the cochlea. All semicircular canals and the vestibule were fully surrounded by bone that was denser than in the former stage (Fig. 6.2). Canals for that carry the vestibular nerves to the ampullae of the semicircular canals and the labyrinthine portion of the facial nerve canal were easily visible.

From the stage of 21-mm petrous length (approximately seven months gestation), the general morphology of the inner ear was similar to its adult form. The cochlear lateral wall and the interscalar septum were dense. The fetuses also had a well-developed ossified modiolus. The bony wall of the semicircular canal arc was thick. An internal auditory meatus of adult-like diameter was found in fetuses with the petrous length of more than 21 mm. The number of the cochlear coils varied little among samples, ranging from 2.6 to 2.8 turns, and seemed unchanged during intrauterine life (Fig. 6.2).

In all specimens, the opening of the oval window (OW) was an elongated ellipse. The opening of the round window, however, was rather varied in shape among both fetal and adult cochleae. Generally, the circular and elliptical shapes were most frequently seen, whilst undefined, irregular shapes were observed in three of the total specimens (see Appendix D.3).

6.2 Repeatability

The intra-observer repeatability of the landmarking and measurements were assessed by repeating the measures three times for three randomly selected specimens (A3, S1 and S6). The smaller the variance within individual specimens (S^2) was, the better the repeatability was. For measurements of each cochlear parameter (Table 6.1), S^2 was very small and the P value was less than 0.001 for all parameters. In addition, the intraclass correlation coefficient (r) was almost equal to one. In shape space, the repeated shape variables were close to each other in the PCA plots (Fig. 6.3). Shape differences among repeated measurements were significantly less than shape differences between specimens ($P < 0.001$ for PC1-PC4 and $P < 0.01$ for PC5; Table 6.1). The findings suggested that the large majority of the variation was due to differences between specimens and that measurements within individual specimens can be considered repeatable.

Table 6.1 The repeatability of measurements and landmarking.

Parameters	ANOVA						Repeatability		
	Variance	Sum of sqrs	df	Mean square	F	Sig.	S^2	S^2A	r
Length	Between gr.	75.5395	2	37.7698	3347.00	***	0.01128	12.5862	0.9991
	Within gr.	0.06770	6	0.01128					
Height	Between gr.	0.36605	2	0.18303	640.00	***	0.00029	0.06091	0.9953
	Within gr.	0.00172	6	0.00029					
Width	Between gr.	5.74033	2	2.87017	4748.00	***	0.00060	0.95652	0.9994
	Within gr.	0.00363	6	0.00060					
Volume	Between gr.	2463.04	2	1231.52	4274.00	***	0.28814	410.411	0.9993
	Within gr.	1.72884	6	0.28814					
OW	Between gr.	2.64937	2	1.32469	836.80	***	0.00158	0.44104	0.9964
	Within gr.	0.00950	6	0.00158					
RW	Between gr.	0.68185	2	0.34093	345.40	***	0.00099	0.11331	0.9914
	Within gr.	0.00592	6	0.00099					
OW/RW	Between gr.	0.69101	2	0.34551	2353.00	***	0.00015	0.11512	0.9987
	Within gr.	0.00088	6	0.00015					
H/W	Between gr.	0.01196	2	0.00598	505.30	***	0.00001	0.00199	0.9941
	Within gr.	0.00007	6	0.00001					

Parameters	ANOVA						Repeatability		
	Variance	Sum of sqrs	df	Mean square	F	Sig.	S ²	S ² A	r
PC1	Between gr.	0.03160	2	0.01580	1455.00	***	0.00001	0.00526	0.9979
	Within gr.	0.00007	6	0.00001					
PC2	Between gr.	0.02747	2	0.01373	609.30	***	0.00002	0.00457	0.9951
	Within gr.	0.00014	6	0.00002					
PC3	Between gr.	0.00149	2	0.00075	73.99	***	0.00001	0.00025	0.9605
	Within gr.	0.00006	6	0.00001					
PC4	Between gr.	0.00046	2	0.00023	28.48	***	0.00001	0.00007	0.9016
	Within gr.	0.00005	6	0.00001					
PC5	Between gr.	0.00013	2	0.00007	15.67	**	0.00000	0.00002	0.8302
	Within gr.	0.00003	6	0.00000					

*** $P < 0.001$; ** $P < 0.01$

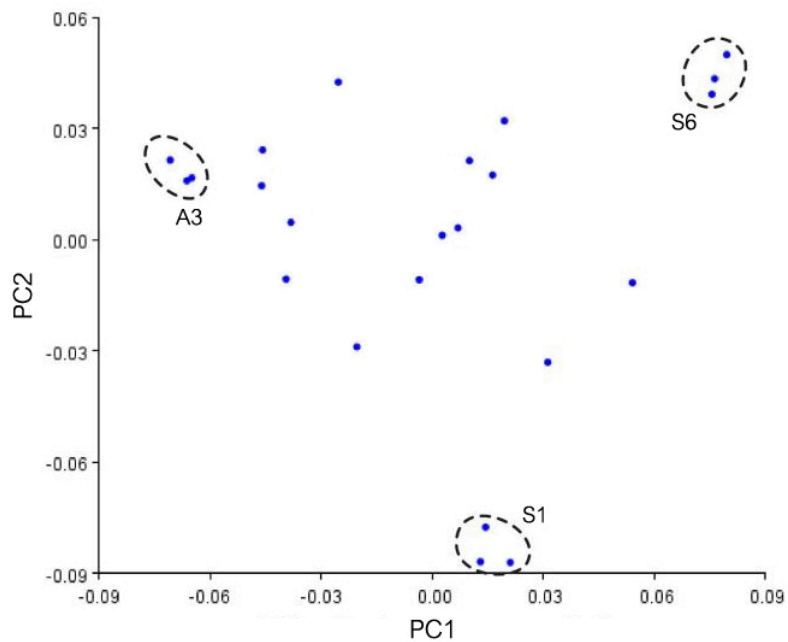


Figure 6.3 Repeatability test in shape space. Shape variation of the human cochlea represented by the scatter plot of PC1 vs PC2. Three specimens (A3, S1 and S6) were measured three times; repeated shape variables plotted closely together in shape space (dashed circles).

6.3 Developmental study: fetal cochleae

In this section, fetal specimens were subdivided into the large and small groups to determine if there were any major growth and/or developmental changes within the fetal cohort. The allometric relationship with the petrous bone and the differences in cochlear form among fetal specimens were examined.

6.3.1 Bivariate analysis—allometry with the length of the petrous bone

The V, OW area and RW area were significantly correlated with the petrous length at the $P < 0.05$ level, whereas the OW/RW ratio showed the same at the $P < 0.01$ level (Table 6.2). Positive correlations with the petrous length were present for both V and RW area, while negative correlations were found in OW area and OW/RW ratio. Reduced major axis regression demonstrated that all variables showing the correlations were strongly negatively allometric with respect to the petrous length, with an allometric coefficient of less than 1 (expected slope for isometry = 1; $P < 0.001$ for all except for RW area ($P < 0.01$)). In other words, these variables do not increase as rapidly as petrous bone length during gestation. It should be noted, however, that the OW/RW ratio is dimensionless and that there is no predicted slope for isometry (or allometry).

Table 6.2 Spearman's rank correlation and RMA regression of cochlear variables with petrous bone length.

Log petrous length vs	r	Sig.	RMA regression		
			Slope	95% CI	Intercept
Log Length	0.3706	ns			
log Height	0.1608	ns			
Log Width	0.2238	ns			
Log Volume cbt	0.6014	*	0.1229	0.0384-0.1644	0.45499
Log OW area sqrt	-0.6783	*	-0.3338	(-0.8934)-(-0.0492)	0.69752
Log RW area sqrt	0.6224	*	0.2757	0.0921-0.4078	-0.16356
Log (OW/RW area)	-0.7552	**	-1.0469	(-1.436)-(-0.272)	1.49010
Log (H/W)	-0.3217	ns			
Log (No. of turns)	-0.2443	ns			

** $P < 0.01$; * $P < 0.05$; ns = not significant.

6.3.2 Differences in the cochlear morphology between large and small fetuses

Univariate analysis and Mann-Whitney U test were used to test for differences between small and large fetuses (Table 6.3 and 6.4). Except for the OW area, no significant differences in cochlear dimensions were observed between large and small fetal groups. The OW area in the group of smaller fetuses, however, was significantly larger than that in the group of large fetuses ($P < 0.05$).

Table 6.3 Summary statistics of cochlear variables in sample groups.

Group	n	L (mm)		H (mm)		W (mm)		V (mm ³)		OW area (mm ²)		RW area (mm ²)		OW/RW area		H/W ratio		No. of turns	
		mean	SD	mean	SD	mean	SD	mean	SD	mean	SD	mean	SD	mean	SD	mean	SD	mean	SD
Adults	5	30.987	0.912	3.265	0.211	7.069	0.165	100.764	2.277	3.399	0.242	2.616	0.721	1.360	0.277	0.462	0.033	2.638	0.052
All fetuses	12	27.276	1.826	3.069	0.196	6.292	0.450	73.085	6.360	3.158	0.518	2.633	0.369	1.230	0.310	0.489	0.038	2.677	0.045
Large fetuses	6	28.206	0.701	3.094	0.217	6.474	0.263	77.334	2.028	2.884	0.262	2.796	0.462	1.056	0.202	0.478	0.036	2.677	0.047
Small fetuses	6	26.346	2.183	3.044	0.190	6.111	0.546	68.836	6.446	3.432	0.585	2.469	0.148	1.403	0.314	0.500	0.040	2.677	0.047

Table 6.4 Significance of Mann-Whitney U tests of cochlear morphology between sample groups.

Pairs	L (mm)	H (mm)	W (mm)	V (mm ³)	OW area (mm ²)	RW area (mm ²)	OW/RW	H/W	No. of turns
Adult - all fetuses	** ^(a)	ns	** ^(a)	** ^(a)	ns	ns	ns	ns	ns
Adult - large fetuses	** ^(b)	ns	** ^(b)	** ^(b)	* ^(b)	ns	ns	ns	ns
Adult - small fetuses	** ^(c)	ns	** ^(c)	** ^(c)	ns	ns	ns	ns	ns
Large fetuses - small fetuses	ns	ns	ns	ns	* ^(d)	ns	ns	ns	ns

** $P < 0.01$; * $P < 0.05$; ns = not significant.

Medians: ^(a)Adult > All fetuses (Length: 31.016 > 27.680, Width: 6.992 > 6.411, Volume: 100.439 > 74.775);

^(b)Adult > Large fetuses (Length: 31.016 > 28.307, Width: 6.992 > 6.568, Volume: 100.439 > 78.217, OW area: 3.432 > 2.956);

^(c)Adult > Small fetuses (Length: 31.016 > 25.531, Width: 6.992 > 5.977, Volume: 100.439 > 66.504);

^(d)Large fetuses < Small fetuses (2.956 < 3.433).

6.3.3 Geometric Morphometrics

The first five PCs represented more than 5% of the total variance each and were therefore investigated further. Together they explained a total of 87.3% of the variance in the whole sample (Fig. 6.4). The overall mean shape was warped to the extremes of the first five PCs to visualize the pattern of variability in cochlear shape described by each PC. Shape variations on PC1 were principally related to changes in the number of whorls and the radius of curvature at the middle turn (Fig. 6.5 and 6.6). The positive extreme of PC1 showed the cochlea having fewer turns but a larger radius of curvature at the middle turn than at the negative extreme. Variations on PC2 mainly represented changes in the radius of curvature at the last turn and the apical-basal compression of the whole cochlea (Fig. 6.5 and 6.6). The cochlea at the negative extreme of PC2 possessed a more apical-basal compression and a smaller radius at the last turn than the cochlea at the positive extreme. The shape change associated with PC3 was the curvature radius at the most basal turn and the expansion at the apex (Fig. 6.7). At the negative extreme, the cochlea had a smaller radius at the most basal turn and a relatively hook-shaped apex. Shape variations on PC4 were related to differences in the angle between the body of the cochlear spirals and the most basal turn (Fig. 6.7 and 6.8); the degree of the angle between them was less at the negative extreme. Finally, PC5 showed differences in the curvature pattern of the most basal turn (Fig. 6.8). The negative extreme had a relatively downward curve of the most basal turn in the direction toward the apex when compared with the opposite extreme.

Overall, in the scatter plots of the first five PCs, the distributions of the large and small fetal groups overlapped and did not separate from each other. Also, no

specimens with unusual shapes were observed. This suggests that there is little shape difference between small and larger fetuses, spanning approximately four to nine months *in utero*.

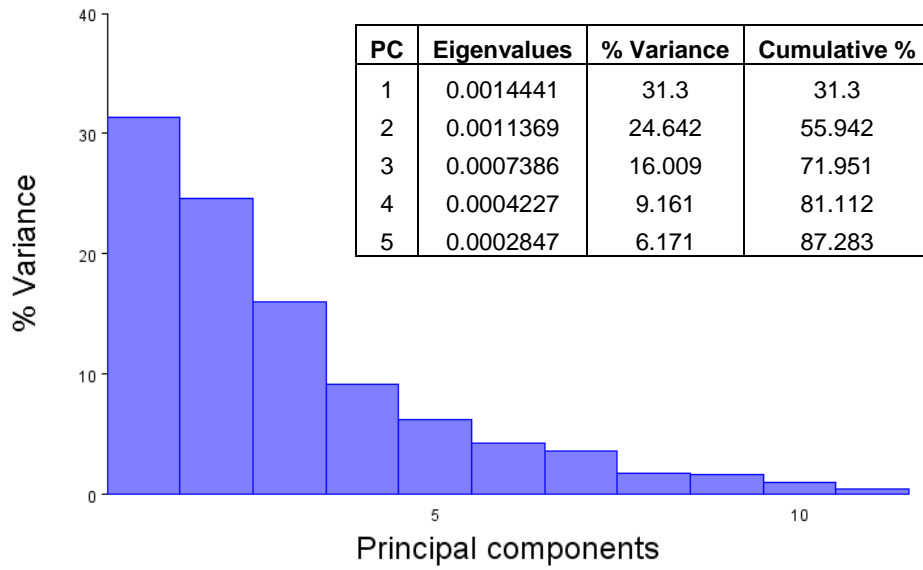


Figure 6.4 Plot of the proportion of variance accounted for each PC. Only PC1 to PC5 explained more than 5% of the total variance.

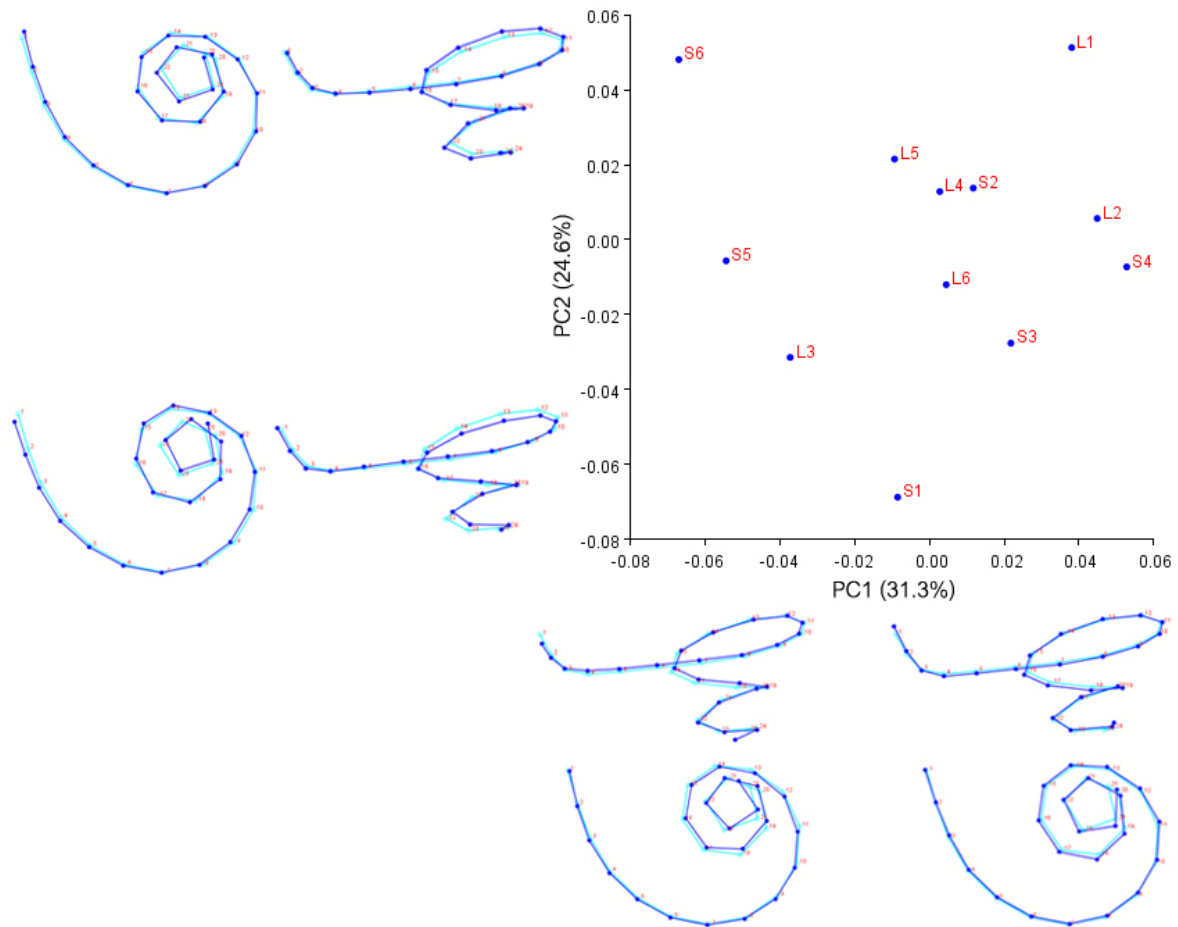


Figure 6.5 Shape variation of the fetal human cochleae described by the scatter plot of PC1 vs PC2. The pattern of shape variability represented by each PC was indicated by the constructed cochlear wireframes. The light blue lines indicated the mean shape (the coordinate (0.0, 0.0)) and the dark blue lines showed the shape at the extreme of each axis. Specimens of large fetuses and small fetuses were represented by 'L' and 'S' symbols, respectively.

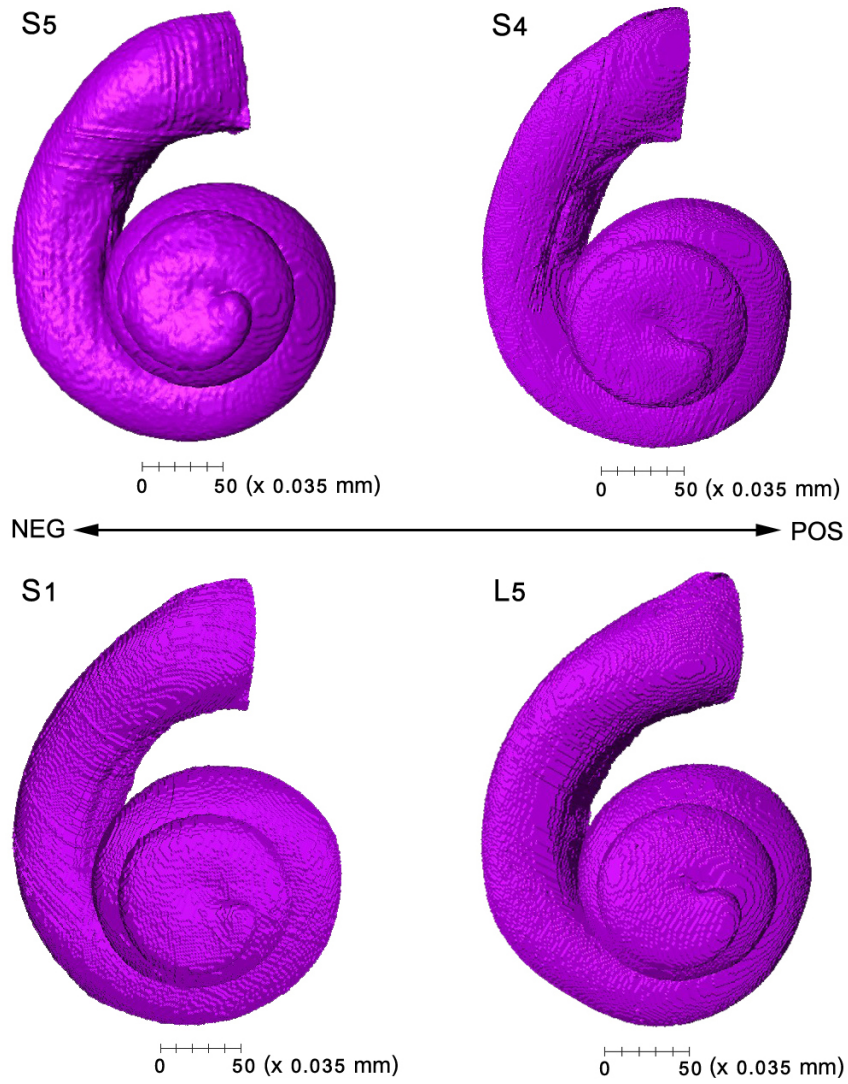


Figure 6.6 Three-dimensional cochlear images of some human specimens along PC1 (S4 and S5) and PC2 (S1 and L5). The arrow line represents PC axes toward the negative extreme (NEG) and positive extreme (POS).

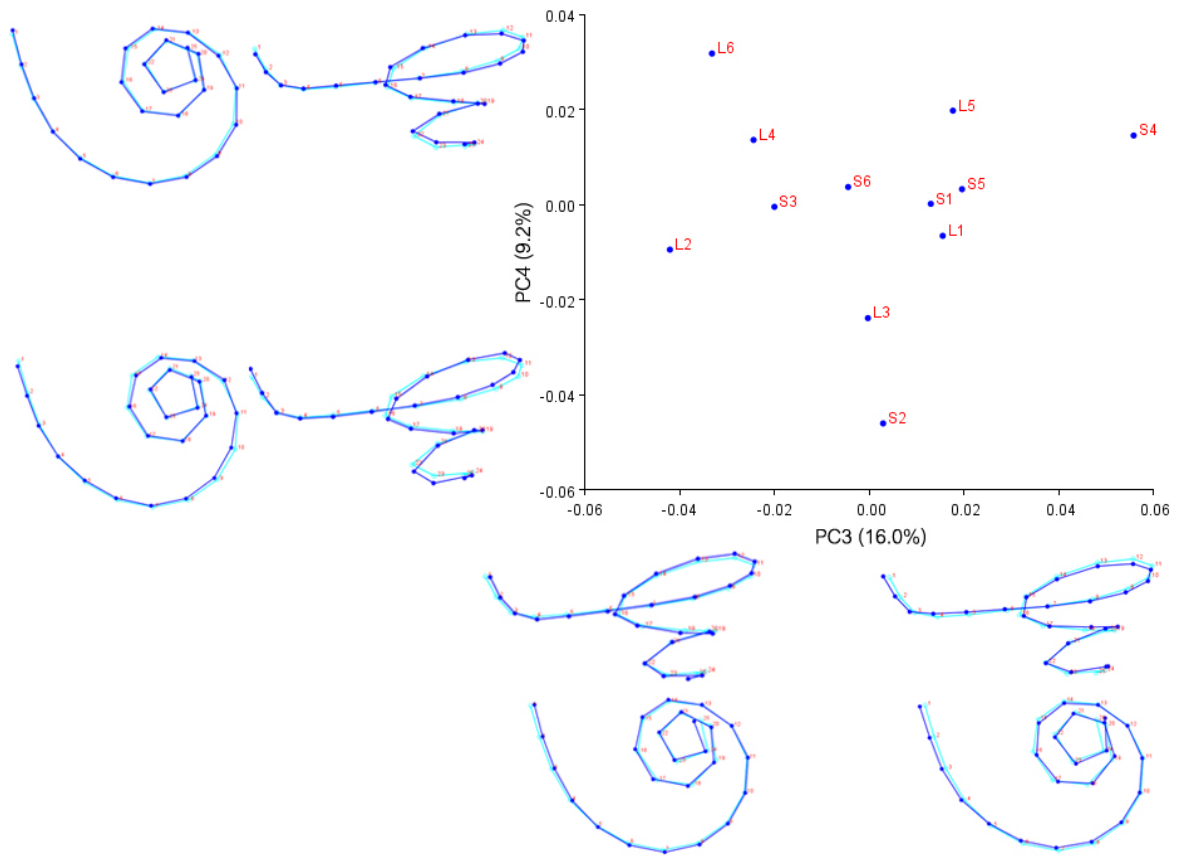


Figure 6.7 Shape variation of the fetal human cochleae described by the scatter plot of PC3 vs PC4. All parameters are the same as Figure 6.5.

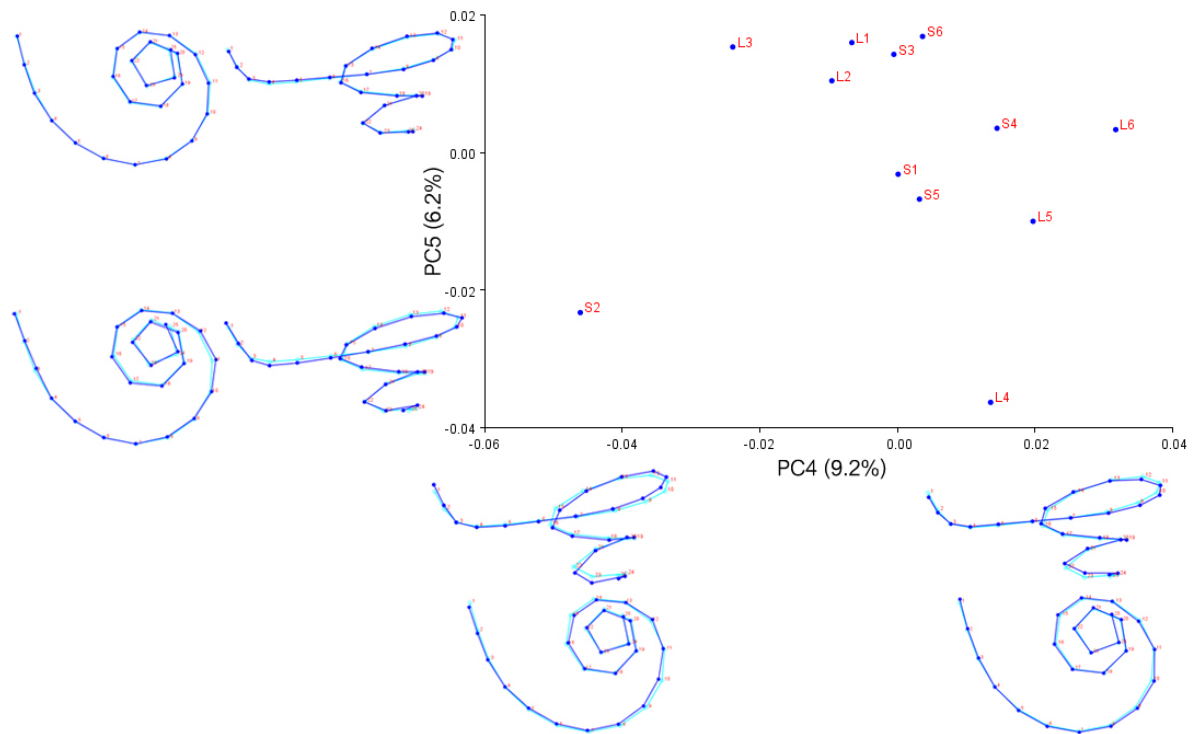


Figure 6.8 Shape variation of the fetal human cochleae described by the scatter plot of PC4 vs PC5. All parameters are the same as Figure 6.5.

To examine the size effects on shape variation, RMA regression analysis of PC scores (shape variables) against the natural log-transformed of centroid size was done. The result showed that there was no statistically significant relationship between the centroid size and the PC scores on the five PC axes (Table 6.5). There was no significant relationship between the petrous bone length and the PC scores either (Table 6.6). The DFA and Mann-Whitney U tests confirmed that there were no significant differences in shape between the cochleae of large fetuses and small fetuses (Table 6.7 and 6.8). These findings indicated that shape changes were not tightly linked to size (or age) differences among fetal cochleae.

Table 6.5 Spearman's rank correlation and RMA regression of PCs with centroid size.

Ln centroid size vs	r	Sig.	RMA regression		
			Slope	95% CI	Intercept
PC1	0.4685	ns			
PC2	-0.2657	ns			
PC3	0.0070	ns			
PC4	0.0280	ns			
PC5	0.3357	ns			

ns = not significant.

Table 6.6 Spearman's rank correlation and RMA regression of PCs with petrous length.

Log petrous length vs	r	Sig.	RMA regression		
			Slope	95% CI	Intercept
PC1	0.3217	ns			
PC2	0.1049	ns			
PC3	-0.3147	ns			
PC4	-0.2797	ns			
PC5	0.0350	ns			

ns = not significant.

Table 6.7 Discriminant function analysis with permutation tests (10,000 iterations) of PC scores across the whole shape space.

Group 1	Group 2	Procrustes dis.	T ² (Sig.)	DFA (%)		Cross-validation (%)	
				Group 1	Group 2	Group 1	Group 2
Large fetuses	Small fetuses	0.5731	ns	67	83	33	33

ns = not significant.

Table 6.8 Mann-Whitney U test of PC scores on PC1-PC5.

Pairs	PC1	PC2	PC3	PC4	PC5
Large fetuses - small fetuses	ns	ns	ns	ns	ns

ns = not significant.

6.4 Developmental study: adult versus fetal cochleae

In this section, all human specimens were included and divided into adults and fetuses. The fetuses were also classified into large and small fetuses. A comparison of the cochlear form between adults and the fetuses is outlined below.

6.4.1 Differences in the cochlear morphology between adults and fetuses

Univariate analysis and Mann-Whitney U test were used in this analysis (Table 6.3 and 6.4). When compared with all fetal specimens, adult specimens showed significant differences in L, W and V at the $P < 0.01$ level. The medians of L, W and V in adults were higher than those in the group of all fetuses. In contrast, no significant differences in H, the number of spiral turns and the size of the OW and RW were seen. The same results were also obtained from the comparison between the cochleae in adults compared with only the small fetus group. When compared to the large fetus group, however, adults showed significant differences in not only L, W, V, but also the OW area ($P < 0.05$). The medians of these significant variables were higher in adults.

6.4.2 Geometric morphometrics

The first five PCs of shape met the criterion of the components that described more than 5% of the variance each. In total, they explained 83.6% of the total variance observed among the specimens (Fig. 6.9). The adult and fetal specimens somewhat overlapped. The overall mean shape was warped along the first five PC axes to visualize the pattern of variability in cochlear shape explained by each PC. Shape variations accounted for by PC1 primarily represented changes in the elongation of the apex influencing the number of spiral turns, and the radius of curvature at the middle and apical turns (Fig. 6.10 and 6.11). The negative extreme of PC1 was characterized by the cochlea with fewer turns, and larger curvature radii at the middle and apical turns. Three out of five adult cochleae were found in this region of the PC. At the other, positive, extreme, only fetal cochleae were found. Variations on PC2 were primarily related to changes in the orientation of first spiral and the radius of curvature of the last spiral (Fig. 6.10 and 6.11). The negative extreme of PC2 showed the cochlea with a smaller radius of the last spiral turn than the positive extreme. For PC3, its shape variations were mainly related to the apical-basal compression of the whole cochlea and the expansion at the apex (Fig. 6.12), which were notably pronounced at the positive extreme. Variations on PC4 represented differences in the angle between the body of the cochlear spirals and the most basal turn (Fig. 6.12 and 6.13). The degree of the angle between them was less at the negative extreme. Lastly, PC5 indicated differences in the curvature pattern of the most basal turn and the last turn (Fig. 6.13). The negative extreme showed a relatively downward curve of the most basal turn in the direction toward the apex and a relatively inward bend of the last turn, whereas the positive extreme showed a

relatively smooth curve of the most basal turn and a relatively outward direction of the last turn.

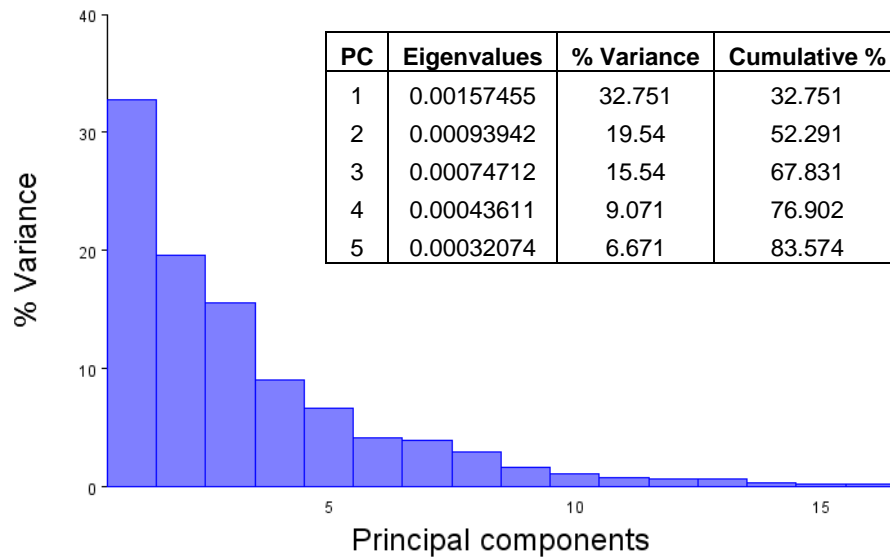


Figure 6.9 Plot of the proportion of variance accounted for each PC. Only PC1 to PC5 described more than 5% of the total variance.

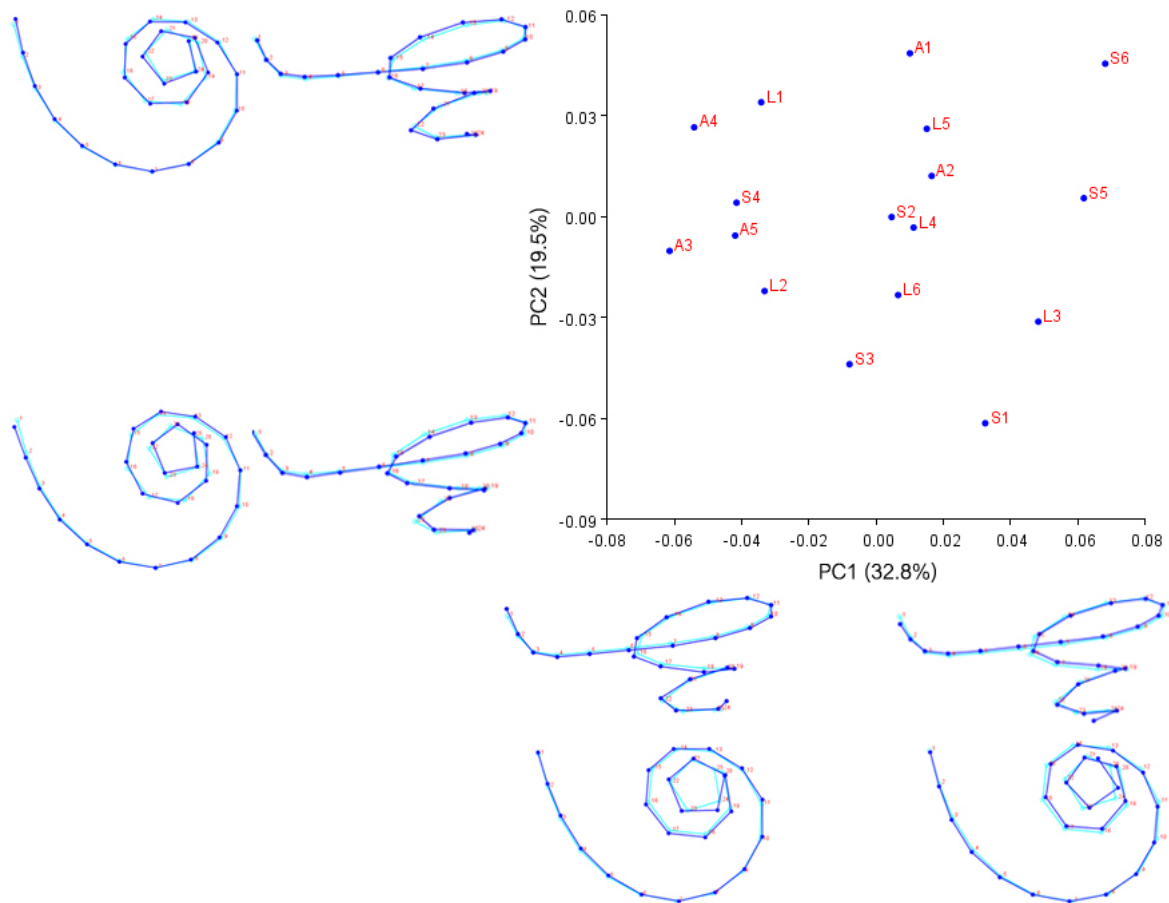


Figure 6.10 Shape variation of the human cochlea described by the scatter plot of PC1 vs PC2. The pattern of shape variability represented by each PC was indicated by the constructed cochlear wireframes. The light blue lines indicated the mean shape (the coordinate (0.0, 0.0)) and the dark blue lines showed the shape at the extreme of each axis. Specimens of adults, large fetuses and small fetuses were represented by 'A', 'L' and 'S' symbols, respectively.

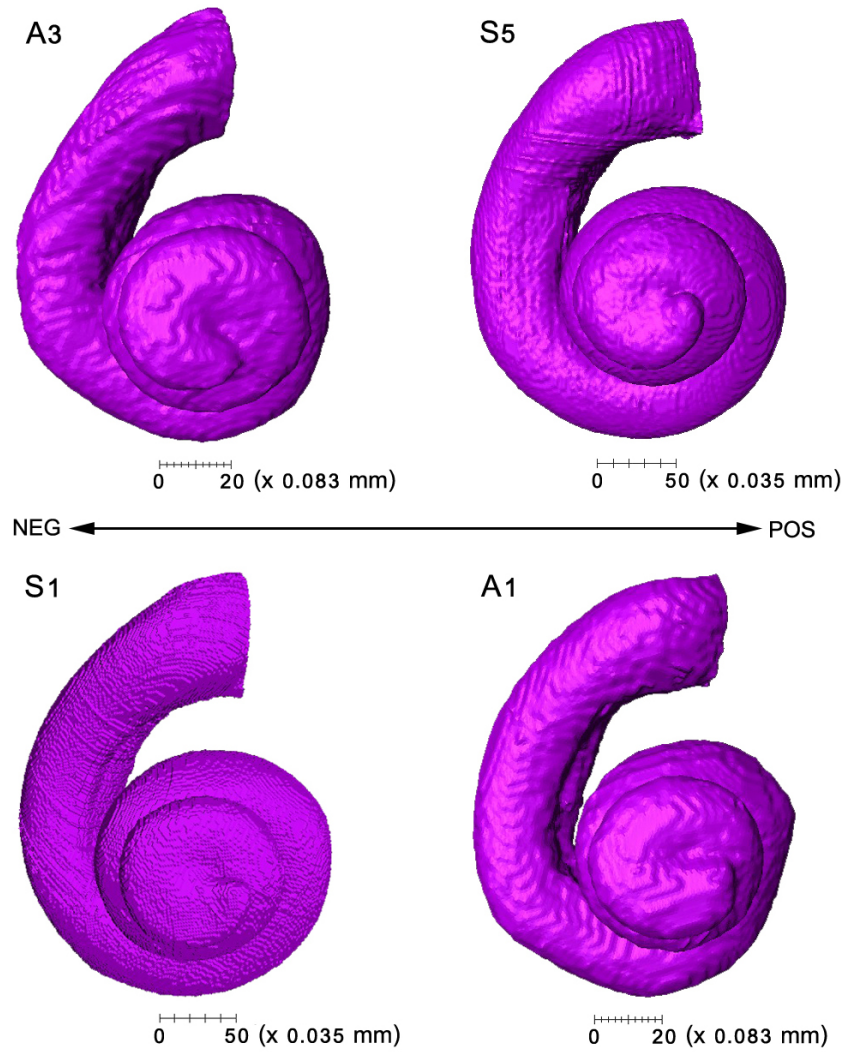


Figure 6.11 Three-dimensional cochlear images of some human specimens along PC1 (A3 and S5) and PC2 (S1 and A1). The arrow line represents PC axes toward the negative extreme (NEG) and positive extreme (POS).

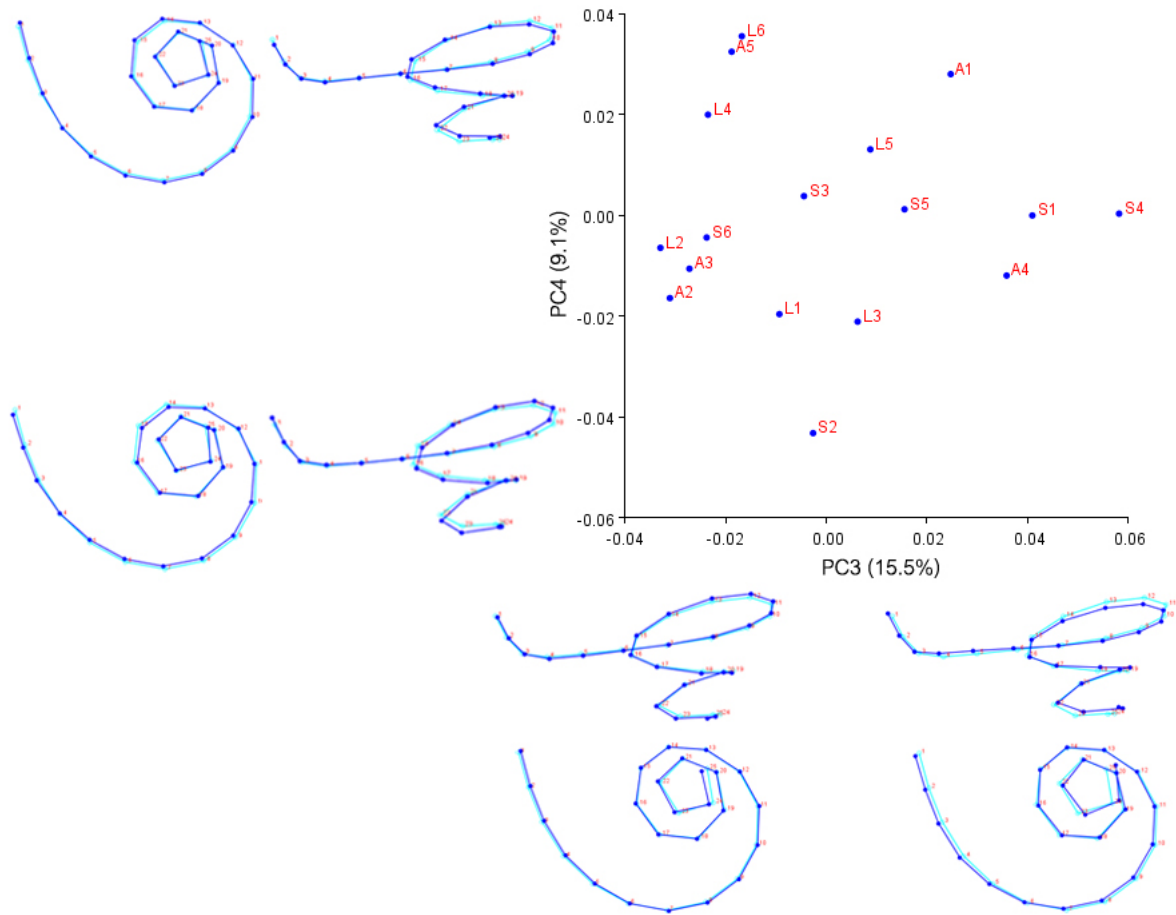


Figure 6.12 Shape variation of the human cochlea described by the scatter plot of PC3 vs PC4. All parameters are the same as Figure 6.10.

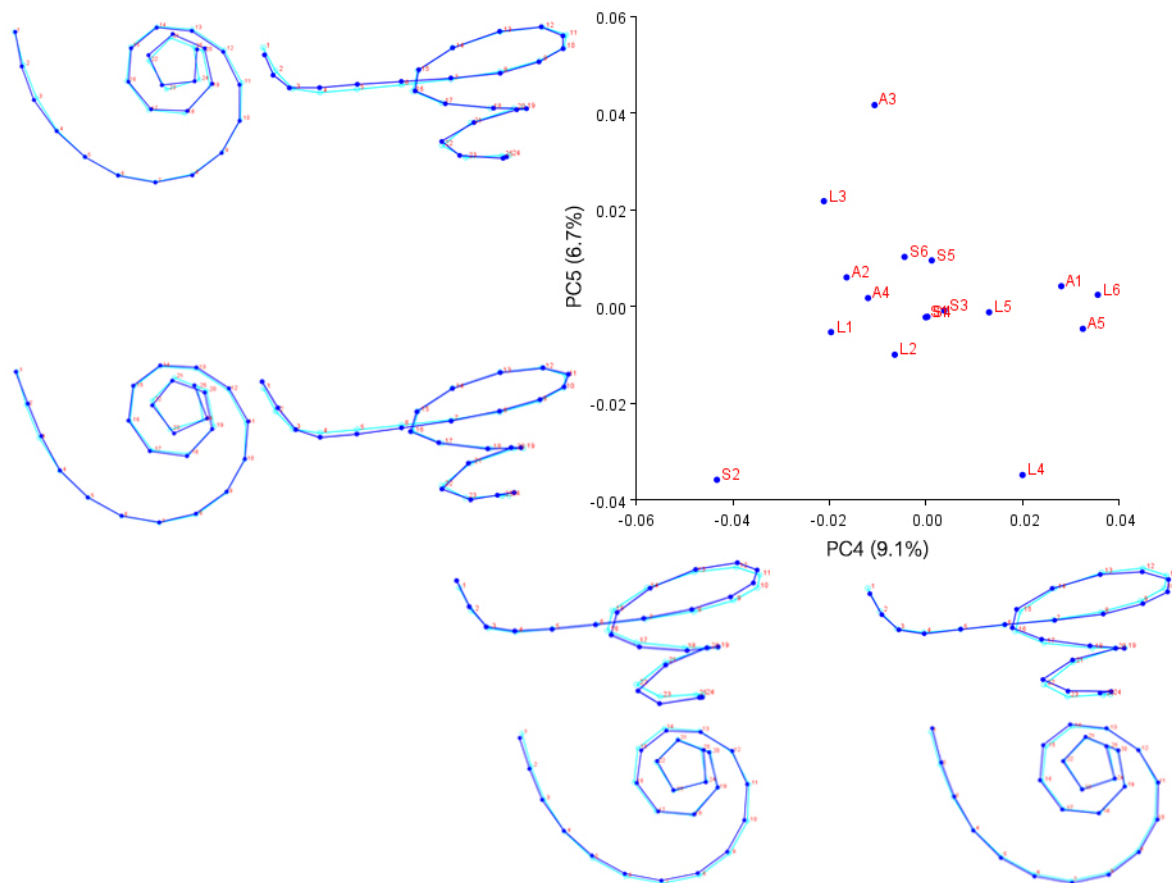


Figure 6.13 Shape variation of the human cochlea described by the scatter plot of PC4 vs PC5. All parameters are the same as Figure 6.10.

Across all five PCs, shape change between adult and fetal cochleae seemed to be related to size, particularly along on PC1. The adult cochlea tended to be found in the plot areas that represented features that were relatively larger, whereas the fetal cochlea tended to be distributed in the areas that represented features that were relatively smaller. The adult and fetal cochleae blended together on other PC axes, so shape variation on these axes was possibly not attributed to size. The significance of size-related shape change was tested using RMA regression of PC scores against natural log-transformed centroid size. The result demonstrated that there was only a significant relationship between the centroid size and scores on PC1 ($P < 0.05$; Table 6.9). This result indicated that size differences were associated

with about 32% of the change in cochlear shape. After removing the allometric effects from shape variables on PC1, however, the adult and fetal datum points blended together on the plot of residual PC1 vs PC2 (Fig. 6.14).

Table 6.9 Spearman’s rank correlation and RMA regression of PCs with centroid size.

Ln centroid size vs	r	Sig.	RMA regression		
			Slope	95% CI	Intercept
PC1	-0.5956	*	-0.5510	(-0.6896)-(-0.33)	1.4133
PC2	0.1299	ns			
PC3	0.0441	ns			
PC4	0.0637	ns			
PC5	0.2647	ns			

* $P < 0.05$; ns = not significant.

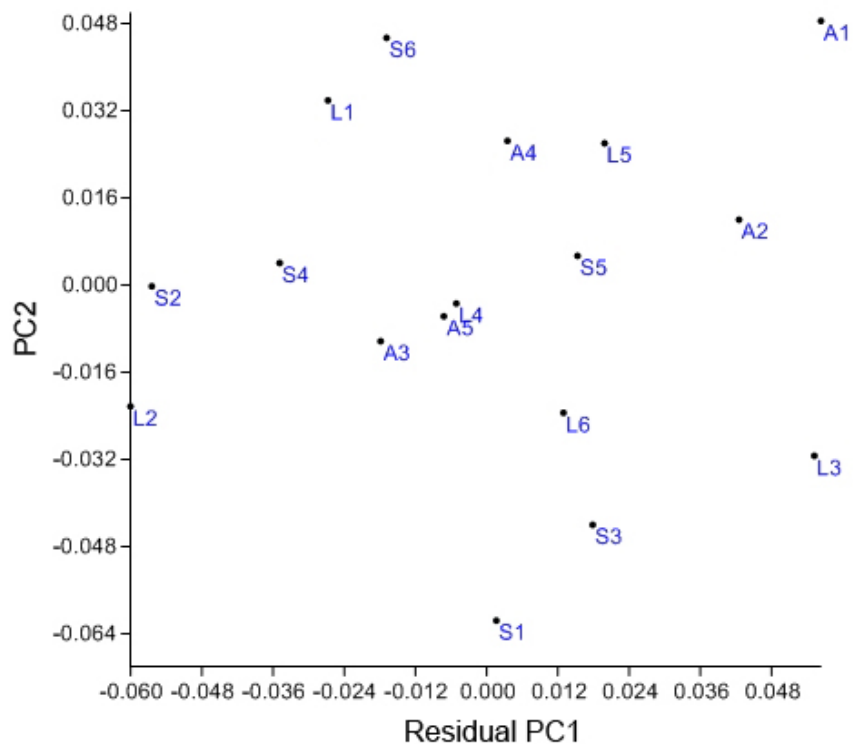


Figure 6.14 Shape variation of the human cochlea described by the scatter plot of residual PC1 vs PC2. Specimens of adults, large fetuses and small fetuses were represented by ‘A’, ‘L’ and ‘S’ symbols, respectively.

Shape residuals for PC1 were also used for shape analysis via Mann-Whitney U test, whereas shape residuals across the whole shape space were used for shape analysis via DFA in MorphoJ software. As shown in Table 6.10 and 6.11, DFA and Mann-Whitney U test demonstrated that adult cochlear shape was not significantly different from fetal cochlear shape at both levels of the whole sample set and separate subgroups (large fetuses and small fetuses).

Table 6.10 Discriminant function analysis with permutation tests (10,000 iterations) of regression residuals across the whole shape space.

Group 1	Group 2	Procrustes dis.	T ² (Sig.)	DFA (%)		Cross-validation (%)	
				Group 1	Group 2	Group 1	Group 2
Adult	All fetuses	0.9013	ns	100	83	0	50
Adult	Large fetuses	0.9553	ns	80	83	20	33
Adult	Small fetuses	0.7068	ns	100	67	40	33

ns = not significant.

Table 6.11 Mann-Whitney U test of regression residuals on PC1, and original PC2-PC5 scores.

Pairs	PC1 residuals	PC2	PC3	PC4	PC5
Adults - all fetuses	ns	ns	ns	ns	ns
Adults - large fetuses	ns	ns	ns	ns	ns
Adults - small fetuses	ns	ns	ns	ns	ns

ns = not significant.

Chapter 7 Discussions and Conclusions

The sense of hearing is fundamentally important for survival as well as reproduction and consequently the associated structures have changed throughout the evolutionary history of the vertebrates. The major evolutionary changes involve the appearance of the ossicles and adaptations of the inner ear sensory organ. In mammals, the cochlea is the receptive organ of hearing. There is a great variation in form of the cochlea across different mammalian species. These morphological variations have been linked to differences of hearing capabilities, particularly pertaining to frequency limit. Mammals are the only vertebrate group showing a widespread distribution of species across land, water and sky, in addition to diverse behaviour from solitary underground digging species through to gregarious swimming species. It is known that such eco-behavioural traits correlate with hearing frequency and hence it is anticipated that the morphology of the mammalian cochlea is as equally diverse. However, little is known about morphological adaptations of the cochlea related to ecology and behaviour. The present study determined variation of form of the adult mammalian bony cochlea. The study also determined whether the bony cochlea carries eco-behavioural traits that can be used to contextualize our understanding of the fossil record.

Presently, observable characteristics of an organism are attributed to evolutionary adaptation and other selection mechanisms. A gradual accumulation of characteristic changes is passed to offspring over many successive generations until the change is large enough to give rise to speciation. The process of accumulation and heredity of change can be seen from development. Thus, ontogenetic studies can yield insights

into evolutionary mechanisms by representing the accumulation of genetic changes over developmental time. The second part of the present study investigated the ontogeny of the human bony cochlea, which may provide basic information useful for clinical implications.

7.1 Adult interspecific study

In this section, the variation of the bony cochlea morphology in relation to hearing frequency and eco-behavioural traits are reviewed. The significant results and interesting points found will be comprehensively discussed with reference to previous literature.

7.1.1 General description of the cochlea in relation to hearing abilities

In the present study, the outer osseous spiral lamina was found to be well-developed in odontocetes and *Eptesicus fuscus* (big brown bat), all of which are species that use high-frequency echolocation. It was present throughout the basal turn, and extended up to at least a half of the entire cochlear length. In other species, the outer bony lamina was absent or occupied only in the basal turn. These results agree with those from many researchers (e.g., Fleischer, 1976; Ketten, 1994; Wartzok and Ketten, 1999; Solntseva, 2010). The length of the outer bony lamina is believed to increase the stiffness of the basilar membrane, leading to high ultrasonic hearing (Ketten, 1994; Wartzok and Ketten, 1999; Vater and Kossl, 2010). The extensive outer lamina is also considered as a hallmark of ultrasonic ears (Wartzok and Ketten, 1999; Solntseva, 2010; Vater and Kossl, 2010).

In odontocetes, the spiral canal was large at the basal and middle turns (Fig. 5.3). The spiral canal houses the spiral ganglion of the acoustic nerve which conveys nerve signals from the cochlea to the central nervous system. Nerve fibers from the ganglion respond only to a relatively restricted range of frequencies (Fleischer, 1976). Consequently, it is possible that the increased number of nerve cells in the spiral ganglion results in better frequency discrimination across the higher range of frequencies used for echolocation (Fleischer, 1976; Solntseva, 2010).

The results from the present study also demonstrated that the scala tympani was relatively larger than the scala vestibuli, extending toward the apical turn, in cetaceans (Fig. 5.3). This feature is different from the common trend in other mammals, where the enlarged scala tympani is generally only found at the basal portion of the cochlea (Fleischer, 1976). It is reported, however, that many subterranean species show a low scala tympani throughout almost entire cochlear spiral (Begall et al., 2007). These findings may indicate, at least to some extent, that there is a relationship between the size of the scala tympani and audible frequency response, although the precise mechanism responsible for this relationship is still unclear. It can be speculated that as the scala tympani terminates at the round window, size of the scala tympani may be indicative of the round window size. The main function of the round window is to relieve sound energy from the inner ear. A smaller round window may reflect a decreased efficiency of dissipating excessive energy. Subterranean mammals favour low-frequency sounds that have lower energy, so they do not necessarily need the large round window (large scala tympani) as found in odontocetes that hear ultrasonic high-frequency sounds.

Concerning the cochlear aqueduct, it was very large in odontocetes and pinnipeds (Fig. 5.3). Møhl (1968) suggested that a large cochlear aqueduct may be useful for underwater bone-conduction in pinnipeds. This, however, is not consistent with the function found in odontocetes. Odontocete ears are fully isolated from the skull, so there are air cushions between them that prevent odontocetes from using bone conduction in water (Wartzok and Ketten, 1999; Nummela et al., 2007). Until now, the function of the cochlear aqueduct in toothed whales has remained unclear.

One particularly noteworthy finding was the poorly developed semicircular canals in marine species, particularly in odontocetes (Fig. 5.1). A feasible explanation is that the cervical vertebrae are fused together in odontocetes (Ketten, 1997; Wartzok and Ketten, 1999; Spoor et al., 2002), and partially fused in sirenians (Gray, 1951), leading to limited head rotation. Due to the restricted head rotation, input signals to the vestibular system are diminished, resulting in degeneration of related vestibular receptors (Ketten, 1997; Wartzok and Ketten, 1999). The reduced canals are also believed to be adaptive features of fully aquatic lifestyle that improve their hydrodynamic performance (Ketten, 1997; Wartzok and Ketten, 1999; Feldhamer et al., 2004). It could be that larger canals take longer to relax back to a state of equilibrium after stimulation. In other words, whilst large canals may be more sensitive, the relaxation times are relatively longer. This means the canals can become saturated after repeated agile movements. Perhaps smaller canals allow for a short response time to keep track of more frequent, repetitive agile movements and reduce the sensitivity to protect from overstimulation.

7.1.2 Allometric relationship with body mass

This study demonstrated that all cochlear size variables, except for the number of cochlear turns, scaled with body mass in a similar manner. These variables were each positively correlated with body mass (Table 5.2) and scaled with strong negative allometry. In other words, as body mass increases, the cochlear size increases at a slower rate. When the data were examined without logarithmic transformations, the cochlear variables in small mammals scaled with positive allometry and then with negative allometry in larger mammals. This indicates that there is a functional limit to cochlear size beyond which there is little benefit, or even potentially some disadvantages. The results of pairwise comparisons of the cochlear variables showed that length, height and width were strongly positively correlated with volume (Table 5.4). This seems reasonable because if the cochlear increases in its linear dimensions, there should be an increase in overall cochlear volume. The results also indicated that length and width had the closest association with the overall change in volume. One interesting point to note is that the number of spiral turns does not show any correlation with the other cochlear variables, including volume. This implies that spiraling is unlikely to be a mechanism to accommodate a larger cochlea within the confines of the petrous bone.

For hearing variables, scaling relationships with body mass were found in relation to the low frequency limit of hearing and the intermeatal distance. The low frequency limit showed a negative correlation, whereas the intermeatal distance showed a positive correlation (Table 5.3). This suggests that the low frequency limit decreases with increasing body mass. In contrast, an increase in body mass is associated with an increase in the intermeatal distance. It appears reasonable to expect that a

mammal with larger body size should have a larger head, resulting in a greater distance between the left and right auditory meatuses. Both variables showed strong negative allometry. Without logarithmic transformations, the rate of change with body mass was greater for small species compared with larger species.

7.1.3 Relationships between the bony cochlear morphology, ecology and hearing abilities

7.1.3.1 The number of cochlear turns

The number of cochlear turns varies considerably across eutherian species. In the present study, it ranges from 4.2 turns in the guinea pig (*Cavia porcellus*) and coypu (*Myocastor coypus*) to 1.75 turns in the bottlenose dolphin (*Tursiops truncatus*) and African manatee (*Trichechus senegalensis*) (Fig. 7.1). Marine mammals have fewer whorls than any other group and differ most significantly from species foraging on or near the ground surface (Fig. 5.15). The number of turns measured in the present study is similar to those documented previously (Gray 1907; Watt, 1917; West 1985; Solntseva, 2010). One exception is the guinea pig. Its cochlea had more turns than that the 3.5-3.75 turns reported by Wysocki's (2005) study. The 4.2 turns reported here, however, is consistent with other studies (e.g., West 1985; Manoussaki et al., 2008; Solntseva, 2010). The average number of spiral turns across all 45 species studied was 2.74 turns, which is similar to the study of Watt (1917), who reported an average of 2.6 whorls across 52 species.

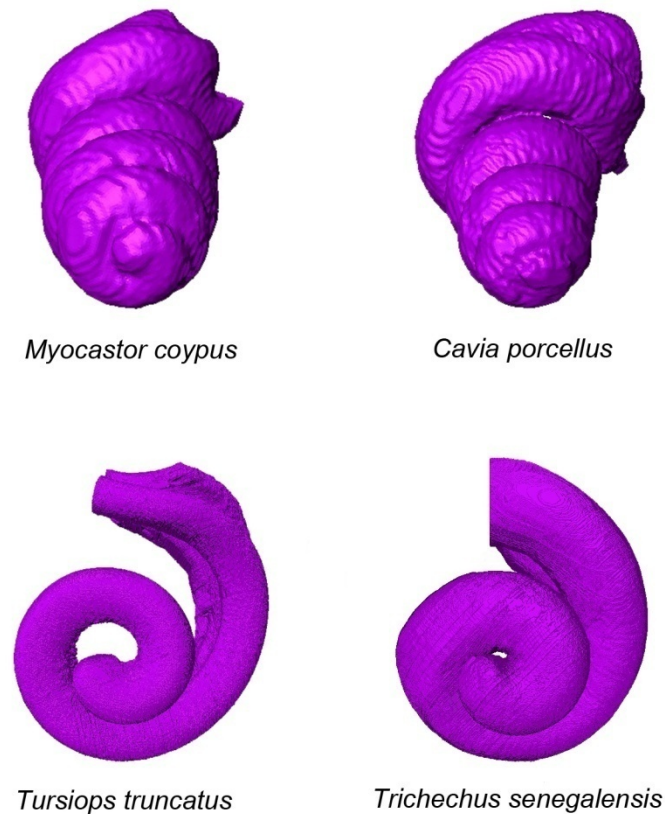


Figure 7.1 The number of cochlear whorls in the four species. The greatest number of turns in the present study (4.2 turns) was found in the coypu (*Myocastor coypus*) and guinea pig (*Cavia porcellus*). The fewest turns (1.75 turns) was found in the bottlenose dolphin (*Tursiops truncatus*) and African manatee (*Trichechus senegalensis*).

That a mammal has a highly coiled cochlea or a flattened cochlea with few turns could be partly due to the spatial limitations of skull. If the area for expansion of the basal turn is limited, an elongation of the cochlea length can be accomplished by increased spiralization (Bruns et al., 1989). This notion, however, appears to contradict findings reported here (as discussed above) and by Watt (1917) showing that number of whorls is not related to changes in cochlear size within the confines of the petrous bone. Further work, incorporating petrous bone size into the analysis as well and focusing on smaller species, in which size scaling is more pronounced, is needed. Image data available for the present study were often cropped to the inner

ear region only and hence petrous size could not be measured. Petrous lengths were available for the developmental study. As discussed later, however, there does not appear to be much significant change in the spiraling of the cochlea during fetal development.

The number of cochlear whorls is also thought to be a measure of efficiency of interpreting sound. In terrestrial mammals, the number of turns shows a significant correlation with hearing range, particularly the frequency range toward low frequencies; mammals with many turns have a greater sensitivity to low frequencies than species with few turns (West, 1985). Moreover, subterranean mammals that are good low-frequency detectors tend to possess greater coiling of the cochlea when compared to their ground-dwelling relatives with poor low-frequency hearing (Lange et al., 2004; Begall et al., 2007). These are supported by the results from Table 5.11, which showed a significantly negative correlation between the low frequency limit of hearing and the number of spiral turns in mammals—an increased number of turns is associated with an extension of hearing range toward lower frequencies. This trend excludes the bats. Many researchers have shown that bats utilizing high-frequency echolocation have an increased number of spiral turns, typically 3.5 turns (Bruns et al., 1989; Solntseva, 2010). It could be argued that the hearing frequency link with the number of turns is an indirect consequence of a closer association between cochlea size and frequency. This suggests that size and coiling carry the link with frequency from size to coiling. Results reported here, however, show no correlation of cochlea size and coiling.

7.1.3.2 The height-to-width ratio of the cochlea

Fleischer (1976) suggested that mammals with a small ratio of height to width (e.g., cetaceans) favour high-frequency hearing, whereas mammals with the greatest ratio (the tower-shaped cochlea) tend to respond best to low frequencies. The height of the cochlea is considered as a function of the number of turns (Solntseva, 2010). The findings of the present study were that marine species had the smallest height-width ratio, whereas underground species had the greatest ratio (Table 5.7); this supports Fleischer's idea. It is well known that odontocetes and sireneans develop the capability of ultrasonic hearing (e.g., Gerstein et al., 1999; Wartzok and Ketten, 1999; Nummela et al., 2007), and underground species show auditory adaptations to their habitat with shifts in hearing range and sensitivity toward lower frequencies (Lange et al., 2004; Lange et al., 2007; Begall et al., 2007). In addition, the results from the ANCOVA showed that the height-width ratio in subterranean mammals was significantly higher than that in terrestrial mammals (Fig. 5.15). This agrees with the result that the cochlear width in subterraneans was significantly less than that in terrestrials; less width enhances the ratio value. Based on Fleischer's hypothesis, these findings support previous studies indicating that subterranean species have a higher sensitivity to the low-frequency range compared to their ground-dwelling counterparts (Lange et al., 2004; Begall et al., 2007). It is noteworthy, however, that no significant difference in this ratio between marine and subterranean mammals was found, despite the fact that both were the smallest and the greatest ratios. This may be due to the small number of marine samples examined in the present study.

7.1.3.3 Cochlear width (the width of the basal turn)

Cochlear width was measured across the first cochlear turn (as per Nemzek et al., 1996). Thus, cochlear width in the present study is equivalent to the width of basal turn. A wide basal cochlear turn can be found in some mammals: e.g., shrews, pinnipeds and particularly echolocating species (Solntseva, 2010). A significant increase in the width of the basal whorl is regarded as one of the most important adaptations to the perception of very high frequencies in echolocating bats and odontocetes (Fleischer, 1976; Habersetzer and Storch, 1992; Solntseva, 2010). The findings of the present study demonstrated that the high frequency limit and the best hearing frequency were significantly positively correlated with cochlear width (Table 5.10 and 5.13). In categorical data analyses independent of body mass, the results also showed that mammal groups with high and with medium high-frequency limits had significantly wider basal turns than the group with a low high-frequency limit (Fig. 5.17). Mammals with a medium best hearing frequency had significantly wider basal turns than mammals with a low best frequency, as well (Fig. 5.18). By contrast, the basal turn in subterranean mammals was relatively narrow compared to other groups with different habitats. Consequently, all data are in an agreement and reflect a wider basal turn as an adaptive feature of improved high-frequency hearing. It is reported that the number of hair cells is associated with frequency discrimination at a given frequency range; in the cochlear regions responsible for the best hearing frequencies, the number of hair cells is generally higher than other regions (Begall and Burda, 2006; Begall et al., 2007). The present study suggests that a wider basal turn (thereby increasing length) may accommodate more hair cells in this region where high frequency sound is primarily perceived, hence enhanced high-frequency response.

7.1.3.4 Cochlear volume

The result showed that cochlear volume was significantly positively correlated with the high-frequency limit of hearing (Table 5.10). Additionally, the present study found that mammals with a medium high-frequency limit had significantly larger cochlear volumes than mammals with a low high-frequency limit (Fig. 5.17). The relationship between the groups with medium and with low best hearing frequency also followed this trend with cochlear volume (Fig. 5.18). These findings contradict previous studies in primates indicating that the high-frequency limit increases with a decrease in cochlear size, independent of body mass (Kirk and Gosselin-Ildari, 2009; Armstrong et al., 2011).

Another result showed that, in terrestrial species, cochlear volume was significantly larger than that in underground species after controlling for body mass (Fig. 5.15). Several previous studies of subterranean hearing reported an association between an enlarged middle-ear cavity and improved low-frequency hearing due to increased middle-ear compliance (Relkin, 1988; Schleich and Vassallo, 2003; Schleich and Busch, 2004; Begall and Burda, 2006), but very little information is available on implications of the cochlear volume. If the idea of Kirk and Gosselin-Ildari (2009) and Armstrong et al. (2011) is applicable for mammals in general, subterranean mammals should have a larger cochlear volume than terrestrials for a given body size. The results, however, suggest this is not the case. The present study suggests that Kirk and Armstrong's proposition may be practical only in primates, whilst for mammals in general, species with larger cochleae tend to detect higher frequency sounds (relatively high high-frequency limit) at a given body size. The question is raised how cochlear size impacts on hearing abilities. One can speculate that the

mass of cochlear fluids (larger mass in larger cochlear size) may have a resonant effect on frequency analysis along the cochlear duct. The exact mechanisms accounting for this relationship remain to be clarified.

7.1.3.5 Cochlear frenestrae

Many studies have examined the area ratio of the tympanum to stapedial footplate. The size of the stapedial footplate is reported to be comparable to that of the oval window (Meng, 1992; Ladeveze et al., 2010; Ekdale, 2013). Thus, this ratio can be represented as the ratio of the tympanum to oval window. Sound propagations (acoustic impedance) in air in the middle ear and in fluid in the cochlea differ greatly, so sound energy tends to be reflected at the interface of these media. This ratio is believed to contribute to the impedance-matching function of the middle ear that decreases the amount of sound reflected at the interface, leading to increased efficiency of sound transmission to the cochlea. Mammals with lower area ratios have poorer impedance matching, resulting in reduced transmission of sound energy to the cochlea (Wilkins et al., 1999; Mason, 2006; Begall et al., 2007). Fossorial and subterranean mammals have lower ratios because of their enlarged footplate areas compared with non-fossorial mammals (Mason, 2001). The low area ratio of the eardrum to the footplate (oval window) is presumed to be related to the poor hearing sensitivity in air in these mammals (Wilkins et al., 1999; Mason, 2001; Schleich and Busch, 2004). In a recent study that combines this ratio with the ossicular lever arm ratio to form a single unit, a relatively large footplate in comparison to the eardrum is indirectly linked to the lower frequency of airborne hearing (Colman and Colbert, 2010).

The size of the round window is also proposed as an additional factor for sound amplification (Scarpa, 1962; Wartzok and Ketten, 1999). The round window and the oval window work on sound energy exchange between the middle and inner ears. Sound vibration from the middle ear entering the cochlea through the oval window is transferred through the hearing receptors into the scala tympani. Pressure waves are then relieved by the round window to the middle ear again. Nevertheless, the implications of the coupling function between them (possibly represented as the area ratio of oval window to round window) has been neglected. In the present study, the results showed that subterranean and fossorial groups had a significantly higher ratio of oval window to round window than terrestrial mammals (Fig. 5.15). The hearing parameters did not show any significant correlation with the oval window-round window ratio across all 45 species (Table 5.10, 5.11 and 5.13). When aquatic species were excluded, however, the high frequency limit and the best frequency hearing were significantly negatively correlated with the oval window-round window ratio (see Appendix D.10 to D.12). This implies that the ratio may be a measure of the efficiency of sound energy exchange; the higher ratio is related to decreased high-frequency airborne hearing. Further investigation of the functional significance of this ratio in airborne hearing could be performed by comparing the ratios between species with a comparable area of the tympanum against available audiometric data. Studying the behaviour of sound propagation in relation to sound density and pressure along the path from the oval window to the round window may also help clarify this point.

Interestingly, the present study found that the area of the oval window was significantly smaller in gregarious mammals than solitary mammals, independent of

body mass (Fig. 5.16). This result can be explained by the function of the area ratio between the eardrum and the footplate (the oval window). If it is assumed to hold the area of the eardrum constant, a smaller oval window will give a higher ratio. This means that the efficiency of energy transmission to the inner ear is increased, thereby enhanced hearing sensitivity in air. Acoustic intraspecific communication may play a major role in animals living in colonies (Begall and Burda, 2006). Thus, it is possible that mammals that form social aggregations possess a relatively small oval window to maintain sensitive audition to promote intraspecific communication.

The present study includes many cochlear and hearing variables and it is likely that some, if not all, of these are inter-dependent to varying degrees, creating a myriad of potential connections. Below is a hypothetical map based on the present study that outlines the most important links and key determinants. The inter-dependencies of the variables are represented as links in the chain below (Fig. 7.2).

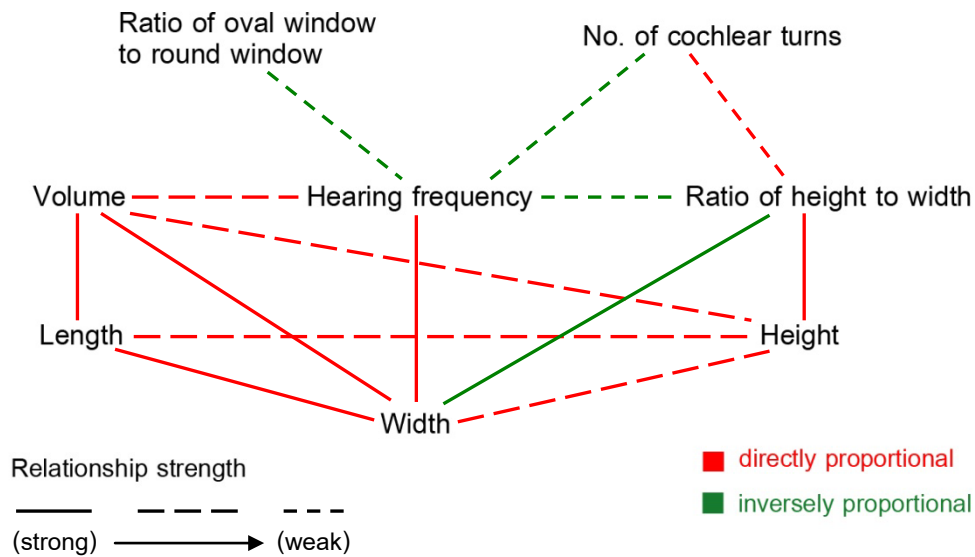


Figure 7.2 The inter-dependencies of cochlear dimensions and hearing frequency. For instance, the relationship between cochlear width and hearing frequency is strong and directly proportional; hearing frequency increases with increasing cochlear width. In contrast, the relationship between the number of spiral turns and hearing frequency is weak and inversely proportional; as the number of turns increases, hearing frequency decreases, or vice versa.

7.1.4 Shape analysis of the cochlea

To date there is little information on the relationships of cochlear shape to hearing frequency and eco-behavioural traits. Published data are largely descriptive and are not tested by statistical methods. Therefore, the present study examines these relationships using geometric morphometrics and statistical analyses. Significant and interesting results will be discussed with reference to previous publications.

7.1.4.1 Shape analysis by principal component analysis

The results showed that scores on PC1, PC3 and PC4 were significantly correlated with centroid size ($P < 0.001$, Table 5.5). Based on the variances of the three axes,

size difference accounted for at least 63% of the shape change. This indicates that size variation plays an important role in shape diversity of the mammalian cochlea (see above regarding size scaling). When considering the cochlear wireframes on all four PCs (Fig. 5.12 and 5.13), many landmarks in the middle and apex of the cochlea had obviously large shifts in their position. This suggests that the changes in the middle and apical portions represent a significant proportion of the size related shape variation of the mammalian cochlea.

Marine species form a separate group from the other mammals throughout the first four PCs. Within this group, the cochlea is characterized by fewer than 2 turns, a large basal turn and a compact middle turn. The radii ratio of the basal turn to the middle turn is relatively high compared to other species. Interestingly, the northern elephant seal (*Mirounga angustirostris*), a phocid species, falls close to marine species (Fig. 5.12 and 5.13). The northern elephant seal is unique among pinnipeds in its behaviour. It favors deep diving and engages in a great deal of acoustic communication under water (Kastak and Schusterman, 1999). Also, the northern elephant seal's ear is assumed to be more adapted for hearing sensitivity underwater compared with other pinniped ears (Kastak and Schusterman, 1998, 1999). As a result, it is possible that its behaviour, adapted for essentially aquatic lifestyle, may be associated with the observed similarity to the cochlea in marine species. There are some differences in hearing abilities among species within this marine group. For example, toothed whales (but not others) can use high ultrasonic echolocation, and the African manatee and the northern elephant seal can use bone conduction mechanism but not toothed whales.

On the plot of PC1 vs PC2, there is a distinct cluster of six species (Fig. 5.12). The cluster includes the prairie dog (*Cynomys ludovicianus*), tuco-tuco (*Ctenomys opimus*), plains viscacha (*Lagostomus maximus*), guinea pig, coypu and tarsier (*Tarsius bancanus*). These species are characterized by a tower-shaped cochlea with more than 3.5 turns. An interesting question arises: why is cochlear shape so different in these six species? It cannot be explained by ecological patterns in relation to habitat, active period and sociality alone since the species do not consistently populate these categories (Table 4.1). Concerning the phylogenetic effect, the six species include a single primate and five rodent species; other closely related species (e.g., *Rattus*) are found elsewhere in the shape space. This suggests that the cluster is not primarily related to phylogeny. Interestingly, the results showed that all six species share a common feature, an inflated auditory bulla. Inflated bullae have been reported in the guinea pig, tuco-tuco and tarsier (Fleischer, 1978; Packer, 1987; Schleich and Vassallo, 2003). Evidence of a bulla in the prairie dog reported here, however, contradicts Heffner et al. (1994), who did not find anatomical specializations in the auditory apparatus. Another potentially important shared feature is that the cochlea in these six species bulges further into the bulla compared to other mammals. It is believed that large bullar size may reflect an adaptation to improved low-frequency hearing (Webster and Webster, 1972; Fleischer, 1978; Packer, 1987). Based on available audiograms and findings from several studies, the guinea pig, prairie dog, tuco-tuco and tarsier appear to rely on low-frequency audition to suit their lifestyles (Packer, 1987; Heffner et al., 1994; Heffner et al., 2001; Schleich and Vassallo, 2003; Ramsier et al., 2012). Information about hearing abilities in the plains viscacha and the coypu is limited. Nonetheless, based on the presence of the inflated bulla and all supporting data, it can be proposed that the

functional selection pressure to hear low frequencies may be the key factor responsible for the similar cochlear shape in these species.

Compliance is one of the main factors that affect sound energy transmission in the middle ear. One of the most important contributors to compliance is the volume of the middle ear (Dallos, 1973; Schleich and Busch, 2004). Greater bullar volume is associated with increased compliance, or reduced stiffness (Relkin, 1988; Schleich and Vassallo, 2003; Schleich and Busch, 2004). Increased compliance results in less sensitivity towards high frequencies and improved transmission of low-frequency sound to the cochlea, which in turn lead to improved low-frequency audition (Relkin, 1988; Schleich and Vassallo, 2003; Schleich and Busch, 2004; Mason, 2006; Begall et al., 2007). The greater exposure of the cochlea to the internal surfaces of the bulla may represent an adaptation of the bony transmission of sound directly into the cochlea. This, too, would favour lower frequency sounds and warrants further investigation, possibly with computational methods such as fluid dynamics.

7.1.4.2 Shape analysis after size correction

Because there were size effects on PC1, PC3 and PC4, shape residuals on these PC axes were calculated with PAST and used to minimise these size effects. After correction for allometry, the overall distribution of species in morphospace was different from uncorrected analysis; none of the groups was clearly distinct from others (Fig. 5.14). In general, this indicates that allometry strongly influences the morphological disparity of the mammalian bony cochlea. Four obligate aquatic species, however, still fell close together throughout the four PCs, as in the uncorrected analysis despite an almost four-fold difference in body mass. This result

strongly supports the idea that marine environment places particularly strong functional demands on the bony cochlear shape. Also, both before and after size-correction, the guinea pig and coypu plotted separately from the others in PC4, which is related to changes in coiling. This may reflect a unique coiling pattern in these two species. A highly-spiraled cochlea is considered a synapomorphic character for their carviomorph group (Ekdale, 2013).

For the comparison between hearing variables and cochlear shape, a significant correlation was found only between the low frequency limit of hearing and PC4 residuals. It may reflect the adaptation of some aspects of cochlear shape to low-frequency hearing.

Discriminant Function Analysis (DFA) and the Mann-Whitney U test were used to examine differences of the cochlear shape between mammalian groups with different eco-behavioural traits or with different hearing parameters. There were some discrepancies between the two methods (Table 5.8 compared to Table 5.9). DFA is a very conservative test, as it spans the whole shape space (as represented by the Procrustes distances) and not just the regions of specific interest. Consequently, the shape space was decomposed into principal components and differences among PC scores were then tested with a Mann-Whitney U test. Different results were probably observed due to these different approaches. Overall, DFA and Mann-Whitney U test typically produced similar results in terms of the significant differences in cochlear shape in relation to habitat and active period. Differences in cochlear shape were noted between species living in the sea, on the ground, and underground. These may reflect the effects of transmission media for sound; i.e., by liquid in marine

mammals, by air in terrestrial species, or by solid (seismic vibration) in subterranean species. The types of transmission media are associated with sound propagation (Begall et al., 2007; Nummela et al., 2007) and may affect animals' hearing characteristics, leading to the adaptation of cochlear shape. Pertaining to the active time, nocturnal species have a different cochlear shape from diurnal species. Nocturnal species would be expected to rely relatively more on hearing than species active during the day (Beecher, 1974). In the darkness, where vision is restricted, prey detection or even predator avoidance via hearing sense would be crucially important for many nocturnal species (Webster and Webster, 1971, 1972; Packer, 1987). Thus, there are possibly some different adaptations of cochlear shape to suit diurnal and nocturnal mammals. The Bonferroni correction is a statistic used to reduce the probability of false-positive results when multiple pairwise tests are performed on a single data set. The analysis is complex but not a permutation test of all possible combinations. In addition, many of the findings were insignificant (and thus corrections cannot be applied). Currently the Bonferroni corrections are not available in MorphoJ. Therefore, it is not possible to use the Bonferroni corrections and seems unlikely that the adjustment would fundamentally alter the conclusions. In summary, although the results here from DFA and Mann-Whitney U test should be considered as tentative, based on the presence of significant results in both methods, it can be concluded that eco-behavioral traits and hearing parameters can be derived, in principle, from shape variation of the mammalian cochlea.

7.1.5 Phylogenetic signal in cochlear shape variation

For shape variation of the whole 45 species, the permutation test showed evidence that is inconsistent with the null hypothesis that there is no phylogenetic signal.

Within mammalian subclades, phylogenetic signal was also present in rodents but not in primates. The uncertainty in the tree lengths used, however, is an important concern for the test of phylogenetic signal (Klingenberg, 2011). Hence, independent contrast analysis was also performed. This analysis is used to minimise the influence of the evolutionary framework between the species. When the independent contrasts of shape in the whole sample were regressed on the contrasts of centroid size, correlations on PC1, PC3 and PC4 were found, indicating the presence of the allometric effects reported earlier. In comparisons between regression lines obtained before and after taking the contrasts on each PC, no significant differences in slopes were noted in both the whole sample and the two subclades. These results suggest that shape variation of the cochlea is mostly, but not wholly, independent of phylogeny. It appears that size has a much greater influence.

7.1.6 The intermeatal distance and adaptations of the bony cochlea in adult mammals

There are three basic cues used for localizing sound sources in the horizontal plane: the interaural time difference (ITD), the interaural level (intensity) difference (ILD) and pinnae cues. Both ITD and ILD require comparing the sounds between two ears. The importance of the ITD cue partly depends on the maximum interaural time difference (μs) which can be measured when sound sources are located between 90° to the left or right. This maximum time difference correlates with the intermeatal distance (time = distance/velocity), which is directly related to head size. Therefore, the present study uses the intermeatal distance as a measure of head size instead of the maximum time difference. Results of the present study showed that the

intermeatal distance was significantly positively correlated with body mass (Table 5.3). In other words, the intermeatal distance increases with increasing body mass.

The selective pressure for sound localization is proposed to be a major cause for increased high-frequency hearing in mammals with small heads or close-set pinnae (Masterton et al., 1969; Heffner et al., 2001; Heffner, 2004). Small species are forced to rely on ILD and pinnae cues to localize sounds. Listening to high frequencies enables small mammals to improve sound localization ability because frequencies that are high enough can be shadowed by their heads, thereby leading to an increased intensity differences of the sounds at the two ears. Similarly, pinnae cues are ineffective at frequencies too low to be modified by the components of the small pinna (Heffner, 2004). High frequencies can be attenuated and reflected by the pinna depending on the angle of the sound source relative to the head. Therefore, small mammals tend to use high frequencies to localize sounds by detecting differences in the degree of sound modification between the two ears. Many publications, however, indicate that there are exceptions to this generalization. For example, low-frequency acuity can be found in many small rodents and subterranean species (Webster and Webster, 1972; Schleich and Vassallo, 2003; Mason, 2006). Small mammals prefer low frequencies rather than high frequencies, if those low-frequency sounds are more important to their survival (Webster and Webster, 1972; Heffner et al., 2001). In other words, there is a balance between accuracy and range, with the latter predominating as determined by the environment and for sounds that need little further interpretation and are used primarily to elicit an immediate response as in, for example, predator avoidance. In the present study, subterranean mammals and a

few rodents (prairie dog and guinea pig) are examples of such species that do not conform to the standard theory.

Subterranean mammals live in long narrow burrows where low-frequency airborne sound is transmitted best (Begall et al., 2007; Lange et al., 2007). In seismic communication in underground life, low frequencies are also transmitted across long distances through the soil substrate with the least amount of attenuation (Nevo et al., 1991; Begall et al., 2007). Airborne sounds in narrow tunnels are either in front or to the rear so localizing sounds in the horizontal and vertical planes by ILD and pinnae cues is less important. Because of the environment where they live, low-frequency hearing appears to be more important than accurate sound localization in these taxa. It is worth noting that the fossorial prairie dog is another small-headed species that extends its hearing frequency toward the low frequency range (Heffner et al., 1994; Heffner, 2004). It spends much time in underground tunnels but still forages on the ground near a burrow entrance (Heffner et al., 1994). Although the hearing ability is similar to that in subterranean mammals, the prairie dog has a better overall sensitivity to sound because it is not an exclusively subterranean species.

Another small rodent that favors low-frequency hearing is the guinea pig (*Cavia porcellus*). It has been suggested this species is descended from a closely related species of wild cavies, such as *C. aperea* or *C. tschudii* (Nowak, 1999). Based on field studies of behaviour, wild cavies spend long periods of time foraging among vegetation patches (Cassini, 1991; Cassini and Galante, 1992). Species that prefer to forage in open environments have a high risk of being attacked from predators. Therefore, these species need to have evolved some abilities to cope with and

minimise the high predation risk. It is suggested that visual sense is a more useful adjunct to hearing for species living in open areas than species in a jungle or cluttered thicket environment (Webster and Webster, 1972). For example, kangaroo rats (*Dipodomys* sp.) inhabit desert environments where the view is quite unobstructed. Major predators of kangaroo rats usually produce low-frequency sounds during the period before the strike (Webster and Webster, 1971). They have morphological adaptations to avoid the predator's strike: large and protruding eyes and inflated auditory bullae (Webster and Webster, 1972; Kotler, 1984). It seems that low-frequency hearing and vision play more significant roles in a kangaroo rats' life than accurate sound localization using high frequencies (Webster and Webster, 1972). Guinea pigs inhabit open areas, like kangaroo rats, and show the same adaptive behaviour that is heightened anti-predator vigilance at a greater distance (Cassini, 1991). Low frequency waves generally travel farther and can alert an animal to more distant danger. Like kangaroo rats, it may be assumed that both vision and low-frequency audition are important in predator avoidance in guinea pigs, so they retain low-frequency hearing and reduce the necessity for accurate high-frequency sound localization. Further investigation, however, is required to clarify this point.

In the present study, mammals with small head size (short intermeatal distance) showed many adaptations of the auditory structures to low-frequency hearing. The tuco-tuco, prairie dog and guinea pig possessed the inflated auditory bullae. Enlarged bullar volume contributes to increased middle-ear compliance, resulting in increased sensitivity to low-frequency sounds (Relkin, 1988; Schleich and Busch, 2004). In addition to increased volume, the auditory bulla in the tuco-tuco was

divided into many subcavities by large and prominent septa (Fig. 7.3). This observation is similar to the findings in their close relatives *Ctenomys sociabilis* (Mason, 2004) and *C. talarum* (Schleich and Busch, 2004). Lay (1972) suggested that these septa buttress the auditory bulla by resisting compression forces that are produced by contractions of muscles at the lower jaw, which pass over the inferior surface of the bulla. The septa direct compression forces toward the base of the external auditory meatus to dissipate. The buttress system and the inflated bulla function together in increasing sensitivity to low-frequency sounds. In subterranean moles, although no inflated bulla was observed, there was a connection between left and right bullae (Fig. 5.5), similar to that reported in the studies of Mason (2003, 2006). Coles et al. (1982) proposed that sound in burrows can be transmitted through the head of subterranean moles and reaches both sides of the eardrum with phase differences, depending on the direction of sound source. This pressure-difference detection system can permit the moles to localize sound at low frequencies (Coles et al., 1982).

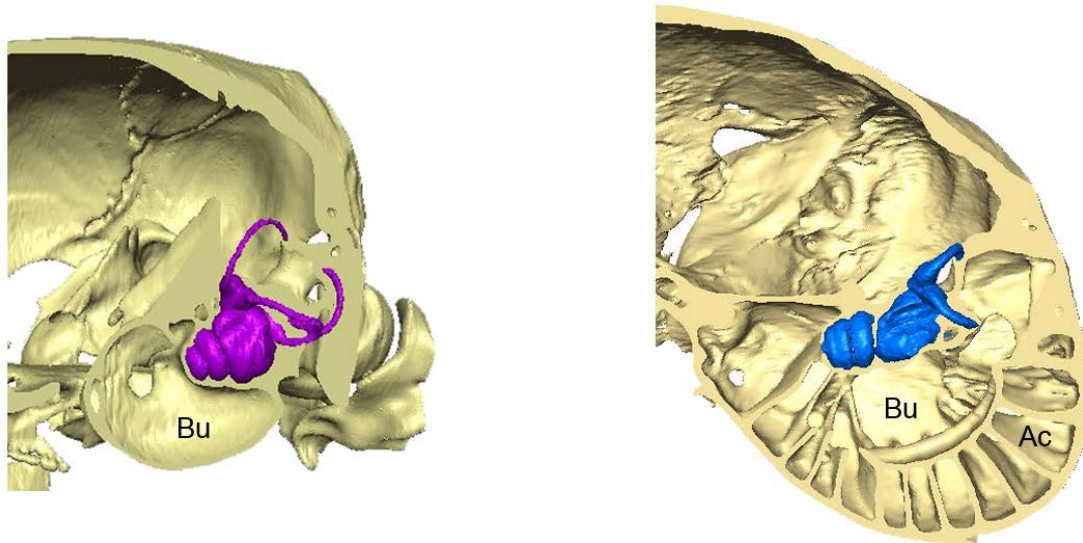


Figure 7.3 The auditory bullae in the rat (left) and in the tuco-tuco (right). The auditory bullae and the cochleae are shown at the plane through the mid-modiolar axis. The bulla in the tuco-tuco is relatively inflated and has many air cavities inside. Bu, auditory bulla; Ac, air cavities.

There are many other characteristics of the middle ear reported to improve low-frequency hearing. For example, a loose articulation between the malleoincudal complex and the tympanic bone, called the freely mobile ossicles, is found in subterranean mammals and guinea pigs (Mason, 2001, 2003; Schleich and Busch, 2004). The middle-ear muscles, the tensor tympani and the stapedius, are considerably reduced or lost among underground mammals (Mason, 2001, 2006). The freely mobile ossicles and the reduced middle-ear muscles reduce the stiffness of the middle ear, thereby increasing transmission at low frequencies (Mason, 2006; Begall et al., 2007). Furthermore, a bony tube enclosing the stapedial artery in subterranean moles helps reduce arterial noise (related to heart rate) and improve low-frequency hearing (Packer, 1987; Mason, 2003, 2006; Fig. 7.4).

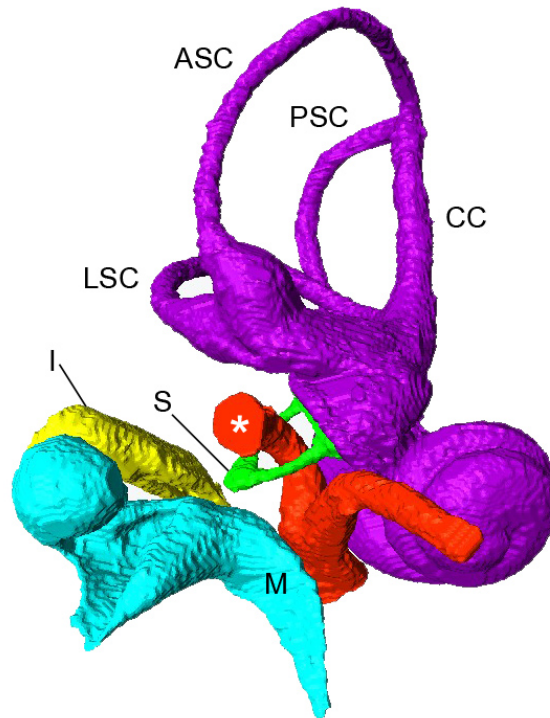


Figure 7.4 The middle-ear ossicles and the inner ear of the Spanish mole (*Talpa occidentalis*). The stapedial artery enclosed by a bony tube (*) passes through the stapedial foramen. ASC, anterior semicircular canal; LSC, lateral semicircular canal; PSC, posterior semicircular canal; CC, common crus; M, malleus; I, incus; S, stapes.

Concerning the adaptation of the cochlear morphology, many small-headed species in the present study showed a high ratio of the oval window to round window. The functional significance of this ratio has remained unclear. This study, however, demonstrated that the high frequency limit and the best hearing frequency were significantly negatively correlated with the ratio of the oval window to round window when aquatic mammals were not included. In other words, as the ratio of the oval window to round window increases, there is a decrease in high-frequency audition. These results correspond to the presence of restricted high-frequency hearing in these small mammals. Accordingly, the size of the cochlear fenestrae and their

interaction may indicate the adaptation of the bony cochlea to sound frequency response in air.

For the adaptation of cochlear shape, the subterranean mammals, prairie dog and guinea pig fell closely together in shape space, near the negative extreme of PC1 (Fig. 5.12). The exceptions, however, were the two talpid moles (*Talpa europaea* and *T. occidentalis*) that were found in the positive region. The negative extreme of PC1 was characterized by the high number of spiral turns and a small radius of curvature at the basal turn. This implies that these small mammals possess a relatively narrow basal turn, contributing to a relatively low value of cochlear width. A wider basal turn is proposed to be an adaptive feature of improved high-frequency hearing (Solntseva, 2010; this study). Moreover, the increased number of turns is associated with an extension of hearing range toward lower frequencies (West, 1985; Lange et al., 2004; Begall et al., 2007; this study). Thus, the similarity in these aspects of cochlear shape on PC1 is indicative of a cochlea with restricted high-frequency response but adaptive specializations for sensitive perception of low frequencies. On the other hand, the two talpid moles possessed a cochlea with only about two turns. The number of cochlear coils may contribute mainly to the shape difference on PC1.

There are many morphological adaptations of the middle ear and the inner ear for promoting low-frequency hearing. As seen in this study, each small species exploits different strategies by means of adaptations that function together to achieve low-frequency audition in their environment.

7.2 Human developmental study

In this section, the development of the cochlea in one species, modern humans, was explored. The study of change and variation of characteristics observed during development may provide important insights into the mechanisms underlying the evolutionary, interspecific variations outlined above.

Data on the development of the prenatal human bony cochlea is limited and yet important for our basic understanding of intrauterine auditory function and congenital ear anomalies as well as evolution. What little data are available apparently contradict each other, with some papers reporting that cochlear form (size and shape) attains its mature state prior to birth, whilst others maintain that changes in the bony cochlea continue after birth. Therefore, specific questions of the present study addressed were: 1) Does the bony cochlea reach a mature-like size prior to birth?; 2) Do shape changes in the bony cochlea cease during gestation, or do postnatal changes occur? Earlier maturation would indicate that the bony phenotype is highly conserved, less plastic and further removed from well established postnatal changes of auditory function amongst humans.

7.2.1 Size maturation of the bony cochlea

The first question asked whether the bony cochlea reaches its adult size prior to birth or not. The results of the present study showed that length, width and volume of the adult cochlea were significantly higher than those in the fetal cochlea (Table 6.4), whereas no significant differences existed between large and small fetuses. The adult cochlea was, on average, bigger than the large fetuses by about 9% in length and width and 23% in volume. These results imply that there is a change in cochlear

size after birth, supporting observations by Turkewitsch (1930), Hardy (1938) and Sercer (1958), contra suggestions that the cochlea achieves adult size and ceases its growth during prenatal period (Eby and Nadol, 1986; Sato et al., 1991; Nemzek et al., 1996; Jeffery and Spoor, 2004). The otic capsule is suggested to be fully ossified during the sixth month of gestation (Bast, 1930; Nemzek et al., 1996; Richard et al., 2010). In contrast, the temporal bone undergoes considerable change during postnatal life (Eby and Nadol, 1986; Nemzek et al., 1996; Lloyd et al., 2010). Hence, based on the present study, the change in bony cochlear size may occur after complete ossification of the otic capsule, particularly in the postnatal period, together with the growth of the temporal bone. It is important to note, however, that there are only five adult cochleae included in this study. It may not be truly representative of the variation amongst adults. Perhaps throwing in more adults from other non-European populations will push the variances together and affect the level of significance in the results, e.g., non-significance of cochlear variables. Jeffery & Spoor (2004) included data on 54 adult individuals. Obtaining micro-CT data to replicate the current study for this many subjects was not feasible. Such data may be in the public domain in the near future, however, and will require a re-appraisal of the findings reported here. Nonetheless, it is important to note that the sampling issues only affect comparisons that establish significant differences. Findings that fetal and adult samples are similar are unlikely to change with the addition of more specimens, as it seems unlikely that the five adults used in the present study would overestimate variance.

Findings reported here showed that the number of spiral turns was not significantly different between adult and fetal cochleae, and between large and small fetal

samples (Table 6.4). In addition, the number of cochlear whorls did not show a significant correlation with the length of the petrous bone during fetal development (Table 6.2). This does not support the hypothesis that spirals increase to accommodate an enlarged cochlea in a small petrous bone. The number of cochlear turns was rather constant between four and nine months of gestation. Moreover, observations of micro-CT images revealed that the bony partition between the cochlear turns was completely ossified around five months of gestation. It has been reported that the fetus responds to sound at five months (Hepper and Shahidullah, 1994). Therefore, the present findings suggest that the adult number of cochlear turns is set during the intrauterine period, approximately at middle gestation. Meanwhile, the fetus begins hearing because acoustic energy can focus at the bony wall and propagate along the radial direction of the cochlea.

The average number of cochlear turns calculated from all specimens was 2.67 turns, ranging from 2.56 to 2.75 turns. Several previous studies reported that the number of human cochlear turns ranged from 2.5 up to 3 turns, although the majority of the cochleae have more than 2.5 and less than 2.75 turns (Hardy, 1938; Nemzek et al., 1996; Biedron et al., 2009). Therefore, those studies are supported by the findings of the present study.

Concerning the round window, although a slight increase in size was observed during fetal development (Table 6.2), there was no significant difference in size between large and small fetuses (Table 6.4). Also, no significant difference was found between adults and fetuses. These results agree with previous studies, reporting the maturation of the round window size before birth (Su et al., 1982;

Bonaldi et al., 1997; Toth et al., 2006; Richard et al., 2010). The time to achieve adult size, however, is not agreed. It is reported to reach adult size by the fourth month of gestation (Bonaldi et al., 1997), near the sixth month (Richard et al., 2010) and even as late as the eighth month (Toth et al., 2006). In the present study, the round window area in the fetuses approaches the adult value first at about the second trimester, most similar to the results of Bonaldi et al. (1997) and Richard et al. (2010). Takahashi et al. (1989) reported that an average surface area of the human round window is about 2.70 mm², which is similar to an area of about 2.63 mm² as reported in the present study.

Previous authors agreed that the oval window reaches its mature size during intrauterine life, although reported different maturation times, from the fourth month of gestation (Bonaldi et al., 1997) to near the ninth month (Richard et al., 2010). These contradict our findings that the oval window area in adults was significantly larger than that in the large fetus group (Table 6.4), indicating that there are some changes after birth. One interesting result is that the oval window area in the small fetus group was also larger than that in the large fetus group (Table 6.4) but not significantly different from that in the adults. The oval window decreased in size during fetal development (Table 6.2). Formation of the oval window is believed to be closely related to development of the stapedial footplate (Zeifer et al., 2000). The ossification process of the stapes proceeds rapidly between the fourth and fifth month of gestation (Nemzek et al., 1996). Also, based on the present micro-CT images at about four months of gestation, the bony layer at the edge of the oval window is rather thin and not clearly visible. Thus, it is possible that the ossification of the oval window may occur during that time. It is supposed that the oval window

area in the small fetus group may be affected by the incomplete ossification itself, resulting in an unsettled bony border and a relatively large area, which in turn leads to non-significance in comparison with the adults. Because the effect of categorization may be a cause for the perceived difference, it should be considered tentative.

Overall, the findings suggest that the round window size achieves its mature state prior to birth, by approximately the second trimester. By contrast, the bony cochlea and the oval window continue to change in size after birth. The pattern of change for the oval window includes an initial reduction in size from midgestation due to ossification process, and then a functionally determined enlargement after birth.

7.2.2 Shape maturation of the bony cochlea

The second question asked whether shape change of the bony cochlea ceases before birth or not. Both DFA and Mann-Whitney U test failed to show significant differences between the large and small fetuses (Table 6.7 and 6.8), and also between the adult and fetal cochleae (Table 6.10 and 6.11). Moreover, the overlapping distributions between specimen groups in PCA were observed both before and after the removal of allometric effects (Fig 6.5, 6.10 and 6.14). These results indicate that the cochlea reach a mature-like shape during intrauterine life and shows little or no changes in shape after birth. Based on the PC plots, shapes of fetal specimens at the second trimester of gestational age start to appear similar to those of adults. Thus, the findings suggest that mature shape is achieved during the second trimester. These results support similar observations described by Jeffery and Spoor (2004) and Moore and Linthicum (2007).

Among fetal specimens, no significant relationship was found between shape variables and centroid size (Table 6.5), meaning that shape variation of the cochlea among fetuses is independent of size differences. In contrast, when all specimens (both adults and fetuses) are examined, the results showed a slight correlation of PC1 scores with centroid size (Table 6.9). This indicates that size difference is associated with about 33% of the cochlear shape variation, primarily in the middle and apical regions. This size-related shape can be explained by the results mentioned above that the adult cochlea has a relatively larger size compared to the fetal cochlea.

Concerning the petrous bone, this study found that the length of the petrous bone was not related to shape variables but was positively correlated with volume (Table 6.2 and 6.6). These findings indicate that, during intrauterine gestation, as the petrous bone increases in size, the cochlea expands slightly (RMA regression slope = 0.12) without much shape changes. It is interesting to note, however, that length, height and width do not show the relationships with the petrous bone length despite the relationship with increased volume. It could be supposed that during development the cochlear cavity may increase in diameter at the lateral sides of the cochlea, thereby no observed changes in length and height. Also, this increased diameter may occur mainly in the parts of the middle and apical turns where the parameter 'width' cannot explain because its value is measured from the basal turn.

The present study revealed that the oval window in all specimens studied has a similar shape; an elongated ellipse. In contrast, the shape of the round window showed a greater variability, including circular, oval, elliptical or irregular shapes.

These shapes can be found in both adults and fetuses. It appears that round window shape is not age-dependent, but subject individual variability. The variability in shape may be due to the uneven growth of different walls of the round window during development *in utero* (Toth et al., 2006).

7.3 Conclusions

Morphological variation on the mammalian bony cochlea is size-related and is tightly constrained by functional requirements of hearing frequency response, which is related to the environment mammals live in. Mammals show adaptations of their hearing ability to acoustic properties in their environment. Communication and sound source determination (important in predator alertness) are main selective pressures on defining the sense of hearing. Indeed, all three parts of the ear (external, middle and inner) play an important role in determining the overall shape of mammalian audiogram, particularly the middle and inner ear.

Some dimensions of the bony cochlea may be indicative of the eco-behavioural niche that a mammal occupies. For example, mammals with the number of spiral turns fewer than two tend to be species inhabiting marine environment. Another example is the size of the oval window in association with the size of the tympanic membrane (tympanum-oval window ratio) and with the size of the round window (oval window-round window ratio). A relatively large oval window is indicative of mammals that live in an environment where low-frequency sounds are preferably transmitted; e.g., underground habitats. By contrast, a small size of the oval window indicates a better transmission of sound energy to the cochlea. Therefore, this can

be found in species relying on intraspecific communication or high-frequency hearing.

The bony cochlea and the middle ear may be indicative of the pattern of evolutionary relationship between mammals. Some mammalian species have similar adaptive features of the ear structures to suit their hearing in the same environment despite distinct phylogenies; for example, similarities between subterranean moles and subterranean rodents used for low-frequency hearing. Also, the northern elephant seal and odontocetes have a similar shape of the bony cochlea used for underwater hearing. These may be considered homoplastic characters arising from convergent evolution. By contrast, some related species sharing a common ancestor evolve different traits of the ear structures to suit different environments. An example is the relationship between the African manatee and the elephant (*Loxodonta africana*) and this is regarded as divergent evolution.

Generally eutherian mammals show differences in the time of onset of hearing, audiogram as well as the cochlear characteristics (e.g., coiling and the number of whorls). During ontogenesis, however, all eutherian cochleae begin their growth from the basal turn towards the apex and form a fully coiled cochlea (more than one turn). Also, the elongated elliptical shape of the oval window opening was observed throughout all eutherians in the present study. It matches with a report on the presence of an elliptical stapedial footplate in only eutherian species (Meng, 1992). This evidence suggests a synapomorphy of eutherians and a descending from a common ancestor. It is noteworthy that the monotreme cochlea is not fully coiled like other mammals but similar to the semilunar-shaped lagena found in reptiles and

birds (Ladhams and Pickles, 1996). The stapes and a round-shaped oval window are also similar to those of birds and reptiles (Gates et al., 1974; Chen and Anderson, 1985; Meng, 1992). The internal morphology of the monotreme cochlea, however, including hearing receptors, has a distinctly mammalian structure. Therefore, it is suggested that the monotreme cochlea is intermediate between that of reptiles and mammals and occupies a transitional position in evolution of mammalian hearing.

Pertaining to development of the human bony cochlea, cochlear shape attains its mature state before birth, whereas the growth in cochlear size may continue after birth. This may indicate phenotypic plasticity of the bony cochlea in response to different environments between life in the womb and after birth. In addition, unlike the oval window, the round window achieves its adult dimensions prior to birth and shows variability in shape. This intraspecific variation is considered phenotypic polymorphism. Further studies of postnatal samples are needed to clarify the extent of any phenotypic plasticity. It seems likely that postnatal changes of auditory detection (e.g., hair cell maturation), connections, and processing in the neocortex would explain the offset between prenatal cochlea shape maturation and subsequent postnatal function. The temporal delay in this form-function relationship is of considerable interest and questions how closely the morphology of the cochlea can be tied to its function both in studies of adults, including extinct taxa, and during ontogeny.

Bibliography

- Adams, D.C., Rohlf, F.J., and Slice, D.E., 2004. Geometric morphometrics: ten years of progress following the 'revolution'. *Ital J Zool*, 71: 5-16.
- Aitkin, L.M., Horseman, B.G., and Bush, B.M.H., 1982. Some aspects of the auditory pathway and audition in the European mole, *Talpa europaea*. *Brain Behav Evol*, 21: 49-59.
- Aitkin, L.M., and Moore, D.R., 1975. Inferior colliculus. II. Developmental of tuning characteristics and tonotopic organization in central nucleus of neonatal cat. *J Neurophysiol*, 38: 1208-1216.
- Alvarez, A., and Perez, S.I., 2013. Two- versus three-dimensional morphometric approaches in macroevolution: insight from the mandible of caviomorph rodents. *Evol Biol*, 40: 150-157.
- Ames, A.L., van Vleet, E.S., and Reynolds, J.E., 2002. Comparison of lipids in selected tissues of the Florida manatee (Order Sirenia) and bottlenose dolphin (Order Cetacea; Suborder Odontoceti). *Comp Biochem Phys B*, 132: 625-634.
- Arjmand, E., Harris, D., and Dallos, P., 1988. Developmental changes in frequency mapping of the gerbil cochlea: Comparison of two cochlea locations. *Hearing Res*, 32: 93-97.
- Armitage, P., 1980. *Statistical methods in medical research*. Blackwell Scientific Publications, Oxford.
- Armstrong, S.D., Bloch, J.I., Houde, P., and Silcox, M.T., 2011. Cochlear labyrinth volume in Euarchontoglires: implications for the evolution of hearing in primates. *Anat Rec*, 294: 263-266.

- Au, W.W.L., and Hastings, M.C., 2008. *Principles of marine bioacoustics*. Springer Science+Business Media, New York.
- Ball, J., Moore, A.D., and Turner, S., 2008. *Ball and Moore's essential physics for radiographers*. 4th ed. Blackwell Publishing, Singapore.
- Barrett, J.F., and Keat, N., 2004. Artifacts in CT: recognition and avoidance. *RadioGraphics*, 24: 1679-1691.
- Bast, T.H., 1930. Ossification of the otic capsule in human fetuses. *Contribut Embryol*, 121: 55-82.
- Beecher, M.D., 1974. Hearing in the owl monkey (*Aotus trivirgatus*): I. auditory sensitivity. *J Comp Physiol Psychol*, 86: 898-901.
- Begall, S., and Burda, H., 2006. Acoustic communication and burrow acoustics are reflected in the ear morphology of the coruro (*Spalacopus cyanus*, Octodontidae), a social fossorial rodent. *J Morphol*, 267: 382-390.
- Begall, S., Lange, S., Schleich, C.E., and Burda, H., 2007. Acoustics, audition and auditory system. In: Begall, S., Burda, H., Schleich, C.E. (Eds.), *Subterranean rodents: news from underground*. Springer-Verlag, Berlin, p. 97-111.
- Bekesy, G. von, 1960. *Experiments in hearing*. McGraw Hill, New York.
- Berta, A., 2009. Pinniped evolution. In: Perrin, W. et al. (Eds.), *Encyclopedia of marine mammals*. 2nd ed. Academic Press, San Diego, p. 861-868.
- Biedron, S., Westhofen, M., and Ilgner, J., 2009. On the number of turns in human cochleae. *Otol Neurotol*, 30: 414-417.
- Bininda-Emonds, O.R.P., Cardillo, M., Jones, K.E., MacPhee, R.D.E., Beck, R.M.D., Grenyer, R., Price, S.A., Vos, R.A., Gittleman, J.L., and Purvis, A., 2007. The delayed rise of present-day mammals. *Nature*, 446: 507-512.

- Birnholz, J.C., and Benacerraf, B.C., 1983. The development of human fetal hearing. *Science*, 222: 516-518.
- Bonaldi, L.V., de Angelis, M.A., and Smith, R.L., 1997. Developmental study of the round window region. *Acta Anat*, 159: 25-29.
- Bookstein, F.L., 1991. *Morphometric tools for landmark data: geometry and biology*. Cambridge University Press, Cambridge.
- Bookstein, F.L., 1998. A hundred years of morphometrics. *Acta Zool Acad Sci Hung*, 44: 7-59.
- Bookstein, F.L., Chernoff, B., Elder, R.L., Humphries, J.M. Jr., Smith, G.R., and Strauss, R.E., 1985. *Morphometrics in evolutionary biology*. Special publication 15. Academy of Natural Sciences Press, Philadelphia.
- Bossy, J., and Gaillard de Collogny, L., 1965. Orientation comparee de la cochlea et du canal semi-circulaire anterieur chez les foetus. *J Franc Oto-Rhino-Laryng*, 14: 727-735.
- Bregman, A., 1990. *Auditory scene analysis: the perceptual organization of sound*. MIT Press, Cambridge.
- Bruckmann, G., and Burda, H., 1997. Hearing in blind subterranean Zambian mole-rats (*Cryptomys* sp.): collective behavioural audiogram in a highly social rodent. *J Comp Physiol A*, 181: 83-88.
- Bruns, V., Burda, H., and Ryan, M.J., 1989. Ear morphology of the frog-eating bat (*Trachops cirrhosus*, Family: Phyllostomidae): apparent specializations for low-frequency hearing. *J Morphol*, 199: 103-118.
- Burda, H., Bruns, V., and Hickman, G.C., 1992. The ear in subterranean Insectivora and Rodentia in comparison with ground-dwelling representatives. I. Sound conducting system of the middle ear. *J Morphol*, 214: 49-61.

- Burda, H., Bruns, V., and Nevo, E., 1989. Middle ear and cochlear receptors in the subterranean mole-rat, *Spalax ehrenbergi*. *Hearing Res*, 39: 225-230.
- Cassini, M.H., 1991. Foraging under predation risk in the wild guinea pig *Cavia aperea*. *Oikos*, 62: 20-24.
- Cassini, M.H., and Galante, M.L., 1992. Foraging under predation risk in the wild guinea pig: the effect of vegetation height on habitat utilization. *Ann Zool Fennici*, 29: 285-290.
- Castele, E.V.D., 2004. *Model-based approach for beam hardening correction and resolution measurements in microtomography*. PhD thesis, University of Antwerp, Belgium.
- Chapla, M.E., Nowacek, D.P., Rommel, S.A., and Sadler, V.M., 2007. CT scans and 3D reconstructions of Florida manatee (*Trichechus manatus latirostris*) heads and ear bones. *Hearing Res*, 228: 123-135.
- Chen, C.S., and Anderson, L.M., 1985. The inner ear structures of the echina—an SEM study. *Experientia*, 41: 1324-1326.
- Cheverud, J.M., 2007. The relationship between development and evolution through heritable variation. *Tinkering: the macroevolution of development: novartis foundation symposium*, 284: 55-70.
- Christensen-Dalsgaard, K., and Carr, C.E., 2008. Evolution of sensory novelty: tympanic ears and the associated neural processing. *Brain Res Bull*, 75: 365-370.
- Cohen, Y.E., Bacon, C.K., and Saunders, J.C., 1992. Middle ear development III: morphometric changes in the conducting apparatus of the Mongolian gerbil. *Hearing Res*, 62: 187-193.

- Coleman, M.N., and Colbert, M.W., 2010. Correlations between auditory structures and hearing sensitivity in non-human primates. *J Morphol*, 271: 511-532.
- Coles, R.B., Gower, D.M., Boyd, P.J., and Lewis, D.B., 1982. Acoustic transmission through the head of the common mole, *Talpa europaea*. *J Exp Biol*, 101: 337-341.
- Conejero, J., 2011. Interpolation algorithms in PixInsight. Available: <http://pixinsight.com/doc/docs/InterpolationAlgorithms/InterpolationAlgorithms.html>. Last accessed 7th October 2013.
- Cucchi, T., Hulme-Beaman, A., Yuan, J., and Dobney, K., 2011. Early Neolithic pig domestication at Jiahu, Henan province, China: clues from molar shape analyses using geometric morphometric approaches. *J Archaeol Sci*, 38: 11-22.
- Dallos, P., 1973. *The auditory periphery*. Academic Press, New York.
- Deza, M.M., and Deza, E., 2009. *Encyclopedia of distances*. Springer-Verlag, Berlin.
- Dryden, I.L., and Mardia, K.V., 1998. *Statistical shape analysis*. John Wiley & Sons, New York.
- Eby, T.L., and Nadol, J.B. Jr., 1986. Postnatal growth of the human temporal bone. Implications for cochlear implants in children. *Ann Otol Rhinol Laryngol*, 95: 356-364.
- Echteler, S.M., Arjmand, E., and Dallos, P., 1989. Developmental alterations in the frequency map of the mammalian cochlea. *Nature*, 341: 147-149.
- Echteler, S.M., Fay, R.R., and Popper, A.N., 1994. Structure of the mammalian cochlea. In: Fay, R.R., Popper, A.N. (Eds.), *Comparative hearing: mammals*. Springer-Verlag, New York, p. 134-171.

- Ekdale, E.G., 2013. Comparative anatomy of the bony labyrinth (inner ear) of placental mammals. *PLoS ONE*, 8: e66624. doi:10.1371/journal.pone.0066624
- Elliott, J.C., and Dover, S.D., 1982. X-ray microtomography. *J Microsc*, 126: 211-213.
- Engelke, K., Graeff, W., Meiss, L., Hahn, M., and Delling, G., 1993. High spatial resolution imaging of bone mineral using computed microtomography. Comparison with microradiography and undecalcified histologic sections. *Invest Radiol*, 28: 341-349.
- Fay, R.R., and Popper, A.N., 2000. Evolution of hearing in vertebrates: the inner ears and processing. *Hearing Res*, 149: 1-10.
- Feddersen, W.E., Sandel, T.T., Teas, D.C., and Jeffress, L.A., 1957. Localization of high frequency tones. *J Acoust Soc Am*, 29: 988-991.
- Feldhamer, G.A., Drickamer, L.C., Vessey, S.H., and Merritt, J.F., 2004. *Mammalogy: adaptation, diversity and ecology*. 2nd ed. McGraw Hill, Singapore.
- Fernandez, C., and Schmidt, R.S., 1963. The opossum ear and evolution of the coiled cochlea. *J Comp Neurol*, 121: 151-159.
- Fettiplace, R., and Hackney, C.M., 2006. The sensory and motor roles of auditory hair cells. *Nat Rev Neurosci*, 7: 19-29.
- Finck, A., Schneck, C.D., and Hartman, A.F., 1972. Development of cochlear function in the neonate Mongolian gerbil (*Meriones unguiculatus*). *J Comp Physiol Psychol*, 78: 375-380.
- Finneran, J.J., and Jenkins, A.K., 2012. Criteria and thresholds for U.S. Navy acoustic and explosive effects analysis. SSC Pacific, USA.

- Fitzgerald, E.M.G., 2006. A bizarre new toothed mysticete (Cetacea) from Australia and the early evolution of baleen whales. *Proc R Soc B*, 273: 2955-2963.
- Fleischer, G., 1976. Hearing in extinct cetaceans as determined by cochlear structure. *J Paleontol*, 50: 133-152.
- Fleischer, G., 1978. Evolutionary principles of the mammalian middle ear. *Adv Anat Embryol Cell Biol*, 55: 1-70.
- Foth, C., Brusatte, S.L., and Butler, R.J., 2012. Do different disparity proxies converge on a common signal? Insights from the cranial morphometrics and evolutionary history of Pterosauria (Diapsida: Archosauria). *J Evol Biol*, 25: 904-915.
- Gans, C., 1992. An overview of the evolutionary biology of hearing. In: Webster, D.B., Fay, R.R., Popper, A.N. (Eds.), *The evolutionary biology of hearing*. Springer-Verlag, New York, p. 3-13.
- Gates, G.R., Saunders, J.C., and Bock, G.R., 1974. Peripheral auditory function in the platypus, *Ornithorhynchus anatinus*. *J Acoust Soc Am*, 56: 152-156.
- Gerstein, R.E., Gerstein, L., Forsythe, S.E., and Blue, J.E., 1999. The underwater audiogram of the West Indian manatee (*Trichechus manatus*). *J Acoust Soc Am*, 105: 3575-3583.
- Gould, E., 1983. Mechanisms of mammalian auditory communication. In: Eisenberg, J.F., Kleiman, D.G. (Eds.), *Advances in the study of mammalian behavior*. Spec. Pub. No. 7, American Society of Mammalogists, p. 265-342.
- Goycoolea, M.V., 2001. Clinical aspects of round window membrane permeability under normal and pathological conditions. *Acta Otolaryngol*, 121: 437-447.
- Goycoolea, M.V., and Lundman, L., 1997. Round window membrane. Structure function and permeability: a review. *Microsc Res Techniq*, 36: 201-211.

- Graham, D.T., and Cloke, P., 2003. *Principles of radiological physics*. 4th ed. Churchill Livingstone, Edinburgh.
- Gray, A.A., 1907. *The labyrinth of animals*. J & A Churchill, London.
- Gray, O., 1951. An introduction to the study of the comparative anatomy of the labyrinth. *J Laryngol Otol*, 65: 681-703.
- Gunz, P., Ramsier, M., Kuhrig, M., Hublin, J.J., and Spoor, F., 2012. The mammalian bony labyrinth reconsidered, introducing a comprehensive geometric morphometric approach. *J Anat*, 220: 529-543.
- Habersetzer, J., and Storch, G., 1992. Cochlea size in extant Chiroptera and middle Eocene microchiropterans from Messel. *Naturwissenschaften*, 79: 462-466.
- Hammer, Ø., Harper, D.A.T., and Ryan, P.D., 2001. PAST: paleontological statistics software package for education and data analysis. *Palaeontol Electron*, 4: 9pp.
- Hanke, W., and Dehnhardt, G., 2013. Sensory biology of aquatic mammals. *J Comp Physiol A*, 199: 417-420.
- Hardie, N.A., MacDonald, G., and Rubel, E.W., 2004. A new method for imaging and 3D reconstruction of mammalian cochlea by fluorescent confocal microscopy. *Brain Res*, 1000: 200-210.
- Hardy, M., 1938. The length of the organ of Corti in man. *Am J Anat*, 62: 393-397.
- Harris, D.M., and Dallos, P., 1984. Ontogenetic changes in frequency mapping of a mammalian ear. *Science*, 25: 741-743.
- Harris, D.M., Rotche, R., and Freedom, T., 1990. Postnatal growth of cochlea spiral in Mongolian gerbils. *Hearing Res*, 50: 1-6.

- Hashimoto, S., Kimura, R.S., and Takasaka, T., 1990. Computer-aided three-dimensional reconstruction of the inner hair cells and their nerve endings in the guinea pig cochlea. *Acta Otolaryngol*, 109: 228-234.
- Hauser, M., 1997. *Evolution of communication*. MIT Press, Cambridge.
- Hay, G.A., and Hughes, D., 1988. *First-year physics for radiographers*. 3rd ed. Bailliere Tindall, London.
- Heath, D.G., Soyer, P.A., Kuszyk, B.S., Bliss, D.F., Calhoun, P.S., Bluemke, D.A., Choti, M.A., and Fishman, E.K., 1995. Three-dimensional spiral CT during arterial portography: comparison of three rendering techniques. *Radiographics*, 15: 1001-1011.
- Heffner, R.S., 2004. Primate hearing from a mammalian perspective. *Anat Rec Part A*, 281A: 1111-1122.
- Heffner, R.S., and Heffner, H.E., 1980. Hearing in the elephant (*Elephas maximus*). *Science*, 208: 518-520.
- Heffner, R.S., and Heffner, H.E., 1993. Degenerate hearing and sound localization in naked mole rats (*Heterocephalus glaber*), with an overview of central auditory structures. *J Comp Neurol*, 331: 418-433.
- Heffner, R.S., Heffner, H.E., Contos, C., and Kearns, D., 1994. Hearing in prairie dogs: transition between surface and subterranean rodents. *Hearing Res*, 73: 185-189.
- Heffner, R.S., Koay, G., and Heffner, H.E., 2001. Audiograms of five species of rodents: implications for the evolution of hearing and the perception of pitch. *Hearing Res*, 157: 138-152.

- Heffner, R.S., Koay, G., and Heffner, H.E., 2006. Hearing in large (*Eidolon helvum*) and small (*Cynopterus brachyotis*) non-echolocating fruit bats. *Hearing Res*, 221: 17-25.
- Heffner, R.S., Koay, G., and Heffner, H.E., 2007. Sound localization acuity and its relation to vision in large and small fruit-eating bats: I. Echolocating species, *Phyllostomus hastatus* and *Carollia perspicillata*. *Hearing Res*, 234: 1-9.
- Hemila, S., Nummela, S., Berta, A., and Reuter, T., 2006. High-frequency hearing in phocid and otariid pinnipeds: an interpretation based on inertial and cochlear constraints. *J Acoust Soc Am*, 120: 3463-3466.
- Hemila, S., Nummela, S., and Reuter, T., 2001. Modeling whale audiograms: effects of bone mass on high-frequency hearing. *Hearing Res*, 151: 221-226.
- Henwood, S., 1999. *Clinical CT techniques and practice*. Greenwich Medical Media, London.
- Hepper, P.G., and Shahidullah, B.S., 1994. Development of fetal hearing. *Arch Dis Child*, 71: F81-F87.
- Hernandez, P.P., Moreno, V., Olivali, F.A., and Allende, M.L., 2006. Sub-lethal concentrations of waterborne copper are toxic to lateral line neuromasts in zebrafish (*Danio rerio*). *Hearing Res*, 213: 1-10.
- Horner, K.C., Serviere, J., and Granier-Deferre, C., 1987. Desoxyglucose demonstration of in-utero hearing in the guinea pig foetus. *Hearing Res*, 26: 327-335.
- Hsieh, J., 1995. Image artifacts, causes and correction. In: Goldman, L.W., Fowlkes, J.B. (Eds.), *Medical CT and ultrasound: current technology and applications*. Advanced Medical Publishing, Madison, p. 487-518.

- Hsieh, J., 2003. *Computed tomography: principles, design, artifacts, and recent advances*. SPIE Press, Bellingham.
- Huangfu, M., and Saunders, J.C., 1983. Auditory development in the mouse: structural maturation of the middle ear. *Journal of Morphology*, 176: 249-259.
- Hyrtl, J., 1845. *Vergleichend-anatomische Untersuchungen über den Menschen und der Säugethiere*. Friedrich Ehrlich, Prague.
- Hyson, R.L., and Rudy, J.W., 1987. Ontogenetic change in the analysis of sound frequency in the infant rat. *Dev Psychobiol*, 20: 189-207.
- Jeffery, N., and Spoor, F., 2004. Prenatal growth and development of the modern human labyrinth. *J Anat*, 204: 71-92.
- Jones, G., and Teeling, E.C., 2006. The evolution of echolocation in bats. *Trends Ecol Evol*, 21: 149-156.
- Junqueira, L.C., and Carneiro, J., 2005. *Basic histology: texts & atlas*. 11th ed. McGraw Hill, Lange.
- Kalender, W.A., 2005. *Computed tomography: fundamentals, system technology, image quality, applications*. 2nd ed. Publicis Corporate Publishing, Erlangen.
- Kalko, E.K.V., 1995. Echolocation signal design, foraging habitats and guild structure in six Neotropical sheath-tailed bats (Emballonuridae). *Symposium of the Zoological Society of London*, 67: 259-273.
- Kardong, K.V., 2006. *Vertebrates: comparative anatomy, function, evolution*. McGraw-Hill, Michigan.
- Kastak, D., and Schusterman, R.J., 1998. Low-frequency amphibious hearing in pinnipeds: methods, measurements, noise, and ecology. *J Acoust Soc Am*, 103: 2216-2228.

- Kastak, D., and Schusterman, R.J., 1999. In-air and underwater hearing sensitivity of a northern elephant seal (*Mirounga angustirostris*). *Can J Zool*, 77: 1751-1758.
- Keithley, E.M., Ryan, A.F., and Woolf, N.K., 1989. Spiral ganglion cell density in young and old gerbils. *Hearing Res*, 38: 125-133.
- Keithley, E.M., Ryan, A.F., and Feldman, M.L., 1991. Cochlear degeneration in aged rats of four strains. *Hearing Res*, 59: 171-178.
- Kendall, D., 1977. The diffusion of shape. *Adv Appl Probab*, 9: 428-430.
- Ketcham, R.A., and Carlson, W.D., 2001. Acquisition, optimization and interpretation of X-ray computed tomographic imagery: applications to the geosciences. *Comput Geosci*, 27: 381-400.
- Ketten, D., 1984. *Correlations of morphology with frequency for odontocete cochlea: systematics and topology*. PhD thesis, The Johns Hopkins University, Baltimore.
- Ketten, D.R., 1994. Functional analyses of whale ears: adaptations for underwater hearing. *Proceedings in Underwater Acoustics*, 1: 264-270.
- Ketten, D.R., 1997. Structure and function in whale ears. *Bioacoustics*, 8: 103-135.
- Ketten, D.R., Odell, D.K., and Domning, D.P., 1992. Structure, function, and adaptation of the manatee ear. In: Thomas, J., Kastelein, R., Supin, A.Y. (Eds.), *Marine mammal sensory systems*. Plenum Press, New York, p. 77-95.
- Kimchi, T., Reshef, M., and Terkel, J., 2005. Evidence for the use of reflected self-generated seismic waves for spatial orientation in a blind subterranean mammal. *J Exp Biol*, 208: 647-659.
- Kirk, E.C., and Gosselin-Ildari, A.D., 2009. Cochlear labyrinth volume and hearing abilities in primates. *Anat Rec*, 292: 765-776.

- Klingenberg, C.P., 2011. MorphoJ: an integrated software package for geometric morphometrics. *Mol Ecol Resour*, 11: 353-357.
- Klingenberg, C.P., Duttke, S., Whelan, S., and Kim, M., 2012. Developmental plasticity, morphological variation and evolvability: a multilevel analysis of morphometric integration in the shape of compound leaves. *J Evol Biol*, 25: 115-129.
- Klingenberg, C.P., and Gidaszewski, N.A., 2010. Testing and quantifying phylogenetic signals and homoplasy in morphometric data. *Syst Biol*, 59: 245-261.
- Kotler, B.P., 1984. Risk of predation and the structure of desert rodent communities. *Ecology*, 65: 689-701.
- Kuhn, J.L., Goldstein, S.A., Feldkamp, L.A., Goulet, R.W., and Jesion, G., 1990. Evaluation of a microcomputed tomography system to study trabecular bone structure. *J Orthopaed Res*, 8: 833-842.
- Laboratory of Comparative Hearing, 2013. *Behavioral Audiograms of Mammals*. Available: http://laboratoryofcomparativehearing.com/Page_2.html. Last accessed 17th May 2013.
- Ladeveze, S., de Muizon, C., Colbert, M., and Smith, T., 2010. 3D computational imaging of the petrosal of a new multituberculate mammal from the Late Cretaceous of China and its paleobiologic inferences. *Comptes Rendus Palevol*, 9: 319-330.
- Ladhams, A., and Pickles, J.O., 1996. Morphology of the monotreme organ of Corti and macula lagena. *J Comp Neurol*, 366: 335-347.
- Lalwani, A.K., 2007. *Current diagnosis & treatment in Otolaryngology: head and neck surgery*. 2nd ed. McGraw-Hill Medical, New York.

- Lange, S., Burda, H., Wegner, R.E., Dammann, P., Begall, S., and Kawalika, M., 2007. Living in a “stethoscope”: burrow-acoustics promote auditory specializations in subterranean rodents. *Naturwissenschaften*, 94: 134-138.
- Lange, S., Stalleicken, J., and Burda, H., 2004. Functional morphology of the ear in fossorial rodents, *Microtus arvalis* and *Arvicola terrestris*. *J Morphol*, 262: 770-779.
- Lay, D.M., 1972. The anatomy, physiology, functional significance and evolution of specialized hearing organs of gerbilline rodents. *J Morphol*, 138: 41-120.
- Lehtonen, T.K., and Lindstrom, K., 2008. Repeatability of mating preferences in the sand goby. *Anim Behav*, 75: 55-61.
- Lenoir, M., Puel, J., and Pujol, R., 1987. Stereocilia and tectorial membrane development in the rat cochlea. *Anat Embryol*, 175: 477-487.
- Lenoir, M., Shnerson, A., and Pujol, R., 1980. Cochlear receptor development in the rat with emphasis on synaptogenesis. *Anat Embryol*, 160: 253-262.
- Liem, K.F., Bemis, W.E., Walker, W.F., and Grande, L., 2001. *Functional anatomy of the vertebrates: an evolutionary perspective*. 3rd ed. Thomson Learning, Belmont.
- Lloyd, S.K.W., Kasbekar, A.V., Kenway, B., Prevost, T., Hockman, M., Beale, T., and Graham, J., 2010. Developmental changes in cochlear orientation—Implications for cochlear implantation. *Otol Neurotol*, 31: 902-907.
- Luo, Z.X., Ji, Q., Wible, J.R., and Yuan, C.X., 2003. An Early Cretaceous tribosphenic mammal and metatherian evolution. *Science*, 302: 1934-1939.
- Luo, Z.X., Ruf, I., Schultz, J.A., and Martin, T., 2011. Fossil evidence on evolution of inner ear cochlea in Jurassic mammals. *Proc R Soc B*, 278: 28-34.

- Maddison, W.P., 1991. Squared-change parsimony reconstructions of ancestral states for continuous-valued characters on a phylogenetic tree. *Syst Zool*, 40: 304-314.
- Manley, G.A., 1972. A review of some current concepts of the functional evolution of the ear in terrestrial vertebrates. *Evolution*, 26: 608-621.
- Manley, G.A., 2000. Cochlear mechanisms from a phylogenetic viewpoint. *P Natl Acad Sci*, 97: 11736-11743.
- Manley, G.A., 2010. An evolutionary perspective on middle ears. *Hearing Res*, 263: 3-8.
- Manley, G.A., 2012. Evolutionary paths to mammalian cochleae. *J Assoc Res Otolaryngol*, 13: 733-743.
- Manley, G.A., Brix, J., and Kaiser, A., 1987. Developmental stability of the tonotopic organization of the chick's basilar papilla. *Science*, 237: 655-656.
- Manoussaki, D., Chadwick, R.S., Ketten, D.R., Arruda, J., Dimitriadis, E.K., and O'Malley, J.T., 2008. The influence of cochlear shape on low-frequency hearing. *P Natl Acad Sci*, 105: 6162-6166.
- Mason, M.J., 2001. Middle ear structures in fossorial mammals: a comparison with non-fossorial species. *J Zool*, 255: 467-486.
- Mason, M.J., 2003. Morphology of the middle ear of golden moles (Chrysochloridae). *J Zool*, 260: 391-403.
- Mason, M.J., 2004. The middle ear apparatus of the tuco-tuco *Ctenomys sociabilis* (Rodentia, Ctenomyidae). *J Mammal*, 85: 797-805.
- Mason, M.J., 2006. Evolution of the middle ear apparatus in Talpid moles. *J Morphol*, 267: 678-695.

- Masterton, B., Heffner, H., and Ravizza, R., 1969. The evolution of human hearing. *J Acoust Soc Am*, 45: 966-985.
- McCormick, C.A., 1999. Anatomy of the central auditory pathways of fishes and amphibians. In: Fay, R.R., Popper, A.N. (Eds.), *Comparative hearing: fish and amphibians*. Springer-Verlag, New York, p. 155-215.
- Meijering, E.H.W., Niessen, W.J., and Viergever, M.A., 2001. Quantitative evaluation of convolution-based methods for medical image interpolation. *Med Image Anal*, 5: 111-126.
- Meng, J., 1992. The stapes of *Lambdopsalis bulla* (Multituberculata) and transformational analyses on some stapedial features in Mammaliaformes. *J Vert Paleontol*, 12: 459-471.
- Meng, J., and Fox, R.C., 1995. Therian petrosals from the Oldman and Milk River Formations (Late Cretaceous), Alberta, Canada. *J Vert Paleontol*, 15: 122-130.
- Meng, J., and Fox, R.C., 1995. Osseous inner-ear structures and hearing in early marsupials and placentals. *Zoo J Linn Soc*, 115: 47-71.
- Moggi-Cecchi, J., and Collard, M., 2002. A fossil stapes from Sterkfontein, South Africa, and the hearing capabilities of early hominids. *J Hum Evol*, 42: 259-265.
- Møhl, B., 1968. Hearing in seals. In: Harrison, R., Hubbard, R., Rice, C., Schusterman, R.J. (Eds.), *The behavior and physiology of pinnipeds*. Appleton—Century, New York, p. 172-195.
- Møhl, B., and Ronald, K., 1975. The peripheral auditory system of the harp seal, *Pagophilus groenlandicus*, (Erxleben, 1777). *Rapp P -v Reun Cons Int Explor Mer*, 169, 516-523.

- Moore, J.K., and Linthicum, F.H., 2007. The human auditory system: a timeline of development. *Int J Audiol*, 46: 460-478.
- Mu, M.Y., Chardin, S., Avan, P., and Romand, R., 1997. Ontogenesis of rat cochlea. A quantitative study of the organ of Corti. *Dev Brain Res*, 99: 29-37.
- Muller, M., 1991. Developmental changes of frequency representation in the rat cochlea. *Hearing Res*, 56: 1-7.
- Muller, M., 1996. The cochlear place-frequency map of the adult and developing Mongolian gerbil. *Hearing Res*, 94: 148-156.
- Nedwell, J., Edwards, B., Turnpenny, A.W.H., and Gordon, J., 2004. *Fish and marine mammal audiograms: a summary of available information*. Subacoustech, Hampshire.
- Nemzek, W.R., Brodie, H.A., Chong, B.W., Babcock, C.J., Hecht, S.T., Salamat, S., Ellis, W.G., and Seibert, J.A., 1996. Imaging findings of the developing temporal bone in fetal specimens. *Am J Neuroradiol*, 17: 1467-1477.
- Nevo, E., Heth, G., and Pratt, H., 1991. Seismic communication in a blind subterranean mammal: a major somatosensory mechanism in adaptive evolution underground. *Proc Natl Acad Sci*, 88: 1256-1260.
- Niemitz, C., 1984. Vocal communication of two tarsier species (*Tarsius bancanus* and *Tarsius spectrum*). In: Niemitz, C. (Eds.), *Biology of tarsiers*. G F Verlag, Stuttgart, p. 129-141.
- Nowak, R.M., 1999. *Walker's mammals of the world*. 6th ed. The Johns Hopkins University Press, Baltimore.
- Nummela, S., 1995. Scaling of the mammalian middle ear. *Hearing Res*, 85: 18-30.
- Nummela, S., Thewissen, J.G.M., Bajpai, S., Hussain, T., and Kumar, K., 2004. Eocene evolution of whale hearing. *Nature*, 430: 776-778.

- Nummela, S., Thewissen, J.G.M., Bajpai, S., Hussain, T., and Kumar, K., 2007. Sound transmission in archaic and modern whales: anatomical adaptations for underwater hearing. *Anat Rec*, 290: 716-733.
- O'Higgins, P., 2000. The study of morphological variation in the hominid fossil record: biology, landmarks and geometry. *J Anat*, 197: 103-120.
- O'Rahilly, R., 1983. The timing and sequence of events in the development of the human eye and ear during the embryonic period proper. *Anat Embryol*, 168: 87-99.
- Packer, D.J., 1987. The influence of carotid arterial sounds on hearing sensitivity in mammals. *J Zool*, 211: 547-560.
- Pansky, B., 1982. *Review of medical embryology*. Macmillan, New York.
- Parsons, K.J., Robinson, B.W., and Hrbek, T., 2003. Getting into shape: an empirical comparison of traditional truss-based morphometric methods with a newer geometric method applied to New World cichlids. *Environ Biol Fish*, 67: 417-431.
- Phillips, M.J, Bennett, T.H, and Lee, M.S., 2009. Molecules, morphology, and ecology indicate a recent, amphibious ancestry for echidnas. *P Natl Acad Sci*, 106: 17089–17094.
- Popper, A.N., and Higgs, D.M., 2009. Fish: hearing, lateral lines (mechanisms, role in behavior, adaptations to life underwater). In: Steele, J.H., Thorpe, S.A., Turekian, K.K. (Eds.), *Marine biology*. Elsevier, London, p. 3754-3761.
- Pujol, R., and Marty, R., 1970. Postnatal maturation in the cochlea of the cat. *J Comp Neurol*, 139: 115-126.
- Pujol, R., Carlier, E., and Devigne, C., 1978. Different patterns of cochlear innervation during the development of kitten. *J Comp Neurol*, 177: 529-536.

- Purcell, D., Johnson, J., Fischbein, N., and Lalwani, A.K., 2003. Establishment of normative cochlear and vestibular measurements to aid in the diagnosis of inner ear malformations. *Otolaryngol Head Neck Surg*, 128: 78-87.
- Puria, S., and Steele, C., 2010. Tympanic-membrane and malleus-incus-complex co-adaptations for high-frequency hearing in mammals. *Hearing Res*, 263: 183-190.
- Ramsier, M.A., Cunningham, A.J., Moritz, G.L., Finneran, J.J., Williams, C.V., Ong, P.S., Gursky-Doyen, S.L., and Dominy, N.J., 2012. Primate communication in the pure ultrasound. *Biol Lett*, 8: 508-511.
- Randall, D., Burggren, W., and French, K., 2002. *Eckert animal physiology: mechanisms and adaptations*. 5th ed. W.H. Freeman, New York.
- Rasband, W.S., 2012. *ImageJ*. Available: <http://imagej.nih.gov/ij/>. Last accessed 6th September 2013.
- Rau, T.S., Würfel, W., Lenarz, T., and Majdani, O., 2013. Three-dimensional histological specimen preparation for accurate imaging and spatial reconstruction of the middle and inner ear. *Int J CARS*, 8: 481-509.
- Reep, R.L., Gaspard III, J.C., Sarko, D., Rice, F.L., Mann, D.A., and Bauer, G.B., 2011. Manatee vibrissae: evidence for a “lateral line” function. *Ann N Y Acad Sci*, 1225: 101-109.
- Reimer, K., 1996. Ontogeny of hearing in the marsupial, *Monodelphis domestica*, as revealed by brainstem auditory evoked potentials. *Hearing Res*, 92: 143-150.
- Relkin, E.M., 1988. Introduction to the analysis of middle-ear function. In: Jahn, A.F., Santos-Sacchi, J. (Eds.), *Physiology of the ear*. Raven Press, New York, p. 103-123.

- Relkin, E.M., and Saunders, J.C., 1980. Displacement of the malleus in neonatal golden hamsters. *Acta Oto-Laryngologica*, 90: 6-15.
- Repenning, C.A., 1972. Underwater hearing in seals: functional morphology. In: Harisson, R.J. (Ed.), *Functional anatomy of marine mammals Vol. 1*. Academic Press, London, p. 307-331.
- Rich, T.H., Hopson, J.A., Musser, A.M., Flannery, T.F., and Vickers-Rich, P., 2005. Independent origins of middle ear bones in monotremes and therians. *Science*, 307: 910-914.
- Richard, C., Laroche, N., Malaval, L., Dumollard, J.M., Martin, Ch., Peoch, M., Vico, L., and Prades, J.M., 2010. New insight into the bony labyrinth: a microcomputed tomography study. *Auris Nasus Larynx*, 37: 155-161.
- Richtsmeier, J.T., Deleon, V.B., and Lele, S.R., 2002. The promise of geometric morphometrics. *Yearb Phys Anthropol*, 45: 63-91.
- Rohlf, F.J., 1998. On applications of geometric morphometrics to studies of ontogeny and phylogeny. *Syst Biol*, 47: 147-158.
- Rohlf, F.J., 1999. Shape statistics: Procrustes superimposition and tangent spaces. *J Classif*, 16: 197-223.
- Rohlf, F.J., and Marcus, L.F., 1993. A revolution in morphometrics. *Trends Ecol Evol*, 8: 129-132.
- Romand, R., 1983. Development of the cochlea. In: Romand, R. (Ed.), *Developmental of auditory and vestibular systems*. Academic Press, New York, p. 47-88.
- Rosowski, J.J., 1994. Outer and middle ears. In: Fay, R.R., Popper, A.N. (Eds.), *Comparative hearing: mammals*. Springer-Verlag, New York, p. 172-247.

- Rosowski, J.J., and Graybeal, A., 1991. What did Morganucodon hear? *Zool J Linn Soc*, 101: 131-168.
- Rubel, E.W., 1978. Ontogeny of structure and function in the vertebrate auditory system. In: Jacobson, M. (Eds.), *Handbook of sensory physiology, Vol IX*. Springer-Verlag, New York, p. 135-237.
- Rubel, E.W., and Ryals, B.M., 1983. Development of the place principle: Acoustic trauma. *Science*, 219: 512-514.
- Rubsamen, R., 1992. Postnatal development of central auditory frequency maps. *J Comp Physiol A*, 170: 129-143.
- Ryan, A.F., and Woolf, N.K., 1988. Development of tonotopic representation in the Mongolian gerbil: A 2-deoxyglucose study. *Dev Brain Res*, 41: 61-70.
- Sanchez-Villagra, M.R., and Schmelzle, T., 2007. Anatomy and development of the bony inner ear in the woolly opossum, *Caluromys philander* (Didelphimorphia, Marsupialia). *Mastozoologia Neotropical*, 14(1): 53-60.
- Sanes, D.H., Mernickel, M., and Rubel, E.W., 1989. Evidence for an alteration of the tonotopic map in the cochlea during development. *J Comp Neurol*, 279: 436-444.
- Sato, H., Sando, I., and Takahashi, H., 1991. Sexual dimorphism and development of the human cochlea. *Acta Otolaryngol*, 111: 1037-1040.
- Sato, M., Henson, M.M., Henson Jr., O.W., and Smith, D.W., 1999. The innervation of outer hair cells: 3D reconstruction from TEM serial sections in the Japanese macaque. *Hearing Res*, 135: 29-38.
- Scarpa, A., 1962. Anatomical observations on the round window. *Arch Otolaryngol*, 75: 16-59.

- Schleich, C.E., and Busch, C., 2004. Functional morphology of the middle ear of *Ctenomys talarum* (Rodentia: Octodontidae). *J Mammal*, 85: 290-295.
- Schleich, C.E., and Vassallo, A.I., 2003. Bullar volume in subterranean and surface-dwelling caviomorph rodents. *J Mammal*, 84: 185-189.
- Schusterman, R.J., 1981. Behavioral of seals and sea lions: a review of their hearing, visual, learning and diving skills. *Psychol Rec*, 31: 125-143.
- Schusterman, R.J., Kastak, D., Levenson, D.H., Reichmuth, C.J., and Southall, B.L., 2000. Why pinnipeds don't echolocate. *J Acoust Soc Am*, 107: 2256-2264.
- Scottish Sensory Centre, 2010. *Auditory localisation*. Available: www.ssc.education.ed.ac.uk/courses/deaf/dnov10i.html. Last accessed 19th June 2013.
- Seeram, E., 2001, *Computed tomography: physical principles, clinical applications, and quality control*. 2nd ed. Saunders, Missouri.
- Seeram, E., 2009, *Computed tomography: physical principles, clinical applications, and quality control*. 3rd ed. Saunders, Missouri.
- Sercer, A., 1958. L'étiopathogénie de l'otospongiose et les facteurs anthropologiques. *Arch Ital Otol Rinol Laryngol*, 69: 1-92.
- Shen, Z., Nacev, A., Sarwar, A., Lee, R., Depireux, D., and Shapiro, B., 2013. Automated fluorescence and reflectance coregistered 3-D tissue imaging system. *IEEE Transactions on Magnetics*, 49: 279-284.
- Sherwood, L., Klandorf, H., and Yancey, P.H., 2005. *Animal physiology: from genes to organisms*. Thomson Learning, Belmont.
- Shibata, T., and Nagano, T., 1996. Applying very high resolution microfocus X-ray CT and 3-D reconstruction to the human auditory apparatus. *Nat Med*, 2: 933-935.

- Silva, M., and Downing, J.A., 1995. *Handbook of mammalian body masses*. CRC Press, Boca Raton, Florida.
- Slice, D.E., 2001. Landmark coordinates aligned by Procrustes analysis do not lie in Kendall's shape space. *Syst Biol*, 50: 141-149.
- Slice, D.E., 2007. Geometric morphometrics. *Annu Rev Anthropol*, 36: 261-81.
- Smith, S.W., 1997. *The scientist and engineer's guide to digital signal processing*. California Technical Publishing, California.
- Solntseva, G.N., 2010. Morphology of the inner ear of mammals in ontogeny. *Russ J Dev Biol*, 41: 94-110.
- Spoor, C.F., 1993. *The comparative morphology and phylogeny of the human bony labyrinth*. PhD thesis, Utrecht University.
- Spoor, F., Bajpai, S., Hussain, S.T., Kumar, K., and Thewissen, J.G.M., 2002. Vestibular evidence for the evolution of aquatic behaviour in early cetaceans. *Nature*, 417: 163-166.
- Spoor, F., Jeffery, N., and Zonneveld, F., 2000. Imaging skeletal growth and evolution. In: Higgins, P.O., Cohen, M. (Eds.), *Development, Growth and Evolution*. The Linnean Society of London, p. 123-161.
- Spoor, F., and Zonneveld, F., 1995. Morphometry of the primate bony labyrinth: a new method based on high-resolution computed tomography. *J Anat*, 186: 271-286.
- Stebbins, W.C., and Sommers, M.S., 1992. Evolution, perception, and the comparative method. In: Webster, D.B., Fay, R.R., Popper, A.N. (Eds.), *The evolutionary biology of hearing*. Springer-Verlag, New York, p. 211-228.
- Steel, K.P., and Barkway, C., 1989. Another role for melanocytes: their importance for normal stria vascularis development in the mammalian inner ear. *Development*, 107: 453-463.

- Steeman, M.E., 2009. A new baleen whale from the Late Miocene of Denmark and early mysticete hearing. *Palaeontology*, 52: 1169-1190.
- Stevenson, D.M., Yin, L., and Stewart, M.A., 2010. X-ray tomography verification for determining phase proportions in volcanic rocks. *Proc. SPIE 7804*, Developments in X-ray tomography VII, 780416 (September 20, 2010); doi:10.1117/12.862109
- Su, W., Marion, M.S., Hinojosa, R., and Matz, G.J., 1982. Anatomical measurements of the cochlear aqueduct, round window membrane, round window niche, and facial recess. *Laryngoscope*, 92: 483-486.
- Takahashi, H., 2005. *Mammalian Crania Photographic Archive*. Available: http://1kai.dokkyomed.ac.jp/mammal/en/index_sci.html. Last accessed 3rd May 2013.
- Takahashi, H., Takagi, A., and Sando, I., 1989. Computer-aided three-dimensional reconstruction and measurement of the round window and its membrane. *Otolaryngol Head Neck Surg*, 101: 517-521.
- Tarnowski, B.I., Schmiedt, R.A., Hellstrom, L.I., Lee, F.S., and Adams, J.C., 1991. Aged-related changes in cochleas of Mongolian gerbils. *Hearing Res*, 54: 123-134.
- Teeling, E.C., 2009. Hear, hear: the convergent evolution of echolocation in bats?. *Trends Ecol Evol*, 24: 351-354.
- Thompson, J.L., and Illerhaus, B., 1998. A new reconstruction of the Le Moustier 1 skull and investigation of internal structures using 3-D- μ CT data. *J Hum Evol*, 35: 647-665.
- Toth, M., Alpar, A., and Patonay, L., and Olah, I., 2006. Development and surgical anatomy of the round window niche. *Ann Anat*, 188: 93-101.

- Turkewitsch, B.G., 1930. Alters- und geschlechtseigenschaften de anatomischen baues des menschlichen knochernen labyrinthes. *Anat Anz*, 70: 225-234.
- Uhen, M.D., 1998. Middle to Late Eocene basilosaurines and dorudontines. In: Thewissen, J.G.M. (Eds.), *The emergence of whales: evolutionary patterns in the origin of cetacea*. Kluwer Academic/Plenum, New York, p. 29-61.
- Uhen, M.D., 2007. Evolution of marine mammals: back to the sea after 300 million years. *Anat Rec*, 290: 514-522.
- van Bergeijk, W.A., 1967. The evolution of vertebrate hearing. In: Neff, W.D. (Ed.), *Contributions to sensory physiology*. Academic Press, New York, p. 1-49.
- Vater, M., and Kossl, M., 2010. Comparative aspects of cochlear functional organization in mammals. *Hearing Res*, 273: 89-99.
- Viscosi, V., and Cardini, A., 2011. Leaf morphology, taxonomy and geometric morphometrics: a simplified protocol for beginners. *PLoS ONE*, 6: e25630. doi:10.1371/journal.pone.0025630
- Walsh, S.A., Barrett, P.M., Milner, A.C., and Manley, G., 2009. Inner ear anatomy is a proxy for deducing auditory capability and behaviour in reptiles and birds. *Proc R Soc B*, 276: 1355-1360.
- Wartzok, D., and Ketten, D.R., 1999. Marine mammal sensory systems. In: Reynolds, J., Rommel, S. (Eds.), *Biology of marine mammals*. Smithsonian Institution Press, p. 117-175.
- Watt, H.J., 1917. The typical form of the cochlea and its variations. *Proc R Soc Lond B*, 89: 410-421.
- Weaver, S.P., and Schweitzer, L., 1994. Development of gerbil outer hair cells after the onset of cochlear function: An ultrastructural study. *Hearing Res*, 72: 44-52.

- Webster, D.B., and Webster, M., 1971. Adaptive value of hearing and vision in kangaroo rat predator avoidance. *Brain Behav Evol*, 4: 310-322.
- Webster, D.B., and Webster, M., 1972. Kangaroo rat auditory thresholds before and after middle ear reduction. *Brain Behav Evol*, 5: 41-53.
- West, C.D., 1985. The relationship of the spiral turns of the cochlea and the length of the basilar membrane to the range of audible frequencies in ground dwelling mammals. *J Acoust Soc Am*, 77: 1091-1101.
- Wever, E.G., 1974. The evolution of vertebrate hearing. In: Keidel, W.D., Neff, W.D. (Eds.), *Handbook of sensory physiology, vol. V-1: auditory system, anatomy, physiology (ear)*. Springer-Verlag, New York, p. 423-454.
- Wilbrand, H., and Rauschnig, W., 1986. Investigation of temporal bone anatomy by plastic moulding and cryomicrotomy. *Acta Radiol Diagn*, 27: 389-394.
- Wilkins, K.T., Roberts, J.C., and Roorda, C.S., and Hawkins, J.E., 1999. Morphometrics and functional morphology of middle ears of extant pocket gophers (Rodentia: Geomyidae). *J Mammal*, 80: 180-198.
- Winter, P., Handley, P., Ploog, D., and Schott, D., 1973. Ontogeny of squirrel monkey calls under normal conditions and under acoustic isolation. *Behaviour*, 47: 230-239.
- Woolf, N.K., and Ryan, A.F., 1988. Contributions of the middle ear to the development of function in the cochlea. *Hearing Res*, 35: 131-142.
- Wysocki, J., 2005. Topographical anatomy of the guinea pig temporal bone. *Hearing Res*, 199: 103-110.
- Xu, Z., Jing, W., Keping, S., Tinglei, J., Yunlei, J., and Jiang, F., 2008. Echolocation calls of *Rhinolophus ferrumequinum* in relation to habitat type and environmental factors. *Acta Ecologica Sinica*, 28: 5248-5258.

- Zatz, L.M., 1981. Basic principles of computed tomography scanning. In: Newton, T.H., Potts, D.G. (Eds.), *Technical aspects of computed tomography*. Mosby, St. Louis, p. 3853-3876.
- Zehnder, A.F., Kristiansen, A.G., Adams, J.C., Kujawa, S.G., Merchant, S.N., and McKenna, M.J., 2006. Osteoprotegrin knockout mice demonstrate abnormal remodeling of the otic capsule and progressive hearing loss. *Laryngoscope*, 116: 201-206.
- Zeifer, B., Sabini, P., and Sonne, J., 2000. Congenital absence of the oval window: radiologic diagnosis and associated anomalies. *Am J Neuroradiol*, 21: 322-327.
- Zelditch, M.L., Swiderski, D.L., Sheets, H.D., and Fink, W.L., 2004. *Geometric morphometrics for biologists: a primer*. Elsevier Academic Press, San Diego.

Appendix A

Procedures in Amira software (v. 5.2.2)

Step-by-step procedures in Amira are summarised below:

A.1 Plane standardization

1. The original inverted TIFF file of an image stack (the source field) was connected to the *ObliqueSlice* module.
2. The *Orientation* and *Translate* ports in the *ObliqueSlice* module were used to adjust position of a slice to find the lateral semicircular canal.
3. The *fit to points* toggle was enabled to click three times at different points on the lateral canal. Now the slice was automatically reset to be parallel to the lateral canal.
4. The *ApplyTransform* module was attached to the source field.
5. That slice of the *ObliqueSlice* module reset from the *fit to points* was connected to the *Reference* connection of the *ApplyTransform* module.
6. The *Lanczos* interpolation was chosen because it is the most accurate interpolation (Conejero, 2011).
7. The *extended* mode was selected to have a new field's size containing the entire source field.
8. The *Apply* button was pressed.
9. A new field with its sampling planes parallel to the lateral canal was created and saved.

A.2 Reconstruction of 3D images

1. The new field after standardization and a *LabelField* object were loaded into the Segmentation Editor.
2. In *Zoom and Data Window* panel, size, contrast and brightness of the image were adjusted for viewing.
3. Segmentation tools (Brush, Magic Wand, Threshold and Blowtool) were manipulated to select areas (voxels) of the inner ear in each current slice. All selected areas were drawn in transparent red colour.
4. The current voxel selection could be modified by the *masking* tool and many filters (growing, shrinking, smoothing and interpolating filters) under the *Selection* menu bar.
5. Selected voxels were assigned to the material of interest (the inner ear) using the '+' button.
6. Polygonal surfaces of the inner ear were reconstructed using the *SurfaceGen* module.
7. The surfaces were smoothed using the *SmoothSurface* module.

A.3 Landmark methods

1. The original source field was connected to the *ObliqueSlice* module.
2. Orientation of an image slice was adjusted to find a plane passing through the mid-modiolar axis.
3. The 3D Length tool in the *Measurement* module was used to draw an axial line on the slice passing the mid-modiolar axis.
4. *LandmarkSet* object from the menu was opened to create two landmarks on the axial line.

5. A special blue module, *ReAlignObliqueSliceByLandmarks.scro*, was loaded.
6. The blue module was connected to the *Data* connection of the *LandmarkSet* object, and also connected to the *ObliqueSlice* connection of the *ObliqueSlice* module. From this step forward, the two landmarks on the axial line functioned as the rotation axis (0-360°) around the mid-modiolar plane.
7. A new *LandmarkSet* object was opened.
8. Once each slice was rotated 22.5 degrees, a single landmark was put at the centre of the cochlear cavity. Landmarks were orderly put from the basal turn to the apex.
9. To quantify shape with geometric morphometrics, another new *LandmarkSet* object was opened to create semi-landmarks. Twenty-five equidistant semi-landmarks were required in this study.
10. At this step, all modules and networks were saved and closed.
11. Coordinates of all 25 semi-landmarks were calculated using my own mathematical formulae created in Microsoft Office Excel 2007.
12. These semi-landmark coordinates were copied into the *LandmarkAscii* file (notepad) of the *LandmarkSet* object in 9).
13. Amira networks were opened again and 25 semi-landmarks should be apparent in the *LandmarkSet* object.

A.4 Measurement of cochlear height

1. The landmark at the inferior edge of the round window and the last landmark at the apex were used to calculate cochlear height.

2. The angle of the rotation axis was adjusted in the *ReAlignObliqueSliceBy-Landmarks.scro* module in order to place the slice through the landmark at the round window.
3. The 3D Angle tool was used to draw a line from the landmark (at the round window) orthogonally projected onto the mid-modiolar axis (axial line).
4. A new *LandmarkSet* object was opened to add a landmark at the intersection of the drawing line and the axial line to determine the coordinate at the intersection.
5. The processes from 2) to 4) were repeated for the last landmark at the apex.
6. Both landmark coordinates at the intersections were used to calculate the distance between them (cochlear height).

A.5 Measurement of cochlear width

1. The landmark at the inferior edge of the round window and the opposite landmark were used to compute cochlear width.
2. The slice was rotated to pass through these two landmarks.
3. Using the 3D Angle tool, a transverse line (the first line) perpendicular to the axial line was drawn from the landmark at the round window to the opposite landmark.
4. When the first line did not pass the opposite landmark, the second line from the opposite landmark was drawn and projected at a right angle onto the first line. The second line was also parallel to the axial line.
5. A new landmark was added at the junction between the first and second lines to determine the coordinate at the junction.
6. Cochlear width was calculated as the distance between the landmark at the round window and the landmark at that junction.

A.6 Measurement of cochlear volume

1. Image data used for 3D-image reconstruction were loaded into the Segmentation Editor.
2. Voxels currently assigned to the inner ear were selected in the Material list.
3. The 2D and 3D checkboxes were checked to switch the inner ear visible in the 2D and 3D viewers. The voxels were displayed in red in the 3D viewer.
4. The 3D lasso tool was chosen from the toolbox and was used to draw a closed curve around unwanted voxels of the vestibular apparatus. The closed curve passed parallel to the groove under the saccular protrusion, and passed the first clear point of the inner osseous lamina.
5. The unwanted voxels were removed using the *Replace* button in the *Selection* panel.
6. Removing and adding voxels were continued in both 2D and 3D viewers until only voxels of the cochlea remained.
7. At the Pool view, the *MaterialStatistics* module was connected to the *LabelField* object.
8. After the *Region* mode was applied, the value of the internal cochlear volume was displayed in a table.

A.7 Measurement of surface area of the cochlear fenestrae

1. The surface of 3D images after smoothing was displayed in the Surface Editor.
2. In the Properties Area of the surface object, the Transform Editor was invoked and the *Apply Transform* button was selected.
3. Again in the Properties Area, the Surface Editor was activated to show the image surface in the 3D viewer with each triangle outlined in black.

4. A slice of the 2D viewer was rotated and translated to pass the edge and region of the oval and round windows.
5. In the Surface Editor's tool bar, interactive tools were used for selecting and highlighting triangles occupying the area of the oval and round windows. Highlighted triangles were drawn in red wireframe.
6. *Buffer* object from the *Surface* menu was opened and the menu entry *Invert Highlights* was chosen. As a result, triangles of the windows became black and other unwanted triangles were red instead.
7. The *remove highlighted triangles from buffer* button in the Surface Editor's tool bar was selected. As a result, only triangles of the windows remained.
8. In the *SurfaceView* module, the *Draw Style, more options* and *Create Surface* were selected sequentially. Therefore a new surface object with only triangles of the windows was created in the Pool view.
9. To compute the area of the windows, the *SurfaceArea* module was connected to the new surface object. Values of surface area of the cochlear fenestrae were displayed in a spreadsheet object.

Appendix B

Module and NEXUS files

B.1 The script of the *ReAlignObliqueSliceByLandmarks.scro* module

```
# Amira-Script-Object v3.0

#$this script show

#
# This script rotates an ObliqueSlice around an axis
# defined by two landmark points.
#

$this proc constructor {} {
    $this newPortDoIt action
    $this newPortConnection obliqueSlice HxObliqueSlice
    $this newPortFloatSlider slider
    $this slider setMinMax 0 360
    $this slider setValue 0
}

$this proc compute {} {
    set data [$this data source]
    if { $data == "" } {
        echo "Error: no LandmarkSet connected as data"
        return
    }
    if { [$data getTypeId] != "HxLandmarkSet" } {
        echo "Error: connected input is not a landmark set"
        return
    }

    if { [$data getNumPoints] < 2 } {
        echo "Error: at least two points are required (only the first 2
points will be used)"
        return
    }
    set p1 [$data getPoint 0 0]
    set p2 [$data getPoint 1 0]

    set os [$this obliqueSlice source]
    if { $os == "" } {
        echo "Error: no ObliqueSlice module found"
        return
    }
    $this obliqueSlice setTightness 1
    set center [list [expr [lindex $p1 0] + ([lindex $p2 0]-[lindex $p1
0])/2.0] \
                    [expr [lindex $p1 1] + ([lindex $p2 1]-[lindex $p1 1])/2.0]
\
                    [expr [lindex $p1 2] + ([lindex $p2 2]-[lindex $p1
2])/2.0]]

    set axis [list [expr [lindex $p2 0]-[lindex $p1 0]] \
                  [expr [lindex $p2 1]-[lindex $p1 1]] \
```

```

        [expr [lindex $p2 2]-[lindex $p1 2]]
    set a1 [list 0 1 1]
    set d1 [list [expr [lindex $a1 1] * [lindex $axis 2] - [lindex $a1 2] *
[lindex $axis 1]] \
        [expr [lindex $a1 2] * [lindex $axis 0] - [lindex $a1 0] *
[lindex $axis 2]] \
        [expr [lindex $a1 0] * [lindex $axis 1] - [lindex $a1 1] *
[lindex $axis 0]]]
    set length [expr sqrt([lindex $d1 0]*[lindex $d1 0] + [lindex $d1
1]*[lindex $d1 1] + [lindex $d1 2]*[lindex $d1 2])]
    set d1 [list [expr [lindex $d1 0]/$length] [expr [lindex $d1
1]/$length] [expr [lindex $d1 2]/$length]]
    set d2 [list [expr [lindex $d1 1] * [lindex $axis 2] - [lindex $d1 2] *
[lindex $axis 1]] \
        [expr [lindex $d1 2] * [lindex $axis 0] - [lindex $d1 0] *
[lindex $axis 2]] \
        [expr [lindex $d1 0] * [lindex $axis 1] - [lindex $d1 1] *
[lindex $axis 0]]]
    set length [expr sqrt([lindex $d2 0]*[lindex $d2 0] + [lindex $d2
1]*[lindex $d2 1] + [lindex $d2 2]*[lindex $d2 2])]
    set d2 [list [expr [lindex $d2 0]/$length] [expr [lindex $d2
1]/$length] [expr [lindex $d2 2]/$length]]

    # d1 and d2 are now orthogonal to the axis defined by the two points
    # we rotate between these two direction vectors
    set alpha [expr [$this slider getValue]/360.0*2.0*3.1415927]
    set res [list [expr cos($alpha)*[lindex $d1 0] + sin($alpha)*[lindex
$d2 0]] \
        [expr cos($alpha)*[lindex $d1 1] + sin($alpha)*[lindex $d2 1]]
\
        [expr cos($alpha)*[lindex $d1 2] + sin($alpha)*[lindex $d2
2]]]
    eval "$os setPlane $center $res"
    $os fire
}

```

B.2 NEXUS file of the phylogenetic tree of 45 mammalian species

```

#NEXUS
[written Mon Aug 06 16:32:40 BST 2012 by Mesquite version 2.75 (build 564)
at njeffery/138.253.145.216]

BEGIN TAXA;
    TITLE Taxa;
    DIMENSIONS NTAX=45;
    TAXLABELS
        Dl Tu Ha Bp Cd Ec Pc Fc Vv Af Pl Tt Me Ll Mi Or Ef Te To Hs Ca
Ss At Tb Dm Ac Gs Gv Xe Ma Cl Cc Mm Rn Mp Cb Pe Ch Cp Lm Mc Co La Ts Ne;

END;

BEGIN TREES;
    Title Imported_trees;
    LINK Taxa = Taxa;
    TRANSLATE
        1 Dl,
        2 Tu,
        3 Ha,

```

4 Bp,
 5 Cd,
 6 Ec,
 7 Pc,
 8 Fc,
 9 Vv,
 10 Af,
 11 Pl,
 12 Tt,
 13 Me,
 14 Ll,
 15 Mi,
 16 Or,
 17 Ef,
 18 Te,
 19 To,
 20 Hs,
 21 Ca,
 22 Ss,
 23 At,
 24 Tb,
 25 Dm,
 26 Ac,
 27 Gs,
 28 Gv,
 29 Xe,
 30 Ma,
 31 Cl,
 32 Cc,
 33 Mm,
 34 Rn,
 35 Mp,
 36 Cb,
 37 Pe,
 38 Ch,
 39 Cp,
 40 Lm,
 41 Mc,
 42 Co,
 43 La,
 44 Ts,
 45 Ne;

```

    TREE Imported_tree_0 =
    ((((((((((1:30.8,2:30.8):28.7,3:59.5):6.4,4:65.9):8.2,5:74.1):13.2,6:87.3):
    1.2,((7:16.8,8:16.8):50.3,(9:59.2,((10:39.3,(11:31.5,(12:26.1,(13:23.9,14:2
    3.9):2.2):5.4):7.8):9.7,(15:34.3,16:34.3):14.7):10.2):7.9):21.4):0.2,17:88.
    7):3.1,(18:30.1,19:30.1):61.7):7.1,((((20:54.1,((21:18.7,22:18.7):2.3,23:21
    .0):33.1):30.9,24:85.0):2.8,(25:41.5,(26:40.5,27:40.5):1.0):46.3):6.8,((28:
    43.6,(29:39.9,(30:9.3,31:9.3):30.6):3.7):41.7,(((32:81.0,((33:28.5,34:28.5)
    :21.4,35:49.9,36:49.9):30.2,37:80.1):0.9):4.1,((38:49.4,39:49.4,40:49.4,41:
    49.4):0.4,42:49.8):35.3):0.2):9.2):4.4):2.4,((43:77.8,44:77.8):15.6,45:93.4
    ):7.9);
  
```

END;

B.3 NEXUS file of the phylogenetic tree of 15 rodent species

```
#NEXUS
[written Mon Aug 06 16:32:40 BST 2012 by Mesquite version 2.75 (build 564)
at njeffery/138.253.145.216]

BEGIN TAXA;

    TAXLABELS    Gv Xe Ma Cl Cc Mm Rn Mp Cb Pe Ch Cp Lm Mc Co;

END;

BEGIN TREES;

    Tree tree1 =
((Gv:43.6,(Xe:39.9,(Ma:9.3,Cl:9.3):30.6):3.7):41.7,((Cc:81.0,(((Mm:28.5,Rn:
28.5):21.4,Mp:49.9,Cb:49.9):30.2,Pe:80.1):0.9):4.1,((Ch:49.4,Cp:49.4,Lm:49.
4,Mc:49.4):0.4,Co:49.8):35.3):0.2);

END;
```

B.4 NEXUS file of the phylogenetic tree of 8 primate species

```
#NEXUS
[written Mon Aug 06 16:32:40 BST 2012 by Mesquite version 2.75 (build 564)
at njeffery/138.253.145.216]

BEGIN TAXA;

    TAXLABELS    Ca Ss At Hs Tb Ac Gs Dm;

END;

BEGIN TREES;

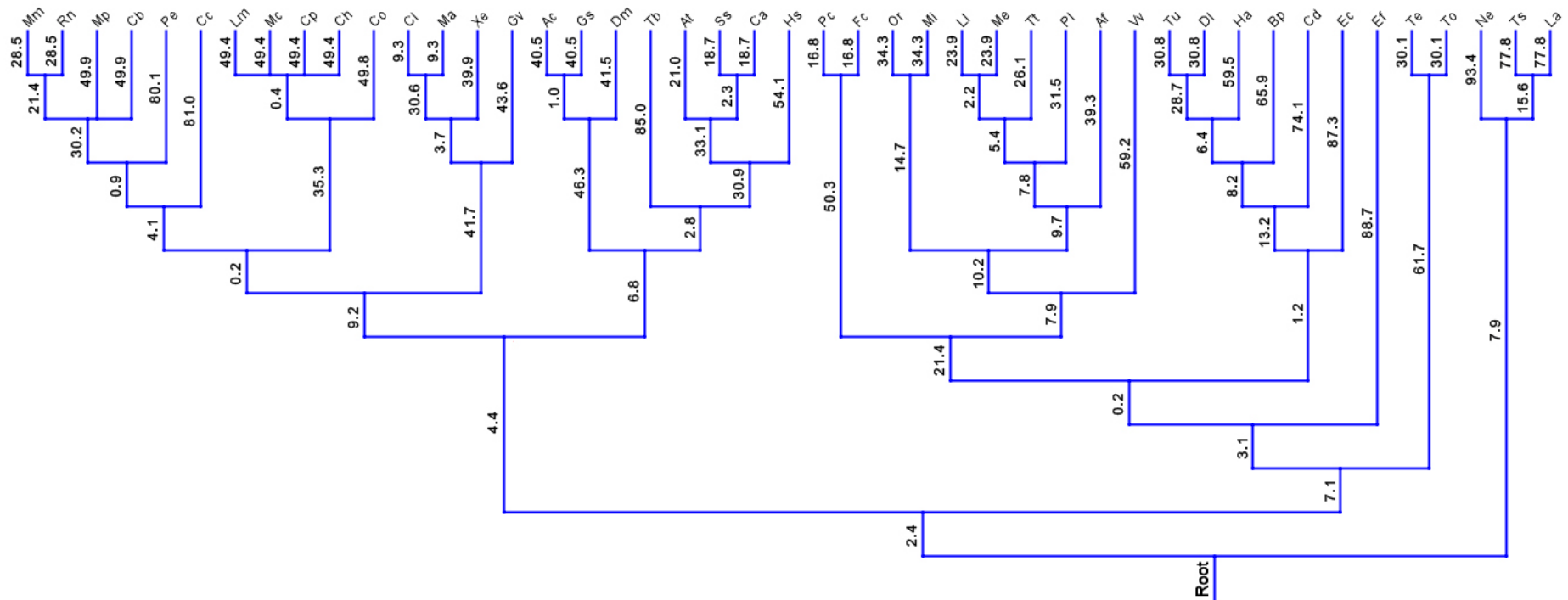
    Tree tree1 =
((((Ca:18.7,Ss:18.7):2.3,At:21.0):33.1,Hs:54.1):30.9,Tb:85.0):2.8,((Ac:40.
5,Gs:40.5):1.0,Dm:41.5):46.3);

END;
```

Appendix C

The phylogenetic tree for 45 mammalian species

The topology and dates of phylogenetic tree for 45 mammalian species studied. All dates are in millions of years. The tree is derived from Bininda-Emonds et al. (2007).



Appendix D

Raw data and statistics

D.1 Taxonomy of 45 mammalian species studied (in alphabetical order).

ID	Species	Common name	Order
Ac	<i>Arctocebus calabarensis</i>	Calabar potto	Primates
Af	<i>Ailurus fulgens</i>	Red panda	Carnivora
At	<i>Aotus trivirgatus</i>	Northern night monkey	Primates
Bp	<i>Bos primigenius</i>	Aurochs	Artiodactyla
Ca	<i>Cebus apella</i>	Brown capuchin	Primates
Cb	<i>Cannomys badius</i>	Lesser bamboo rat	Rodentia
Cc	<i>Castor canadensis</i>	American beaver	Rodentia
Cd	<i>Camelus dromedarius</i>	Dromedary	Artiodactyla
Ch	<i>Cryptomys hottentotus</i>	Common mole rat	Rodentia
Cl	<i>Cynomys ludovicianus</i>	Prairie Dog	Rodentia
Co	<i>Ctenomys opimus</i>	Highland Tuco-tuco	Rodentia
Cp	<i>Cavia porcellus</i>	Guinea pig	Rodentia
DI	<i>Delphinapterus leucas</i>	Beluga whale	Cetacea
Dm	<i>Daubentonia madagascariensis</i>	Aye-aye	Primates
Ec	<i>Equus caballus</i>	Domestic horse	Perissodactyla
Ef	<i>Eptesicus fuscus</i>	Big brown bat	Chiroptera
Fc	<i>Felis catus</i>	Cat	Carnivora
Gs	<i>Galago senegalensis</i>	Senegal bushbaby	Primates
Gv	<i>Glaucomys volans</i>	Southern flying squirrel	Rodentia
Ha	<i>Hippopotamus amphibius</i>	Hippopotamus	Artiodactyla
Hs	<i>Homo sapiens</i>	Human	Primates
La	<i>Loxodonta africana</i>	Savanna elephant	Proboscidea
LI	<i>Lutra lutra</i>	Otter	Carnivora
Lm	<i>Lagostomus maximus</i>	Plains viscacha	Rodentia
Ma	<i>Marmota monax</i>	Woodchuck	Rodentia
Mc	<i>Myocastor coypus</i>	Coypu	Rodentia
Me	<i>Mephitis</i> sp.	Skunk	Carnivora
Mi	<i>Mirounga angustirostris</i>	Northern elephant seal	Pinnipedia
Mm	<i>Mus musculus</i>	Mouse	Rodentia
Mp	<i>Microtus pennsylvanicus</i>	Meadow vole	Rodentia
Ne	<i>Neamblysomus</i> sp.	Golden mole	Insectivora
Or	<i>Odobenus rosmarus divergens</i>	Walrus	Pinnipedia
Pc	<i>Puma concolor</i>	Cougar	Carnivora
Pe	<i>Pedetes capensis</i>	Springhare	Rodentia
Pl	<i>Procyon lotor</i>	Common raccoon	Carnivora
Rn	<i>Rattus norvegicus</i>	Rat	Rodentia
Ss	<i>Saimiri sciureus</i>	Common squirrel monkey	Primates

ID	Species	Common name	Order
Tb	<i>Tarsius bancanus</i>	Horsfield's tarsier	Primates
Te	<i>Talpa europaea</i>	European mole	Insectivora
To	<i>Talpa occidentalis</i>	Spanish mole	Insectivora
Ts	<i>Trichechus senegalensis</i>	African manatee	Sirenia
Tt	<i>Taxidea taxus</i>	American badger	Carnivora
Tu	<i>Tursiops truncatus</i>	Bottlenosed dolphin	Cetacea
Vv	<i>Vulpes vulpes</i>	Red fox	Carnivora
Xe	<i>Xerus erythropus</i>	African ground squirrel	Rodentia

D.2 Shapes of the round window in 45 eutherian mammals.

Species	Shapes			
	Circular	Elliptical	Bean	Undefined
<i>Mus musculus</i>	•			
<i>Puma concolor</i>		•		
<i>Glaucomys volans</i>		•		
<i>Felis catus</i>	•			
<i>Vulpes vulpes</i>			•	
<i>Ailurus fulgens</i>		•		
<i>Mephitis sp.</i>				•
<i>Loxodonta africana</i>		•		
<i>Equus caballus</i>	•			
<i>Bos primigenius</i>		•		
<i>Arctocebus calabarensis</i>	•			
<i>Tarsius bancanus</i>	•			
<i>Aotus trivirgatus</i>	•			
<i>Daubentonia madagascariensis</i>	•			
<i>Camelus dromedarius</i>		•		
<i>Procyon lotor</i>	•			
<i>Saimiri sciureus</i>	•			
<i>Cebus apella</i>	•			
<i>Rattus norvegicus</i>	•			
<i>Homo sapiens</i>		•		
<i>Galago senegalensis</i>	•			
<i>Cavia porcellus</i>		•		
<i>Cynomys ludovicianus</i>		•		
<i>Pedetes capensis</i>		•		
<i>Lagostomus maximus</i>		•		
<i>Taxidea taxus</i>				•

Species	Shapes			
	Circular	Elliptical	Bean	Undefined
<i>Microtus pennsylvanicus</i>				•
<i>Marmota monax</i>		•		
<i>Xerus erythropus</i>		•		
<i>Talpa europaea</i>		•		
<i>Talpa occidentalis</i>		•		
<i>Neamblysomus</i> sp.		•		
<i>Ctenomys opimus</i>		•		
<i>Cryptomys hottentotus</i>		•		
<i>Cannomys badius</i>	•			
<i>Eptesicus fuscus</i>		•		
<i>Odobenus rosmarus divergens</i>		•		
<i>Mirounga angustirostris</i>		•		
<i>Lutra lutra</i>		•		
<i>Castor canadensis</i>		•		
<i>Myocastor coypus</i>		•		
<i>Hippopotamus amphibius</i>			•	
<i>Tursiops truncatus</i>		•		
<i>Trichechus senegalensis</i>				•
<i>Delphinapterus leucas</i>		•		

Note: Between the circular and elliptical shapes, if the major axis is 1.25 times longer than the minor axis, the shape will be regarded as the ellipse.

D.3 Shapes of the round window in 17 human specimens.

Specimen ID	Categories	Shapes		
		Circular	Elliptical	Undefined
A1	Adult	•		
A2	Adult			•
A3	Adult		•	
A4	Adult		•	
A5	Adult		•	
L1	Large fetus	•		
L2	Large fetus	•		
L3	Large fetus		•	
L4	Large fetus		•	
L5	Large fetus			•
L6	Large fetus	•		
S1	Small fetus		•	
S2	Small fetus		•	
S3	Small fetus		•	
S4	Small fetus			•
S5	Small fetus	•		
S6	Small fetus	•		

Note: Between the circular and elliptical shapes, if the major axis is 1.25 times longer than the minor axis, the shape will be regarded as the ellipse.

D.4 Raw data of measurements of the cochlear variables in 45 mammalian species.

Species	Spiral turns	L (mm)	H (mm)	W (mm)	V (mm ³)	OW area (mm ²)	RW area (mm ²)	OW/RW area	H/W
<i>Mus musculus</i>	1.875	5.213	0.596	0.990	1.420	0.096	0.240	0.400	0.602
<i>Puma concolor</i>	2.8125	27.094	3.146	5.460	118.655	5.859	8.073	0.726	0.576
<i>Glaucomys volans</i>	2.6875	10.904	1.702	1.657	5.731	0.448	0.428	1.047	1.027
<i>Felis catus</i>	3	20.551	2.953	3.150	37.935	1.997	4.747	0.421	0.937
<i>Vulpes vulpes</i>	3	19.766	3.156	3.637	45.379	2.190	3.574	0.613	0.868
<i>Ailurus fulgens</i>	2.125	15.115	1.903	3.043	24.416	0.984	2.017	0.488	0.625
<i>Mephitis</i> sp.	2.75	16.205	1.764	3.057	19.283	1.044	1.799	0.580	0.577
<i>Loxodonta africana</i>	2.25	35.796	4.348	7.710	322.715	16.447	12.360	1.331	0.564
<i>Equus caballus</i>	2.4375	31.346	2.898	6.989	114.865	4.686	7.181	0.652	0.415
<i>Bos primigenius</i>	2.1875	25.701	3.191	6.097	122.624	2.365	6.579	0.359	0.523
<i>Arctocebus calabarensis</i>	2.5	16.039	2.439	2.855	21.671	0.741	0.729	1.016	0.854
<i>Tarsius bancanus</i>	3.75	16.643	2.253	2.508	13.529	0.712	0.831	0.857	0.898
<i>Aotus trivirgatus</i>	3.0625	18.739	1.637	3.345	16.436	0.838	1.128	0.743	0.489
<i>Daubentonia madagascariensis</i>	2.25	16.216	1.955	3.743	28.750	1.118	2.228	0.502	0.522
<i>Camelus dromedarius</i>	2.3125	28.918	3.230	6.760	121.886	6.373	11.429	0.558	0.478
<i>Procyon lotor</i>	2.5	18.355	3.246	2.907	41.980	1.405	2.680	0.524	1.117
<i>Saimiri sciureus</i>	2.9375	19.708	1.775	3.984	20.319	0.701	1.310	0.535	0.446
<i>Cebus apella</i>	3.125	24.948	2.516	4.655	36.607	1.198	2.157	0.555	0.540
<i>Rattus norvegicus</i>	2.4375	8.207	1.340	1.634	4.183	0.351	0.613	0.573	0.820
<i>Homo sapiens</i>	2.6375	30.987	3.265	7.069	100.764	3.399	2.616	1.360	0.462
<i>Galago senegalensis</i>	2.75	13.517	1.701	2.387	12.630	0.581	0.463	1.255	0.713
<i>Cavia porcellus</i>	4.1875	19.476	3.768	2.626	16.551	0.952	1.205	0.790	1.435

Species	Spiral turns	L (mm)	H (mm)	W (mm)	V (mm ³)	OW area (mm ²)	RW area (mm ²)	OW/RW area	H/W
<i>Cynomys ludovicianus</i>	3.5625	13.291	1.664	1.696	7.914	1.107	1.081	1.024	0.981
<i>Pedetes capensis</i>	2.6875	16.087	2.348	2.977	20.881	1.506	2.617	0.575	0.789
<i>Lagostomus maximus</i>	3.5	17.874	3.134	2.766	24.759	1.829	1.967	0.930	1.133
<i>Taxidea taxus</i>	3.25	26.547	3.127	4.556	64.467	3.047	2.463	1.237	0.686
<i>Microtus pennsylvanicus</i>	2.5	7.042	1.166	1.244	2.268	0.414	0.200	2.065	0.937
<i>Marmota monax</i>	3	14.483	1.561	2.478	11.547	1.365	1.210	1.128	0.630
<i>Xerus erythropus</i>	3.125	13.912	1.842	2.081	9.512	0.979	0.588	1.665	0.885
<i>Talpa europaea</i>	2	5.439	0.908	1.049	1.655	0.494	0.561	0.880	0.866
<i>Talpa occidentalis</i>	2.1875	5.791	1.119	0.988	1.646	0.471	0.346	1.363	1.133
<i>Neamblysomus</i> sp.	3	8.312	1.386	1.214	2.558	0.802	0.497	1.614	1.141
<i>Ctenomys opimus</i>	3.625	15.807	2.699	1.682	7.675	1.103	0.891	1.238	1.605
<i>Cryptomys hottentotus</i>	3.375	10.346	1.826	1.153	2.854	0.422	0.303	1.394	1.584
<i>Cannomys badius</i>	3.0625	13.227	1.970	1.933	9.267	0.928	0.511	1.818	1.019
<i>Eptesicus fuscus</i>	2.125	8.010	0.848	1.519	2.857	0.160	0.234	0.684	0.558
<i>Odobenus rosmarus divergens</i>	2.5	32.369	4.551	6.582	352.861	4.440	15.440	0.288	0.691
<i>Mirounga angustirostris</i>	1.8125	33.486	3.465	9.197	266.583	10.979	24.732	0.444	0.377
<i>Lutra lutra</i>	2.8125	17.699	2.021	3.650	30.958	2.035	3.635	0.560	0.554
<i>Castor canadensis</i>	2.75	17.942	2.271	3.145	41.138	2.419	2.437	0.993	0.722
<i>Myocastor coypus</i>	4.1875	23.966	4.185	2.453	27.349	1.188	1.613	0.736	1.706
<i>Hippopotamus amphibius</i>	3.125	44.503	5.202	8.434	317.127	13.302	24.405	0.545	0.617
<i>Tursiops truncatus</i>	1.75	31.876	3.843	8.213	142.067	4.614	7.835	0.589	0.468
<i>Trichechus senegalensis</i>	1.75	30.713	4.525	7.020	342.215	22.288	22.100	1.008	0.645
<i>Delphinapterus leucas</i>	2	35.403	3.365	9.823	157.902	5.416	7.705	0.703	0.343

D.5 Significance of ANCOVA pairwise comparison of groups whilst controlling for log body mass — Habitats.

Groups	Log L (mm)	Log H (mm)	Log W (mm)	Log V (mm ³)	Log (No. of Turns)	Log OW area (mm ²)	Log RW area (mm ²)	Log (OW/RW area)	Log (H/W)
Ter-Foss	ns	ns	*(a)	ns	ns	ns	ns	** (b)	ns
Ter-Sub	ns	ns	*** (c)	*** (c)	ns	ns	ns	** (d)	** (d)
Ter-Sem	ns	ns	ns	ns	ns	ns	ns	ns	ns
Ter-Mar	ns	ns	ns	ns	*(e)	ns	ns	ns	ns
Fos-Sub	ns	ns	ns	ns	ns	ns	ns	ns	ns
Fos-Sem	ns	ns	ns	ns	ns	ns	ns	ns	ns
Fos-Mar	ns	ns	ns	ns	** (f)	ns	ns	ns	ns
Sub-Sem	ns	ns	ns	ns	ns	ns	ns	ns	ns
Sub-Mar	ns	ns	ns	ns	ns	ns	ns	ns	ns
Sem-Mar	ns	ns	ns	ns	ns	ns	ns	ns	ns

Adjusted means: ^(a)Ter > Fos (0.522 > 0.427); ^(b)Fos > Ter (0.056 > -0.172); ^(c)Ter > Sub (Log W: 0.492 > 0.285, Log V: 1.347 > 0.376);

^(d)Sub > Ter (Log OW/RW: 0.133 > -0.174, Log H/W: 0.023 > -0.163); ^(e)Ter > Mar (0.422 > 0.289); ^(f)Fos > Mar (0.516 > 0.194)

D.6 Significance of ANCOVA pairwise comparison of groups whilst controlling for log body mass — Sociality.

Groups	Log L (mm)	Log H (mm)	Log W (mm)	Log V (mm ³)	Log (No. of Turns)	Log OW area (mm ²)	Log RW area (mm ²)	Log (OW/RW area)	Log (H/W)
S - G	ns	ns	ns	ns	ns	** (a)	ns	ns	ns

Adjusted mean: ^(a)S > G (0.289 > 0.111)

D.7 Significance of ANCOVA pairwise comparison of groups whilst controlling for log body mass — High frequency limit.

Groups	Log L (mm)	Log H (mm)	Log W (mm)	Log V (mm ³)	Log (No. of Turns)	Log OW area (mm ²)	Log RW area (mm ²)	Log (OW/RW area)	Log (H/W)
HHL-MHL	ns	ns	ns	ns	ns	ns	ns	ns	ns
HHL-LHL	ns	ns	*(a)	ns	ns	ns	ns	ns	ns
MHL-LHL	*(b)	ns	** (b)	*** (b)	ns	ns	ns	ns	ns

Adjusted means: ^(a)HHL > LHL (0.593 > 0.451); ^(b)MHL > LHL (Log L: 1.335 > 1.228, Log W: 0.64 > 0.477, Log V: 1.690 > 1.380)

D.8 Significance of ANCOVA pairwise comparison of groups whilst controlling for log body mass — Low frequency limit.

Groups	Log L (mm)	Log H (mm)	Log W (mm)	Log V (mm ³)	Log (No. of Turns)	Log OW area (mm ²)	Log RW area (mm ²)	Log (OW/RW area)	Log (H/W)
HLL-MLL	ns	ns	ns	ns	ns	ns	ns	ns	ns
HLL-LLL	ns	ns	ns	ns	*(a)	ns	ns	ns	ns
MLL-LLL	ns	ns	ns	ns	ns	ns	ns	ns	ns

Adjusted mean: ^(a)LLL > HLL (0.468 > 0.334)

D.9 Significance of ANCOVA pairwise comparison of groups whilst controlling for log body mass — Best hearing frequency.

Groups	Log L (mm)	Log H (mm)	Log W (mm)	Log V (mm ³)	Log (No. of Turns)	Log OW area (mm ²)	Log RW area (mm ²)	Log (OW/RW area)	Log (H/W)
HBF-MBF	ns	ns	ns	ns	ns	ns	ns	ns	ns
HBF-LBF	ns	ns	ns	ns	ns	ns	ns	*(b)	ns
MBF-LBF	ns	ns	** (a)	** (a)	ns	ns	ns	ns	ns

Adjusted means: ^(a)MBF > LBF (Log W: 0.579 > 0.423, Log V: 1.523 > 1.243); ^(b)LBF > HBF (-0.007 > -0.224)

D.10-D.12 Spearman's rank correlation and RMA regression of residual cochlear variables with hearing parameters (marine and semi-aquatic mammals are excluded).

Log high frequency limit vs	r	Sig.	RMA regression		
			Slope	95% CI	Intercept
Residual log OW area squared	-0.0816	ns			
Residual log RW area squared	0.4765	*	1.4752	0.747-1.929	1.6717
Residual log (OW/RW area)	-0.7187	***	-0.9944	(-1.206)-(-0.542)	1.5632

*** $P < 0.001$; * $P < 0.05$; ns = not significant.

Residual log low frequency limit vs	r	Sig.	RMA regression		
			Slope	95% CI	Intercept
Residual log OW area squared	-0.3263	ns			
Residual log RW area squared	-0.2035	ns			
Residual log (OW/RW area)	-0.1088	ns			

ns = not significant.

Log best hearing frequency vs	r	Sig.	RMA regression		
			Slope	95% CI	Intercept
Residual log OW area squared	-0.2557	ns			
Residual log RW area squared	0.2974	ns			
Residual log (OW/RW area)	-0.6534	**	-1.8006	(-2.428)-(-0.456)	0.6115

** $P < 0.01$; ns = not significant.

D.13 Scores on PC1-PC4 in the adult interspecific study.

Species	5% cut-off rule				ln Centroid size
	PC1 score (45.4%)	PC2 score (22.4%)	PC3 score (11.7%)	PC4 score (6.9%)	
<i>Mus musculus</i>	0.30194	0.09534	-0.01068	0.15634	0.97898
<i>Puma concolor</i>	-0.00301	-0.18837	0.10256	-0.07127	2.47345
<i>Glaucomys volans</i>	-0.30345	-0.10566	-0.01256	-0.06517	1.52336
<i>Felis catus</i>	-0.06507	-0.13200	0.05307	-0.06736	2.21881
<i>Vulpes vulpes</i>	-0.18181	-0.02760	0.10279	-0.02221	2.20772
<i>Ailurus fulgens</i>	0.29363	-0.04798	-0.10939	0.13410	1.98657
<i>Mephitis</i> sp.	-0.07498	-0.24825	-0.01813	-0.02413	1.89339
<i>Loxodonta africana</i>	0.38812	0.05651	-0.01247	0.07180	2.92032
<i>Equus caballus</i>	0.30526	-0.07967	-0.06448	-0.02713	2.72201
<i>Bos primigenius</i>	0.35302	0.01133	-0.05553	-0.00617	2.59899
<i>Arctocebus calabarensis</i>	0.00438	-0.22293	-0.16299	0.03436	1.92957
<i>Tarsius bancanus</i>	-0.24752	0.30308	-0.04582	0.10234	1.77359
<i>Aotus trivirgatus</i>	-0.17202	-0.10808	0.22697	0.10291	1.93794
<i>Daubentonia madagascariensis</i>	0.40227	0.08880	0.02048	0.04588	2.10951
<i>Camelus dromedarius</i>	0.37829	0.03882	-0.03471	-0.02748	2.68738
<i>Procyon lotor</i>	-0.03598	-0.18060	-0.14977	-0.02285	2.13432
<i>Saimiri sciureus</i>	0.06018	-0.30883	0.10478	0.02868	2.05262
<i>Cebus apella</i>	-0.11368	-0.23391	0.17388	0.06795	2.25697
<i>Rattus norvegicus</i>	0.13444	-0.08845	-0.19816	0.04891	1.39620
<i>Homo sapiens</i>	0.19330	-0.22116	0.02062	-0.06141	2.64437
<i>Galago senegalensis</i>	-0.24321	-0.15894	-0.09404	-0.05618	1.76184
<i>Cavia porcellus</i>	-0.12351	0.27655	-0.22793	-0.24336	2.00754
<i>Cynomys ludovicianus</i>	-0.23389	0.39201	-0.09130	0.04359	1.52449
<i>Pedetes capensis</i>	0.11111	-0.16315	-0.05263	-0.09001	2.02457
<i>Lagostomus maximus</i>	-0.25698	0.35881	-0.00687	0.03120	1.98639
<i>Taxidea taxus</i>	-0.27218	-0.02251	0.18149	0.11529	2.29483
<i>Microtus pennsylvanicus</i>	-0.15800	-0.10937	-0.20679	-0.01371	1.18623
<i>Marmota monax</i>	-0.25826	-0.17397	0.06677	0.01554	1.71214
<i>Xerus erythropus</i>	-0.38187	0.15823	0.09862	0.07958	1.67385
<i>Talpa europaea</i>	0.21300	0.09567	-0.15188	0.16165	1.05707
<i>Talpa occidentalis</i>	0.07997	-0.01686	-0.25478	0.14839	1.04706
<i>Neamblysomus</i> sp.	-0.37780	-0.07003	-0.04960	-0.01243	1.17893
<i>Ctenomys opimus</i>	-0.29487	0.34889	-0.04485	0.05274	1.72420
<i>Cryptomys hottentotus</i>	-0.41291	0.18092	0.01505	0.02707	1.32459
<i>Cannomys badius</i>	-0.38022	0.07131	0.11758	0.01279	1.61680
<i>Eptesicus fuscus</i>	0.28685	0.00555	-0.11572	0.19601	1.31335
<i>Odobenus rosmarus divergens</i>	0.17406	-0.16329	-0.01051	-0.10979	2.72091
<i>Mirounga angustirostris</i>	0.35946	0.20242	0.22181	-0.09700	2.99497
<i>Lutra lutra</i>	-0.09203	-0.18936	0.08107	-0.06986	2.05633
<i>Castor canadensis</i>	-0.26727	-0.09413	0.07933	-0.04681	2.00911
<i>Myocastor coypus</i>	-0.02466	0.14203	-0.21682	-0.34058	2.10956

Species	5% cut-off rule				In Centroid size
	PC1 score (45.4%)	PC2 score (22.4%)	PC3 score (11.7%)	PC4 score (6.9%)	
Hippopotamus amphibius	-0.12240	-0.09162	0.09136	0.04104	2.94065
Tursiops truncatus	0.35721	0.20702	0.22017	-0.07540	2.89024
Trichechus senegalensis	0.32735	0.21365	0.21587	-0.10565	2.92422
Delphinapterus leucas	0.37373	0.19979	0.20413	-0.06222	3.01020

D.14 Raw data of measurements of cochlear variables in human specimens.

Specimen	Gestational ages on tins (months)	Spiral turns	L (mm)	H (mm)	W (mm)	V (mm ³)	OW area (mm ²)	RW area (mm ²)	OW/RW area	H/W
A1		2.6875	31.461	3.185	7.201	100.341	3.670	3.401	1.079	0.442
A2		2.6875	29.615	3.501	6.923	103.647	3.554	3.384	1.050	0.506
A3		2.5625	30.771	3.344	7.289	101.918	3.045	1.999	1.523	0.459
A4		2.625	32.070	3.351	6.941	97.475	3.295	1.986	1.659	0.483
A5		2.625	31.016	2.945	6.992	100.439	3.432	2.308	1.487	0.421
L1	9	2.625	28.810	2.952	6.685	78.078	3.056	2.940	1.040	0.442
L2	9	2.625	27.382	3.183	6.019	79.285	3.089	3.404	0.907	0.529
L3	8	2.6875	27.525	3.385	6.631	78.737	2.856	2.424	1.178	0.510
L4	9	2.75	27.836	2.841	6.318	78.356	2.439	3.241	0.753	0.450
L5	6	2.6875	28.777	2.932	6.505	74.548	2.747	2.390	1.150	0.451
L6	8	2.6875	28.906	3.273	6.687	75.002	3.118	2.378	1.311	0.489
S1	7	2.6875	25.682	3.277	6.101	67.072	3.186	2.640	1.207	0.537
S2	7	2.6875	25.172	2.779	5.852	65.059	2.568	2.532	1.014	0.475
S3	6	2.625	29.311	3.225	6.740	81.552	3.680	2.352	1.565	0.479
S4	5	2.625	28.743	3.003	6.750	65.936	3.170	2.616	1.212	0.445
S5	5	2.6875	25.381	3.077	5.853	64.342	3.723	2.393	1.556	0.526
S6	4	2.75	23.788	2.903	5.368	69.054	4.264	2.283	1.867	0.541

Note: A1-A5 are adult specimens.

D.15 Scores on PC1-PC5 in the human developmental study (adults + fetuses).

Specimen	5% cut-off rule					In Centroid size
	PC1 score (32.8%)	PC2 score (19.5%)	PC3 score (15.5%)	PC4 score (9.1%)	PC5 score (6.7%)	
A1	0.01006	0.04852	0.02471	0.02799	0.00416	2.64921
A2	0.01650	0.01204	-0.03105	-0.01645	0.00600	2.61244
A3	-0.06148	-0.01027	-0.02715	-0.01065	0.04165	2.64437
A4	-0.05421	0.02651	0.03583	-0.01200	0.00170	2.66996
A5	-0.04197	-0.00570	-0.01878	0.03244	-0.00466	2.62827
L1	-0.03423	0.03392	-0.00929	-0.01965	-0.00534	2.57879
L2	-0.03324	-0.02222	-0.03291	-0.00648	-0.01001	2.51661
L3	0.04826	-0.03131	0.00625	-0.02114	0.02174	2.57786
L4	0.01116	-0.00334	-0.02348	0.01995	-0.03489	2.53568
L5	0.01507	0.02606	0.00876	0.01304	-0.00123	2.57392
L6	0.00654	-0.02341	-0.01675	0.03552	0.00237	2.57682
S1	0.03245	-0.06154	0.04092	-0.00007	-0.00228	2.50926
S2	0.00458	-0.00019	-0.00260	-0.04328	-0.03589	2.45447
S3	-0.00791	-0.04397	-0.00442	0.00378	-0.00088	2.61201
S4	-0.04159	0.00409	0.05815	0.00029	-0.00217	2.57737
S5	0.06182	0.00540	0.01555	0.00117	0.00949	2.48079
S6	0.06820	0.04541	-0.02375	-0.00444	0.01023	2.41082

D.16 Scores on PC1-PC5 in the human developmental study (only fetuses).

Specimen	5% cut-off rule					In Centroid size
	PC1 score (31.3%)	PC2 score (24.6%)	PC3 score (16.0%)	PC4 score (9.2%)	PC5 score (6.2%)	
L1	0.03806	0.05127	0.01552	-0.00661	0.01597	2.57879
L2	0.04487	0.00562	-0.04211	-0.00951	0.01041	2.51661
L3	-0.03723	-0.03148	-0.00027	-0.02392	0.01534	2.57786
L4	0.00276	0.01282	-0.02443	0.01358	-0.03636	2.53568
L5	-0.00935	0.02149	0.01766	0.01975	-0.01003	2.57392
L6	0.00449	-0.01205	-0.03320	0.03178	0.00331	2.57682
S1	-0.00848	-0.06881	0.01299	0.00013	-0.00317	2.50926
S2	0.01172	0.01374	0.00292	-0.04609	-0.02331	2.45447
S3	0.02180	-0.02766	-0.02003	-0.00050	0.01425	2.61201
S4	0.05278	-0.00730	0.05584	0.01451	0.00352	2.57737
S5	-0.05437	-0.00569	0.01958	0.00323	-0.00679	2.48079
S6	-0.06705	0.04805	-0.00447	0.00367	0.01687	2.41082

Appendix E

Abstracts for international conferences

Abstract for International Congress of Vertebrate Morphology, Spain 2013

Morphological Adaptations of the Rodent Inner Ear

Thanakul Wannaprasert and Nathan Jeffery

Rodents place varied functional demands on their sense of hearing and balance to meet the requirements of a broad range of ecological niches and diverse behaviours, from solitary and slow moving subterranean species through to gregarious semi-aquatic species and gliding species. Here we aim to capture and document potentially related adaptations of the organs of hearing, the cochlea, and of balance, the semicircular canals. Techniques including, for example, micro-CT, 3D reconstruction, and geometric morphometrics were used to study morphological variations of the bony inner ear across 15 rodent species. The cochleae were examined for changes of form (size and shape) whilst the canals were examined for variations in their planar orientations. Results revealed a considerable range of variation of rodent cochlear morphology, represented at one end by the typical mammalian condition seen in, for example, *Rattus norvegicus* and at the other end by a derived spring like cochlea seen in, for example, *Cavia porcellus* and *Myocastor coypus*. Potential links with hearing, ecology and behaviour were explored but proved inconclusive ($p > 0.05$). Results for the canal orientations indicated that the canals of fast moving species (e.g. *Pedetes capensis*) are no closer to orthogonal than those of slower moving species (e.g. *Cryptomys hottentotus*).

test the female choice hypothesis because male olive baboons of all ranks follow consorting pairs and compete for access to viable females. In the current study, males were observed contesting consorts during nearly half ($n=34$) of all observed consorts ($n=73$). If calls function as a signal to male partners to continue consorting, it is likely that female calls are related to whether a consort is contested. Females called more often during uncontested than contested copulations ($\chi^2=4.452$, $df=1$, $p<0.05$), and when their male partner was high-ranking versus low-ranking ($\chi^2=4.735$, $df=1$, $p<0.05$). Variability in individual female's acoustic patterns based on partner rank and time in female's cycle is addressed. Our results lend support for the female choice hypothesis for the evolution of copulation calls, and demonstrate that female mate preferences can be reflected in behaviors outside of those typically incorporated in female choice studies.

We would like to thank the following organizations and institutions for contributing to the funding of this project: The Leakey Foundation, International Primatological Society, American Society of Primatologists, Sigma Xi, Animal Behavior Society, and The Ohio State University Department of Anthropology.

The placement of the maxillo-zygomatic suture in primate midfacial skeleton: An investigation on Old World Monkeys and New World Monkeys.

QIAN WANG¹, JANA MAKEDONSKA², CRAIG BYRON³ and DAVID STRAIT².
¹Division of Basic Medical Sciences, Mercer University School of Medicine, ²Department of Anthropology, University at Albany, ³Department of Biology, Mercer University.

Craniofacial sutures are weak points compared to rigid bone on the skull thence they must be shielded from unduly high stresses so as not to disrupt vital growth processes and skeletal functions. Thus, it is hypothesized that the placement of sutures should maximize their growth potentials yet minimize their negative biomechanical impacts, especially in areas under high stress during dietary activities, such as the midface. Specifically, for any given suture, it is hypothesized that suture position would be different in skulls of different form adapted to different dietary ecology. In this study, we investigated the position of the Maxillo-Zygomatic suture (MZS) in five species of Old World Monkeys (OWM) and six species of New World Monkeys (NWM) by calculating the relative Zygoma breadth compared to the facial breadth at the level of the inferior rim of the orbit. Results demonstrated that the ZMS in NWM has a more lateral position compared to that in OWM. Consequently, the ratio of facial surface vs. temporal surface of the Zygoma in NWM is relatively smaller than that in OWM, which is coupled with different configuration patterns in the orbital and pterion areas. Variation is also present within closely related taxa. For example, the ZMS is more laterally placed in *Cebus apella* than in *C. albifrons*.

These findings suggest different bone interaction patterns related to differences in dietary ecology. The significance of the placement of sutures thus warrants careful ontogenetic, phylogenetic, and biomechanical studies.

Supported by NSF HOMINID BCS-0725126, BCS-0725183.

Size and shape maturation of the human cochlea.

THANAKUL WANNAPRASERT¹, FRED SPOOR² and NATHAN JEFFERY¹.
¹Institute of Ageing & Chronic Disease, University of Liverpool, United Kingdom, ²Dept. Human Evolution, Max Planck Institute for Evolutionary Anthropology, Germany.

Previous studies suggest that the human cochlea attains a size within the adult range as early as 23 weeks in utero, but 3D shape changes have as yet not been assessed. Here we document the shape component of form change of the human fetal cochlea and test whether the shape is distinct from that seen among adults. We collected microCT data for 12 fetuses ranging from 16 to 39 weeks in utero and data for 5 adults. Each cochlea was reconstructed in 3D and a spline function was fitted along the centre of the duct. A total of 25 landmarks were placed at equidistant points along the line and were subjected to form analysis. Measurements of cochlear length, width, height and volume were also collected. Findings indicate that there is little difference of cochlea shape between fetuses and adults but, in contrast to previous studies, a small difference of size was observed.

Analyses revealed a significant correlation ($p<0.05$) of PC1 scores with centroid size. This was associated with shape changes primarily in the apical region. Discriminant function analysis found no significant differences of cochlear shape in pairwise comparisons between the smallest fetuses, largest fetuses and adults. Mann-Whitney Tests suggest that the adult cochlea is on average significantly bigger than the largest fetuses in terms of length (+10%), width (+10%) and volume (+30%). These results suggest that whilst the general coiled shape is reached at an early stage of development, there may be size related morphological changes after birth.

TW was funded by a scholarship from the Royal Thai Embassy, London.

Earliest evidence of distinctive modern human-like hand morphology from West Turkana, Kenya.

CAROL V. WARD¹, MATTHEW W. TOCHERI², J. MICHAEL PLAVCAN³, FRANK H. BROWN⁴ and FREDRICK K. MANTH⁵.
¹Pathology and Anatomical Sciences, University of Missouri, ²Human Origins Program, National Museum of Natural History, Smithsonian Institution, ³Anthropology, University of Arkansas, ⁴College of Mines and Earth Sciences, University of Utah, ⁵Earth Sciences, National Museums of Kenya.

Despite recent discoveries of relatively complete hands from two early hominin species (*Ardipithecus ramidus* and *Australopithecus sediba*), fundamental questions remain about the evolution of human-like hand anatomy and function. These questions are driven by the paucity of hominin hand fossils between 1.8 and 0.8 million years old. In 2010, a team from the West Turkana Paleontology Project of the National Museums of Kenya recovered a hominin third metacarpal (KNM-WT 51260) from the newly discovered site of Kaitio. Kaitio is located in northern Kenya west of Lake Turkana and dates to about 1.4 Ma. In all ways, this bone resembles that of a modern human in overall proportions and morphology. The metacarpal is long, falling within the upper range of modern European and African American males, and is one of the longest hominin third metacarpals known among Neandertals and early modern humans. Notably, KNM-WT 51260 displays a well-developed styloid process, the most distinctive features of the human and Neandertal hand, not present in earlier hominins. The morphological similarity of KNM-WT 51260 to human third metacarpals, and its spatio-temporal context, suggests that this fossil is attributable to *Homo erectus sensu lato*. KNM-WT 51260 shows that modern human-like hand morphology and function was present within a behavioral context characterized by Acheulean technology. It provides the earliest evidence of a key shared derived characteristic of modern human and Neandertal hands, and suggests that the distinctive complex of radial carpometacarpal joint features in the human hand arose early in the evolution of the genus *Homo*.

Funding provided by the LSB Leakey Foundation and University of Missouri Research Council.

Ancient DNA and the metagenomics of disease.

CHRISTINA WARINNER. Anthropology, University of Oklahoma, Centre for Evolutionary Medicine, University of Zürich.

High-throughput genomic and proteomic sequencing has opened up dramatic new opportunities to study health and disease, and the demonstrated success of applying these techniques to archaeological material is revolutionizing the field of paleopathology. The recent discovery that human dental calculus preserves abundant, high quality microscopic and biomolecular remains opens up further possibilities and extends the application of these techniques to non-mummified remains previously thought to be out of reach for most biomolecular studies of ancient disease. This paper presents new results from combined metagenomic and metaproteomic analyses of human dental calculus specimens collected from four Medieval individuals with osteological evidence of periodontitis (Dalheim, Germany, c. 1100 CE). We document the presence of more than 500 bacterial taxa known to inhabit the human oral cavity, including 16 bacterial pathogens associated with periodontal disease and caries infection. We further identify